Determination of the Optimum Conditions in Evaluation of Kiwi Juice as Green Corrosion Inhibitor of Steel in Hydrochloric Acid

Khalid Hamid Rashid
Lecturer
Chemical Engineering Department-University of Technology-Baghdad
Email: alhadidikhalid@yahoo.com

ABSTRACT

The corrosion protection of low carbon steel in 2.5 M HCl solution by kiwi juice was studied at different temperatures and immersion times by weight loss technique. To study the determination of the optimum conditions from statistical design in evaluation of a corrosion inhibitor, three variables, were considered as the most dominant variables. These variables are: temperature, inhibitor concentration (extracted kiwi juice) and immersion time at static conditions.

These three variables are manipulated through the experimental work using central composite rotatable Box – Wilson Experimental Design (BWED) where second order polynomial model was proposed to correlate the studied variables with the corrosion rate of low carbon steel alloy to estimate the coefficients by nonlinear regression analysis method based on Rosenbrock and Quasi-Newton estimation method in as few experiments as possible to determinate of the optimum conditions of the proposed polynomial adopted via *STATISTICA* software. The parametric study on corrosion inhibition process using response surface methodology (RSM) is presented in this paper.

The study shows that the immersion time and temperature of corroding medium had shown negative dependence of great significance in increase the corrosion rate while the other studied variable (i.e. inhibitor concentration) had shown large positive dependence in reduce the corrosion rate of low carbon steel alloy.

Optimum conditions for achieving the minimum corrosion rate are obtained from optimizing the above correlation and are found as follow: 42.86 °C temperature of corroding medium, 29.29 cm^3/L inhibitor concentration and 2.65 h immersion time. In these circumstances, the value of inhibition efficiency obtained was 96.09 %. It could be concluded that Box-Wilson experimental design was adequately applicable in the optimization of process variables and that kiwi juice sufficiently inhibited the corrosion for low carbon steel at the conditions of the experiment.

Keywords: RSM; corrosion inhibition; kiwi juice; hydrochloric acid solution

إيجاد الظروف المثلى في تقييم عصير الكيوي كمانع تآكل طبيعي للحديد في حامض الهيدروكلوريك

خالد حامد رشيد
مدرس
قسم الهندسة الكيمياوية - الجامعة التكنلوجية – بغداد

الخلاصة

تم دراسة حماية تآكل حديد منخفض الكاربون في محلول حامض الهيدروكلوريك (2.5 مولاري) بأستخدام عصير الكيوي كمثبط لعملية التاكل عند مختلف درجات الحرارة وفترات زمن غمر بأستخدام تقنية فقدان الوزن لحساب معدلات التآكل. لدراسة تحديد الظروف المثلى من التصميم الأحصائي في تقييم أداء مثبط عملية تآكل أُخذت بنظر الأعتبار ثلاثة متغيرات

أعتبرت الأكثر تأثيرًا على عملية التآكل. العوامل المؤثرة هي درجة الحرارة و تركيز المثبط (عصير الكيوي) و فترة زمن غمر عند ظروف ساكنة.
المتغيرات الثلاثة تم معالجتها من خلال تصميم التجارب العملية بإستخدام طريقة التصميم الدوار المركب المركزي (Box-Wilson) لربط المتغيرات أعلاه بمعادلة متعددة الحدود من الدرجة الثانية التي تشير الى العلاقة بين المتغيرات الثلاثة ومعدل التآكل لسبيكة الحديد منخفض الكاربون من خلال إيجاد المعاملات بأستخدام طريقة تحليل التراجع والأرتداد اللاخطي المعتمدة على طريقة حساب (Rosenbrock and Quasi-Newton) بأقل عدد تجارب ممكن لتحديد الظروف المثلى للمعادلة المفترضة المتعددة الحدود المعتمدة بواسطة (*STATISTICA* software). ذكرت دراسة العوامل على عملية تثبيط التاكل بأستخدام منهج سطح الأستجابة في هذه المقالة.
الدراسة تبين بأن زمن الغمر ودرجة حرارة محلول التآكل لها تأثيرا سلبيا في زيادة معدل التآكل في حين أن المتغير الآخر (تركيز المثبط) كان له تأثيرا أيجابيا كبيرا في تقليل معدل تآكل سبيكة حديد منخفض الكاربون . تم إستخراج الظروف المثلى للتجارب للحصول على أقل معدل تآكل وهي : درجة حرارة محلول التآكل 42.86 °C , تركيز المثبط 29.29 cm^3/L و زمن غمر 2.65 h. وعند هذه الظروف , قيمة كفاءة المادة المانعة للتاكل كانت 96.09 %. أستنتج من النتائج بأن التصميم العملي Box-Wilson قابل للتطبيق على نحو ملائم في أختيار الأفضل لمتغيرات العملية وعصير الكيوي له التأثيرعلى نحو كافي في تثبيط تآكل الحديد منخفض الكاربون عند ظروف التجربة.

الكلمات الرئيسيه: RSM ، تثبيط تآكل ، عصير كيوي ، محلول حامض الهيدروكلوريك

1. INTRODUCTION

In the chemical and engineering industry experimental designs are particularly applied to study of process variables and how they affect on the product, **Perry**, and **Green**, **2000**.

Three basic types of statistically designated experiments are most often used in chemical and engineering industry. These are 1. Fractional-Factorial design. 2. Box-Wilson design. 3. Factorial design. Box-Wilson designs and, in particular, the two-level Box-Wilson design, have been treated in the literature both theoretically and from application point of view, **Box** and **Hunto**, **2005**. However, it's desirable here to review briefly their major characteristics:

Consider the weight loss resulting from corrosion of a low carbon steel specimen has to be determined as function of temperature, inhibitor concentration and immersion time, and let the two levels of temperature, inhibitor concentration and immersion time. The experiments carried out under these conditions are presented in the experimental design.

Many metals and alloys which used in different human activities are susceptible to different mechanisms of corrosion due to their exposure to different corrosive media. Among these, low carbon steel is very important. One of the methods used to reduce the rate of metallic corrosion is addition of inhibitors. Many studies have been carried out to find suitable compounds to be used as corrosion inhibitors for this metal in different aqueous solutions. These studies reported that there are a number of organic and inorganic compounds which can inhibit corrosion of steel, **Musa**, **et al.**, **2010**, **Khadom**, **et al.**, **2009**, **Yaro**, **et al.**, **2000**. Many researchers were conducted to examine some naturally occurring substances as corrosion inhibitors for different metals in various environments, **El-Etre**, **et al.**, **2005**, **El-Etre**, **2003**.

The use of inhibitors is an important method of protecting materials against deterioration. Inhibitors are chemicals that often work by adsorbing themselves on the metallic surface by forming a film, **Ebenso**, **et al.**, **2009**, **Noor, 2008**, **Ebenso**, **et al.**, **2008**, **Oguzie**, **2006**, **Gazquez**, **2006**. Most corrosion inhibitors are either synthesized from cheap raw materials or are chosen from organic compounds containing electronegative functional groups and л-electrons in triple or conjugated double bonds. The sites of aromatic rings and hetro atoms (such as S, N, O and P) are the major adsorption centers for these inhibitors, **Dubey**, and **Sing, 2007**. Broad spectra of organic compounds are available as corrosion inhibitors. Of these, only very few are actually used in practice. This is partly due to the fact that desirable properties of an inhibitor usually

extend beyond those simply related to metal protection. Considerations of cost, toxicity, availability and environmental friendliness are of considerable important. Accordingly, the replacement of some toxic, expensive chemical inhibitors by inhibitors obtained from natural sources is necessary. Apart from being readily available, cheap and a renewable source of materials, naturally occurring substances are eco-friendly and ecologically acceptable. Naturally occurring substances are biodegradable and do not contain heavy metals or other toxic compounds. Among the so-called "green corrosion inhibitors" are organic compounds that act by adsorption on the metal surface, such as extracts of natural substances, **Raja**, and **Sethuraman**, **2008**. The efficiency of these organic corrosion inhibitors is related to the presence of polar functional groups with S, O or N atoms in the molecule, heterocyclic compounds and л-electrons. The polar function is usually regarded as the reaction center for the establishment of the adsorption process, **Roberge**, **1999**. One of these natural compounds is fruits. Fruit is a rich source of chemicals such as vitamins, minerals, organic acids and phenolic compounds. The kiwi juice includes different level of phenolic compounds. The hydroxybenzoic acids and hydroxycinnamic acids are the most common compounds in kiwi fruits, **Keith**, **2012**. Note that the kiwi juice extract use for the first time as natural inhibitor in this article to the corrosion of low carbon steel alloy in hydrochloric acid solution. **Alaneme**, and **Olusegun**, **2012** have studied the inhibitive property of lignin extract of sun flower (tithonia diversifolia) as green corrosion inhibitor in 1 M H_2SO_4 solution using experimental design. **Da Rocha**, **et al**., **2012** have studied the inhibitive action of grape pomace extract as green corrosion inhibitor against the corrosion of carbon steel in a 1 mol L^{-1} HCl solution using weight loss measurements. **Afia, et al**., **2014** have studied the inhibitive property of acid garlic essential oil as a green corrosion inhibitor in a 1 M HCl solution by weight loss method of monitoring corrosion rate.

Therefore, the present study of inhibition of kiwi juice on low carbon steel corrosion and the optimization of the independent variables is necessary, as well as important to the environment.

The experiments discussed in this work were designed to optimize the inhibition of low carbon steel by extracted kiwi juice where several variables, including temperature, inhibitor concentration and immersion time would influence the corrosion rate.

Design of experiment is a statistical procedure that can reduce significantly the number of experiment, keeping however, the reliability of the conclusions at high standard. The traditional experimental method, one factor at a time approach can hardly be used to establish relationships among all the experimental input factors and the output responses. Even though the traditional approach can be useful in finding predominate factors in this situation, it is difficult to observe the optimum value of the working parameters as no interaction among them is considered. To solve this problem and obtain a probable optimum, design of experiment (DOE) offers a better alternative to study the effect of variables and their responses with minimum number of experiments, **Giovanilton**, **et al**., **2011**, **Montgomery**, **2005**. A Box-Wilson is used to evaluate two or more factors simultaneously. The treatment is combination of level of the factors. The advantages of Box-Wilson design over one-factor-at-a-time experiment are that they are more efficient and they allow interactions to be detected. .

The aim of the present work is to investigate the influence of the operating parameters (temperature, inhibitor concentration of extracted kiwi juice and immersion time) on corrosion rate of low carbon steel alloy in hydrochloric acid solution under optimum conditions that are obtained by using Box-Wilson techniques, then estimation of the inhibition efficiency of extracted kiwi juice as green corrosion inhibitor in order to find a naturally, cheap and environmentally safe substance that could be used for inhibition purposes.

2. EXPERIMENTAL WORK

2.1 Metal Preparation

The material of working electrodes used in this study is low carbon steel in foil coupons of a tag shape were used as specimens. This material is cut of specimens by dimensions of (2×3×0.2 cm). Analysis of these specimens was carried out at National Center for Construction Laboratories and Research /Baghdad/Iraq. **Table 4** shows the nominal and the analytical chemical compositions of material used in this work. This analysis indicates that the main elements of material are within the standard limits.

2.2 Extraction of Inhibitor

Completely fresh ripe kiwi fruit weighing 2 kg was purchased from the local market (Baghdad-Iraq). The fruits washed in cold running tap water followed by distilled water, dried with clean tissue, and extracted the crust from it and then was squeezed mechanically to get corresponding juice. The resulting juice nomination in order to get a homogeneous solution. In this process, 1/2 liter of kiwi juice was obtained. The extracted juice was kept frozen at - 4 °C in glass graduated cylinder until further experiment. The concentrations of inhibitor were closer as 5, 15, 25, 35 and 45 cm^3/L kiwi juice concentration.

2.3 Box-Wilson Experimental Design (BWED) and Optimization of Variables

The running expense for each experiment is relatively high which leads to need of design of experiment. The design of experiment is a statistical tool which helps to minimize the number of experiments so that appropriate data will be collected, the minimum number of experiments will be performed to acquire the necessary technical information and suitable statistical methods will be used to analyze the collected data. The initial task of this stage is to find out the key process control parameters with their ranges and performance evaluation parameter (output) that is to be measured. The levels of each variable represent the range for which the effect of that variable is desired to be known.

Box-Wilson experimental design is easy to apply to many engineering situations, making it a powerful yet simple tool and a series of tests for characterizing a physical mechanism. These series of experiments have been developed which efficiently serve as a basic deriving the mathematical model of process, **Jeff**, and **Michael**, **2009**. For three variables, the quadratic polynomial equation can be represented as follows:

$$Y = B_0 + B_1X_1 + B_2X_2 + B_3X_3 + B_{11}X_1^2 + B_{22}X_2^2 + B_{33}X_3^2 + B_{12}X_1X_2 + B_{13}X_1X_3 + B_{23}X_2X_3 \quad (1)$$

A preliminary step is to set up the relationships between the coded level and the corresponding real variables, which are required in the determination of experimental range by the following equation.

$$X_{coded} = \frac{X_{real} - X_{center}}{\frac{X_{center} - X_{min}}{\sqrt{k}}} \quad (2)$$

The coded variables take the value between -2 and 2 in accordance with the central composite rotatable suggested by Tarantino, **Tarantino**, **2010**.

The range of real variables for the system could be represented in **Table 1**.

The expression of coded level for the system is estimated from Eq. (2)

$$X_1 = \frac{T - 45}{8.66} \quad (3)$$

$$X_2 = \frac{C - 25}{11.55} \quad (4)$$

$$X_3 = \frac{t - 3}{1.15} \quad (5)$$

Where:
T = Temperature of corroding medium (°C)
C = Inhibitor Concentration (cm^3/L)
t = Immersion Time (h)
Table 2 shows the relationship between the coded level and corresponding real variables.
The number of experiments that must be done shown in **Table 3**.

2.4 Experimentation

The cleaning procedure was as follows: The specimens were first degreased with analar benzene and acetone at 25 °C, and then annealed in a vacuum oven at 550 °C for 1.5 h and cooled to room temperature. Specimens were abraded in sequence under running tap water using emery paper of grade numbers 220,320,400 and 600, rinsed with running tap water followed by distilled water, dried with clean tissue, immersed in acetone and benzene, and kept in desiccator over silica gel bed until time of use. The specimens were completely submerged in 200 cm^3 corrosion solution at 2.5 M HCl, 30, 37.5, 45, 52.5 and 60 °C, and 5, 15, 25, 35 and 45 cm^3/L kiwi juice concentration for a period of time 1, 2, 3, 4 and 5 h. After each experiment the specimens were washed with running tap water followed by distilled water, dried with clean tissue, immersed in acetone and benzene, and kept in desiccators over silica gel bed to dry, then weighed by high accuracy electronic balance.

3. RESULTS AND DISCUSSION

The corrosion of low carbon steel in 2.5 M HCl solution containing various concentrations of inhibitor at different temperatures and immersion times was studied by weight loss measurments. The corrosion rate of low carbon steel was determined using the relation:

$$C.R = \frac{Weight\ loss\ (g)}{Area\ (m^2)\ x\ Time\ (day)} \quad (6)$$

$C.R$: Corrosion rate (g/m^2. day) (gmd)

The percentage inhibition efficiency (IE (%)) was calculated at optimum conditions using the relationship, **Alaneme**, and **Olusegun**, **2012**:

$$IE\% = \frac{W_{uninhibt} - W_{inhibit}}{W_{uninhibit}} \times 100 \quad (7)$$

Where $W_{uninhibt}$ and $W_{inhibit}$ are the corrosion rates in absence and presence of inhibitor respectively.

Table 5 will be first fitted through nonlinear regression analysis to estimate the coefficients of the proposed model. **Table 5** also shows the corrosion rate of the specimens that reached through the experimental work and the predicated corrosion rate, which are designed according to the central composite rotatable design method.

3.1 Response Surface Methodology:

Response Surface Methodology (RSM) can be regarded as a statistical technique for optimizing the objective functions through some mathematical methods. Basically, this involves doing several experiments. Using the result of one experiment, direction for what to do next is provided, **Lenth**, **2010**. The field of RSM consists of the experimental strategy for exploring the space of the process or independent variables, empirical statistical modeling to develop an appropriate approximating relationship between the yield and process variables and optimization methods for finding the values of process variables that produce desirable values of the response, **Acherjee**, **et al.**, **2009**. The main objective of RSM is to find the combination of factor levels to achieve the optimal response.

In the present work the RSM is used to study the parametric effect of process parameters on corrosion rate. The result of experiment is used to develop the regression model as discussed in the following section. The effect of temperature, inhibitor concentration and immersion time on corrosion rate is shown graphically in **Fig. 3** through **Fig. 5** by constructing the response surface and contour diagram.

Multiple regression analysis (MRA) is one of the most widely used statistical techniques for analyzing multifactor data, **Davim**, **et al.**, **2008**. In the present work a regression model is developed by establishment of correlation between the process control parameters such as temperature, inhibitor concentration and immersion time with the output parameter namely corrosion rate, one can use this relationship in various algorithms. A quadratic regression model for response corrosion rate ($C.R$) is developed based on experimental results using the coded data of the central composite rotatable design, **Table 6** the coefficients of the 2nd order polynomial were estimated by implementing nonlinear least squares regression analysis technique based on Rosenbrock and Quasi-Newton estimation method via the *STATISTICA* software of version 10.1 can be used for estimation of coefficients B_0, B_1,…., B_{23}. This model will help to predict the response as a function of independent variables and their interactions.

In order to obtain the second-order response surface model equation the following equation may be assumed:

$$Y = B_0 + \sum_{i=1}^{n} B_i X_i + \sum_{i=1}^{n} B_{ii} X_i^2 + \sum_{i<j}^{n} B_{ij} X_i X_j + e_i \quad (8)$$

Where Y is the predicted response, B_0 the intercept coefficient, B_i the linear terms, B_{ii} the squared terms, B_{ij} the interaction terms, X_i and X_j are coded levels of the process control variables, the residual, e_i measures the experimental error of the observation number and n is the total number of designed variables, **Jian-Ping**, **et al.**, **2007**, **Montgomery**, **2005**. The coefficients of the model for the corresponding response are estimated using multiple regression analysis technique included in RSM. The response surfaces of corrosion rate can be expressed by the following quadratic equation in terms of coded values and real units.

$$C.R_{weight\ loss\ (gmd)} = 70.41 + 8.73\,T - 18.44\,C + 10.42\,t + 10.24\,T^2 + 22.34\,C^2 + 12.56\,t^2 - 0.34\,T \times C + 7.42\,T \times t + 1.11\,C \times t \quad (9)$$

Where, T = Temperature (°C)
C = Concentration of Inhibitor (cm^3/L)
t = Immersion Time (h)

3.2 Statistical and Mathematical Analysis:

From **Table 5**:
$e_i = (C.R_E - C.R_P)$
An estimation of the experimental error variance (S_r^2) is obtained by dividing the residual sum of squares (e_i) by number of degree of freedom(γ); where:

$$\gamma = N_i - N_{\text{coff}} \quad (10)$$

Where:
N_i: No. of experiments
N_{coff}: No. of coefficients in the model

$$\gamma = 18 - 10 = 8 \quad (11)$$

$$S_r^2 = \sum e_i^2/\gamma \quad (12)$$

The estimated variance of coefficients (S_b^2) is then calculated by the following formula:

$$S_b^2 = S_r^2/\sum X^2 \quad (13)$$

The significant coefficient can be estimated by comparing the value of (B^2/S_b^2) to the critical value $F_{0.95(1,8)} = 0.29$ of the F-distribution at 95% level of confidence, **Jeff**, and **Michael**, **2009**. The results of these calculations are shown in **Table 7** for low carbon steel alloy. The final form of the proposed model was as follows:

$$C.R_{weight\ loss\ (gmd)} = 70.41 + 8.73\,T - 18.44\,C + 10.42\,t + 10.24\,T^2 + 22.34\,C^2 + 12.56\,t^2 + 7.42\,T \times t \quad (14)$$

The accuracy of an empirical model can also be done by means of statistical parameters, for example, correlation coefficient. The correlation coefficient (R^2) is a statistical measure of the strength of correlation between the predicted and measured values, **Devore**, **2005**. For the current problem, the following result is obtained: $R^2 = 0.895$. **Fig. 2** shows predicted corrosion rate by Eq. (14) against experimental one.

3.3 Inhibition Optimization Result and Estimating the Percentage Inhibition Efficiency:

According to Eq. (14), using *POLYMATH* software version 4.02 in terms of minimum corrosion rate, the optimum values were obtained. The optimum values of the studied variables in coded and real form are listed in **Table 8** below for low carbon steel alloy. A validation experiment was conducted at the specified optimized values and the results were used to calculate the response (corrosion rate). The practical value of the corrosion rate at the optimum conditions was comparable with the theoretical value and the result was closed.

The percentage inhibition efficiency at the optimum conditions can be calculated from the Eq. (7).

$$IE\% = \frac{0.1049 - 0.0041}{0.1049} \times 100 = 96.09\ \%$$

3.4 Influence of Process Parameters on Corrosion Rate:

The aim of this study was to find a corrosion rate whose features would have been previously defined from the operative conditions extracted from the quadratic mathematical model.
Because the direct exploitation of the equation was delicate, it was convenient to restore it under a graphic representation; while fixing one of the three factors of the survey, it was possible to represent the response surface materializing the surface of regression in a three-dimensional space. It was also possible to project the equation in a design under isoresponse curves, interpreted as card curves level.

A. Evolution of corrosion rate as a function of the temperature and the concentration of corrosion inhibitor:

Fig. 3 shows the evolution of the corrosion rate as a function of the temperature and the concentration of corrosion inhibitor (extracted kiwi juice). It can be seen that the inhibitor concentration has a strong influence on the tentative response. The minimal corrosion rate is obtained for an inhibitor concentration of 0.37 in coded variable, i.e., 29.29 cm^3/L in real variable. Considering simultaneous effects of temperature and inhibitor concentration is presented in **Fig. 3** contour plot. The figure shows, in high temperature (60 °C), the increase of corrosion rate is higher than in lower temperature (30 °C). This is also in close agreement with the research done by, **Da Rocha, et al., 2012**.

B. Evolution of corrosion rate as a function of the temperature and the immersion time:

Fig. 4 shows the synergism between the two factors: the temperature and immersion time in corrosion rate at inhibitor concentration 29.29 cm^3/L. It can be noted that the effect of the immersion time differed according to the corrosion rate's variation. This effect becomes positive and even more important when the corrosion rate is degraded (reduced). Analysis of corrosion rate as effects of interaction between temperature and immersion time is shown in **Fig. 4** contour plot. The model shows a decrease followed by growing of corrosion rate due to temperature and immersion time at the optimum condition of inhibitor concentration 29.29 cm^3/L and this in agreement with, **Alaneme**, and **Olusegun**, **2012**.

C. Evolution of corrosion rate as a function of the concentration of corrosion inhibitor and the immersion time:

Fig. 5 represents the evolution of the corrosion rate as a function of the inhibitor concentration and the immersion time. This figure shows that the corrosion rate initially decreased when the inhibitor concentration and immersion time increased. This evolution was however more accentuated up to a concentration of 29.29 cm^3/L kiwi juice until it reaches a minimum value of corrosion rate at 2.65 h, which contributes to the great tendency of corrosion protection causes decrease in corrosion rate then it begins to increase again with increasing the inhibitor concentration and immersion time. **Fig. 5** contour plot presents a polynomial surface response relating to effect of inhibitor concentration and immersion time on corrosion rate. It is shown that different corrosion rate is observed for inhibitor concentration and immersion time. Immersion time increased corrosion rate from 70-220 gmd along the immersion time setting (1-5

h). Concentration of inhibitor from 5-45 cm^3/L has decreased corrosion rate from 270-70 gmd. This is also in close agreement with the research done by, **Afia, et al., 2014**.

4. CONCLUSION

1. The results of experiment are extended to develop the second order polynomial regression model of the objective function (corrosion rate) in terms of three variables (i.e., temperature of corroding medium, inhibitor concentration and immersion time) using response surface methodology (RSM) gives Eq. (14), which adequately describes the behavior of the process throughout the studied range.
2. The three variables effect on the corrosion rate in following order:

   Inhibitor concentration > Immersion time > Temperature**.**
3. The green corrosion inhibitor made up the kiwi juice extract successfully reduced the corrosion rates of low carbon steel alloy in 2.5 M HCl solution.
4. The optimum conditions as predicted from Eq. (14) is 42.86 °C temperature of corroding medium, 29.29 cm^3/L inhibitor concentration and 2.65 h of immersion time for low carbon steel alloy.
5. Kiwi juice extract acts as a corrosion inhibitor of low carbon steel with inhibition efficiency of 96.09 % under the optimum conditions.
6. The corrosion rate of low carbon steel alloy in 2.5 M HCl solution in presence of kiwi juice extract, increases with increasing temperature and immersion time, and decreased with increasing concentration of inhibitor.
7. The analysis of statistical central composite rotatable Box–Wilson Experimental Design (BWED), generally, shows that the interaction effects on the corrosion rate by weight loss technique (within the studied range) is less pronounced compared with the main and square variables except the interaction effect of ($T \times t$) in presence of extracted kiwi juice.

ACKNOWLEDGEMENT

The author would like to thank National Center for Construction Laboratories and Research /Baghdad/Iraq for financial support.

5. REFERENCES

- Acherjee, B., Misra, D., Bose, D. and Venkadeshwaran, K., 2009, *Prediction of Weld Strength and seam Width for Laser Transmission Welding of Thermoplastic using Response Surface Methodology*, Optics & Laser Technology, No. 41, PP. 956-967.

- Afia, L., Benali, O., Salghi, R., Ebenso, E. E., Jodeh, S., Zougagh, M. and Hammouti, B., 2014, *Steel Corrosion Inhibition by Acid Garlic Essential Oil as a Green Corrosion Inhibitor and Sorption Behaviour,* Int J. Electrochem. Sci., Vol. 9, PP. 8392-8406.

- Alaneme, K. K. and Olusegun, S. J., 2012, *Corrosion Inhibition Performance of Lignin Extract of Sum Flower (Tithonia Diversifolia) on Medium Carbon Low Alloy Steel Immersed in H_2SO_4 Solution*, Leonardo Journal of Sciences, Vol. 20, No. 1-6, PP. 59-70.

- ASTM, Annual book, 2004, *Engineering Handbook-Technical Information*, 1st Edition, Huyett.

- Box, H. and Hunto, 2005, *Statistics for Experiments*, 2nd Edition, John-Wiley and Sons, Inc., New York, USA.

- Da Rocha, J. C., Ponciano Gemes, J.A.C., Delia, E., Gil Cruz, A. P., Cabral, L. M.C., Torres, A. G. and Monteiro, M. V. C., 2012, *Grape Pomace Extracts as Green Corrosion Inhibitors for Carbon Steel in Hydrochloric Acid Solutions*, Int. J. Electrochim. Sci., Vol. 7. PP. 11941-11956.

- Davim, J.P., Oliveira, C. and Cardoso, A., 2008 ,*Predicting the Geometric form of Clad in Laser Cladding by Powder Using Multiple Regression Analysis (MRA)*,Materials and Design, No.29, PP.554-557.

- Devore, P., 2005, *The Exploration and Analysis Data*, 5th Edition Thomson Learning, Belmont, USA.

- Dubey, A. K. and Sing, G., 2007, *Corrosion Inhibition of Mild Steel Using Brijj-30*, Portugaliae Electrochimica Acta, Vol. 25, PP. 205-219. http://dx.doi.org/10.4152/pea.200702205

- Ebenso, E.E., Eddy, N.O. and Odongenyi, A.O., 2009, *Inhibition of the Corrosion of Mild Steel by Methocarbamol*, Portugaliae Electrochimica Acta, Vol. 27, PP. 13-22.

- Ebenso, E.E., Eddy, N.O. and Odongenyi, A.O., 2008, *Corrosion Inhibitive Properties and Adsorption Behaviour of Ethanol Extract of Piperguinensis as a Green Corrosion Inhibitor for Mild Steel in* H2SO4, African Journal of Pure and Applied Chemistry, Vol. 4, PP. 107-115.

- El-Etre, A. Y., Abdallah, M. and El-Tantawy, Z. E., 2005, *Corrosion Inhibition of Some Metals Using Lawsonia Extract*, Corros. Sci., No. 47, PP. 389-395.

- El-Etre, A. Y., 2003, Corros. Sci., No. 45, P. 2485.

- Gazquez, J. L., 2006, *Quantum Chemical Study of the Inhibitive Properties of 2-Pyridyl-Azoles*, The Journal of Physical Chemistry, Vol. 110, PP. 8928-8934. http://dx.doi.org/10.1021/jp057143y

- Giovanilton, F. S., Fernando, L. C. and Andrea, L.O., 2011, *Application of Surface Methodology for Optimization of Biodiesel Production by Trans esterification of Soybeam Oil with Ethanol*, Fuel Processing Technology, Vol. 92, PP. 407-413. http://dx.doi.org/10.1016/j.fuproc.2010.10.002

- Jeff Wu, C. F. and Michael, S.H., 2009, *Experiments: Planning, Analysis and Optimization*, 2nd Edition, John-Wiley and Sons, Inc., New York, USA.

- Jian-Ping, W., Yong-Zhen, C., Xue-Wu G. and Han-Qing, Y., 2007, *Optimization of Coagulation-Flocculation Process for A Paper-recycling Wastewater Treatment Using Response Surface Methodology*, Colloids and surfaces A: Physicochem. Eng. Aspects, No. 302, PP.204-210.

- Keith, S., 2012, *Kiwi fruit Overview of Potential Health Benefits*, Nutrition and Food, Vol. 47, No. 3, PP.133-147.

- Khadom, A. A., Yaro, A. S., Al Taie, A. S. and Kadum, A. A. H., 2009, *Electrochemical, Activations and Adsorption Studies for The Corrosion Inhibition of Low Carbon Steel in Acidic Media*, Portug. Electrochim. Acta, Vol. 27, No. 6, PP. 699-712.

- Lenth, R. V., 2010, *Response-Surface Methods in R Using RSM*, Journal of Statistical Software, No.28, July.

- Montgomery, D.C., 2005, *Design and Analysis of Experiments*, 6th Edition, John Wiley and Sons, New York, USA.

- Musa, A. Y., Khadom, A. A., Kadhum, A. A., Mohamad, A. B. and Takriff, M. S., 2010, *Kinetic Behavior of Mild Steel Corrosion Inhibition by 4-Amino-5-Phenyl-4H-1,2,4-Trizole-3-Thiol*, J. Taiwan Inst. Chem. Eng., No.41, PP. 126-128.

- Noor, E. A., 2008, *Comparative Study of Corrosion Inhibition of Mild Steel by Aqueous Extract of Fenugreek Seeds and Leaves in Acidic Solution*, Journal of Engineering and Applied Sciences, Vol. 4, PP. 23-30.

- Oguzie, E. E., 2006, *Adsorption and Corrosion Inhibitive Properties of Azadirechtaindica in Acid Solution*, Pigment and Resin Technology, Vol. 35, PP. 334-340. http://dx.doi.org/10.1108/03699420610711335

- Perry, R.H. and Green, D.W., 2000, *Chemical Engineering Handbook*", 8th Edition, McGraw-Hill, United States.

- Raja, P. B. and Sethuraman, M. G., 2008, *Natural Products as Corrosion Inhibitor for Metals in Corrosive Media-A review*, Mater. Lett., Vol. 62, PP. 113-116.

- Roberge, P. R., 1999, *Corrosion Inhibitors, in: Handbook of Corrosion Engineering*, McGraw-Hill, New York, PP. 833-862.

- Tarantino, L., 2010, *Design and Analysis of Industrial Experiments*", 1st Edition, Tetra Pak.

- Yaro, A. S., Abdul Masih, N. Sh. and Khadom, A. A., 2000, *The Influence of Temperature on Corrosion Inhibition of Carbon Steel in Air –Saturated 7N H_3PO_4 by Potassium Iodide*, Iraqi, J. Chem. Petrol. Eng., No. 1, PP.83-87.

Table 1. The experimental range of variables.

Temperature (°C)	Inhibitor Concentration (cm^3/L)	Immersion Time (h)
30-60	5-45	1-5

Table 2. Real and coded of the independent variables used in RSM study.

Variables	Levels				
$X_1,\ X_2,\ X_3$	-2	-1	0	1	2
$X_1 = \text{Temperature (°C)}$	30	37.5	45	52.5	60
$X_2 = \text{Inhibitor Concentration } (cm^3/L)$	5	15	25	35	45
$X_3 = \text{Immersion Time (h)}$	1	2	3	4	5

Table 3. Sequence of experiments according to central composite rotatable experimental design.

Exp. No.	Coded Variables			Real Variables		
	X_1	X_2	X_3	Temp. (°C)	Inhibitor Conc. (cm^3/L)	Immersion Time (h)
1	-1	-1	-1	37.5	15	2
2	1	-1	-1	52.5	15	2
3	-1	1	-1	37.5	35	2
4	1	1	-1	52.5	35	2
5	-1	-1	1	37.5	15	4
6	1	-1	1	52.5	15	4
7	-1	1	1	37.5	35	4
8	1	1	1	52.5	35	4
9	-2	0	0	30	25	3
10	2	0	0	60	25	3
11	0	-2	0	45	5	3
12	0	2	0	45	45	3
13	0	0	-2	45	25	1
14	0	0	2	45	25	5
15	0	0	0	45	25	3
16	0	0	0	45	25	3
17	0	0	0	45	25	3
18	0	0	0	45	25	3

Table 4. A nominal, **Astm**, **2004** and analytical chemical composition (wt. %) of low carbon steel alloy.

Metal	Fe	C	Mn	Si	P	S	Cr	Mo	Ni	Al
Nominal	Rem.	0.02-0.13	0.3-0.6	0.002	0.004	0.005	0.024	0.0008	0.014	0.003
Analytical	Rem.	0.040	0.309	0.004	0.005	0.007	0.021	0.0009	0.010	0.004

Table 5. Two-level central composite rotatable experimental design of the independent variables with the observed, predicted values and experimental error for the response.

Exp. No.	Coded Variables			Real Variables			Exp. Corrosion Rate	Predicted Corrosion Rate	Corresponding residual
	X_1	X_2	X_3	Temp. (°C)	Inhibitor Conc. (cm^3/L)	Immersion Time (h)	$C.R_E$ (gmd)	$C.R_p$ (gmd)	$e_i = C.R_E - C.R_P$
1	-1	-1	-1	37.5	15	2	100.53	123.04	-22.51
2	1	-1	-1	52.5	15	2	125.88	126.33	-0.45
3	-1	1	-1	37.5	35	2	110.17	84.61	25.56
4	1	1	-1	52.5	35	2	111.45	86.54	24.91
5	-1	-1	1	37.5	15	4	130.44	126.81	3.63
6	1	-1	1	52.5	15	4	162.76	159.79	2.97
7	-1	1	1	37.5	35	4	121.82	92.83	28.99
8	1	1	1	52.5	35	4	175.49	124.45	51.04
9	-2	0	0	30	25	3	90.35	93.92	-3.57
10	2	0	0	60	25	3	103.87	128.84	-24.97
11	0	-2	0	45	5	3	219.09	196.64	22.45
12	0	2	0	45	45	3	71.89	122.87	-50.98
13	0	0	-2	45	25	1	100.33	99.82	0.51
14	0	0	2	45	25	5	112.44	141.49	-29.05
15	0	0	0	45	25	3	63.45	70.41	-6.95
16	0	0	0	45	25	3	65.32	70.41	-5.09
17	0	0	0	45	25	3	61.87	70.41	-8.54
18	0	0	0	45	25	3	62.45	70.41	-7.96

Table 6. The coefficient values of the predicted correlation.

Coeff.	B_0	B_1	B_2	B_3	B_{11}	B_{22}	B_{33}	B_{12}	B_{13}	B_{23}
Value	70.41	8.73	-18.44	10.42	10.24	22.34	12.56	-0.34	7.42	1.11
Correlation Coefficient (R^2)			0.895			Proportion of Variance			0.67	
Final Value of loss function			10042.18							

Table 7. Analysis of variance (ANOVA) for the fitted model.

Constant Estimated	ΣX^2	Estimated Coefficient (B)	Variance $Sb^2 = Sr^2/\Sigma X^2$	F-value $= B^2/Sb^2$	$F_{0.95(1,8)} = 0.29$
B_1	16	8.73	78.4539	0.97	S*
B_2	16	-18.44	78.4539	4.33	S
B_3	16	10.42	78.4539	1.38	S
B_{11}	16	10.24	78.4539	1.34	S
B_{22}	16	22.34	78.4539	6.36	S
B_{33}	16	12.56	78.4539	2.01	S
B_{12}	8	-0.34	156.9078	0.001	NS**
B_{13}	8	7.42	156.9078	0.35	S
B_{23}	8	1.11	156.9078	0.01	NS

(*) Significant
(**) Non-significant

Table 8. Optimum values of the process variables for minimum corrosion rate.

Variables	Optimum Values (low carbon steel alloy)	
	Coded	Real
X_1 = Temperature (°C)	-0.25	42.86
X_2 = Inhibitor Concentration (cm^3/L)	0.37	29.29
X_3 = Immersion Time (h)	-0.30	2.65
Function Minimum (Corrosion rate, gmd)	62.35	

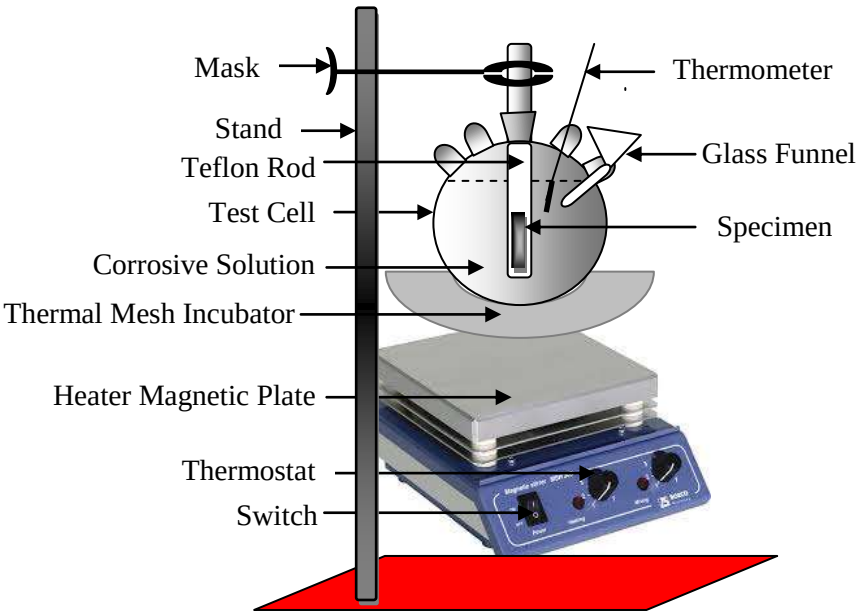

Figure 1. Experimental set-up for weight loss investigation.

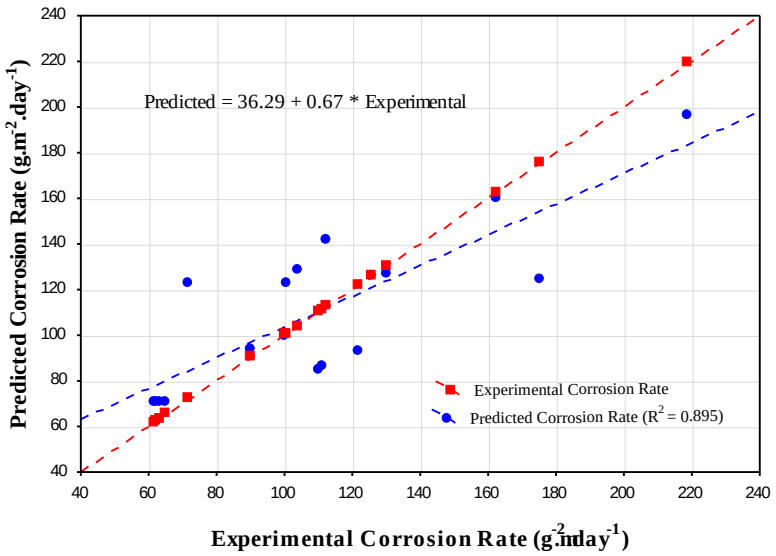

Figure 2. Predicted corrosion rate versus experimental corrosion rate.

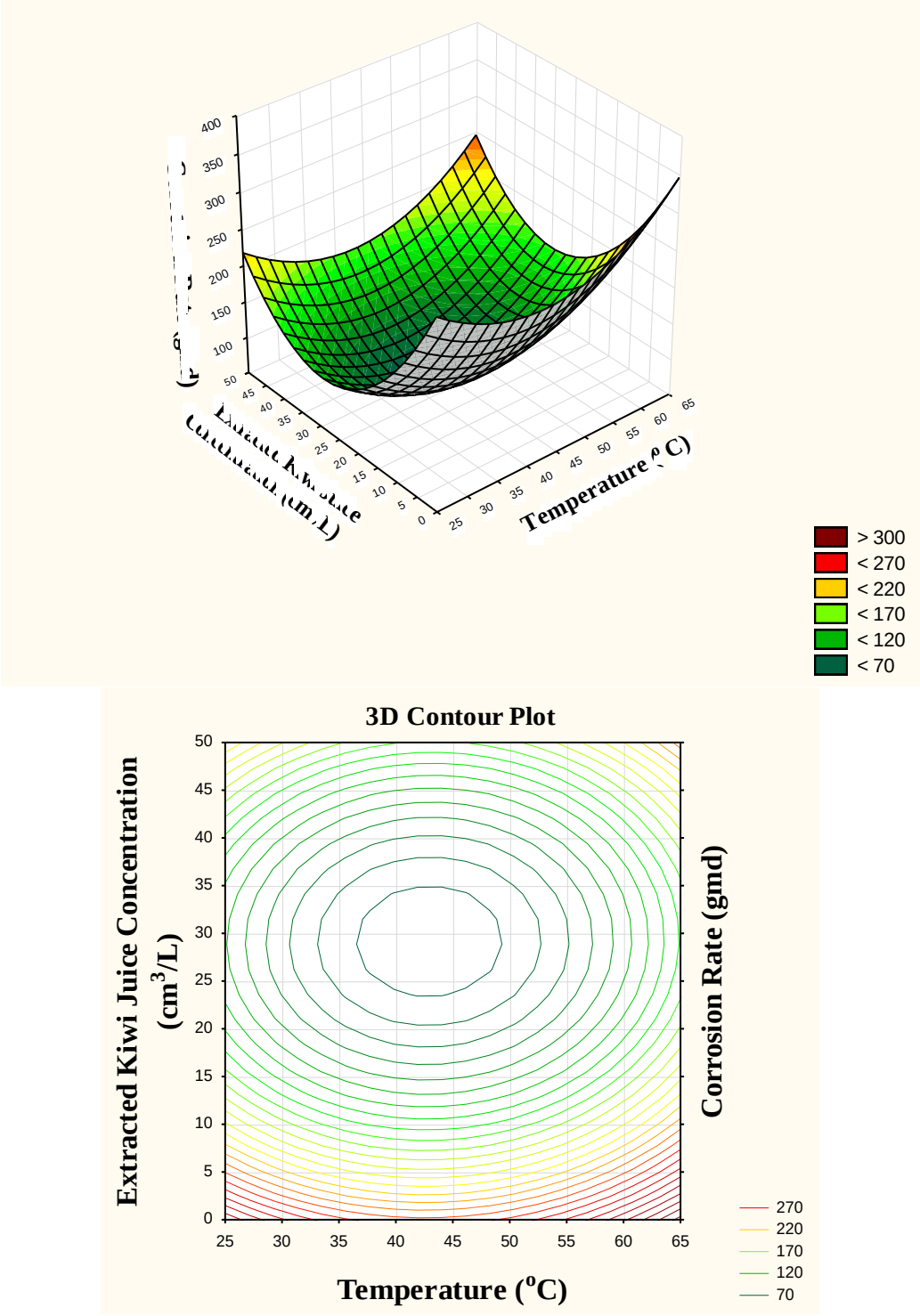

Figure 3. Response surface plot (top) and contour plot (bottom) showing the variation of corrosion rate as a function of the temperature and extracted kiwi juice concentration at the optimum value (2.65 h).

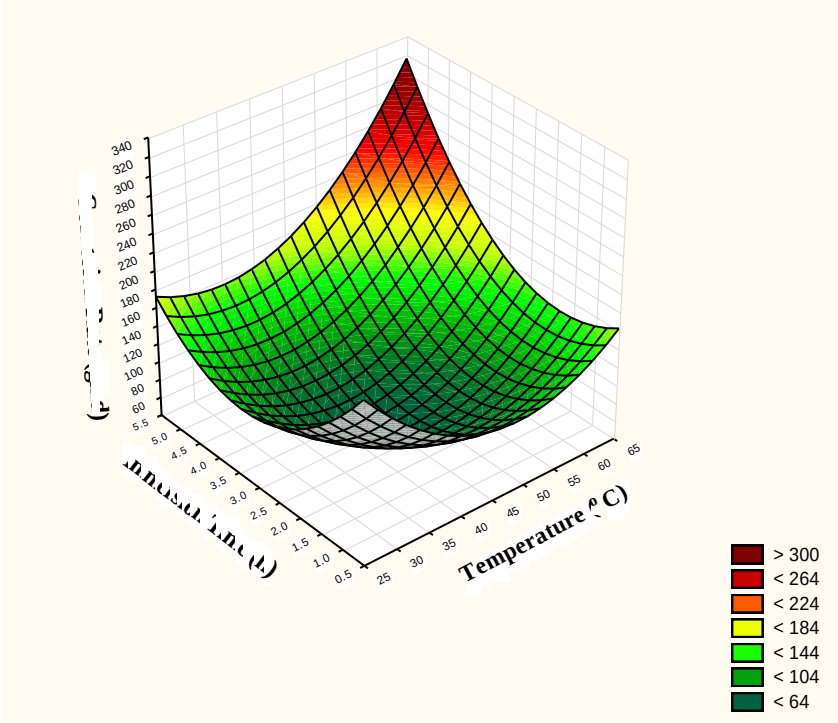

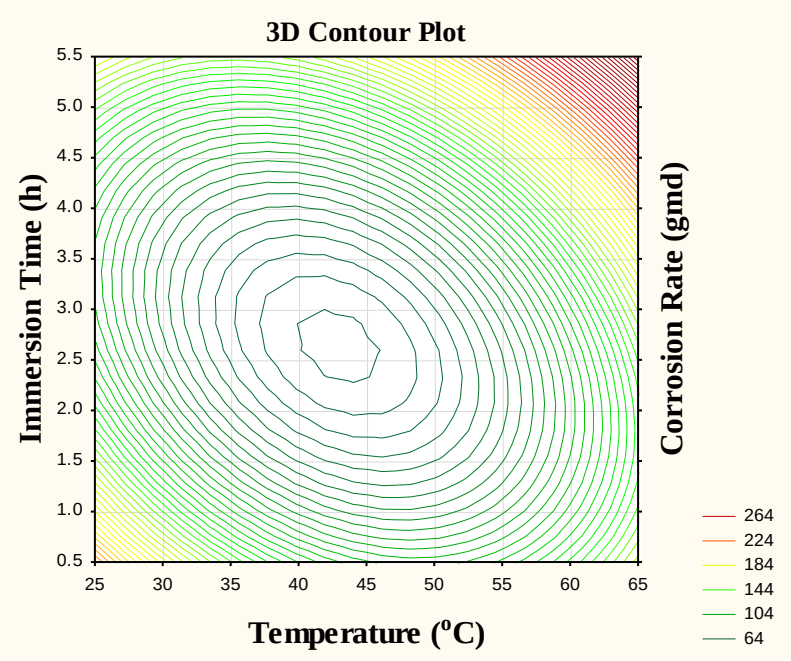

Figure 4. Response surface plot (top) and contour plot (bottom) showing the variation of corrosion rate as a function of the temperature and immersion time at the optimum value (29.29 cm^3/L).

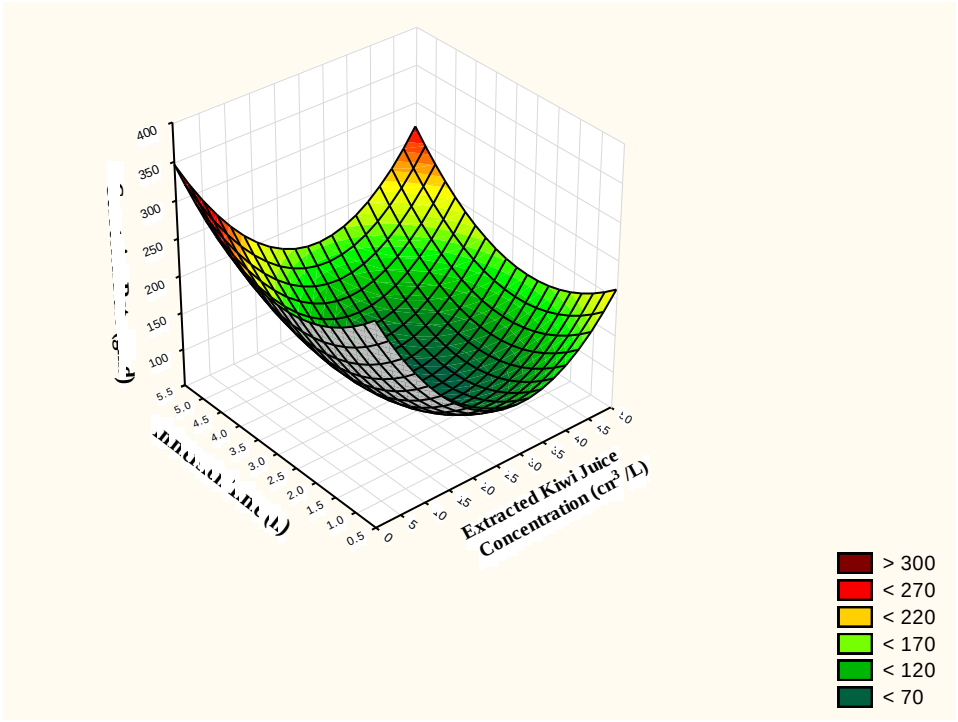

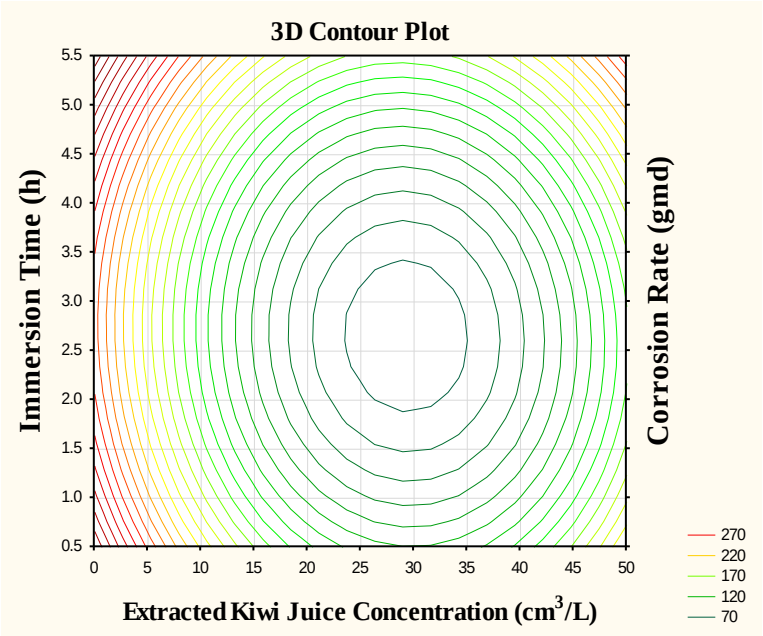

Figure 5. Response surface plot (top) and contour plot (bottom) showing the variation of corrosion rate as a function of the extracted kiwi juice concentration and immersion time at the optimum value (42.86 °C).

Influence of Internal Sulfate Attack on Some Properties of High Strength Concrete

Nada Mahdi Fawzi
Professor
College of Engineering, University of Baghdad
email: naljalawi@yahoo.com

Zena K.Abbas
Lecturer
College of Engineering, University of Baghdad
email: zka_abbas@gmail.com

Hussein Ali Jaber
Engineer
College of Engineering, University of Baghdad
email: hussein_7610@yahoo.com

ABSTRACT

One of the most important problems that faces the concrete industry in Iraq is the deterioration due to internal sulfate attack , since it reduces the compressive strength and increases the expansion of concrete. Consequently, the concrete structure may be damage .The effects of total and total effective sulfate contents on high strength concrete (HSC) have been studied in the present study.

The research studied the effect of sulfate content in cement , sand and gravel , as well as comparing the total sulfate content with the total effective SO_3 content. Materials used were divided into two groups of SO_3 in cement ,three groups of SO_3 in sand ,and two groups of SO_3 in gravel.

The results show that considering the total effective sulfate content is better than the total content of sulfates since the effect of sulfate in each constituent of concrete, depends on it's granular size .The smaller the particle size of the material the more effective is the sulfate in it. Therefore, it is recommended to follow the Iraqi specification for total effective sulfate content, because it gives more flexibility to the use of sand and gravel with higher sulfate content.

The results of compressive strength at 90-days show that the effect of total effective SO_3 content of (2.647% , 2.992% , 3.424%) that correspond to total sulfate of (3.778%, 3.294%, 4.528%) decrease the compressive strength by (7.53%, 11.44%, 14.59%) respectively.

Key words: internal sulfate attack, total effective sulfate content, high strength concrete, total sulfate content, particle size.

تأثير هجوم الاملاح الكبريتية الداخلية على بعض خواص الخرسانة عالية المقاومة

ندى مهدي فوزي
أستاذ
كلية الهندسة – جامعة بغداد

زينة خضير عباس
مدرس
كلية الهندسة – جامعة بغداد

حسين علي جابر
مهندس
كلية الهندسة - جامعة بغداد

الخلاصة

واحدة من أهم المشاكل التي تواجه صناعة الخرسانة في العراق هي التدهور بسبب هجوم الكبريتات الداخلية، نظرا لانه يقلل من مقاومة الانضغاط ويسبب حدوث تمدد في الخرسانة. وبالتالي،قد يسبب الضرر للمنشاء الخرساني.
في الدراسة الحالية تم دراسة تأثيركل من الاملاح الكبريتية الكلية والاملاح الكبريتية الكلية الفعالة على الخرسانة عالية المقاومة.
يدرس البحث تأثير محتوى الكبريتات في السمنت والرمل والحصى، وكذلك مقارنة المحتوى الكلي للكبريتات مع المحتوى الكلي للكبريتات الفعالة. وقد تم تقسيم المواد المستخدمة في البحث الى مجموعتين من محتوى (SO_3) في السمنت، وثلاث مجموعات من (SO_3) في الرمل، ومجموعتين من (SO_3) في الحصى.
بينت النتائج أنه يمكن اعتبار المحتوى الكلي للاملاح الكبريتية الفعالة أفضل من المحتوى الكلي من الكبريتات نظرا لانه يعتمد على حجم الحبيبة للمادة المستخدمة.ان المادة ذات أصغر حجم حبيبي تكون من المواد أكثر فعالية في تأثير الكبريتات .وبالتالي، فمن المستحسن أن تتبع المواصفات العراقية لمجموع محتوى الاملاح الكبريتية الكلية الفعالة لأنه يعطي مزيدا من المرونة لاستخدام الرمل والحصى مع المحتوى العالي من الكبريتات.
أظهرت النتائج خلال عمر سبعة ايام أن تأثير المحتوى الكلي الفعال للSO_3 (2.647٪، 2.992٪، 3.424٪) التي تتقابل مع الكبريتات الكلية (3.778٪، 3.294٪، 4.528٪) يقلل من المقاومة بنسب (5.26٪، 7.44٪، 12.45 ٪) على التوالي.

الكلمات الرئيسية: هجوم الاملاح الكبريتية الداخلي , محتوى الاملاح الكلية الفعالة ,الخرسانة عالية المقاومة , محتوى الاملاح الكلي ,الحجم الحبيبي.

1. INTRODUCTION

High strength concrete is a type of high performance concrete generally with a specified compressive strength of (40MPa) or higher, the production of high strength concrete requires a comprehensive research and more attention to quality control than the conventional concrete **ACI 363.2R, 1998**. High strength concrete is needed to implement the structural elements into service at much earlier age, such as maximize the spaces , construction of long span structures such as bridges and enhance the durability of bridge decks **ACI 363.2R, 1998**. New vanguard producers of ready mixed concrete are directing their promotion efforts toward commercialization of high strength concrete (60MPa and more).Some of the basic concepts that need to be understood for high strength concrete are ; The aggregate should be strong and durable, the aggregate need not necessarily be hard and of high strength but need to be compatible, in terms of stiffness and strength, with the cement paste, high strength concrete mixtures , generally , need to have a low water-cementitious material ratios (w/cm). W/cm ratios can be in the range of(0.23 to 0.35) and the use of air entrainment in high strength concrete will greatly reduce the strength potential **James, 1989, and Ron Burg, 1993**. Internal sulfate attack results from the reaction between sulfate in concrete constituents (water , cement , sand and gravel) .The reaction between these constituents, which have calcium aluminates, and water forms calcium sulphoaluminate . The hazard is

illustrated in the materials which cause high tensile stresses leading to expansion and disruption of concrete **Skalny, and Odler, 2002**.

Raof, 1970 considered Calcium sulfate (gypsum) more dangerous for this type of attack , because of the addition of gypsum to the cement at the grinding stage to control the hydration speed and setting of cement paste .

The deleterious action of internal sulfate attack is brought about by an excessive SO_3 content in the finer material or, less often, in the aggregate used. Under these conditions , the whole volume of the material is affected more-or-less uniformly. The extent of damage depends on the composition of the mixture, the curing conditions, and the environment to which the object of concern is exposed **Skalny, and Odler, 2002**.

The optimum SO_3 content, at which higher mechanical properties and little tendency to expanding are obtained, is at SO_3 equal to 5 (% by weight of cement).Further increase in sulfates content in concrete after this optimum value shows a considerable reduction in mechanical properties; compressive strength, flexural strength , U.P.V and rebound number. Nonetheless, there is some recovering with advance in age at which the affected mixtures retrieve some of their lost strength **Al-Ameeri, and Issa, 2013**.

The cement made with clinker containing somewhat high percentages of SO_3 and low alkali had relatively slower strength development and higher resistance to sulfate attack than classical cement with similar chemical composition **Sayed Horkoss, et al., 2011**.

Al-Rawi, et al., 2002 found that the allowable sulfate content in sand could be increased without a significant loss in strength provided that sulfate content in cement is reduced . They presented the theory of effective sulfate content in concrete constituents and developed the following Eq.(1) which is based on this theory :

$$SO_3(\text{effective}) = 0.9 - 0.25\ \sqrt{F.M} \quad \text{.....(1)}$$

This theory implies that sulfates in cement are more effective than sulfate in sand and sulfates in sand are more effective than that in coarse aggregates. Sulfates in cement could be more than double as effective as sulfates in sand, the same is applicable with the case of sulfate in sand compared with sulfate in coarse aggregate .It will also be used to calculate the effective SO_3 content in the present work **Al-Rawi, et al., 2002**.The different between al-Rawi work and the present work is the method of sulfate content in constituents of concrete which is used naturally contaminated in the present work.

Sulfate problem in fine aggregate increases with time in Iraq and the construction companies face several difficulties to find fine aggregate within the specification with regard to sulfate content. The possibility of adjusting fine aggregate content in concrete mixes is studied to facilitate using fine aggregate with sulfate content higher than that studied by the Iraqi Specification limit to (0.5%), but the total sulfate content of the mix is to be within the **IQS, No.45, 1984**.

In coarse aggregate, the presence of gypsum coatings is the major source of contamination **Saco, and Rassam, 1989**. Work done by **Sharif, et al., 1993** indicates that no gypsum exists in the interior mineral composition of coarse aggregate .By using X-ray Microscopic atomic absorption , and Auto analyzer they found that the gypsum exists only at the external surface of coarse aggregate.

The quality of mixing water plays an important role in the strength of the resulting concrete . Impurities in water may interfere with the setting of cement and adversely affect the strength and

may lead to corrosion of reinforcement . Drinking water satisfies specification of quality assurance for mixing and curing of concrete, most specification **BS 3148, 1980** put an upper limit for sulfate not exceed (1000 ppm), The **ASTM C94, 2003** gives the use of the wash water (SO_3 not exceed 3000 ppm)and the **I.Q.S 1703, 1992** limited (SO_3 not exceed 100 ppm) in water as SO_3% (by weight) as reported by **Al-Salihi, 1994**.

1.1 Objectives

The objectives of this research can be summarized as follows:

1. The research is conducted to produce high strength concrete according to ACI 211.4R(2008) .
2. It also demonstrates the correlation between the total and total effective SO_3% content with (HSC) at different ages.

2. MATERIALS CHARACTERISTICS

2.1 Cement

Ordinary Portland cement (OPC) (Type I) as (cement 1 and cement 2) under commercial name of (Al-Kufa) was used for HSC mixes throughout work. The chemical analysis and physical properties of the cement used are given in **Tables 1** and **2.** The results conform to, **IQS, No.5, 1984**.

2.2 Fine Aggregate

Al-Obeidi (sand 1) , Al-Ekhaider (sand 2) and sand 3 which mixed from (sand 1 and sand 2) natural sands of 4.75 mm maximum size was used as fine aggregate in HSC mixes. Some properties of the three natural fine aggregates are illustrated in **Table 3** according to **IQS, No.45, 1984**.The grading of fine aggregates is shown in **Fig 1**.

2.3 Coarse Aggregate

Aggregate predominately retained on the No.4 (4.75mm) sieve, in this work crushed coarse aggregate with a nominal size of (19 mm) was used and it was obtained from Al-Nibaai region as (gravel 1 and gravel 2). Some properties of coarse aggregate are illustrated in **Table 4** according to **IQS, No.45, 1984** ,**Fig. 2** illustrate the gradation used throughout the investigation.

2.4 High Range Water Reducing Admixture (HRWRA)

A super plasticizer which is known commercially as Flowcrete PC-200 was used as a high range water-reducing agent . It is a highly effective superplasticizer with a slight set retarding effect which produces free-flowing concrete in hot climates . Also a substantial water reducing agent promotes high , early and ultimate strength .

The dosage of this superplasticizer that was recommended by the manufacturer was (0.7-2.5) % by weight of cement . Exact dosage rates depend on type of the effect required, quality of cement , aggregate , water cement ratio and ambient temperature therefore , in many cases, it is advisable to carry out trial mixes . This admixture conforms to the **ASTM**

C494, 2006 type G .**Table 5** shows some physical and chemical analysis of the superplasticizer (PC-200).

2.5 Water

The water used in HSC mixes was potable water for both casting and curing of specimens.

3. PREPARATION OF CUBE SAMPLES

3.1 Mix Design

The design of concrete mixes to achieve characteristic compressive strength of (60) MPa at 28 days is made according to the American Method **ACI 211.4R, 2008**. Cement content is (512.5 kg/m³) and W/C ratio is 0.32. The slump required for all mixes is (75-100 mm). According to the mix design procedure, the mix proportion is (1: 1.44: 1.87). Mixes of HSC have been investigated by using two percentages of SO_3 in cement (type I with SO_3 content =2%) and (type I with SO_3 content=2.75%) ,These mixes have been studied by using different percentages of sulfate in fine aggregate of (0.3, 3.1, 5.3)%, and in coarse aggregate of (0.06,0.72)% and then its effect on the compressive strength, flexural strength, ultrasonic pulse velocity, density, and absorption at the age of 7, 28 , and 90 day.

3.2 Measurement of Workability of the HSC

Workability is one of the most important features defining the fresh properties of concrete and can be defined as a measure of the ability of concrete to be mixed, handled, transported and most important its ability to be placed without loss in homogeneity and with less air voids. A slump test is a suitable test to determine the workability for all types of concrete mixes ; This test is performed according to **ASTM C143, 2006**.

Several slump tests have been carried out to choose the appropriate dosage of HRWRA to give workability of (75 -100 mm) slump for all mixes.

3.3 Cube Mould and Curing

Mixing process was performed by manually operated mixer according to **ASTM C192, 2006**. Firstly, sand was well mixed with the cement to attain a uniform mix. then, gravel was added to the mix and the whole dry materials were well mixed for about (2) minutes. The required amount of tap water and HRWRA were then added gradually and the whole constituents were mixed for further (2) minutes to get a homogenous mix.

After mixing, the concrete mix was placed in the standard cubic steel moulds Specimens (100*100*100) mm which used for compressive strength , ultrasonic , absorption , and density test. The specimens were compacted using a vibrating table for sufficient period about (20 sec), in addition to the use of a metal rod to remove any entrapped air as much as possible. Then , the concrete surface was leveled and smoothed by means of trowel, and the specimens were covered with nylon sheet for 24 hrs at laboratory temperature to prevent evaporation of moisture from the fresh concrete. After, moulds were opened and cured permanent (continuous) water curing until testing date.

4. DETERMINATION OF THE TEST RESULTS

4.1 Compressive strength

Compressive strength test was measured on 100 mm cube for the determination of average compressive strength according to, **B.S. 1881: part 116, 1983** using a compression testing machine with a capacity of (2000 KN).

Specimens were kept under curing method conditions until testing. The loading rate used in the test was 0.3 N/mm² per second. The test was conducted at ages of 7, 28 and 90 days.

4.2 Flexural strength (Modulus of rupture)

The (100*100*400) mm concrete prisms were used for flexural strength. Test was carried out according to **ASTM C293, 2006** .The flexural strength (modulus of rupture) is calculated using the formula:

$$Fr = 3PL /2BD^2 \quad \ldots\ldots\ldots\ldots (2)$$

4.3 Ultrasonic Pulse Velocity

The ultrasonic pulse velocity (U.P.V.) is one of the non-destructive tests of concrete. Samples of (100*100*100) mm were used in the test according to **ASTM C597, 2006** using a device commercially known as (PUNDIT). The ultrasonic pulses have a wide range frequencies between (24-200) kHz, although the (55 kHz) and the (82 kHz) versions will normally be used for site or laboratory testing of concrete **Bungey, and millard, 2010**.

4.4 Density

Density test was performed on a (100*100*100) mm concrete cubes according to **ASTM C642, 2006**. The density of concrete cubes is determined in dry air by measuring the dimensions and weight of specimens using the measurement device (vernier) and the electrical scale.

4.5 Water Absorption

This test was carried out on (100*100*100) mm samples according to British Standard **B.S. 1881-part 122, 1983**. Three specimens are placed in a drying oven. So that each one was not less than 25 mm from any heating surface or from each other.

5. DISCUSSIONS of TEST RESULTS

Table 6 shows the mix designation and sulfate content for all HSC mixes. **Table7** shows the compressive strength and flexural strength results for all HSC mixes at different ages . **Fig.3** and **Fig.4** shows the relation between the reduction in compressive strength with the total effective SO_3% and total SO_3% at different ages. **Fig.5** , **Fig.6** and **Fig.7** shows the relationships between the compressive strength and age of the HSC specimens for different percentages of sulfate content in cement, sand and gravel at 7 , 28 and 90 days . **Fig.8** and **Fig.9** shows the relation between the reduction in flexural strength with the total effective SO_3% and total SO_3% at different ages. **Fig.10** , **Fig.11** and **Fig.12** shows the relationships between the flexural strength and age of the HSC specimens for different percentages of sulfate content in cement, sand and gravel at 7 ,28 and 90 days .The HSC specimens having low sulfate content such as reference mix exhibit an increase in compressive strength with increasing of curing age, while concrete specimens having the higher

percentages of sulfate content such as (MCSHG) mix exhibit slight increase in compressive strength with increasing of curing age .This complies with studies carried out by, **Al-Rawi, et al., 2002,** and **Al-Salihi, 1994.**

In general, the results show that concrete mixes with the lower sulfate content gives a good results for compressive strength due to fill voids by hydration products and increase the density and decrease permeability of concrete .This complies with studies carried out by **Samaa ali, 2010**.

The highest percentages of sulfate content decreasing the compressive strength values at different ages from (5-40)% at 7 days, (6-41)% at 28 days , and (7-42)% at 90 day and decreasing the flexural strength values at different ages from (3-28)% at 7 days, (4-29)% at 28 days , and (6-32)% at 90 day with the increase in the values of total SO_3% and total effective SO_3%,but total effective SO_3% show a good correlation with the decreasing in compressive strength and flexural strength than the total SO_3% content. The trend of (Ultrasonic pulse velocity and density) is compatible with the compressive strength . The trend of absorption results is adverse with the compressive strength results because of sulfate action which absorb more water when the concentration of it increase **Fig.13** shows the effect of total effective SO_3% sulfate content on U.P.V ,density & absorption at 7 ,28 and 90 days .This fact according to the particle size of concrete constituent, the cement which has the higher fineness than sand and coarse make high surface area causing high reaction and high solubility with the sulfate **Al-Rawi, et al., 2002**.

There exist several factors that affect the strength development of concrete having different mixes. These factors are: fineness of the particles of the concrete constituent which are related to the effective SO_3% in materials, The percentages of SO_3% content in cement , in coarse and in fine aggregate, the size and shape of aggregate, concrete porosity, and chemical attack.

Concerning the above factors, the reference mix whose sulfate contents SO_3 (2%) in cement showed higher values of compressive strength , flexural strength , U.P.V and density when the (OPC) is of a low SO_3 in cement ,Thus, the quantity of expansive ettringite becomes less in the cement paste of concrete **Neville, 2010**.

In the fine aggregate when (SO_3%) content increases, the compressive strength of concrete decreases as compared to the reference HSC with SO_3 (0.3%), this is complies with the results of **Al-Salihi, 1994**.The (SO_3) ions which react with C_3A in cement to produce calcium sulphoaluminate causes expansion of concrete which therefore , may reduce the strength.

6. CONCLUSION

Depending on the results of the experimental work which has been done to investigate the effect of internal sulfate attack on HSC, the following conclusions can be drawn from analysis of these results:

1. The increase in total effective sulfate content in concrete causes an decrease in density of concrete about (0.38 - 4.8) at 90 days, but total effective sulfate content is more related linearly with this decrease than the total sulfate content.
2. The reduction in the SO_3 content in cement would allow using higher percentages of sulfate in aggregates used in concrete.
3. The total effective SO_3 shows a good correlation with the conducted result of all tests as compared with the total SO_3, so that the total effective SO_3 gives a good indication of the possibility of using material in concrete.

4. The reduction in the compressive strength ranged about (7-40%) at 7-days for mixes with total effective SO_3 content of (2.6-6.9%) and with total SO_3 content of (3.77-11.72%) (by weight), and the reduction is about (11-42%) in the compressive strength at 90-days of test, these result show a good resistance in HSC to the sulfate action at different ages.
5. Increasing the SO_3 content in cement has a more significant effect than increasing the SO_3 content in fine aggregate, fine aggregate has a more significant effect than increasing the SO_3 content in the coarse aggregate on the properties of concrete .This reduction is due to the surface area and fineness of cement .The total effective SO_3 which depends on the particle size of the materials shows a good trend with the increment in sulfate content in concrete constituent.HSC mixes suffer significant deterioration in all its properties.
6. The compressive strength, flexural strength ,U.P.V, and density results decrease at early ages about (5-40)% ,(3-28)% ,(1-10)% ,(0.38-4.8)% respectively with the increase in total effective SO_3 content of (2.6-6.9%) .
7. The absorption results increase about (-7 to -68)% with the increase in total effective SO_3 content of (2.6-6.9%) .

REFERENCES

- Abbas S. Al-Ameeri, Rawaa H. Issa, March-April 2013, *Effect of Sulfate on The Properties of Self Compacting Concrete Reinforced By Steel Fiber*, International journal of civil engineering and technology volume 4, issue 2, ,pp.270-287.

- ACI 363.2R, 1998, *State-of-the-Art Report on High Strength Concrete*, ACI International Farmington Hills, MI, www.aciint. org.

- ACI Committee 211.4R, 2008, *Guide for Selecting Proportions for High Strength Concrete With Portland Cement.*

- Al - Salihi, R. A., 1994, *Proposed Revision of Iraqi Specification for Concrete Constituent to Cape with Post War Are*, M. Sc. thesis University of Baghdad.

- Al-Rawi R.S., Al-Salihi R.A., and Ali, N.H., 2002, *Effective Sulfate Content in Concrete Constituent*, In: Concrete for extreme conditions ,Dhir R.K, McCarthy M. Newlands M.D., eds, Thomas Telford publishing, London, Great Britain.pp.(499-506).

- ASTM C143, 2006, *Standard Test Method for Slump of Hydraulic Cement Concrete*.

- ASTM C150, 2006, *Standard Specification for Cement.*

- ASTM C192, 2006, *Standard Practice for Making and Curing Concrete Test Specimens in The Laboratory*.

- ASTM C293, 2006, *Standard Test Method for Flexural Strength of Concrete*, Using Simple Beam With Center-Point Loading.
- ASTM C494,2006, *Standard Specification for Chemical Admixtures for Concrete*.
- ASTM C597, 2006, *Standard Test Method for Pulse Velocity Through Concrete*.
- ASTM C642, 2006, *Standard Test Method for Density, Absorption, and Voids in Hardened Concrete*.
- B.S.1881, Part 116, 1989, Method *for Determination of Compressive Strength of Concrete Cubes*, British Standards Institution.
- B.S.1881, Part 122, 1983, *Method for Determination of Water Absorption*, British Standards Institution.
- Bungey J.H , Millard S.G, 2010, *Testing of Concrete in Structure* " 3rd edition pp.(50).
- Iraqi Specification, No.45, 1984, *Aggregate from Natural Sources for Concrete and Construction*.
- Iraqi standards (IQS) , No.5, 1984, *Iraq Standard Specification for Portland Cements*,Baghdad, Iraq .
- James E. Cook, October 1989, *10,000 psi Concrete*, ACI Concrete International, Farmington Hills, MI.
- Jan Skalny, Jacques Marchand, and Ivan Odler, 2002, *Sulfate Attack on Concrete*.
- Neville, A.M., 2010, *Properties of Concrete*, Longman Group, 4th and Final Edition, PP.(18-87), (508-677).
- Ron Burg, November 1993, *The Concrete Producer*,Getting Started with High-strength Concrete .
- Saco, Z. and Rassam , D., 1989, *The Effect of Gypsum Coatings on Coarse Aggregates Upon The Properties of Concrete* , 5th Edition , Conferee of SRC , Vol.4 , part 1 , Baghdad.

- Samaa ali, 2010, *The Effect of Cement and Admixture Types On The Resistance of High Performance Concrete to Internal Sulfate Attack*, M. Sc. thesis University of Baghdad.

- Sayed Horkoss, Roger Lteif, and Toufic Rizk, 2011, *Influence of The Clinker SO3 On The Cement Characteristics*, Cement and Concrete Research.

- Sharif , J.A. et al., 1993 وزارة الاسكان , " دراسة مسودة المواصفة القياسية لتعيين المواد الضارة في الركام الخشن " والتعمير المركز القومي للمختبرات الانشائية , بغداد .

- رؤ وف زين العابدين " الرمال العراقية " مركز بحوث البناء, تشرين أول 1970

NOMENCLATURE

F.M = fineness modulus of aggregate.
Fr = flexural strength, (MPa).
P = maximum applied load indicated by tested machine, (N).
L = average length of specimen, (mm).
B = average width of specimen, (mm).
D = average depth of specimen, (mm).

Table 1. Chemical composition and main compounds of cement 1& cement 2*

Oxide composition	**cement 1 % by weight**	**cement 2 % by weight**	***IQS (No.5:1984) limits***
Lime (CaO)	62.14	61.55	----
Silica (SiO_2)	20.70	20.24	----
Alumina (Al_2O_3)	5.96	6.25	----
Iron oxide (Fe_2O_3)	3.34	3.39	----
Sulfate (SO_3)	2	2.75	$\leq$ 2.8%
Magnesia (MgO)	3.94	3.96	$\leq$ 5%
Loss on Ignition (L.O.I.)	1.07	0.95	$\leq$ 4%
Lime saturation Factor (L.S.F.)	0.90	0.90	0.66-1.02
Insoluble residue (I.R.)	0.60	0.40	$\leq$ 1.5%
Main compounds (Bogue's equations) **			
C_3S	38.49	41.71	----
C_2S	28.99	27.88	----
C_3A	10.83	10.64	----
C_4AF	10.32	10.16	----

* The tests were carried out in the Laboratory of the Kufa Cement Plant ..
** According to, ***ASTM C 150, 2006***.

Table 2. Physical properties of cement 1& cement 2

Properties Physical	Test Result cement 1**	Test Result cement 2**	*IQS (No.5:1984) limits*
Specific surface area, Blaine method, m^2/kg *	313.1	321.5	≥ 230
Setting time , Vicat's Method Initial setting , hr : min Final setting , hr : min	 90 2:30	 90 2:30	 ≥ 45 minutes ≤ 10 hours
Compressive strength MPa 3-days 7-days	 27.2 35	 28.4 35.2	 ≥15 ≥23

* The tests were carried out in the Laboratory of the Kufa Cement Plant .
** cement 1= SO_3 %(2) , cement 2 =SO_3 %(2.75).

Table 3. Properties of fine aggregate*

Sieve size (mm)	Passing% of sand 1**	Passing% of sand 2**	Passing% of sand 3**	Limits of Iraqi spec. No.45/1984/Zone 2
10	100	100	100	100
4.75	95	92	91	90-100
2.36	79.29	83.7	85.1	75-100
1.18	65	73.8	70.7	55-90
0.6	45.43	49.2	48.6	35-59
0.3	13.71	19.3	21.6	8-30
0.15	2.71	4	3	0-10
Physical properties	Physical properties of sand 1	Physical properties of sand 2	Physical properties of sand 3	Limits of Iraqi spec. No.45/1984
Fineness modulus	2.98	2.78	2.8	-
Specific gravity	2.76	2.53	2.6	-
Absorption%	1.2	1.21	1	-
SO_3%	0.3	5.3	3.1	≤ 0.5%
Dry rodded density kg/m^3	1680	1675	1672	-

* Performed in laboratory of Building Materials-University of Baghdad.
** sand 1 = SO_3 %(0.3) , sand 2 = SO_3 %(5.3) , sand 3 (mix sand 1 & sand 2) = SO_3 %(3.1).

Table 4. Properties of coarse aggregate*

Sieve size (mm)	Passing % of gravel 1**	Passing % of gravel 2**	Limits of Iraqi spec. No.45/1984 (5-20)mm
37.5	100	100	100
20	95.35	96.13	95-100
10	31.38	33.9	30-60
4.75	2.48	3.4	0-10
Physical properties	Physical properties of gravel 1	Physical properties of gravel 2	Limits of Iraqi spec. No.45/1984
Specific gravity	2.56	2.57	-
Absorption %	0.56	1.14	-
SO_3 %	0.06	0.72	$\leq 0.1\%$
Dry rodded density kg/m³	1600	1550	-

* Performed in laboratory of Building Materials-University of Baghdad.
** gravel 1 = SO_3 %(0.06) , gravel 2 = SO_3 %(0.72)

Table 5. Technical description of superplasticizer (PC-200) *

Properties	Technical description
Type	Synthetic dispersion
Colour	Light yellow liquid
Specific gravity	1.05 kg/l @ 25°C
Freezing point	- 1°C approximately
Air entrainment	Less than 2% at normal dosage

* Technical description according to Don Gonstruction Products Ltd www.donconstruction.eo. uk.

Table 6. Mix designation and sulfate content for all HSC mixes

Set No.	Sulfate content % in Mix			Slump of Mixes (75-100) mm	Total SO_3% of Mixes	Total effective SO_3% of Mixes
	SO_3% in cement	SO_3% in sand	SO_3% in gravel			
MRef	2	0.3	0.06	100	2.544	2.238
MG	2	0.3	0.72	99	3.778	2.669
MC	2.75	0.3	0.06	95	3.294	2.988
MCG	2.75	0.3	0.72	90	4.528	3.419
MSm	2	3.1	0.06	90	6.576	4.181
MSmG	2	3.1	0.72	87	7.810	4.614
MCSm	2.75	3.1	0.06	87	7.326	4.932
MCSmG	2.75	3.1	0.72	85	8.560	5.364
MSh	2	5.3	0.06	83	9.744	5.779
MShG	2	5.3	0.72	82	10.978	6.211
MCSh	2.75	5.3	0.06	80	10.494	6.529
MCShG	2.75	5.3	0.72	78	11.728	6.961

Table 7. Compressive strength and flexural strength results for all HSC mixes at different ages.

Set No.	Total SO_3% of Mixes	Compressive strength (MPa)			Flexural strength (MPa)		
		7 days.	28 days.	90 days.	7 days.	28 days.	90 days.
MRef	2.544	51.72	61.7	71.7	7.47	8.47	10.26
MG	3.778	49.0	57.98	66.3	7.23	8.13	9.68
MC	3.294	47.87	55.2	63.5	7.13	7.85	9.44
MCG	4.528	45.28	52.09	61.24	7.02	7.78	9.32
MSm	6.576	43.79	51.55	59.3	6.89	7.68	9.02
MSmG	7.810	42.2	49.68	57.08	6.73	7.26	8.67
MCSm	7.326	39.8	47.3	54.35	6.5	7.02	8.47
MCSmG	8.560	38.3	45.2	51.82	6.32	6.78	8.11
MSh	9.744	36.33	42.1	48.3	6.05	6.62	7.78
MShG	10.978	34.77	40.8	45.56	5.85	6.29	7.53
MCSh	10.494	33.03	38.22	43.41	5.7	6.18	7.26
MCShG	11.728	31.0	36.2	41.45	5.35	5.95	7.02

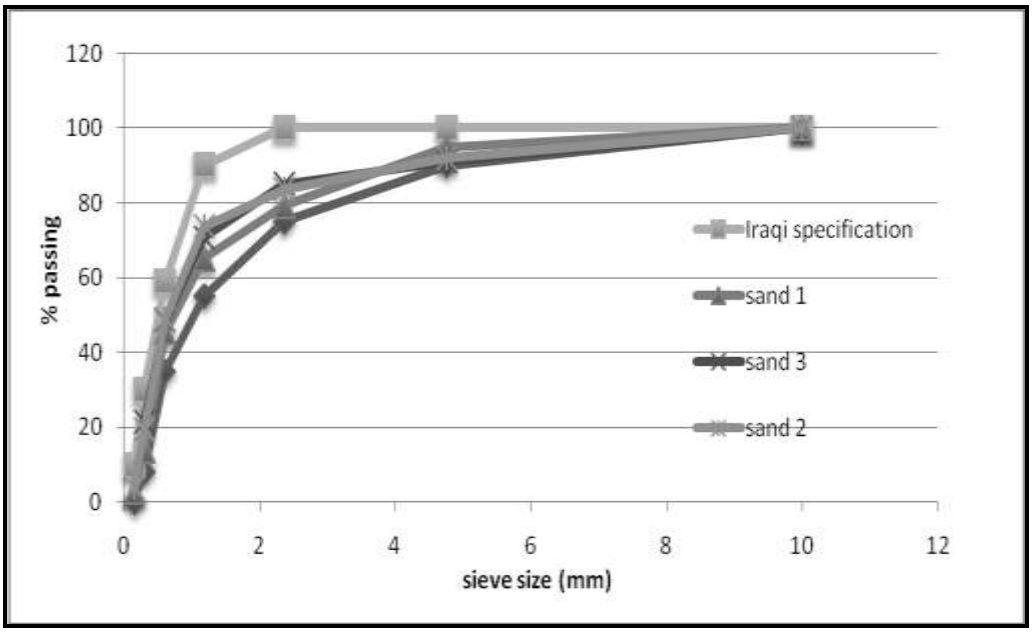

Figure 1. Grading curve for used fine aggregate with (sand 1),(sand 2) and (sand 3).

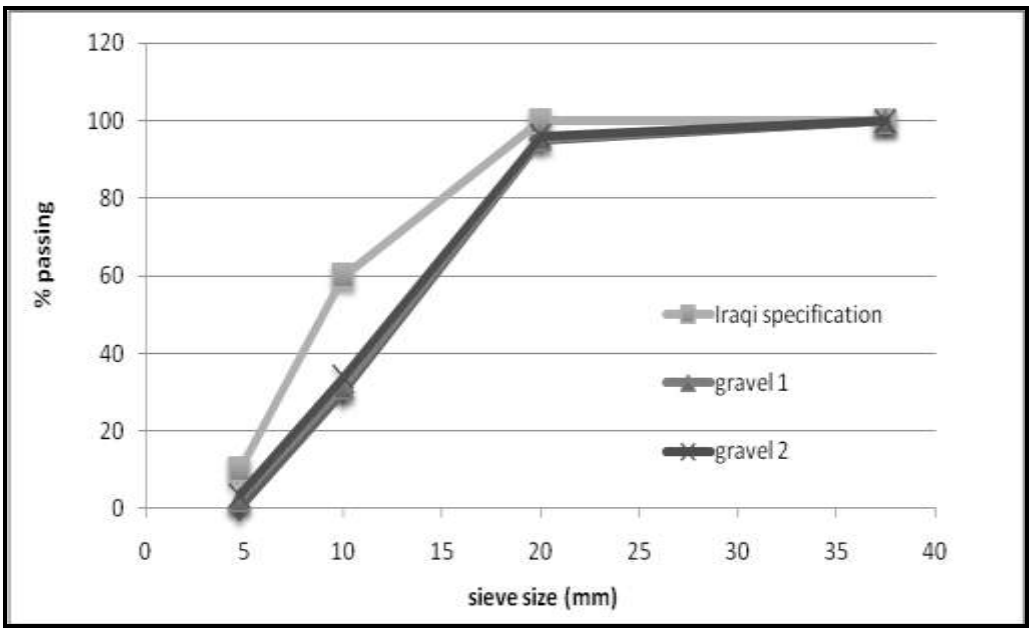

Figure 2. Grading curve for used coarse aggregate with (gravel 1) and (gravel 2).

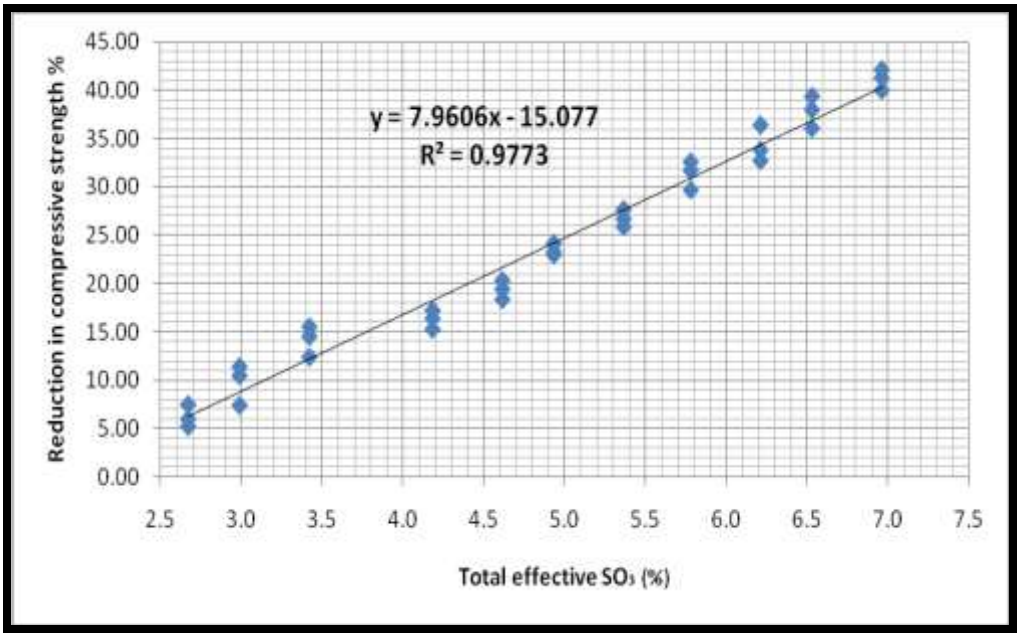

Figure 3. Relation between total effective SO_3% and reduction in compressive strength at different ages.

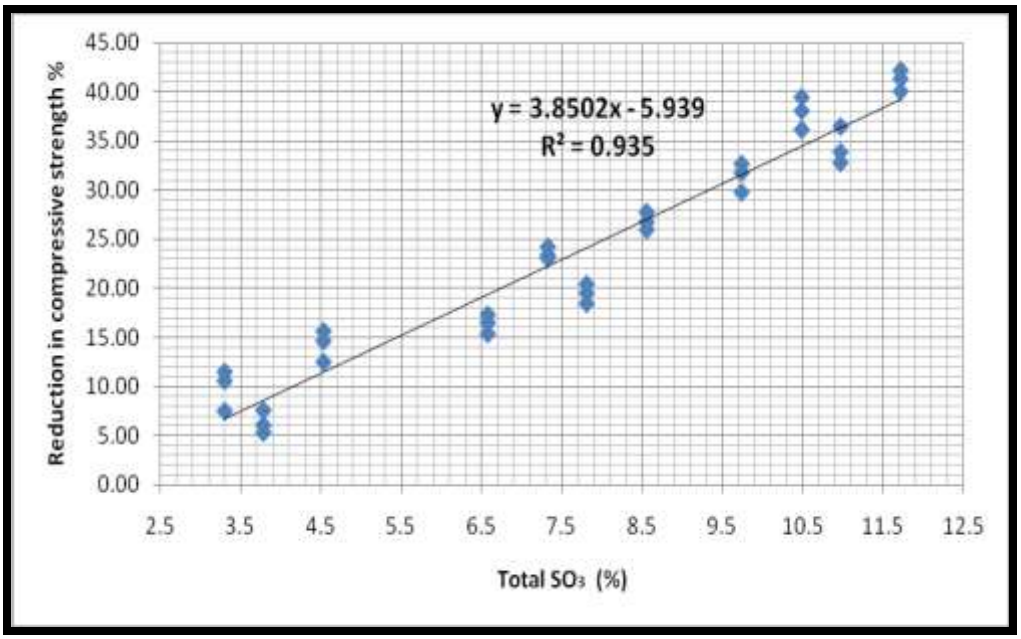

Figure 4. Relation between total SO_3% and reduction in compressive strength at different ages.

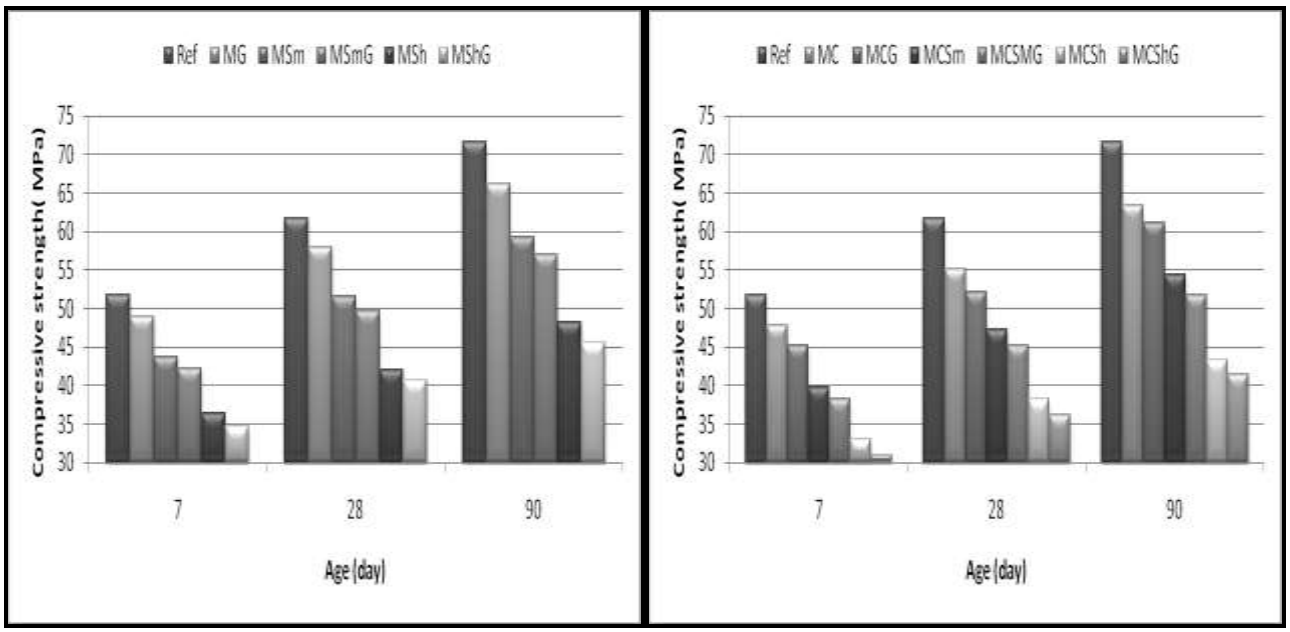

5.a. Cement 1 **5.b. Cement 2**

Figure 5. Effect of different sulfate content in cement on compressive strength at different ages.

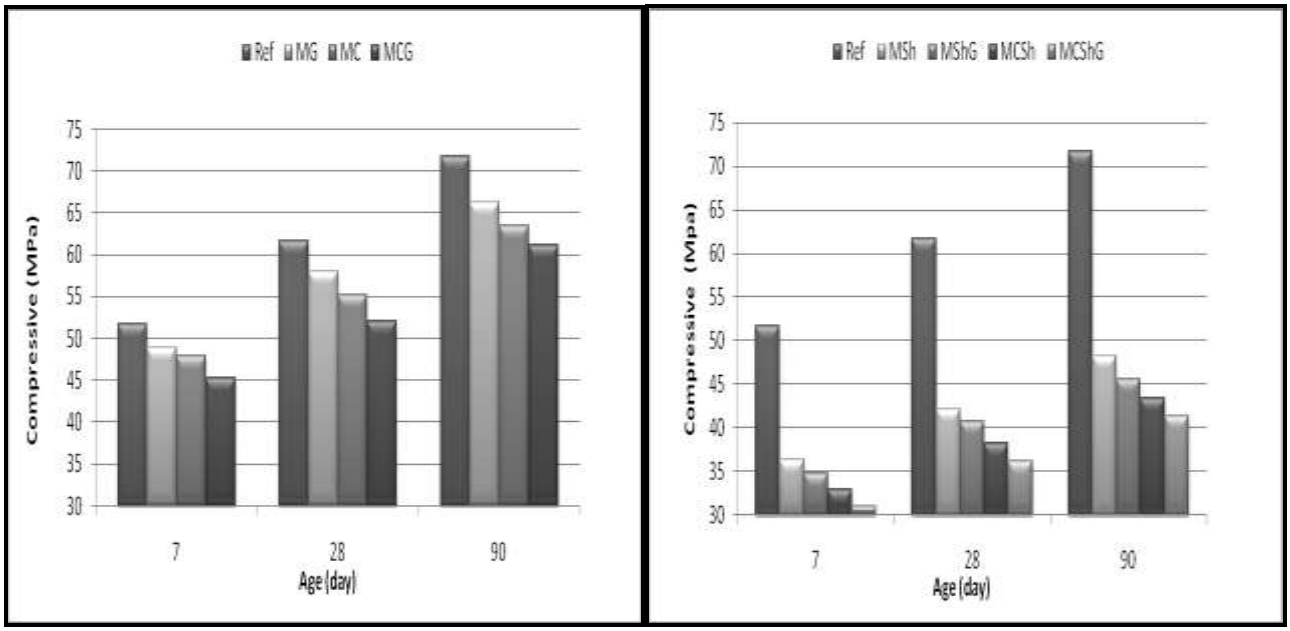

6.a. Sand 1 **6.b. Sand 2**

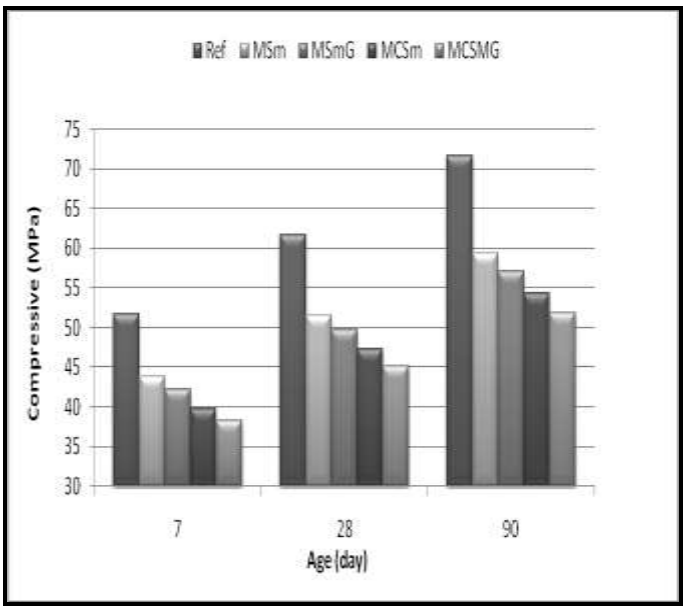

6.c. Sand 3 (mix sand 1 & sand 2)

Figure 6. Effect of different sulfate content in fine aggregate on compressive strength at different ages.

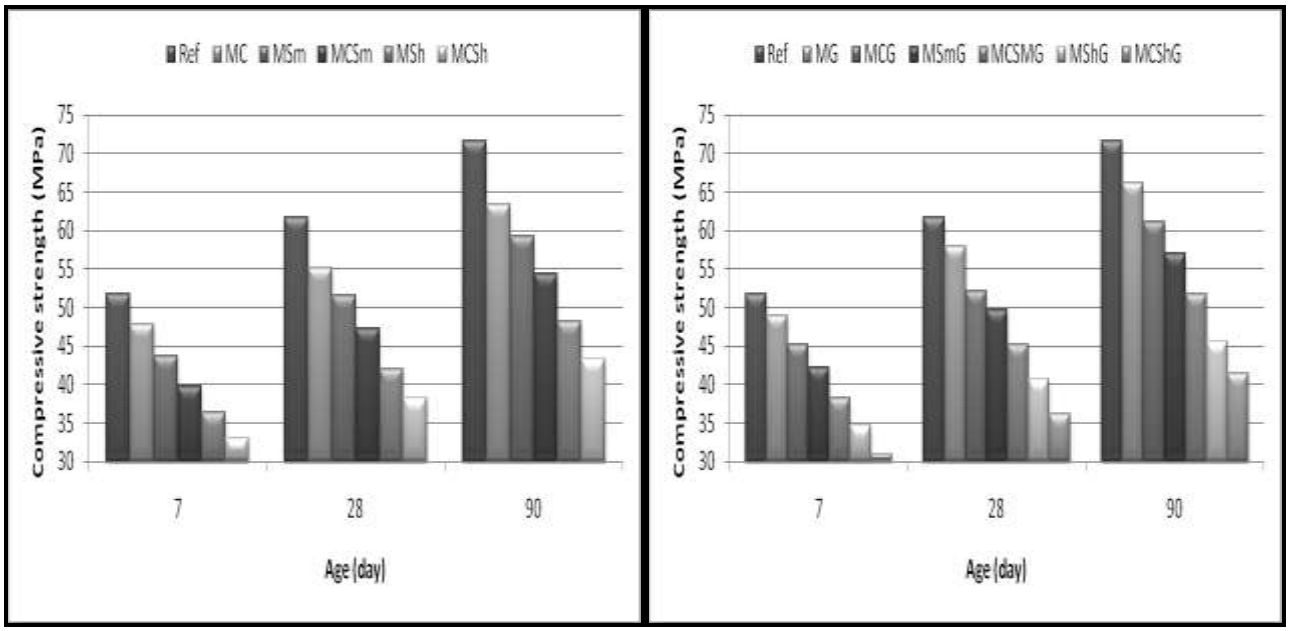

7.a. Gravel 1 **7.b. Gravel 2**

Figure 7. Effect of different sulfate content in coarse aggregate on compressive strength at different ages.

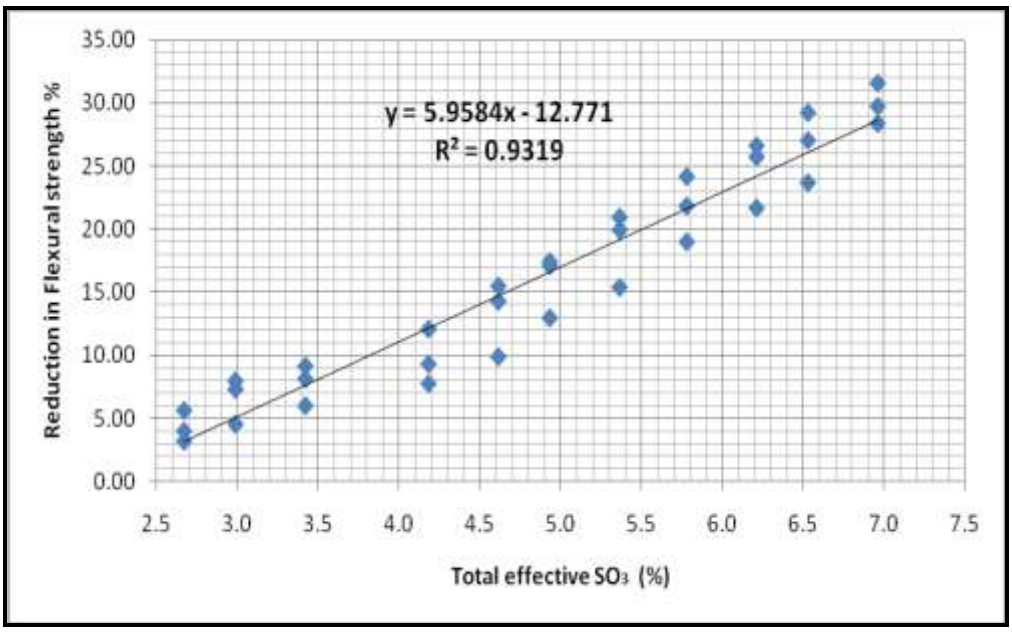

Figure 8. Relation between total effective SO_3% and reduction in flexural strength at different ages.

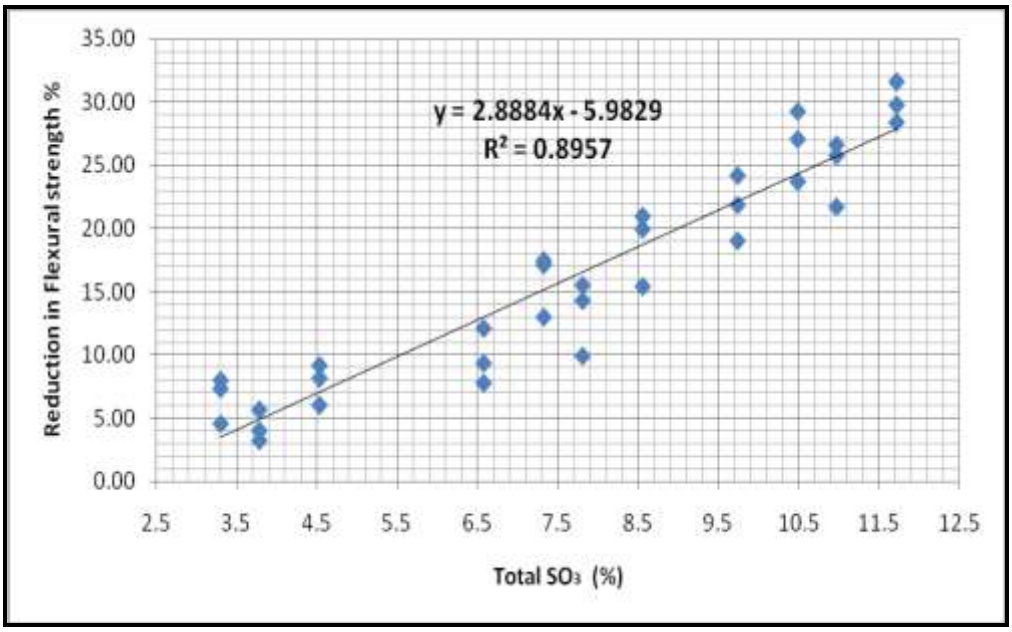

Figure 9. Relation between total SO_3% and reduction in flexural strength at different ages.

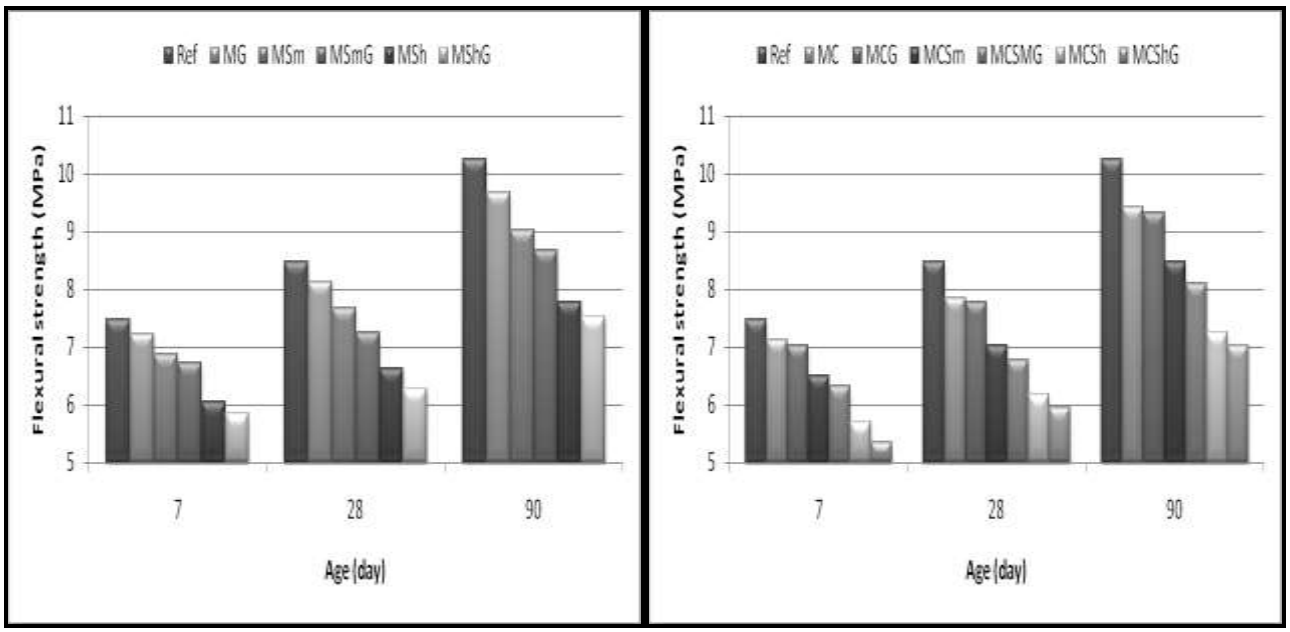

10. a. Cement 1 **10.b. Cement 2**

Figure 10. Effect of different sulfate content in cement on flexural strength at different ages.

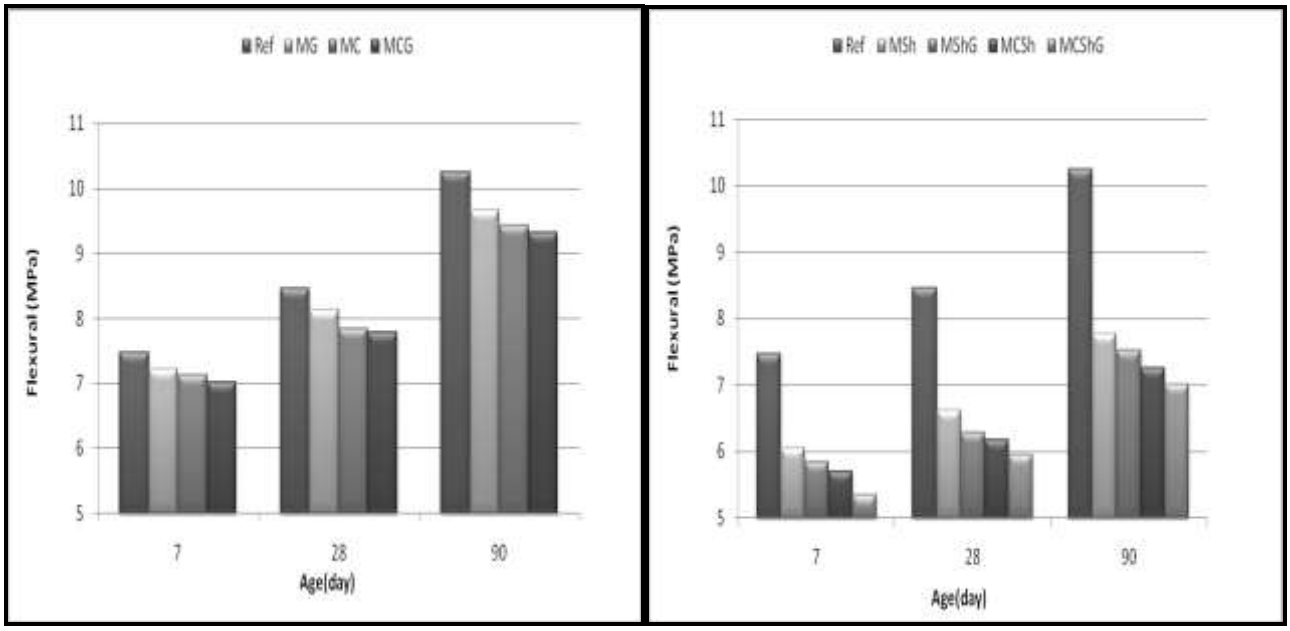

11.a. Sand 1 **11.b. Sand 2**

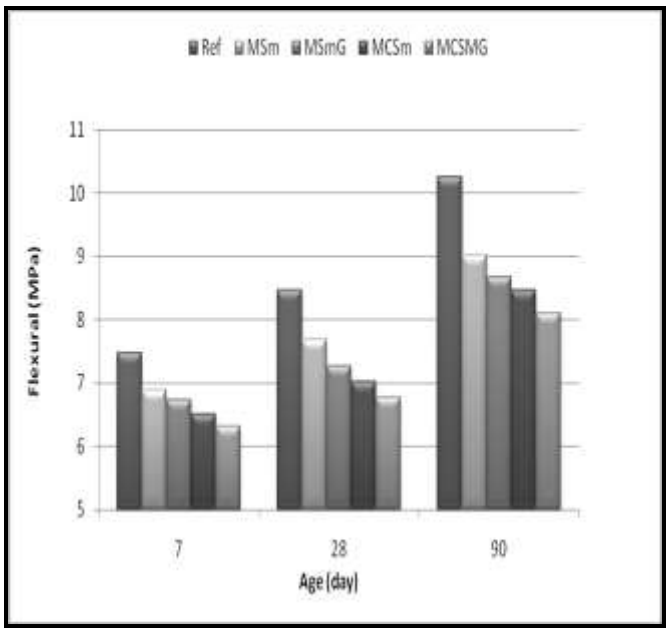

11.c. Sand 3 (mix sand 1 & sand 2)

Figure 11. Effect of different sulfate content in fine aggregate on flexural strength at different ages.

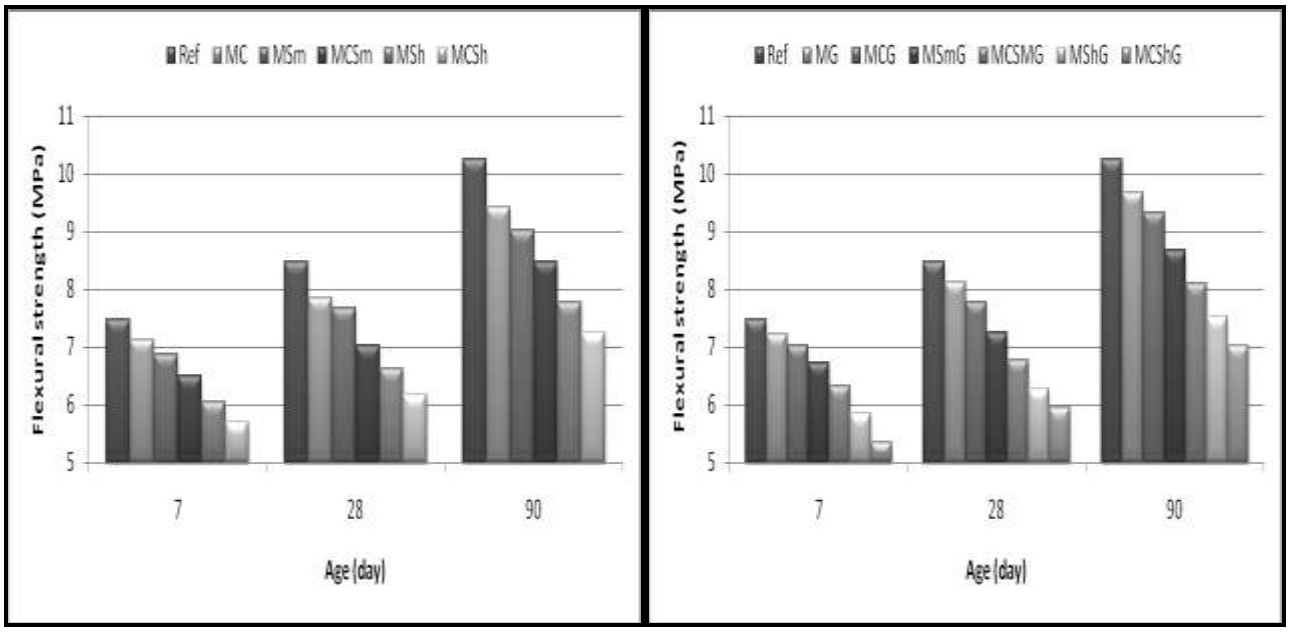

12.a. Gravel 1 **12.b. Gravel 2**

Figure 12. Effect of different sulfate content in coarse aggregate on flexural strength at different ages.

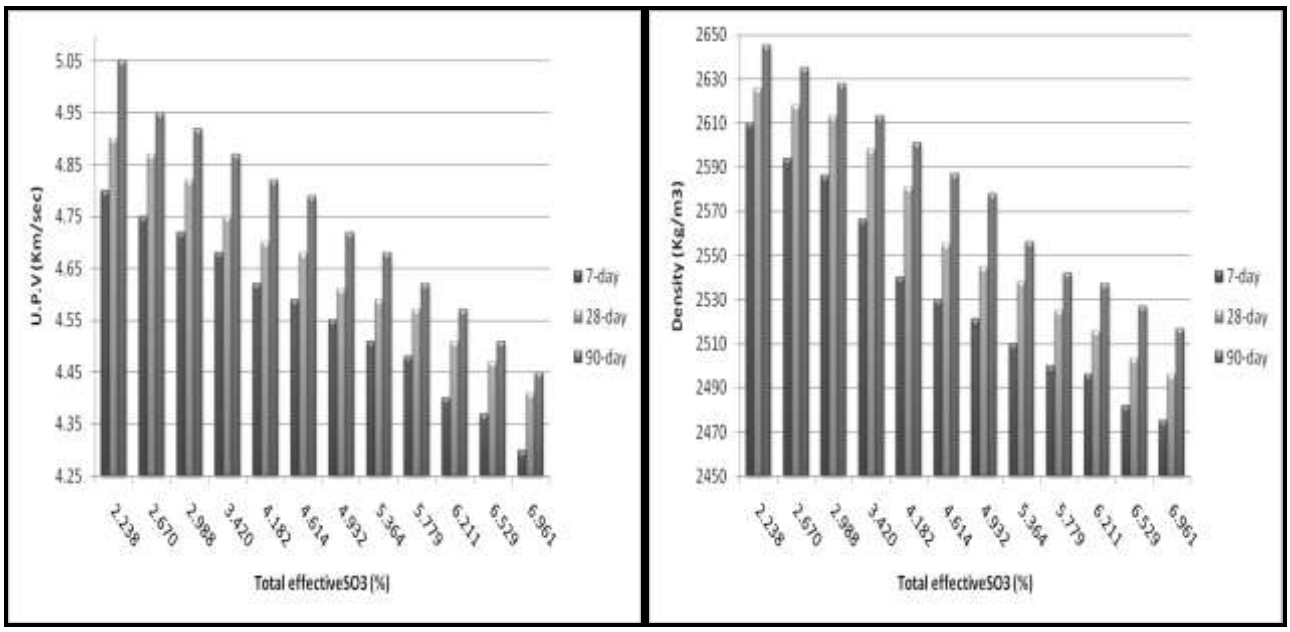

13.a. U.P.V **13.b. Density**

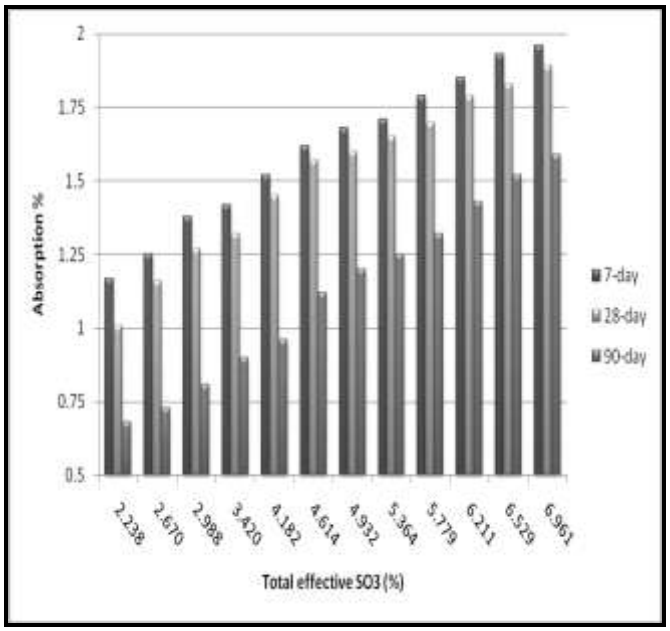

13.c. Absorption

Figure 13. Effect of total effective SO_3% sulfate content on U.P.V ,density & absorption at 7 , 28 and 90 days.

Mechanical Properties of High Performance Concrete Containing Waste Plastic as Aggregate

Asst. Prof. Dr. Abdulkader Ismail Al-Hadithi
Dams and Water Resources Engineering Department
College of Engineering
University of Anbar , Iraq
Email: al_hadithi2000@yahoo.com

Mahmood Fawzi Ahmed Alani
Department of Civil Engineering
College of Engineering
University of Baghdad, Iraq
Email: mahmodmfa81@gmail.com

ABSTRACT

The world's population growth and the increasing demand for new infrastructure facilities and buildings , present us with the vision of a higher resources consumption, specially in the form of more durable concrete such as High Performance Concrete (HPC) . Moreover , the growth of the world pollution by plastic waste has been tremendous. The aim of this research is to investigate the change in mechanical properties of HPC with added waste plastics in concrete. For this purpose 2.5%, 5% and 7.5% in volume of natural fine aggregate in the HPC mixes were replaced by an equal volume of Polyethylene Terephthalate (PET) waste , got by shredded PET bottles. The mechanical properties (compressive, splitting tensile, and flexural strength) evaluated at the ages of (7 ,28, 56 and 91) days while the static modulus of elasticity tested at (28 and 91) days . The results indicated that HPC containing PET-aggregate presented lower compressive strength and static elasticity . The splitting strength displayed an arising trend at the initial stages, however, they have a tendency to decrease after a while. On the other hand, flexural strength results gave better modulus of rapture at all ages of curing , as compared with reference concrete specimens.

Key words: High Performance Concrete, mechanical properties, Polyethylene Terephthalate (PET), PET-aggregate .

الخواص الميكانيكية للخرسانة عالية الاداء والمحتوية على المخلفات البلاستيكية كركام

أ.م.د. عبد القادر اسماعيل عبد الوهاب الحديثي
قسم هندسة السدود والموارد المائية
كلية الهندسة / جامعة الانبار

محمود فوزي احمد العاني
قسم الهندسة المدنية
كلية الهندسة / جامعة بغداد

الخلاصة

ان تزايد استهلاك المصادر الطبيعية نتيجة نمو سكان العالم وتنامي الطلب على المباني الجديدة ومرافق البنية التحتية ، وخاصة المنشآت التي تستخدم فيها الخرسانة عالية الأداء لأغراض الديمومة . يضاف الى هذا ، ان نمو التلوث بالفضلات البلاستيكية في العالم بات نموا هائلا .ان الهدف من هذا البحث هو دراسة التغيير في الخواص الميكانيكية للخرسانة عالية الاداء والمضاف اليها مخلفات المواد البلاستيكية . لهذا الغرض تم استبدال (2.5% , 5% و 7.5%) من حجم الركام الناعم بنسب مكافئة من الركام البلاستيكي الذي تم الحصول عليه من مثروم مخلفات القناني البلاستيكية (بولي اثيلين تيريفثاليت) . تم تقييم الخواص الميكانيكية (مقاومة الانضغاط , مقاومة الانشطار ومقاومة الانثناء) بأعمار (56,28,7 و91) يوم في حين تم قياس معامل المرونة بعمر (28 و 91) يوم . أظهرت النتائج إلى انخفاض مقاومة الانضغاط ومعامل المرونة عند زيادة محتوي الركام البلاستيكي في حين كان سلوك الخرسانة عالية الاداء في مقاومة الشد الانشطاري يميل للزيادة عند اضافة مخلفات البلاستيك ثم تنخفض عند زيادة نسبة الاستبدال . من ناحية أخرى، اعطت نتائج مقاومة الانثناء تحسن في معامل الكسر ولكافة نسب الاستبدال مقارنة مع عينات الخرسانة المرجعية غير المحتوية على مثروم الركام البلاستيكي .

الكلمات الرئيسية : الخرسانة عالية الاداء , الخواص الميكانيكية , بولي اثيلين تيريفثاليت , الركام البلاستيكي

1 . INTRODUCTON

Concrete is the most used man-made material in the world since its invention. Worldwide, about three tonnes of concrete are used annually per person. Concrete comprises three major fractions, aggregate: binder and water. The aggregate fraction in concrete is about 75 % of its total volume and therefore it plays a vital role in the overall performance of concrete, **Brito, and Saikia, 2013** . The environmental impact caused by the increase in the extraction of natural resources and higher CO_2 emissions has given rise to the search for more efficient, environmentally-friendly constructions. To address these needs, high Performance Concrete (HPC) , has been employed to increase the durability and economic service life of slender structures, to decrease the specific energy consumption and to reduce the environmental impact of these activities , **Isaia, 2000** . The improvement of mechanical and durability performances of concrete in their service life can indirectly reduce the CO_2 emission by increasing their service life and reducing the requirements of materials for repairing, **Brito, and Saikia, 2013 .**

The modern life style along with the new technologies caused more waste materials productions for which the disposing problem exist. Most of the waste materials are non-disposal and remain for hundreds and thousands of years in the environment, **Rahmani, et al., 2013** .

Since plastic is a non-biodegradable material, land-filling using plastic would mean preserving the harmful material forever. Land-filling of plastic is also dangerous due to its slow degradation rate and bulky nature, **Saikia ,and Brito, 2012** .These non-biodegradable waste materials along with population growth have caused the environmental crisis all around the world, **Rahmani, et al., 2013**.Polyethylene Terephthalate (PET) is one of the most common consumer plastics used and is widely employed as a raw material to realize products such as blow bottles for soft-drink use and to containers for the packaging of food and other consumer goods, **Afroz, et al., 2013**.

Total plastic consumption has been increasing in recent years and so contributing to an ever-growing volume in the plastic waste stream .This is considered a serious environmental threat, especially in Asia , where demand has been growing in China and India . The estimated production of plastic bottles in India alone was about 20,000 million between 2005 and 2006 . Western Europe consumes about 60 million tonnes of plastics a year, resulting in about 23 million tonnes of plastics waste , **Silva, et al., 2013** .

In 2007 it is reported a world's annual consumption of PET drink covers of approximately 10 million tons, which presents perhaps 250 milliards bottles. This number grows about up to 15% every year , **Afroz, et al., 2013**.

The use of waste materials as aggregate in concrete preparation can consume vast amounts of waste materials. This can solve problems of lack of aggregate on construction sites and reduce environmental problems related to aggregate mining and waste disposal , **Saikia , and Brito, 2014**.

1.1 Objective of the Study

The objective of this study is to offer an attractive low-cost material with consistent properties , and improve the sustainability in concrete industry by using PET waste as an aggregate in HPC , which have benefits such as decreasing the usage of natural resources, the wastes consumption, avoiding the environmental pollution and economizing energy .

2. MATERIALS AND EXPERIMENTAL WORK

2.1 Materials

2.1.1 Cement

Iraqi Ordinary Portland cement manufactured in the north of Iraq with trade mark of (Al-Mass) was used in casting all specimens throughout the experimental work. **Tables (1) and (2)** show the physical properties and chemical analysis respectively. The results indicate that the cement confirms to the Iraqi Specifications **I.Q.S. 5/1984**.

2.1.2 Fine aggregate

Natural sand supplied from (Al-Ukhaydir) area was used for preparing mixes , with maximum aggregate size of 4.75mm. The sieve analysis and physical properties of this aggregate are shown in **Table (3)**. It conforms to the Iraqi Specifications **I.Q.S. No.45/1984** Zone 2.

2.1.3 Coarse aggregate

Crushed gravel supplied from (Al-Nibaee) region in Baghdad City was used for preparing mixes. It has nominal maximum aggregate size 14mm . The sieve analysis and physical properties of this aggregate are shown in **Table (4)** . It conforms to the Iraqis specifications **I.Q.S. No.45/1984**.

2.1.4 Water

The water used for both mixing and curing was potable water from the water-supply network system (tap water) .

2.1.5 Silica fume

Silica fume of Jordanian origin densified type was used throughout this work as a partial replacement of cement . **Tables (5) and (6)** show the physical properties and chemical analysis of silica fume respectively. The results indicate that the properties of silica fume used are comply with **ASTM C1240-05** standard specification.

2.1.6 Superplasticizer

A high range water reducing admixture (superplasticizer) commercially known as Hyperplast PC260 , which complies with **ASTM C494-10 Type F**, was used in this research .

2.1.7 Waste plastic (PET-aggregate)

2.1.7.1 Preparation of plastic PET- aggregate

In this study, PET particles as shown in **Plate (1)** are provided by grinding waste PET bottles and used as fine aggregates in concrete. These PET particles were produced as shown in the following steps:

- Collecting the PET bottles needed for research from disposal area .
- Removing the cover and trade label .
- Washing the bottles and spreading them to dry out .
- Shredding and grinding the bottles to smaller size as that of sand by plastic granulator machine (blade mill) as shown in **Plate (2)** , used for plastic manufacturing plant located in Hit city west of Iraq .

- Then ,the obtained particles were separated ,through sieves and subsequently reassembled according to the sieve size (10 mm) ; the particles passed this sieve were used as fine aggregate , while the coarser one were re-grinded again .

2.1.7.2 Physical and mechanical properties of PET-aggregate

After production of PET-aggregate , it was analyzed in terms of some physical properties such as density and sieve analysis. **Table (7)** and **Table (8)** present the sieve analysis, measured physical and mechanical properties of PET particles , respectively . It can noted from **Table (7)** the sieve analysis of PET-aggregate do not comply with natural sand grading as shown in **Table (3)** due to character of plastic texture and shape of plastic pieces which it is usually be flaky , irregular , sharp edge and angular particle , while the natural fine aggregate is usually be spherical and granulated particles . Moreover it is important to focusing on sustainability of natural sources, negative environmental impact of plastic waste and reduce the coast of construction .

2.2 Experimental Work

2.2.1 Mix design and proportions of HPC

The mix design was made according to the American method (**ACI 211.4R-08**). The reference concrete mixture was designed to obtain the required compressive strength of cube equals to (60 MPa) at 28 day. The cementitious content (cement + silica fume) is (510 kg/m^3) with partial replacement of cement weight by(10%) silica fume , the water to cementitious materials (w/cm) ratio is (0.29) , coarse aggregate is (1160 kg/m^3) and fine aggregate is (660 kg/m^3) , the dosage of superplasticizer which was (0.8 L/100Kg of cementitious materials) in order to have a required slump (175mm) for reference mix only . Finally , the waste plastic (PET-aggregate) was used as partial replacement of natural sand in three volume percentage (2.5 , 5 , 7.5)% .The details of the mixes used throughout this study are given in **Table (9)** .

2.2.2 Procedure of concrete mixing

An electrical rotary mixer was used to batch all specimens with 0.1 m3 capacities. The coarse and fine aggregate wetted to be in saturated surface dry (SSD) conditions .The ingredients were initially mixed by hand in dry condition (cement + silica fume) , and (fine aggregate + PET-aggregate). Firstly, the coarse aggregate and some of the mixing water were added to the mixer and mixed thoroughly. While the mixer was running , the fine aggregate and PET- aggregate were added with the remaining water. Without stopping the mixer the cementitious materials (cement + silica fume) were added and the solution of (water + SP) was added gradually. The concrete was mixed, after all ingredients were in the mixer, for (3-4) min , followed by a 2 minutes stop, and the mixing was manually continued, especially for the portions not reached by the blades of the mixer. Then the mixer was operated for 2 minute to attain homogeneous, uniform in color and consistency concrete .

2.2.3 Preparation of specimens

The molds were well cleaned and the internal surfaces were oiled to prevent adhesion with concrete after hardening. The molds were filled with concrete in layers of (50) mm depth , and each layer was compacted by a vibrating table for a sufficient period to remove any entrapped air as possible. After completing consolidation, the surfaces of the specimens have been leveled by hand trawling. The specimens are covered with Nylon sheets to prevent evaporation of mixing water from concrete, and they have been left about 24hours in the

laboratory. After remolding the specimens curing process was done by completely immersion the specimens in water storage tank until the time of testing.

2.3 Testing Hardened Concrete

2.3.1 Compressive strength test

The compressive strength test was determined according to (**B.S.1881: part 116)**, using 100 mm cubes. The compressive strength cubes were tested using a standard testing machine (TINIUS OLSEN). The average compressive strength value of three cubes was recorded for each testing age (7, 28 , 56 and 91 days).

2.3.2 Splitting tensile strength

Splitting tensile strength was conducted on cylinders of (100mm diameter and 200mm height according to **ASTM C496-04** . The average of three cylinders was recorded for each testing age (7, 28 , 56 and 91) days respectively for splitting tensile strength.

2.3.3 Flexural strength (modulus of rapture)

Flexural strength of concrete was measured on (100×100×400 mm) prism specimens in conformity with **ASTM C293-10**, at ages of (7 , 28 ,56 and 91 days) . The prisms were subjected to center-point loading using the testing machine (SANS Testing Machine), and the average value of three specimens in each mix was taken .

2.3.4 Static modulus of elasticity

The static modulus of elasticity was performed according to the **ASTM C469-02** , The test was carried out at age of 28, and 91 days using cylinders of (150×300) mm , and the cylinder specimens were grinding top surface to be smooth and level. The average value of three cylinders was calculated at each result.

3. RESULTS AND DISCUSSTION

3.1 Compressive Strength

The effect of PET-aggregate content as partial replacement of sand on the compressive strength in comparison to concrete without plastic aggregate illustrated in **Fig.(1)** , the results indicate that the compressive strength decreases with the increase of PET-aggregate content . This trend can be attributed to the reduction in adhesive strength between the surface of the PET- aggregate and the cement paste. Another factor is the mismatch of particle size and shape between natural and plastic waste aggregates, , **Saikia , and Brito, 2014**. Additionally, PET-aggregate is considered to be a hydrophobic material, so this property may restrict the water movement necessary for cement hydration from entering through the structure of the concrete specimens during the curing period, **Ismail, and AL-Hashmi, 2008**.

On the other hand , It is observed from **Table (10)** and **Fig.(2)** , that the all specimens exhibit an increase in compressive strength with the progress of age. This increase in compressive strength is due to the continuity of cement hydration process which forms a new hydration product within the concrete matrix .

3.2 Static Modulus of Elasticity

The **Fig.(3)** indicated that the value of modulus of elasticity decreased with the increase in plastic aggregate content , and the minimum value was (40.53 , 42.16 GPa) for mix(M7.5) at 28 and 91 days respectively. The values of modulus of elasticity for all HPC mixes shown

in **Table (11)** . The reduction in modulus of elasticity can be attributed to the small modulus of elasticity of PET particles; the poor bond between the matrix and plastic aggregates can also contribute to this drop and can be nominated as another reason for this phenomenon, **Rahmani, et al., 2013** .

3.3 Splitting Tensile Strength

The results of splitting tensile strength for various types of HPC specimens at age (7, 28, 56 and 91) days are presented in **Table (12)** . The relationship between splitting tensile strength and various ratios of waste plastic aggregate is shown in **Fig.(4)** . Generally while the rate of sand replacement with PET-aggregate particles increases, the splitting strength have an increasing tendency at first, but it declines after a while . As shown in **Fig.(4)** , the 2.5% replacement of sand volume with PET particles, leads to increases in splitting strength with compared to (M0), while the substitution of (5% and 7.5%) of the sand volume with PET particles caused sharply reduction in splitting tensile strength. In fact , for (M2.5) with low percentages of PET-aggregate content, when the load reaches to its maximum the probability of inter locking between the PET-aggregate on the fractured surfaces increases due to the special shape of the PET particles and their flexibility **.** But when the PET-aggregate percentage increases, because of the weak cohesion between the texture and the PET particles, the smooth surface of the plastic particles and the fact that the strength of the PET-aggregate is lower than that of the natural aggregate , cause a weaker bonding between these particles and the cement paste. As a result, the splitting tensile strength decreases gradually, **(Yadav,2008. Rahmani, et al., 2013 . Brito, and Saikia, 2013 . Saikia , and Brito, 2014.)**

3.4 Flexural Tensile strength

The results of the flexural strength tests for the all HPC mixtures M0 ,M2.5, M5, and M7.5 are illustrated in **Fig.(5)**. As shown in **Fig.(5)** and **Table (13)** , the maximum values of flexural strength was for mix (M2.5), then the strength of flexural trend to drops for mixes (M5 and M7.5) , but still in values higher than control HPC (M0) . This behavior is mainly attributed to the fibro-form, flaky shape and particles size of PET-aggregate , which acts as a fibers role in concrete by the increase in crack resistance of the composite and ability of fibers to resist forces after the concrete matrix has cracked. Furthermore , The plastic PET-aggregates can delay crack initiation and prolong the crack propagation interval thereby increasing structural strength, **Brito, and Saikia, 2013** .

4 . CONCLUSIONS

The main conclusions that can be drawn from this study are:

- The compressive strength values of all waste plastic HPC mixtures tend to decrease below the values for the reference concrete mixtures with increasing the PET-aggregate ratio at all curing ages. The percentage of decreasing in compressive strength for plastic

HPC were (12.49, 17.49 and 27.02) % for M2.5 , M5 and M7.5 respectively compared with M0 at 28 days .

- Regardless of the percentage content of PET-aggregate and curing time, the modulus of elasticity of HPC containing PET-aggregate are lower than those of the reference concrete. This property decrease as the content of PET-aggregate increases. The minimum values were (40.53 , 42.16 GPa) for mix (M7.5) at 28 and 91 days , respectively.
- The HPC specimens containing various amounts of PET particles , exhibited different behaviors in splitting tensile strength. So that 2.5% replacement of fine aggregates with PET particles yielded the optimum splitting tensile strength (4.01 MPa) at 28 days . On the other hand, with further increase of PET-aggregate contents, the splitting tensile strengths were decreased by (11.6 and 13.17)% for M5 and M7.5 at 28 days respectively.
- HPC containing PET-aggregate gives better modulus of rapture at all ages of curing , as compared with reference concrete specimens. The maximum increase was (20.85)% for M2.5 at 28 days with respect to M0 , while the flexural strength for mixes (M5 and M7.5) decrease below M2.5 , but were still higher than (M0) by (11.36 and 10.42) % .

REFERENCES

- ACI Committee 211.4R-08, 2008 , *Guide for Selecting Proportions for High-Strength Concrete Using Portland Cement and Other Cementitious Materials,* American Concrete Institute , First Printing December 2008, pp. (1- 25) .
- Afroz, M., Hasan, M.J., and. Hasan, Md. M., 2013, *Performance of Plain Pet Fibres To Enhance The Mechanical Behavior of Concrete Under Tension and Shear* , International Journal of Science, Engineering and Technology Research (IJSETR) Vol. 2, Issue 9, September , pp. (1668-1672) .
- ASTM C 469-02 ϵ1,2006, *Standard Test Method for Static Modulus of Elasticity and Poisson's Ratio of Concrete in Compression*, American Society for Testing and Materials , April , pp. (1-5) .
- ASTM C1240-05,2005, *Standard Specification for the Use Silica Fume Used in Cementitious Mixtures*, American Society for Testing and Materials , pp. (1-7).
- ASTM C293-10, 2010, *Standard Test Method for Flexural Strength of Concrete (Using Simple Beam With Center-Point Loading)*, American Society for Testing and Materials , pp.(1-3) .
- ASTM C496-04, 2004, *Standard Test Method for Splitting Tensile of Cylindrical Concrete Specimens* ,American Society for Testing and Materials , pp. (1-5) .
- B.S.1881, Part 116,1989, *Method for Determination of Compressive Strength of Concrete Cubes*, British Standards Institution .
- de Brito, J., and Saikia, N., 2013, *Recycled Aggregate in Concrete, Use of Industrial, Construction and Demolition Waste*, Springer-Verlag London .

- Iraqi Specification, No.45, 1984, *Aggregate from Natural Sources for Concrete and Construction*.
- Iraqi Specification, No.5,1984, *Portland Cement*.
- Isaia,G.C., 2000, *High-performance concrete for sustainable constructions*, Waste Management Series ,Vol.1, pp. 344-354 .
- Ismail, Z. Z. , and AL-Hashmi , E. A. , 2008, *Use of waste plastic in concrete mixture as aggregate replacement*, Waste Management Vol.28, pp. 2041–2047 .
- Rahmani, E. , Dehestani, M., Beygi , M.H.A., Allahyari, H. , and Nikbin, I.M., 2013, *On the mechanical properties of concrete containing waste PET particles*, Construction and Building Materials , Vol.47, pp. 1302–1308 .
- Saikia , N. , and de Brito, J. , 2014, *Mechanical properties and abrasion behaviour of concrete containing shredded PET bottle waste as a partial substitution of natural aggregate*, Construction and Building Materials , Vol.52, pp. 236–244 .
- Saikia , N., and de Brito, J., 2012 , *Use of plastic waste as aggregate in cement mortar and concrete preparation* , Construction and Building Materials , Vol.34, pp. 385–401.
- Silva, R.V. , de Brito, J., and Saikia, N.,2013 , *Influence of curing conditions on the durability-related performance of concrete made with selected plastic waste aggregates* , Cement and Concrete Composites, Vol.35 , pp. 23–31.
- Yadav , I. S. ,2008, *Laboratory Investigations Of The Properties Of Concrete Containing Recycled Plastic Aggregates*, M.Sc. Thesis, Civil Engineering Department, Thapar University, May .

List of Abbreviations

M0	High performance concrete content (0)% PET-aggregate replacement of sand by volume
M2.5	High performance concrete content (2.5)% PET-aggregate replacement of sand by volume
M5	High performance concrete content (5)% PET-aggregate replacement of sand by volume
M7.5	High performance concrete content (7.5)% PET-aggregate replacement of sand by volume

Table 1. Physical properties of cement used throughout this work.

Physical properties	Test result	Limits of Iraqi spec. No.5/1984
Specific surface area, Blaine Method, (m^2/kg).	300	> 230
Setting time : -Initial setting (hrs: min) -Final setting (hrs: min)	 1:40 4:00	 ≥ 45 min ≤ 10 hrs
Compressive strength of mortar (MPa): 3-days 7-days	 21 27	 ≥ 15 ≥ 23
Soundness % (Autoclave)	0.02	≤ 0.8

Table 2. Chemical composition and main compounds of ordinary portland cement.

Oxide composition	Abbreviation	by weight%	Limits of Iraqi spec. No.5/1984
Lime	CaO	61	-
Silica	SiO_2	19.84	-
Alumina	Al_2O_3	5.28	-
Iron oxide	Fe_2O_3	4.2	-
Magnesia	MgO	2.49	≤ 5%
Sulphate	SO_3	2.48	≤ 2.8% , when C_3A more than 5%
Loss on Ignition	L.O.I.	3.8	≤ 4%
Lime saturation Factor	L.S.F.	0.92	0.66-1.02
Insoluble residue	I.R.	1.13	≤ 1.5% **
Main compounds (Bogues eq.)		**by weight of cement%**	
Tricalcium silicate (C_3S)		48.9	
Dicalcium silicate (C_2S)		20.26	
Tricalcium aluminate (C_3A)		6.89	
Tetracalcium aluminoferrite (C_4AF)		12.77	

Table 3. Grading and physical properties of fine aggregate.

Sieve size (mm)	Passing%	Limits of Iraqi spec. No.45/1984/Zone 2
10	100	100
4.75	94	90-100
2.36	79.4	75-100
1.18	65.4	55-90
0.6	51.5	35-59
0.3	19	8-30
0.15	3.7	0-10
Physical properties		**Limits of Iraqi spec. No.45/1984**
Fineness modulus : 2.87		-
Specific gravity: 2.68		-
Absorption : 1.66%		-
Dry rodded density: 1800 kg/m³		-
Sulfate Content		**Limits of Iraqi spec. No.45/1984**
SO_3: 0.2 %		≤ 0.5%

Table 4. Grading and physical properties of coarse aggregate.

Sieve size (mm)	Passing%	Limits of Iraqi spec. No.45/1984 Nominal size (5-14)mm
20	100	100
14	99.9	90-100
10	72	50-85
5	8.5	0-10
Physical properties		**Limits of Iraqi spec. No.45/1984**
Specific gravity: 2.76		-
Absorption : 0.23 %		-
Dry rodded density: 1650 kg/m³		-
Sulfate content		**Limits of Iraqi spec. No.45/1984**
SO3: 0.02 %		≤ 0.1%

Table 5. physical properties of SF.

Physical properties	SF Results	ASTM C1240-05 requirements
Percent retained on 45µm (No. 325) sieve, max, %	7	**≤ 10**
Strength Activity Index with Portland cement at 7 days, min % of control	116	**≥ 105**
Specific surface area (m^2/g)	20	**≥ 15**
Bulk density (kg/ m^3)	480	
Moisture content	0.74	≤ 3 %
Physical form and Color	grey to dark grey powder	

Table 6. Chemical analysis of SF.

Oxide Composition	Oxide content %	ASTM C1240-05 Requirements
SiO_2	91.44	Min. 85.0%
Al_2O_3	0.05	-
Fe_2O_3	0.03	-
MgO	0.24	-
CaO	1.04	-
SO_3	0.11	-
L.O.I	4.12	Max. 6.0%

Table 7. Sieve analysis of PET-aggregate.

Sieve size (mm)	Passing%
10	100
4.75	98
2.36	35
1.18	4.2
0.6	1
0.3	0.7
0.15	0.4

Table 8. PET –aggregate particles specification.

Physical properties	Results
Bulk Density (ASTM C29 -09 / Dry Rodded)	447 kg/m^3
Specific gravity	1.285
Water Absorption (24 hr)	0.00%
Thickness	(1 – 0.14) mm
Shape of particles	Flaky and fiberform particles and some pellets pieces with max. size 4.75 mm
Color	crystalline white to blue sky

Table 9. HPC mix proportions used through this work

Items	M0	M2.5	M5	M7.5
Cement kg/m^3	459	459	459	459
Silica fume kg/m^3	51	51	51	51
Water l/m^3	148	148	148	148
SP Liters/100 kg of cementitious materials	0.8	0.8	0.8	0.8
w/cm	0.29	0.29	0.29	0.29
Coarse Aggregate kg/m^3	1160	1160	1160	1160
Fine Aggregate kg/m^3	660	642.8	626.3	609.8
PET-aggregate kg/m^3	0	7.9	15.8	23.7
Average compressive strength at 28 days (MPa)	69	60.38	56.93	50.35

Table 10. Compressive Strength Test Results for all HPC mixes

Mix Symbol	PET-aggregate(%)	Compressive Strength MPa			
		7 days	28 days	56 days	91 days
M 0	0	59.73	69	71.15	74.17
M 2.5	2.5	53.9	60.38	64.1	66.8
M 5	5	49.6	56.93	58.22	62.1
M 7.5	7.5	45.44	50.35	56.1	61.23

Table 11. Static modulus of elasticity for all HPC mixes

Mix Symbol	PET-aggregate(%)	Static Modulus of Elasticity (GPa)	
		28 days	91 days
M 0	0	43.08	46.94
M 2.5	2.5	40.81	43.72
M 5	5	40.77	43.45
M 7.5	7.5	40.53	42.16

Table 12. Splitting tensile strength test results for all HPC mixes

Mix Symbol	PET-aggregate(%)	Splitting Tensile Strength (MPa)			
		7 days	28 days	56 days	91 days
M 0	0	3.74	3.87	3.95	4.08
M 2.5	2.5	3.83	4.01	4.12	4.2
M 5	5	3.23	3.42	3.78	3.95
M 7.5	7.5	3.18	3.36	3.52	3.64

Table 13. Flexural tensile strength test results for all HPC mixes

Mix Symbol	PET-aggregate(%)	Flexural Tensile Strength (MPa)			
		7 days	28 days	56 days	91 days
M 0	0	8.62	9.11	10.48	11.38
M 2.5	2.5	10.64	11.51	11.87	12.04
M 5	5	10.17	10.31	10.89	11.65
M 7.5	7.5	10.03	10.17	10.62	11.57

Plate 1. Sample of (PET- aggregate).

Plate 2. Plastic granulator machine.

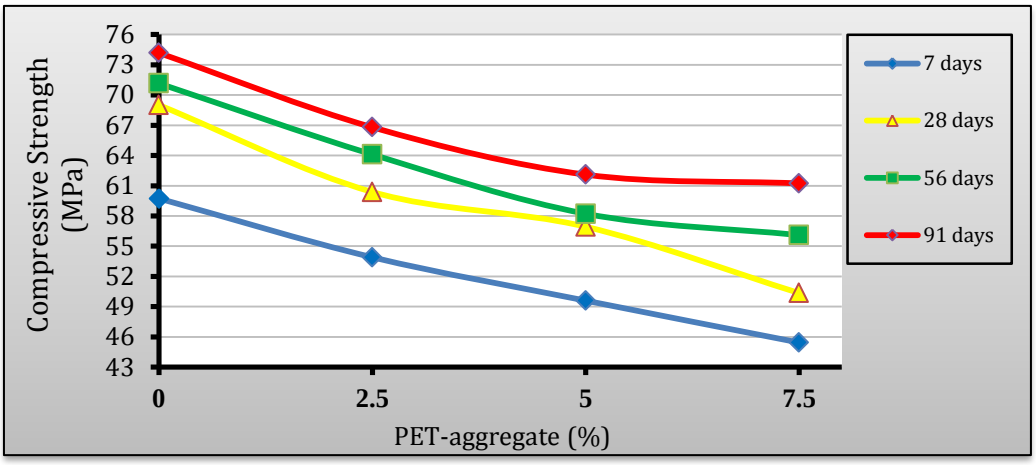

Figure 1. The effect of PET-aggregate content on compressive strength of HPC at different curing ages.

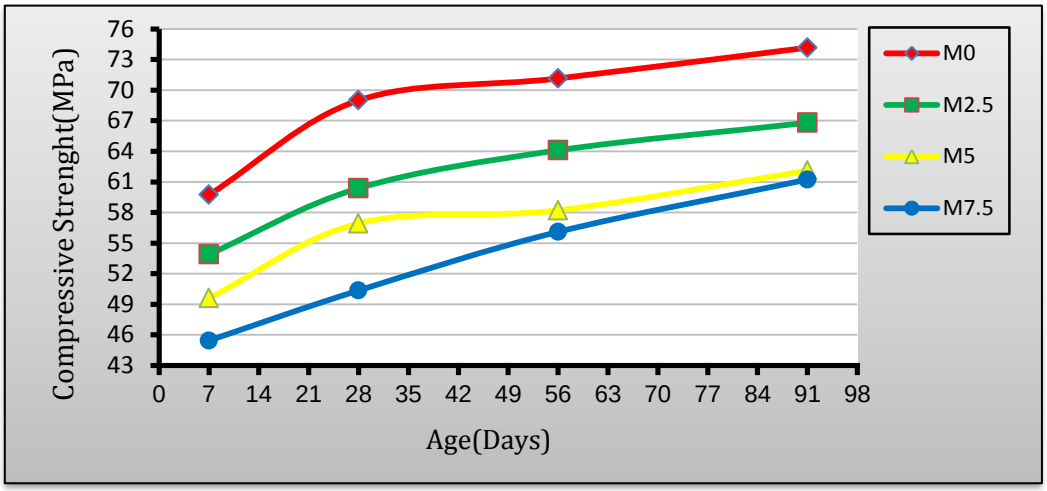

Figure2.: Compressive strength development at different curing ages for all types of HPC.

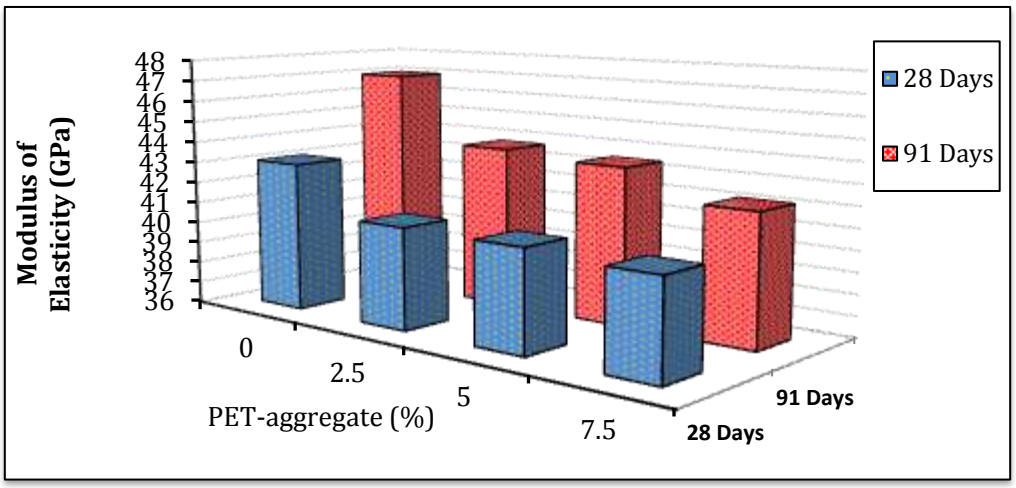

Figure 3. Effect of PET-aggregate on static modulus of elasticity at different curing ages.

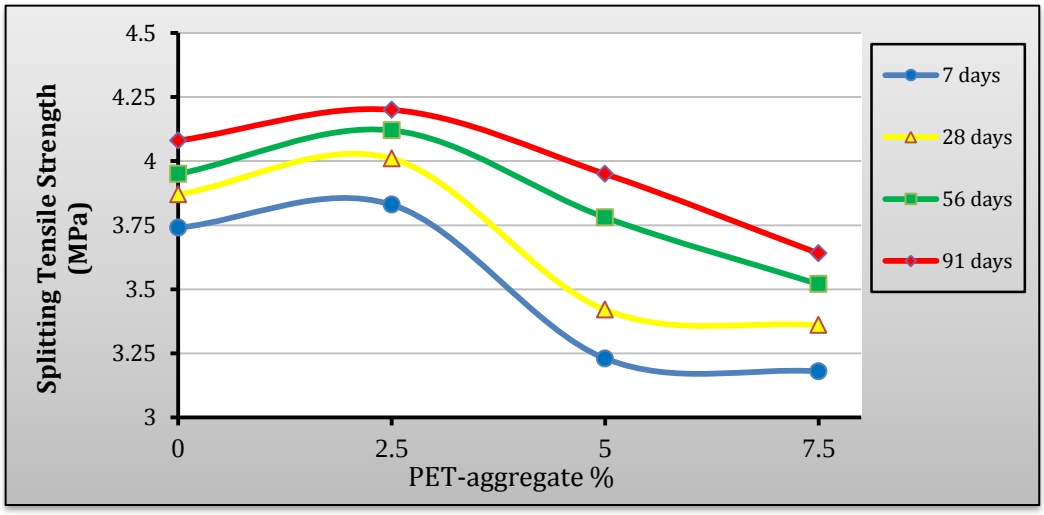

Figure 4. Relationship between splitting tensile strength and PET-aggregate content at different curing ages.

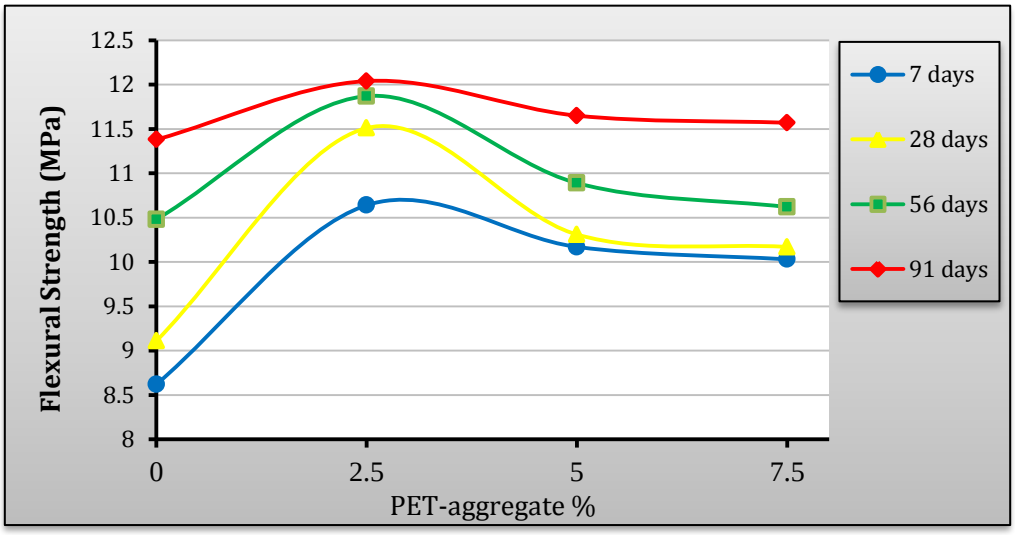

Figure 5. Relationship between flexural strength and PET-aggregate content at different curing ages.

تطوير برنامج عمل لتأثير المخاطر على تحقيق المشاريع الانشائية

أ.م.د. انتصار كاظم رشيد
قسم الهندسة المدنية
كلية الهندسة / جامعة بغداد

الخلاصة:

حاول المختصون في ادارة الانتاج والعمليات تطوير استراتيجية معينة لمواجهة المخاطر الناجمة عن نشاطات المنظمة والمتمثلة بالهدر بمختلف انواعه وبناءً على ذلك فإن ادارة المخاطر في اطارها المعاصر تمثل ظاهرة نوعية جديدة، ولايمكن لهذه الظاهرة ان تأخذ ابعادها التطبيقية إلا بتطوير ثقافة المنظمة تجاه المخاطر وتتعامل مع كافة جوانبها وترسم السبل الكفيلة لمعالجتها ضمن برنامج تكاملي، ويستلزم ذلك توفر مهارات جديدة ونظم معلومات دقيقة قادرة على التنسيق بين الاطراف المتعددة داخل المنظمة.

يهدف البحث الى تطوير برنامج عمل لتحليل العلاقة بين تاثير المخاطر ومراحل تحقيق المشروع ، وعلاقة تاثير المخاطر مع نوع العقد الانشائي، واخيراً علاقة تاثير المخاطر مع نوع الاعمال الانشائية. لقد حددت في هذا البحث عدد من المخاطر التي حدثت فعلاً من دراسة عدد من مشاريع البناء المنجزة وتمت الدراسة النظرية للبحوث والمصادر العلمية السابقة ومقابلة واستبيان عدد من خبراء صناعة التشييد لتحديد مدى تأثير هذه المخاطر في كل من هذه المحاور الثلاثة في المشاريع الانشائية في العراق لغرض الاستجابة لها وادارتها. توصلت الدراسة الى مجموعة من الاستنتاجات اهمها وجود اسبقية متباينة لحدوث المخاطر مما يثبت بأن هناك علاقة بين هذه الاسبقية ومرحلة المشروع ونوع العقد والعمل الانشائي، وعلى ضوء ما تم التوصل اليه ولغرض الاستفادة من مميزات الحاسوب الآلي فقد تم استخدام البرنامج الحاسوبي (Vanguard Software System) لبناء شجرة القرار واتخاذ اجراءات الاستجابة للمخاطر حسب اسبقيتها في الحدوث.

الكلمات الرئيسية: ادارة المخاطر، الاستجابة للمخاطر، مراحل تحقيق المشروع، العقود الانشائية، الاعمال الانشائية

Development of a Blueprint Impact System of the risks on construction projects Implementation

Asst. Prof.Dr. Entisar Kadhim Rasheed
Department of Civil Engineering
College of Engineering
Baghdad University
E-mail:int.pros_62@yahoo.com

ABSTRACT

In Production and Operations Management the specialists have tried to develop a strategy to counter the risks arising from the activities of the organization and of waste of various types and therefore the risk management in the contemporary framework represents a phenomenon of new quality, and can not be this phenomenon to take practical dimensions, but the development of culture of the organization towards the risks and deal with all aspects and paint ways to address them within an integrated program, and requires new skills and systems provide accurate information capable of coordination between the various parties within the organization.

The research aims to develop a blue print to analyze the relationship between the impact of risk and stages of implementing of the project and, the effect of risk relationship with the type of contract, and the impact of risks to do with the type of construction works. In this paper a number of risks has been identified that have already occurred from the study of a number of construction projects completed and theoretical studies and interview a number of construction industry experts to determine the extent of the impact of these risks in each of these three axes in construction projects in Iraq for the purpose of responding and management.

The study found a set of conclusions such as existing of priority in happiness of risks which proof that there is an relationship between the risks and sort of stage, contract and constructional work. In the light of what has been reached for the purpose of benefiting from the computer automated features a program have been used (Vanguard Software System) to build the decision tree in order to manage the risks according to their priority in happiness.

Key words: risk management, risk response, the stages of implementing of the project, construction contracts, construction works

1. المقدمة:

ان مشاريع التشييد تصمم وتنفذ حسب احتياجات صاحب العمل وضمن برنامج عمل وكلفة معقولة واذا لم يكن صاحب العمل هو المنفذ فانه يحتاج الى مقاول ذي خبرة كافية لتحمل المسؤولية ومنها مسؤولية ادارة المخاطر. ان التحديات التي تواجه صناعة التشييد في العراق وخاصة في الظروف الحالية تحتم على العاملين فيها التفكير الجدي من اجل دفع عجلة التقدم في مجال المقاولات نحو الأفضل. تعترض مدير المشروع مسؤولية بناء المشروع المعرض للعديد من المخاطر ضمن الميزانية المحددة للمشروع. ويدرك مهندسو الكلفة والانشاء الحاجة الكبيرة للتحسينات في مجال كلفة المشروع، وبناءً على ما تقدم اصبحت الحاجة ضرورية لتحليل وادارة المخاطر في كل مشروع من المشاريع الانشائية لتحقيق أهداف المشروع ومنها الكلفة.

يقدم هذا البحث برنامج عمل لتحليل علاقة تاثير مخاطر فعلية تم جمعها من عدد من المشاريع الانشائية المنفذة مع نوع العقد والعمل الانشائي فضلاً عن علاقة تاثيرها مع كل مرحلة من مراحل تحقيق المشروع الانشائي وبالاعتماد على التحليل الاحصائي للبيانات المستقاة من استمارات الاستبيان لعدد من الخبراء في مجال صناعة التشييد وتحديد اسبقية حدوثها باستخدام برنامج التحليل الشبكي (ANP) مع استخدام البرنامج الحاسوبي (Vanguard Software System) لبناء شجرة القرار لغرض اتخاذ اجراء الاستجابة المناسبة وحسب اسبقية المخاطر في حدوثها وذلك لتقنين هذه المخاطر بصورة مسبقة وهذا ما يعرف بادارة المخاطر.

2. مراجعة البحوث السابقة:

1.2 مفهوم المخاطر:

يعد التحديد الواضح لمفهوم المخاطر امراً بالغ الاهمية لانه يمثل الاساس الموضوعي لاستيعاب دورها ومهامها ، وتعتبر المخاطرة من المصطلحات التي ترد دائماً في ادبيات ادارة الاعمال فهناك مخاطر صناعية في مجال ادارة الانتاج والعمليات ومخاطر تسويقية في مجال ادارة التسويق ومخاطر مالية في مجال ادارة الموارد المالية وفي الحياة العملية فان مصطلح المخاطرة يتكرر استخدامه ليدل على حالة عدم التاكد (Uncertainty)، وفي هذا الصدد عرف (محفوظ حمدون الصواف واخرون، 2013) المخطر بأنه اي فعالية او نشاط لا يضيف قيمة للسلعة او الزبون او انه اي نشاط غير مرغوب في العملية الانتاجية يؤدي الى الهدر في الموارد المختلفة للمنظمة كالمعيب والمعاد والمرتجع والتالف والفاقد والوقت الضائع.

هناك وجهة نظر تشير الى ان المخاطرة هي حدث محتمل له تأثير سلبي فقط في اهداف مشروع معين. وقد نشأت هذه الفكرة من مفهوم عدم التأكد (Uncertainty) الذي ينتج عنه نتيجتان مختلفتان، اما ضياع الفرصة التي ينجم عنها الربح أو المخاطرة التي ينجم عنها الخسارة، (Malcolm,1997)، كما اشار (العداي ، 1978) على ان المخاطرة هي حادث يؤدي الى خسارة في حين عرفه (Allen & Duvall, 1987) بأنه التباين غير المستحب عن الواقع.

كما تمثل المخاطرة من وجهة نظر (James, 2001) اي شئ قد يحدث ويمكن ان ينشأ عنه اي تأثير ضار على الكلفة، جدولة الوقت، الجودة، نطاق المشروع. وعرفه (Duncan, 2009) بأنه الحدث غير المؤكد أو مجموع الملابسات والتي عند وقوعها ستؤثر على اتمام اهداف المشروع. وتم تعريف المخاطر بانها احتمالية حدوث أية حادثة مستقبلية والتي يمكن أن تؤثر على الخطط الموضوعة للمشروع ومنها المالية والزمنية وبالتالي الانحراف عما مخطط له (علاء،2013)، ان هذا البحث يميل الى التعريف الاخير للمخطر ويؤيده.

2.2 مفهوم ادارة المخاطر:

ان مصطلح ادارة المخاطر يضم شقين الاول ادارة والثاني مخاطرة ، فالإدارة وفق المفهوم الشائع تعني التخطيط والتنظيم والرقابة ، الما المخاطرة فهي التباين في ماهو متوقع (محمد علي ، 2004). تعرف ادارة وتحليل المخاطر بأنها العملية التي تمكن من معرفة المخاطر وتحليل تلك المخاطر باستخدام الطريقة المناسبة ومن ثم وضع الحل المناسب الذي يزيل تلك المخاطرة او يقلل من تأثيرها وبذلك تزيد من نجاح المشروع وتحقيق اهدافه (Taylor et al, 1997). ان تحليل وادارة المخاطر في المشروع تعتبر عملية مستمرة ويمكن ان تبدأ في اي مرحلة من دورة المشروع ويمكن ان تدوم وتستمر الى ان تصبح تكاليف استخدامها اكثر من فائدتها المحتملة والتي يمكن كسبها، وكلما تقدم المشروع تقل المخاطر وبهذا فان فعالية استخدام تحليل وادارة المخاطر تميل الى التقلص لذلك فانه من المستحسن استخدامها في الاطوار المبكرة من دورة حياة

المشروع (Malcolm,1997). كما تعرف بأنها مجال التوصل لمنع المخاطرة والتقليل من حجم الخسائر عند حدوثها والعمل على عدم تكرارها من خلال دراسة اسباب حدوث كل مخاطرة لتلافيها مستقبلاً ، كما تمتد ادارة المخاطر الى تدبير الاموال لتعويض المشروع عن الخسائر التي تحدث كي لا يتوقف عن العمل والانتاج (عاطف، 2008).

3.2 مراحل ادارة المخاطر:

تتطلب ادارة المخاطر وجود ادارة فعالة لوضع استراتيجية يتأشر من خلالها تحديد وتشخيص المخاطر التي يتعرض لها المشروع ثم تقييم حجم الخسائر المحتملة لكل المخاطرة من هذه المخاطر ومن ثم تحديد الطريقة المناسبة لمواجهة كل منها بالتنسيق مع اطراف المشروع، وفي هذا السياق حدد (الهاشمي ،2004) مراحل ادارة المخاطر كما يلي:

- مرحلة تحديد الاهداف
- مرحلة التحديد والاكتشاف
- مرحلة تقييم المخاطر
- مرحلة اختيار استراتيجية لمواجهة المخاطرة
- مرحلة التنفيذ
- مرحلة الرقابة.

فما يتعلق بالمراحل الثلاثة الاولى فهي تعتبر بمثابة التمهيد الأولي لمرحلة اختيار الستراتيجية الملائمة للمواجهة، أما المرحلة الخامسة فانها تهتم بتنفيذ الاستراتيجية التي تم اختيارها من قبل المنظمة من خلال إشراك كافة العاملين بتنفيذها، وفي المرحلة السادسة والاخيرة يتم اجراء المتابعة والمراقبة لملاحظة التغييرات التي تتطلب مراجعة وتنقيح السياسات التي تتعامل مع المخطر ونتائج هذه السياسات.

4.2 تصنيف المخاطر:

تتعرض المشاريع الانشائية الى العديد من المخاطر التي تؤثر على اهداف المشروع المتمثلة بالمدة والكلفة والجودة وتحول دون تحقيقها ويصنف العديد من الباحثين ومنهم الباحث (Mohammad A.Mustafa, 1991) تلك المخاطر الى عدة اصناف وكما يلي:

- مخاطر القضاء والقدر وتشمل: فيضان، زلزال، حريق ---- الخ
- المخاطر الطبيعية وتشمل: الأضرار للمنشأ، الأضرار للمعدات، إصابات العمال، السرقة للمواد والمعدات
- المخاطر المالية والاقتصادية وتشمل: التضخم اللاقتصادي، مشاكل التمويل او التدفق المالي لدى صاحب العمل، العجز المالي للمقاول ---- الخ
- المخاطر السياسية والبيئية وتشمل: تغيير القوانين والتعليمات، الحروب والاضطرابات المدنية، تأخر المصادقات والموافقات والتراخيص، التلوث وتعليمات التأمين، نزاعات الملكية --- الخ
- مخاطر التصميم وتشمل: نقص في التصميم، عيوب في التصميم، نقص في المواصفات، تغيير في التصميم
- مخاطر متعلقة بالموقع وتشمل: نزاعات وإضراب العمال، ضعف انتاجية العمال، عيوب في العمل، اختلاف ظروف الموقع

وبناءً على ماسبق فقد صنف البحث المخاطر الفعلية المستقاة من المشاريع الانشائية المنفذة كمخاطر يتم دراستها في هذا البحث، الى مخاطر تنظيمية، مخاطرمكانية، مخاطر فنية، مخاطر سياسية ومخاطر مالية.

3. عقود المقاولات في قطاع التشييد:

عرف القانون المدني عقد المقاولة بانه (عقد يتعهد به أحد الطرفين أن يصنع شيئاً أو يؤدي عملاً لقاء أجر يتعهد به الطرف الآخر) (القانون المدني،1951) ويشمل هذا التعريف انواع عديدة من العقود ومنهاعقد المقاولات الانشائية والذي يعرف بأنه عقد يتعهد به شخص بإنشاء و/أو صيانة و/أو تشغيل مشروع هندسي لحساب شخص لقاء أجر معين بموجب الشروط والخرائط المعدة لتنفيذه (انطوان، 1985)، ويمكن تصنيف عقد المقاولات الانشائية الى الانواع التالية:

1.3 مقاولة المبلغ المقطوع (جملة) Lump Sum Contract

وتسمى ايضاً مقاولة الكلفة الكلية ويكون المبلغ الكلي ثابتاً ويغطي مصاريف العمل كافة بموجب وثائق المناقصة وفي مثل هذه المقاولات تكون الأعمال المطلوب تنفيذها محددة ابتداءً وموصوفة وصفاً كاملاً من خلال توفير المخططات الكاملة والمواصفات وبذلك يتمكن المقاول من تسعير المقاولة وتحديد المبلغ المقطوع الذي سيتم التعاقد عليه (Edward Whitticks، 2005). تعتبر مقاولة تسليم المفتاح (TurnKey Contract) من مقاولات الجملة، ويلجأ اليها في المشاريع المستعجلة التخصصية جداً أو الستراتيجية مثل مخازن خاصة أو مشاريع صناعية أو عسكرية والتي يتعهد المقاول فيها بإعداد التصاميم الكاملة والتنفيذ والصيانة وذلك وفقاً لمتطلبات صاحب العمل للمشروع المطلوب تنفيذه، لذا يمكن اعتبار عقد تسليم المفتاح ايضاً هو من عقود التصميم والبناء مع بعض الفروقات.

2.3 مقاولة جدول الكميات والاسعار Bill of Quantities and Rates Contract

إن هذا النوع هو الأكثر شيوعاً في العراق حيث ان معظم المقاولات الإنشائية تكون على أساس تسعير جداول الكميات وتتوافر في هذه الحالة تصاميم تفصيلية كاملة مع المواصفات الفنية للمواد والعمل والشروط العامة والخاصة وبذلك تتوافر معلومات كاملة لغرض تسعير جميع الأعمال وفي هذا النوع تقل الخلافات حول تسعير التغييرات وتقييم المطالبات مالياً أثناء التنفيذ (Edward Whitticks، 2005).

3.3 مقاولة جدول الأسعار Schedule of Rates Contract

يستخدم هذا الاسلوب في الحالات التي تتطلب سرعة التنفيذ مع عدم وجود تصور عن كميات الفقرات التنفيذية بشكلٍ دقيق حيث يتم الاتفاق مع المقاول على جدول بأسعار وحدات فقرات الأعمال المتوقع تنفيذها في المشروع، وتكون هذه الاسعار أساساً لحساب كلفة العمل المنجز أو إحتساب السلف، وفي هذا الاسلوب يستوجب إعتماد أقصى درجات الدقة في اختيار المقاول المتمرس ذي الخبرة الجيدة لتفادي سوء التخمين للاسعار ومن ثم وقوع المقاول بمشاكل الخسارة وعرقلة تقدم العمل (Edward Whitticks,2005).

4.3 مقاولة الكلفة زائداً Cost – plus Contract

أن هذا النوع من المقاولات لا يعطي حداً للكلفة الكلية إذ ان صاحب العمل يدفع تكاليف التنفيذ كافةً من شراء المواد وتشغيل الأيدي العاملة والمعدات وكلف المقاولات الثانوية مضافاً اليها مبلغ معين تعويضاً عن الخدمات والمعلومات التقنية التي يقدمها المقاول ولتغطية النفقات الإدارية وفوائد إستثمار رأس المال المستغل ويكون المبلغ المضاف اما حسب مبدأ التنافس أو التفاوض بين المقاول وصاحب العمل (راجي، 1995)، ويقسم هذا النوع من المقاولات الى ثلاثة أنواع:

- مقاولة الكلفة زائداً مبلغ مقطوع كأجور وأرباح يتفق عليها إبتداءً.
- مقاولة الكلفة زائداً نسبة معينة من المصروفات يتفق عليها إبتداءً.
- مقاولة الكلفة زائداً نسبة معينة من الكلفة بسقف أعلى.

5.3 مقاولة التصميم والتنفيذ Design and Build Contract

وفي هذه الطريقة من التعاقد يتم النعاقد مع شركة إنشاءات محددة والاستفادة من خبرتها في مرحلة التصميم الهندسي على وجه الخصوص، حيث يكلف صاحب العمل المقاول الرئيسي للقيام بأعمال التصميم والتنفيذ وبذلك فان المسؤولية التقنية تنحصر من ناحية التصميم والتنفيذ في جهة واحدة (المقاول)، وتكون احتمالية تنفيذ المشروع في زمن قياسي، ويكثر استخدام هذه الطريقة في المشاريع الكبيرة وذات الطبيعة الصناعية كمحطات تكرير النفط.

4. جمع البيانات وتحليلها :

1.4 تحديد المخاطر:

تم تحديد اهم المخاطر التي حدثت فعلاً وذلك بتجميعها من عقود مقاولات لعدد من المشاريع الانشائية قيد الدراسة والتي شملت (مشاريع الكهرباء، الطرق والجسور، المباني، المستشفيات، المشاريع النفطية، شبكات الماء والمجاري، الابنية المدرسية) في عموم المحافظات في العراق اضافة الى المراجعة النظرية للبحوث والادبيات وعدد من المقابلات مع خبراء في مجال صناعة التشييد ونتائج الاستبيان، وبذلك تم تصنيف هذه المخاطر والبالغ عددها (42) مخطر والتي ادت الى تغييرات في الكلفة والوقت وجودة المشروع وكما يلي: مخاطر تنظيمية، مخاطر مكانية، مخاطر فنية، مخاطر مالية ومخاطر سياسية كما موضحة في جدول رقم (1). يتضح من الدراسة الاولية للبيانات الحقلية هذه والتي جمعت من هذه المشاريع مايلي:

- ان المخاطر توزعت بشكل متباين على جميع انواع الاعمال الانشائية.
- ان اكثر عدد مرات حدوث للمخاطر في هذه المشاريع هي المخاطر الفنية تليها المخاطر المكانية ثم التنظيمية ثم السياسية واخيراً المخاطر المالية،
- ان العدد الكلي كحد اعلى للمخاطر مجتمعة كانت في مشاريع المعالجة وشبكات المياه أما المشاريع الاخرى فكان العدد اقل.

2.4 تحليل المخاطر وعلاقتها مع مرحلة المشروع الانشائي:

لغرض تحقيق اي مشروع انشائي فانه يمر بأربعة مراحل وكما يلي :

- مرحلة تحديد الفكرة (مرحلة القرار) Decision phase
- مرحلة التصميم Design phase
- مرحلة التعاقد واعداد مستندات المقاولة Contracting and contract documents phase
- مرحلة التنفيذ Execution phase

ومن ثم التشغيل والصيانة ، ولدراسة العلاقة بين تاثير المخاطر ومراحل تحقيق المشروع الانشائي تم تصميم استمارة استبيان تتضمن محورين المحور الاول : يهدف الى الحصول على معلومات عامة لافراد العينة المختارة من المستبينين كالاختصاص، التحصيل الدراسي، قطاع العمل، المركز الوظيفي وعدد سنوات الخبرة اما المحور الثاني فتضمن السؤال عن راي الخبير عن اي مرحلة من مراحل تحقيق المشروع الانشائي تؤثر المخاطر، وزعت عدد من استمارات الاستبيان الى مدراء

المشاريع الانشائية ومهندسين في المكاتب الاستشارية وفي شركات المقاولات القطاع العام والخاص واساتذة الجامعات ودعم الاستبيان بالمقابلات الشخصية مع هؤلاء الخبراء وقد استرد منها (34) استمارة اعتمدت لاغراض التحليل.

1.2.4 تحليل البيانات:

استخدم البرنامج الحاسوبي (Excel) لمعالجة البيانات، يوضح الجدولان رقم (2) و(3) نسبة المستبينين من حيث طبيعة عملهم وسنوات الخبرة . لقد تبين ان اكثر من نصف حجم العينة من المستبينين لديهم خبرة اكثر من (15) سنة مما يزيد من وثوقية المعلومات التي وفرها المستبينون لتصوير الواقع من خلال خبرتهم في مجال صناعة التشييد.

هناك عدة مقاييس للاحتمال والتأثير للمخاطر عند استبدال المقياس الكيفي بأرقام عند التحليل الاحصائي وقد اعتمد المقياس الآتي (منى واخرون،2012):

المقياس	منخفض جداً	منخفض	متوسط	عالي
المجال %	10 – 0	30 – 11	60 – 31	60 <

2.2.4 تحليل نتائج تأثير المخاطر وعلاقتها مع مرحلة المشروع الانشائي:

تم احتساب النسبة المئوية لاجابات المستبينين لكل مرحلة من مراحل تحقيق المشروع الانشائي، وقد اختيرت اجابة المخاطرة ذات نسبة المئوية للتاثير أكبرمن (30% وفق المقياس أعلاه) اي تأثير متوسط او عالي كأساس لإجراء البحث، يتضح من تحليل الاجوبة ما يلي مايلي :

- ان نسبة (97.6 %) من اجابات المستبينين اشارت الى ان النسبة الأكبر لهذه المخاطر يكون تأثير حدوثها في مرحلة التنفيذ للمشروع وبنسبة (متوسطة الى عالية) حسب المقياس أعلاه عدا المخاطرة (عدم توفر المخططات للشبكات الخدمية المارة خلال الموقع كالمخططات الكهربائية, الهاتف, الماء,وغيرها) المخاطرة (اختلاف طبيعة الارض) المخاطرة (تبديل موقع العمل) فأشارت نسبة الاجابات الى ان تاثير حدوث هذه المخاطر يمكن ان يكون في مرحلة التصميم.
- كما ويتضح ايضاً ان اكبر نسبة للاجابات لتاثير المخاطر في مرحلة التنفيذ كانت للمخاطرة (سوء الظروف الجوية) والبالغة (97.05882 %) يليه المخاطرة (المناسبات الدينية والعطل المفاجئة) والبالغة (94.11765 %).
- اما المخاطرة (عدم وضوح الالتزامات التعاقدية) المخاطرة (ارض المشروع مستملكة من قبل الدولة ولكن لم يتم تسديد استحقاقات المالكين) فأشارت الاجابات الى ان تأثير حدوثهما يكون اكثر في مرحلة التعاقد للمشروع .
- برغم ان النسب المئوية للاجابات في مرحلة القرار كانت منخفضة الا ان ذلك لايمنع من التخطيط لتحديد اجراءات الاستجابة المناسبة لها ابتداءً من هذه المرحلة، اما المخاطر الاخرى فقد توزعت بين مراحل المشروع الاخرى وبنسب منخفضة الى منخفضة جداً.

ان هذه النتائج تعني ضرورة انتباه المعنيين الى اتخاذ اجراءات الاستجابة المطلوبة لمعالجة هذه المخاطر في تلك المراحل وتدريب العاملين على هذه الاجراءات ورصد الميزانية المطلوبة مقدماً وقبل حدوثها.

5. عملية التحليل الشبكي Analytic Network Process (ANP):

وهي عملية إتخاذ القرارات والاعتماد عليها في التغذية الاسترجاعية والتي وضعها الاستاذ والعالم العراقي توماس ساعاتي، ان هياكل AHP (Analytic Hierarchy Process) تضع مشكلة القرار في تسلسل هرمي مع هدف، ومعايير

القرار، وبدائل، في حين أن هياكل ANP تضعها على أنها شبكة. كلاهما يستخدم نظام المقارنات المزدوجة للهيكل لقياس أوزان مكونات الهيكل، وأخيرا إلى تحديد رتبة (اسبقية) البدائل في القرار. استخدم برنامج (ANP) حيث اجريت (648) مقارنة مزدوجة للنسب المئوية للاجوبة لايجاد الاسبقية (priority) للمخاطر وبترتيب تنازلي لكل صنف على حدة من اصناف المخاطر وكما في الشكل رقم (1) والذي يوضح نموذج من عملية التحليل الشبكي هذه، وقد لوحظ من البرنامج اختلاف قيمة هذه الاسبقية للمخطر الواحد بين كل مرحلة واخرى ما يثبت علاقة المخاطرة مع نوع المرحلة كما في الجدول رقم (4) الذي يعرض نموذجاً لهذا الاختلاف في الاسبقية، وكذلك تم عرض جميع نتائج التحليل الشبكي في الجدول رقم (5).

6. العلاقة بين تأثير المخاطر ونوع العقد الانشائي:

لدراسة تأثير هذه المخاطر (42) المخاطرة ونوع العقد الانشائي للمشروع ، صمم استبيان مغلق لعدد من انواع العقود للمقاولات الانشائية التقليدية وهي: عقد الجملة، عقد تسليم المفتاح (وذلك لان عقد تسليم المفتاح يعتبر وكما ذكر سابقاً من عقود مقاولات الجملة لذا تضمنه الاستبيان لبيان هل هناك فرق في تاثير المخاطر في كل منهما ؟) اضافة الى عقد جداول الكميات والاسعار، عقد جدول الاسعار، عقد الكلفة زائداً وعقد التصميم والتنفيذ، حيث تضمن الاستبيان السؤال الأول عن نسبة تأثير كل مخاطرة في كل نوع من انواع هذه العقود وذلك لاتخاذ اجراءات الاستجابة لهذه المخاطر. وقد اختيرت خمسة اجابات وهي : نسبة التأثير منخفضة جداً، منخفضة، متوسطة، عالية، عالية جداً، والسؤال الثاني عن نسبة تأثير كل مخاطرة في كل نوع من أنواع الأعمال الانشائية في المشاريع، ثم وزعت استمارات الاستبيان على عدد من الخبراء في صناعة التشييد تم استرداد (38) استمارة وقد اختلف التحصيل الدراسي وعدد سنوات الخبرة للمستبينين اذ لوحظ ان اكثر من (60%) من حجم العينة كانت خبرتهم اكثر من (15) سنة وهذا مؤشر الى موثوقية اجاباتهم. لقد تم انتخاب اجوبة المستبينين للمخاطر (عالية ومتوسطة الاهمية اي ذات نسبة الاجابة للتاثير أكبر من 30% وفق المقياس أعلاه) لكل مخطر من المخاطر ولكل عقد من عقود المقاولات ليتم تحليلها ومعرفة الاسبقية للمخاطر.

7. تحليل نتائج تأثير المخاطر وعلاقتها مع نوع العقد الانشائي:

يتضح من تحليل النسب المئوية لاجوبة المستبينين تأكيدها جميعاً على ان نسبة تأثير المخاطر في عقد التصميم والتنفيذ تكون نسبة (منخفضة الى منخفضة جداً) وقد يعزى ذلك الى تحمل المقاول المسؤولية كاملة وبذلك عليه مواجهة هذه المخاطر واتخاذ ما يلزم لإدارتها، كذلك فان نسبة المخاطر في عقد الكلفة زائداً تكون نسبة (منخفضة الى منخفضة جداً) وقد يكون ذلك بسبب طبيعة هذا العقد حيث لاتوجد مخططات او أية بيانات يعتمد عليها المقاول وان صاحب العمل هو الذي يتحمل المخاطر. أما بقية العقود فقد توزعت المخاطر بنسب مختلفة بينها حيث يلاحظ ان المخاطر المالية بشكل عام كانت بنسب (متوسطة الى عالية) تليها المخاطر المكانية والفنية ثم التنظيمية ، اما المخاطر السياسية فكانت نسب تأثيرها (منخفضة الى منخفضة جداً).

وقد استخدم برنامج (ANP) حيث اجريت (972) مقارنة مزدوجة للنسب المئوية للاجوبة لايجاد الاسبقية وبترتيب تنازلي بين مخاطر كل صنف على حدة من اصناف المخاطر وكما في الجدول رقم (5)، وقد لوحظ من البرنامج اختلاف قيمة هذه الاسبقية للمخاطرة الواحدة بين كل عقد واخر وهذا يثبت علاقة المخطر بنوع العقد الانشائي.

8. العلاقة بين تأثير المخاطر ونوع العمل في المشروع الانشائي:

السؤال الثاني للاستبيان اعلاه كان لدراسة تاثير الـ (42) مخاطرة هذه في كل نوع من انواع اعمال مختلفة للمشاريع الانشائية وهي: اعمال الكهرباء، شبكات الماء والمجاري، الابنية السكنية، المستشفيات، ابنية المدارس، ابنية المعامل، والطرق والجسور ، وقد اختيرت خمسة اجوبة هي: نسبة تأثير منخفضة جداً، منخفضة، متوسطة، عالية، وعالية جداً. لقد تم انتخاب اجوبة المستبينين للمخاطر (عالية ومتوسطة الاهمية اي ذات نسبة الاجابة للتاثير أكبر من 30% وفق المقياس أعلاه) لكل مخطر من المخاطر ولكل نوع من انواع الاعمال الانشائية ليتم تحليلها ومعرفة الاسبقية للمخاطر.

9. تحليل نتائج تأثير المخاطر وعلاقتها مع نوع العمل الانشائي في المشروع:

يتضح من تحليل النسبة المئوية لاجوبة المستبينين ان المخاطر توزعت على جميع انواع الاعمال الانشائية لكن المخاطر المالية كانت بالمرتبة الاولى حيث بلغت نسبة تأثيرها (متوسطة) في الغالب وهذا لايتطابق مع التحليل لبيانات المخاطر الفعلية للمشاريع التي ظهرت فيها ان المخاطر المالية بالمرتبة الاخيرة ويتضح من البحث ان المخاطر المالية هي مخاطر اساسية ولها الدور الكبير في جميع الاعمال الانشائية فمن المعقول ان تحتل المرتبة الاولى كما توصل لها تحليل نتائج الاستبيان ، تليها المخاطر الفنية ثم التنظيمية ثم المكانية وأخيراً المخاطر السياسية حيث كانت نسب تأثيرها منخفضة الى منخفضة جداً وهذه النتائج تتطابق الى حد ما مع ترتيب المخاطر الفعلية.

ايضاً استخدم برنامج (ANP) حيث اجريت (1134) مقارنة مزدوجة للنسب المئوية للاجوبة لايجاد الاسبقية وبترتيب تنازلي بين مخاطر كل صنف على حدة من اصناف المخاطر وكما في الجدول رقم (5)، وقد لوحظ من البرنامج اختلاف قيمة هذه الاسبقية للمخاطرة الواحدة بين كل نوع عمل انشائي الى اخر وهذا يثبت علاقة المخاطرة بنوع العمل الانشائي.

10. البرنامج الحاسوبي:

لقد تم استخدام البرنامج الحاسوبي (Vanguard Software System) الذي له خاصية بناء شجرة القرار، هذه الشجرة تجمع المدخلات وتنظمها ثم تعرض هذه البيانات في شجرة من عدد من الفروع اعتماداً على هذه المدخلات التي زود بها البرنامج وتتألف من الجذر الذي يظهر الاساس والعنوان للمشكلة ثم الفروع حيث تظهر المعلومات مفصلة حول كيفية الحل وذلك للتوصل الى القرار النهائي حول اية مشكلة تواجه المهندس او اي مختص اخر حيث ان هذا البرنامج يستخدم في عدة اختصاصات كالادارة والطب والعلوم الاخرى. ان السبب في استخدام شجرة القرار هو سهولة الاستخدام والجودة في تنظيم المشكلة المعقدة حيث يتم تقسيمها بداية الى جزئين بسيطين او اكثر ثم يقوم البرنامج بالتعامل معها وانشاء (Diagram) يتماشى مع المشكلة ويكون الحل بشكل شجرة هرمية متدرجة لاتكون مجرد حلاً لمشكلة العمل بل ايضاً الى عرض هذا الحل على الآخرين.

لقداعتمدت نتائج الاستبيان وما تم التوصل اليه من نتائج عملية التحليل الشبكي ANP في تحديد الاسبقية للمخاطر وعلاقتها مع نوع مرحلة المشروع ثم مع نوع العقد الانشائي واخيراً مع نوع العمل الانشائي وكما مبين في الجدول رقم (5) واعتمدت كقاعدة معلومات عند بناء شبكة القرار هذه وكما مبين في الاشكال رقم (2) و (3) و (4) للتوصل الى القرار حول الاسبقية للمخاطر من اجل اتخاذ الاجراءات اللازمة لادارتها. تم بناء شجرة القرار باستخدام البرنامج من خلال عدة خطوات ابتداءً من النقر على الاختيار(File) ثم (New) ثم اختيار(Decision Tree) من بين الاختيارات ثم النقر على (Long Names) فيظهر اول مستطيل ممثلاً لجذر الشجرة والذي يعبر كما ذكر أعلاه عن المشكلة المراد حلها ثم يبدأ البرنامج برسم الفروع حيث ان كل فرع يمثل أحد تصنيفات المخاطر ثم انواعها وصولاً الى القرار الذي يجب اتباعه من خلال

تغذية الفروع بنتائج الاستبيان والتحليلات هذه كمدخلات ويبين الشكل رقم (5) تتابع خطوات البرنامج الحاسوبي المقترح لصناعة أحد قرارات الاسبقية للمخاطر (على سبيل المثال اسبقية المخاطر وعلاقتها مع نوع العقد الانشائي)، فبعد الانتهاء من مرحلة بناء شجرة القرار وبالنقر على ايكونة التشغيل (Run) تظهر الشاشة كما موضحة في الشكل (5- أ) لتحديد تصنيف المخاطرة فاذا تم اختيار المخاطر التنظيمية (Organizational) على سبيل المثال تظهر الشاشة الثانية كما في الشكل (5 – ب) لتأكيد تصنيف المخاطرة وبالضغط على (OK) تظهر الشاشة الثالثة كما في الشكل (5 – جـ) وهي الاستفسار عن نوع المخاطر المتوقع حدوثها في ذلك المشروع ضمن تصنيف المخاطر المختارة وهي (المخاطر التنظيمية) وبالنقر على (OK) تظهر الشاشة الاخيرة كما في الشكل (5 – د) لتمثل القرار الذي يجب اتباعه لادارة تلك المخاطر. ان هذا البرنامج يمكن استخدامه من قبل صاحب العمل او الاطراف الاخرى المعنية بادارة المخاطر.

11. الاستنتاجات والتوصيات:

لقد تم دراسة تأثير المخاطر التي حدثت فعلاً في عدد من المشاريع الانشائية وقد توصل البحث الى العديد من الاستنتاجات من اهمها مايلي:

1- لوحظ ان المخاطر تحدث في جميع مراحل تحقيق المشروع وتتركز في مرحلة التنفيذ.
2- ان المخاطر توزعت بشكل متباين على جميع انواع العقود والاعمال الانشائية التي تناولها البحث.
3- ان اكثر عدد مرات حدوث للمخاطر في هذه المشاريع هي المخاطر الفنية تليها المخاطر المكانية ثم التنظيمية ثم السياسية واخيراً المخاطر المالية،
4- ان العدد الكلي كحد اعلى للمخاطر مجتمعة كانت في مشاريع المعالجة وشبكات المياه أما المشاريع الاخرى فكان العدد اقل.
5- لوحظ ان هناك اسبقية لحدوث المخاطر تم تنظيمها في برنامج عمل لكي يشير الى ضرورة اتخاذ اجراءات الاستجابة لها قبل غيرها.
6- كذلك لوحظ ان قيمة الاسبقية تختلف باختلاف المرحلة وباختلاف العقد والعمل الانشائي مما يدل على العلاقة الوثيقة بين المخاطر وهذه المحاور

كما ويوصي البحث بعدد من التوصيات منها:

1- ضرورة الاهتمام بدراسة المخاطر وتاثيرها منذ المراحل الاولى للمشروع.
2- ضرورة الانتباه الى اسبقية حدوث هذه المخاطر للتركيز على ادارة الاهم منها ثم المهم.
3- ضرورة الانتباه الى العلاقة بين اسبقية حدوث المخاطر ومرحلة تحقيق المشروع ونوع العقد والعمل الانشائي.
4- استخدام البرنامج المقترح لتسهيل معرفة اسبقية حدوث المخاطر وادارتها.

ويقترح البحث استخدام البرنامج (Vanguard Software System) في حل مشاكل انشائية اخرى كمشكلة تحديد الموارد في المشاريع الانشائية.

المصـادرالعربية:

- علاء محسن مهدي،" إدارة المخاطر المسببة للمطالبات في المشاريع الانشائية الحكومية"، رسالة ماجستير، كلية الهندسة، جامعة بغداد 2013.
- محفوظ حمدون الصواف، ماجد محمد صالح،" ادارة الجودة الشاملة كأداة لتقليل المخاطر، دراسة ميدانية في معمل النسيج الحكومي الموصل "، 2013.
- بسمة محمد علي، " واقع ادارة الخطر وأهميته في المنظمات الصناعية ، دراسة ميدانية في معمل الغزل والنسيج في الموصل، رسالة ماجستير، كلية الادارة والاقتصاد، جامعة الموصل، 2004.
- عاطف عبد المنعم، محمد محمود الكاشف، سيد كاسب، " تقييم وإدارة المخاطر "، مركز تطوير الدراسات والبحوث، كلية الهندسة، جامعة القاهرة، مؤسسة فورد، 2008.
- مختار محمود الهاشمي، ابراهيم حمودة، " مقدمة في مبادئ الخطر والتأمين (بين التطور والتطبيق) دار الجامعة للطباعة والنشر، الاسكندرية، 2000.
- منى حمادة و د.محمد نايفة و د.عمر عاموري،" إدارة مخاطر التشييد لمشاريع التشييد في سورية"، مجلة جامعة دمشق للعلوم الهندسية، المجلد الثامن والعشرون، العدد الأول ،2012.
- القانون المدني رقم (40) لسنة 1951، وزارة العدل، مطبعة الحكومة، بغداد، 1951.
- انطوان زحلان،" صناعة الانشاءات العربية"، ترجمة: عطا عبد الوهاب، مركز دراسات الوحدة العربية، بيروت، 1985.
- محمد صبحي ابو صالح وعدنان محمد عوض،" مقدمة في الاحصاء"، جامعة اليرموك، إربد، الاردن، الناشر: جون وايلي وابناءه، نيويورك، 1983.
- زكي راجي العاني، " متطلبات تحسين الأساليب المعتمدة في تنفيذ المشاريع الإنشائية في العراق "، ندوة حسابات الكلف، وزارة الإسكان والأعمار، بغداد، 1995.

المصادر الاجنبية:

- Malcolm, N.E. and McKennon, J. ,"A Process Driven Approach to Integrated Environments", Proceedings INCOSE International Symposium 1997.
- Duncan Cartlidge Frice " Quantity Surveyor's Project Book", First Edition, Elsevier Science and Technology, Department in Oxford, UK, 2009.

- James P. Lewis " Project Planning, Scheduling and Control a Hands-On Guide o Bringing Projects in On Time and On Budget", Third Edition, McGraw-Hill Companies, Inc-U.S.E, 2001.
- Taylor,I and Bassler, J.," Application of ANSI Standard to Space Station Resources", Proceedings INOSE International,1997.
- Mohammad A. Mustafa, Jamal F. Al-Bahar, " Project Risk Analytic Assessment Using the Hierarchy Process ", IEEE, 1991.
- Edward Whitticks, " Construction Contracts ,Gulf publishing company, 2005.

جدول رقم (1) المخاطر التي حدثت فعلاً في المشاريع الانشائية قيد البحث

تصنيف المخاطر	ت	المخاطر	تصنيف المخاطر	ت	المخاطر
تنظيمية	م1-	عدم توفر المخططات للشبكات الخدمية المارة خلال الموقع كالمخططات الكهربائية, الهاتف, الماء,وغيرها)		م22-	تأخر اكمال التصاميم او تغيير في التصميم
	م2-	المناسبات الدينية والعطل المفاجئة		م23-	عدم تطابق المخططات (انشائي , معماري) او وثائق العقد
	م3-	ضعف التنسيق والاتصالات بين صاحب العمل والمقاول		م24-	نزاعات خلال مرحلة التشييد بين اطراف العمل
	م4-	تصنيع القطع الكونكريتية الجاهزة في اماكن بعيدة عن العمل		م25-	جدولة غير دقيقة للمشروع
	م5-	عدم توفر المعلومات الضرورية (تأخر وصول المخاطبات الرسمية الى موقع العمل)	سياسية	م26-	تدهور الاوضاع الامنية في المشروع بالاضافة الى تكرار تفجير المعدات
	م6-	عدم وضوح الالتزامات التعاقدية		م27-	تأخر وصول المواد بسبب الاجراءات الامنية
	م7-	تأخر المصادقة على المخططات التنفيذية من قبل الجهة الاستشارية		م28-	بسبب احداث امنية لم يستطع المقاول استلام الموقع
	م8-	تأخر المباشرة بالعمل في المشروع		م29-	ظروف الحرب (استقرار وحدة عسكرية في المشروع لمدة طويلة)
	م9-	حدوث مشاكل داخلية بين اعضاء فريق المقاول		م30-	حدوث اضرار في بعض اجزاء المشروع بسبب الاحداث الامنية
مكانية	م10-	تأخر في تسليم الموقع الى المقاول بسبب عدم تهيئة الموقع		م31-	تعرض المشروع الى اطلاقات نارية نتيجة احداث امنية
	م11-	وجود عوائق في الموقع كالمياه الجوفية, انابيب المياه, تاسيات كهربائية --- الخ	مالية	م32-	عدم كفاية التخصيصات المالية لاكمال الاعمال
	م12-	عدم تخصيص مكان لرمي الانقاض		م33-	تاخيرانجاز الفقرات بسبب عدم توفرالسيولة المالية لدى المقاول (عدم التحكم بالتدفق النقدي)
	م13-	سوء الظروف الجوية		م34-	التضخم وتقلبات الاسعارخلال فترة تنفيذ المشروع
	م14-	اختلاف طبيعة الارض		م35-	ارتفاع كبير في اسعار حديد التسليح
	م15-	تبديل موقع العمل		م36-	عدم امكانية الاستفادة من المشروع بسبب وجود نواقص كالمصاعد

	م16-	ضيق المساحة داخل الموقع وصعوبة حركة المعدات وعدم توفر مكان لتجهيز المواد، اضافة الى الزخم المروري في المنطقة		م37-	مطالبة المقاول بفرق سعر لارتفاع اسعار المواد بسبب التاخير
	م17-	صعوبة الوصول الى الموقع (الموقع في منطقة نائية)		م38-	تأخر استلام السلف التشغيلية وفق العقد لحين اكمال الاجراءات القانونية
فنية	م18-	فروقات بين التنفيذ والمواصفات المطلوبة نتيجة لسوء فهم المخططات والمواصفات		م39-	ارض المشروع مستملكة من قبل الدولة ولكن لم يتم تسديد استحقاقات المالكين
	م19-	تلزيم العمل لمقاول غير كفوء		م40-	وفاة المقاول
	م20-	تأخر وصول بعض المواد والتجهيزات من بلد المنشأ		م41-	تأخر تنفيذ بعض الفقرات بسبب عدم استملاك المناطق المحرمة للمشروع
	م21-	عدم دقة المسوحات المتعلقة بموقع المشروع من قبل الطرف الاول		م42-	تأخر اجراءات تحويل العمل الى الورثة

جدول رقم (2) : التحصيل الدراسي لافراد العينة

التحصيل الدراسي	التكرار	النسبة المئوية
بكالوريوس هندسة	23	68
ماجستير هندسة	4	12
دكتوراه هندسة	7	20
المجموع	34	%100

جدول رقم (3) : سنوات الخبرة لافراد العينة

سنوات الخبرة	التكرار	النسبة المئوية	
10 – 5	6	18	44 % اقل من 15 سنة
15 – 11	9	26	
اكثر من 15	19	56	56 % اكثر من 15 سنة
المجموع	34	%100	

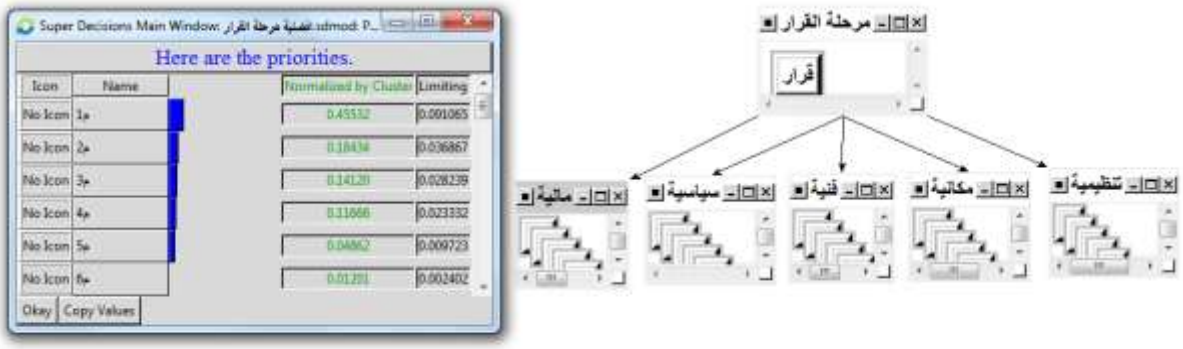

شكل رقم (1): نموذج من عملية التحليل الشبكي ANP

جدول رقم (4): نموذج من نتائج تحليل الشبكة التحليلية ANP لعلاقة تاثير المخاطر ومرحلة المشروع الانشائي

المخاطر	مرحلة تحديد الفكرة (مرحلة القرار)	مرحلة التعاقد	مرحلة التصميم	مرحلة التنفيذ
تنظيمية	(0.45532) أ1	(0.41724) أ1	(0.41753) أ1	(0.33688) أ1
	(0.18434) أ2	(0.22673) أ2	(0.17360) أ2	(0.26735) أ2
	(0.14120) أ3	(0.12321) أ3	(0.12964) أ3	(0.15717) أ3
	(0.11666) أ4	(0.00000) أ4	(0.12062) أ4	(0.09829) أ4
	(0.04862) أ5	(0.05370) أ5	(0.07088) أ5	(0.06076) أ5
	(0.00000) أ6	(0.10390) أ6	(0.03275) أ6	(0.03092) أ6
	(0.00000) أ7	(0.04286) أ7	(0.01093) أ7	(0.00000) أ7

جدول رقم (5): نتائج عملية التحليل الشبكي ANP – الاسبقية للمخاطر

مرحلة المشروع / نوع العقد / نوع العمل الانشائي	مخاطر تنظيمية										مخاطر مكانية										مخاطر فنية			
	م1	م2	م3	م4	م5	م6	م7	م8	م9	م10	م11	م12	م13	م14	م15	م16	م17	م18	م19	م20	م21
القرار	•	•	•	•	•						•	•		•	•	•	•	•		•	•
التعاقد	•	•	•		•	•	•			•	•	•		•	•			•	•	•	•
التصميم	•	•	•	•	•	•	•			•	•	•	•	•	•			•	•	•	•
التنفيذ	•	•	•	•	•	•				•	•	•	•	•	•			•	•	•	•
الجملة	•	•	•	•	•	•				•	•	•	•	•				•	•	•	•
تسليم المفتاح + جدول الكميات والاسعار + جدول الاسعار + الكلفة زائداً + التصميم والتنفيذ	•	•	•	•	•	•				•	•	•	•	•	•			•		•	•
مشاريع الكهرباء + شبكات الماء والمجاري + الابنية السكنية + المستشفيات + ابنية المعامل + الطرق والجسور	•	•	•	•	•	•				•	•	•	•	•	•			•	•	•	•
الابنية المدرسية	•	•	•	•	•	•	•			•	•	•	•	•	•			•	•	•	•
	مخاطر فنية					مخاطر سياسية					مخاطر مالية										
	م22	م23	م24	م25	م26	م27	م28	م29	م30	م31	م32	م33	م34	م35	م36	م37	م38	م39	م40	م41	م42
القرار	•						•	•	•		•						•	•	•	•	•
التعاقد	•	•			•	•	•	•	•		•	•	•	•	•	•	•	•			
التصميم	•	•			•		•	•	•	•	•	•	•	•	•						
التنفيذ	•	•			•	•	•	•	•		•	•	•	•	•	•	•				
الجملة	•	•			•	•	•	•	•		•	•	•	•	•	•	•	•			
تسليم المفتاح + جدول الكميات والاسعار + جدول الا سعار + الكلفة زائداً + التصميم والتنفيذ	•	•			•	•	•	•	•		•	•	•	•	•	•	•				
مشاريع الكهرباء + شبكات الماء والمجاري + الابنية السكنية + المستشفيات + ابنية المعامل + الطرق والجسور	•	•			•	•	•	•	•		•	•	•	•	•	•	•				
الابنية المدرسية	•	•			•	•	•	•	•		•	•	•	•	•	•	•				

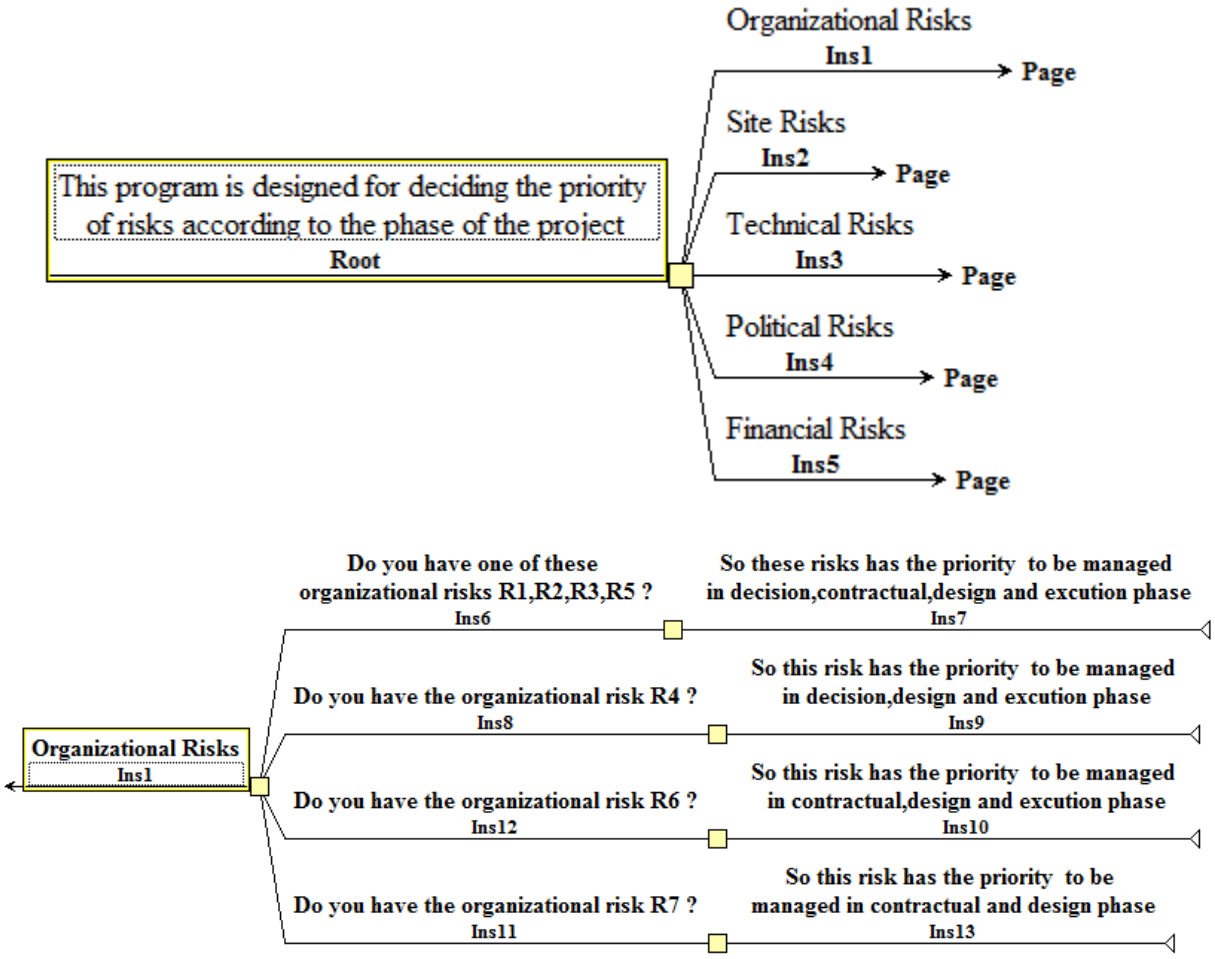
This program is designed for deciding the priority of risks according to the phase of the project
Root
Organizational Risks
Ins1
Page
Site Risks
Ins2
Page
Technical Risks
Ins3
Page
Political Risks
Ins4
Page
Financial Risks
Ins5
Page
Organizational Risks
Ins1
Do you have one of these organizational risks R1,R2,R3,R5 ?
Ins6
So these risks has the priority to be managed in decision,contractual,design and excution phase
Ins7
Do you have the organizational risk R4 ?
Ins8
So this risk has the priority to be managed in decision,design and excution phase
Ins9
Do you have the organizational risk R6 ?
Ins12
So this risk has the priority to be managed in contractual,design and excution phase
Ins10
Do you have the organizational risk R7 ?
Ins11
So this risk has the priority to be managed in contractual and design phase
Ins13

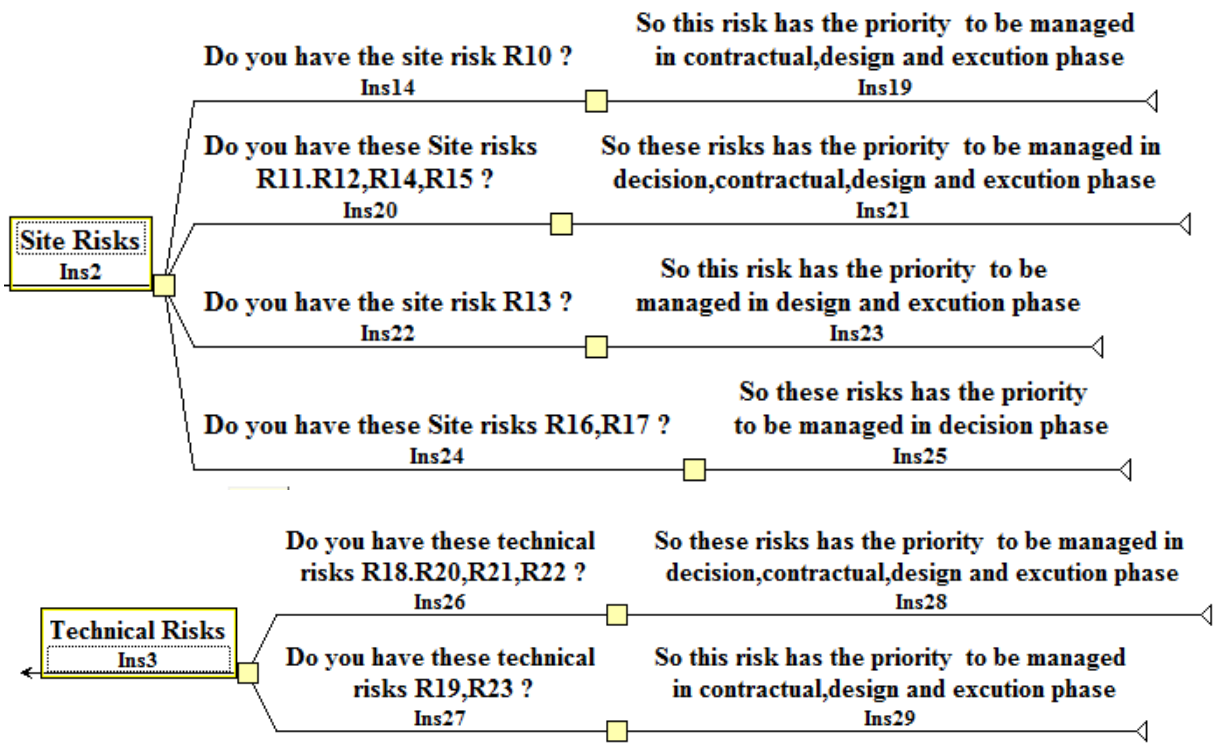
Site Risks
Ins2
Do you have the site risk R10 ?
Ins14
So this risk has the priority to be managed in contractual,design and excution phase
Ins19
Do you have these Site risks R11.R12,R14,R15 ?
Ins20
So these risks has the priority to be managed in decision,contractual,design and excution phase
Ins21
Do you have the site risk R13 ?
Ins22
So this risk has the priority to be managed in design and excution phase
Ins23
Do you have these Site risks R16,R17 ?
Ins24
So these risks has the priority to be managed in decision phase
Ins25
Technical Risks
Ins3
Do you have these technical risks R18.R20,R21,R22 ?
Ins26
So these risks has the priority to be managed in decision,contractual,design and excution phase
Ins28
Do you have these technical risks R19,R23 ?
Ins27
So this risk has the priority to be managed in contractual,design and excution phase
Ins29

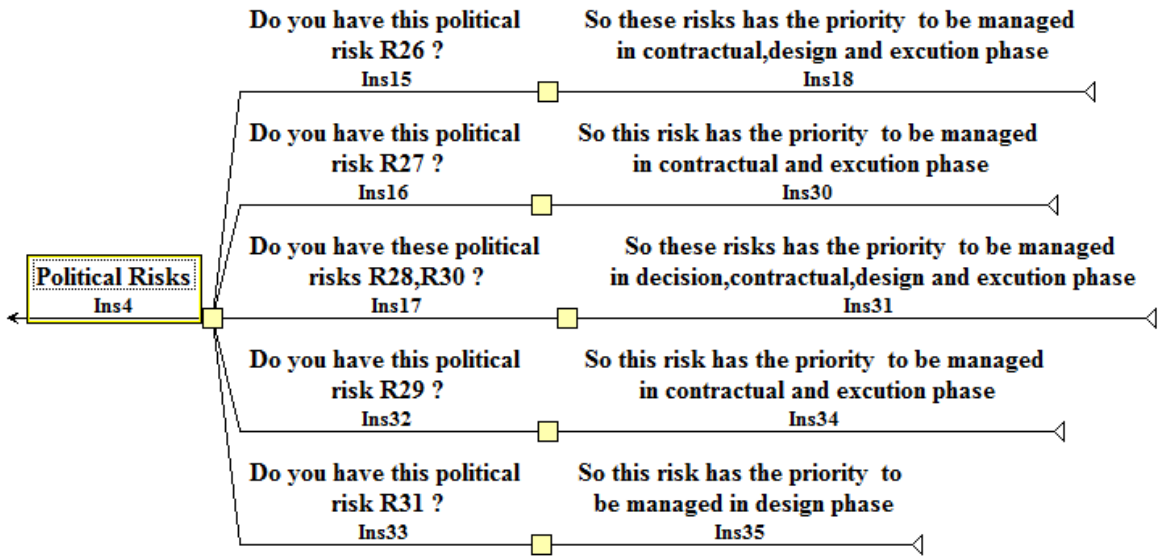

شكل رقم (2): شجرة القرار لبرنامج Vanguard Software System لصناعة القرار لادارة الاسبقية للمخاطر مع نوع المرحلة للمشروع

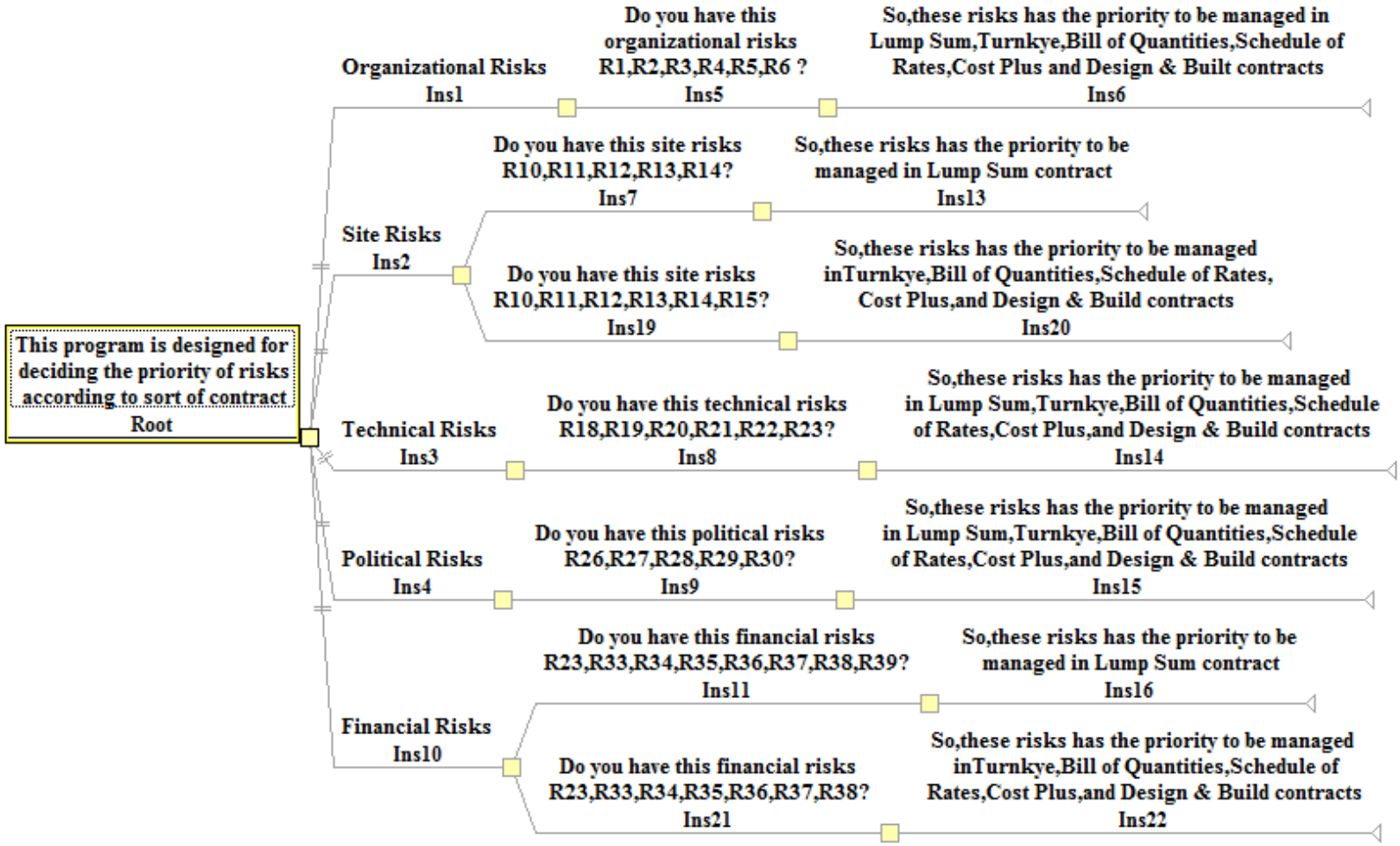

شكل رقم (3): شجرة القرار لبرنامج Vanguard Software System لصناعة القرار لادارة الاسبقية للمخاطر مع نوع العقد

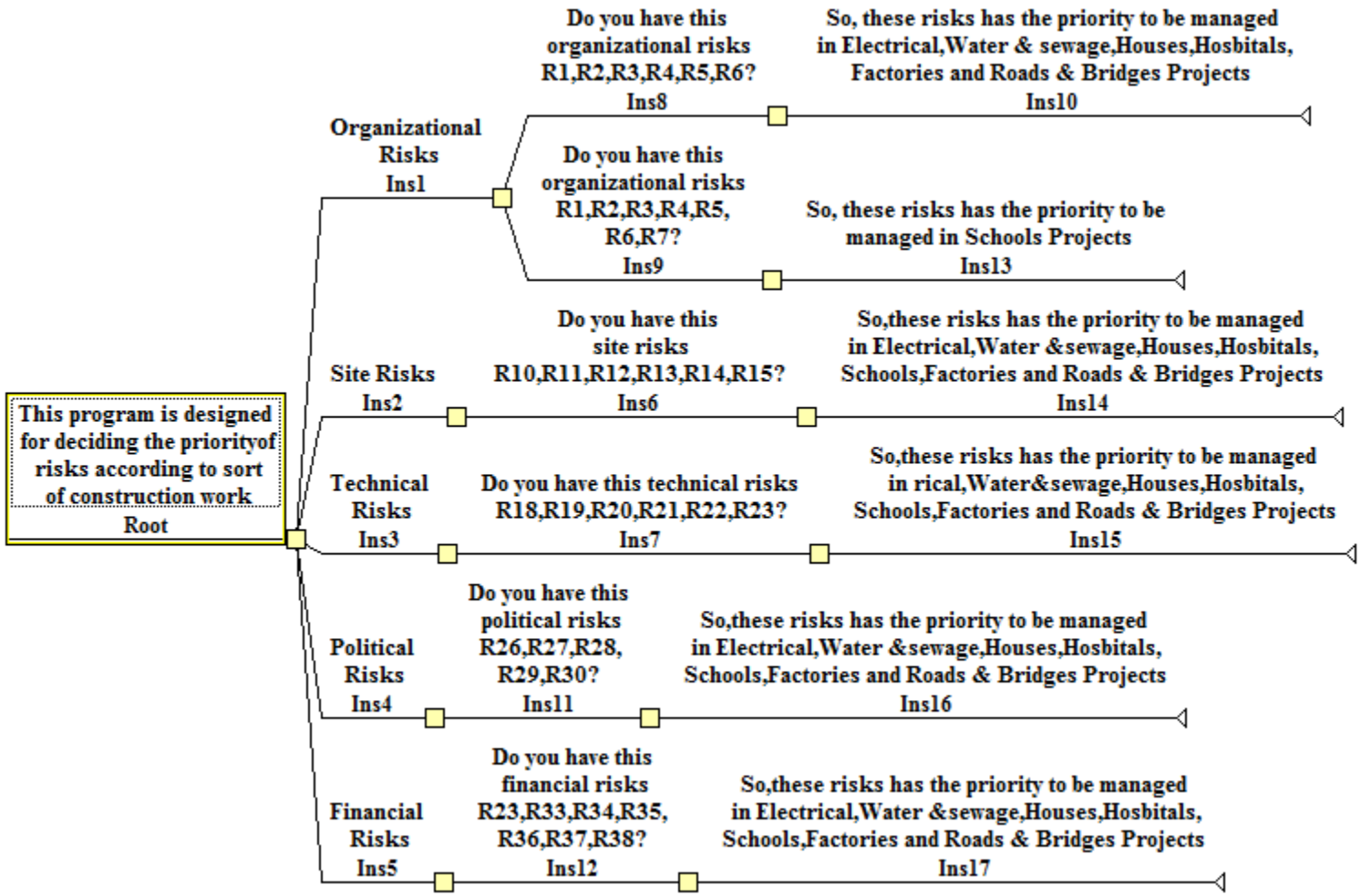

شكل رقم (4): شجرة القرار لبرنامج Vanguard Software System لصناعة القرار لادارة الاسبقية للمخاطر مع نوع العمل في المشروع الانشائي

الشكل رقم (5 – أ): تحديد تصنيف المخاطر

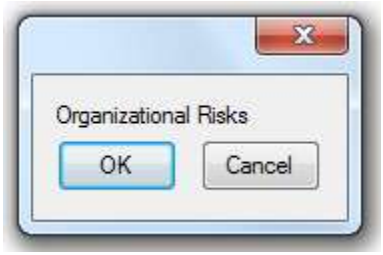

الشكل رقم (5 – ب): لتأكيد اختيار تصنيف المخاطرة

الشكل رقم (5 – جـ): انواع المخاطر ضمن التصنيف المختار

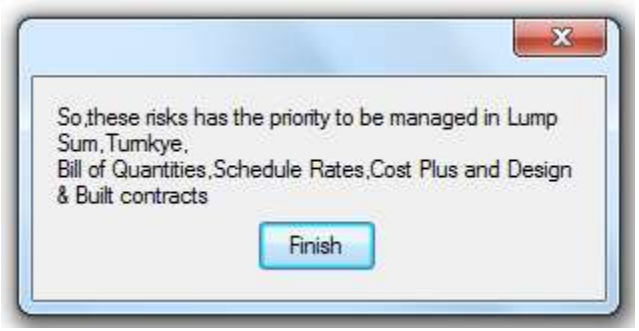

الشكل رقم (5 – د): القرار المطلوب لادارة المخاطر

الشكل رقم (5): خطوات البرنامج المقترح لصناعة قرار الاسبقية للمخاطر مع نوع العقد الانشائي (على سبيل المثال) بعد بناء شجرة القرار

Determination of the Optimum Conditions in Evaluation of Kiwi Juice as Green Corrosion Inhibitor of Steel in Hydrochloric Acid

Khalid Hamid Rashid
Lecturer
Chemical Engineering Department-University of Technology-Baghdad
Email: alhadidikhalid@yahoo.com

ABSTRACT

The corrosion protection of low carbon steel in 2.5 M HCl solution by kiwi juice was studied at different temperatures and immersion times by weight loss technique. To study the determination of the optimum conditions from statistical design in evaluation of a corrosion inhibitor, three variables, were considered as the most dominant variables. These variables are: temperature, inhibitor concentration (extracted kiwi juice) and immersion time at static conditions.

These three variables are manipulated through the experimental work using central composite rotatable Box – Wilson Experimental Design (BWED) where second order polynomial model was proposed to correlate the studied variables with the corrosion rate of low carbon steel alloy to estimate the coefficients by nonlinear regression analysis method based on Rosenbrock and Quasi-Newton estimation method in as few experiments as possible to determinate of the optimum conditions of the proposed polynomial adopted via *STATISTICA* software. The parametric study on corrosion inhibition process using response surface methodology (RSM) is presented in this paper.

The study shows that the immersion time and temperature of corroding medium had shown negative dependence of great significance in increase the corrosion rate while the other studied variable (i.e. inhibitor concentration) had shown large positive dependence in reduce the corrosion rate of low carbon steel alloy.

Optimum conditions for achieving the minimum corrosion rate are obtained from optimizing the above correlation and are found as follow: 42.86 °C temperature of corroding medium, 29.29 cm^3/L inhibitor concentration and 2.65 h immersion time. In these circumstances, the value of inhibition efficiency obtained was 96.09 %. It could be concluded that Box-Wilson experimental design was adequately applicable in the optimization of process variables and that kiwi juice sufficiently inhibited the corrosion for low carbon steel at the conditions of the experiment.

Keywords: RSM; corrosion inhibition; kiwi juice; hydrochloric acid solution

إيجاد الظروف المثلى في تقييم عصير الكيوي كمانع تآكل طبيعي للحديد في حامض الهيدروكلوريك

خالد حامد رشيد
مدرس
قسم الهندسة الكيمياوية - الجامعة التكنلوجية – بغداد

الخلاصة

تم دراسة حماية تآكل حديد منخفض الكاربون في محلول حامض الهيدروكلوريك (2.5 مولاري) بأستخدام عصير الكيوي كمثبط لعملية التاكل عند مختلف درجات الحرارة وفترات زمن غمر بأستخدام تقنية فقدان الوزن لحساب معدلات التآكل. لدراسة تحديد الظروف المثلى من التصميم الأحصائي في تقييم أداء مثبط عملية تآكل أُخذت بنظر الأعتبار ثلاثة متغيرات

أعتبرت الأكثر تأثيرًا على عملية التآكل. العوامل المؤثرة هي درجة الحرارة و تركيز المثبط (عصير الكيوي) و فترة زمن غمر عند ظروف ساكنة.
المتغيرات الثلاثة تم معالجتها من خلال تصميم التجارب العملية بإستخدام طريقة التصميم الدوار المركب المركزي (Box-Wilson) لربط المتغيرات أعلاه بمعادلة متعددة الحدود من الدرجة الثانية التي تشير الى العلاقة بين المتغيرات الثلاثة ومعدل التآكل لسبيكة الحديد منخفض الكاربون من خلال إيجاد المعاملات بأستخدام طريقة تحليل التراجع والأرتداد اللاخطي المعتمدة على طريقة حساب (Rosenbrock and Quasi-Newton) بأقل عدد تجارب ممكن لتحديد الظروف المثلى للمعادلة المفترضة المتعددة الحدود المعتمدة بواسطة (*STATISTICA* software). ذكرت دراسة العوامل على عملية تثبيط التاكل بأستخدام منهج سطح الأستجابة في هذه المقالة.
الدراسة تبين بأن زمن الغمر ودرجة حرارة محلول التآكل لها تأثيرا سلبيا في زيادة معدل التآكل في حين أن المتغير الآخر (تركيز المثبط) كان له تأثيرا أيجابيا كبيرا في تقليل معدل تآكل سبيكة حديد منخفض الكاربون . تم إستخراج الظروف المثلى للتجارب للحصول على أقل معدل تآكل وهي : درجة حرارة محلول التآكل 42.86 °C , تركيز المثبط 29.29 cm^3/L و زمن غمر 2.65 h. وعند هذه الظروف , قيمة كفاءة المادة المانعة للتاكل كانت 96.09 %. أستنتج من النتائج بأن التصميم العملي Box-Wilson قابل للتطبيق على نحو ملائم في أختيار الأفضل لمتغيرات العملية وعصير الكيوي له التأثيرعلى نحو كافي في تثبيط تآكل الحديد منخفض الكاربون عند ظروف التجربة.

الكلمات الرئيسيه: RSM ، تثبيط تآكل ، عصير كيوي ، محلول حامض الهيدروكلوريك

1. INTRODUCTION

In the chemical and engineering industry experimental designs are particularly applied to study of process variables and how they affect on the product, **Perry**, and **Green**, **2000**.

Three basic types of statistically designated experiments are most often used in chemical and engineering industry. These are 1. Fractional-Factorial design. 2. Box-Wilson design. 3. Factorial design. Box-Wilson designs and, in particular, the two-level Box-Wilson design, have been treated in the literature both theoretically and from application point of view, **Box** and **Hunto**, **2005**. However, it's desirable here to review briefly their major characteristics:

Consider the weight loss resulting from corrosion of a low carbon steel specimen has to be determined as function of temperature, inhibitor concentration and immersion time, and let the two levels of temperature, inhibitor concentration and immersion time. The experiments carried out under these conditions are presented in the experimental design.

Many metals and alloys which used in different human activities are susceptible to different mechanisms of corrosion due to their exposure to different corrosive media. Among these, low carbon steel is very important. One of the methods used to reduce the rate of metallic corrosion is addition of inhibitors. Many studies have been carried out to find suitable compounds to be used as corrosion inhibitors for this metal in different aqueous solutions. These studies reported that there are a number of organic and inorganic compounds which can inhibit corrosion of steel, **Musa**, **et al.**, **2010**, **Khadom**, **et al.**, **2009**, **Yaro**, **et al.**, **2000**. Many researchers were conducted to examine some naturally occurring substances as corrosion inhibitors for different metals in various environments, **El-Etre**, **et al.**, **2005**, **El-Etre**, **2003**.

The use of inhibitors is an important method of protecting materials against deterioration. Inhibitors are chemicals that often work by adsorbing themselves on the metallic surface by forming a film, **Ebenso**, **et al.**, **2009**, **Noor, 2008**, **Ebenso**, **et al.**, **2008**, **Oguzie**, **2006**, **Gazquez**, **2006**. Most corrosion inhibitors are either synthesized from cheap raw materials or are chosen from organic compounds containing electronegative functional groups and л-electrons in triple or conjugated double bonds. The sites of aromatic rings and hetro atoms (such as S, N, O and P) are the major adsorption centers for these inhibitors, **Dubey**, and **Sing, 2007**. Broad spectra of organic compounds are available as corrosion inhibitors. Of these, only very few are actually used in practice. This is partly due to the fact that desirable properties of an inhibitor usually

extend beyond those simply related to metal protection. Considerations of cost, toxicity, availability and environmental friendliness are of considerable important. Accordingly, the replacement of some toxic, expensive chemical inhibitors by inhibitors obtained from natural sources is necessary. Apart from being readily available, cheap and a renewable source of materials, naturally occurring substances are eco-friendly and ecologically acceptable. Naturally occurring substances are biodegradable and do not contain heavy metals or other toxic compounds. Among the so-called "green corrosion inhibitors" are organic compounds that act by adsorption on the metal surface, such as extracts of natural substances, **Raja**, and **Sethuraman**, **2008**. The efficiency of these organic corrosion inhibitors is related to the presence of polar functional groups with S, O or N atoms in the molecule, heterocyclic compounds and л-electrons. The polar function is usually regarded as the reaction center for the establishment of the adsorption process, **Roberge**, **1999**. One of these natural compounds is fruits. Fruit is a rich source of chemicals such as vitamins, minerals, organic acids and phenolic compounds. The kiwi juice includes different level of phenolic compounds. The hydroxybenzoic acids and hydroxycinnamic acids are the most common compounds in kiwi fruits, **Keith**, **2012**. Note that the kiwi juice extract use for the first time as natural inhibitor in this article to the corrosion of low carbon steel alloy in hydrochloric acid solution. **Alaneme**, and **Olusegun**, **2012** have studied the inhibitive property of lignin extract of sun flower (tithonia diversifolia) as green corrosion inhibitor in 1 M H_2SO_4 solution using experimental design. **Da Rocha**, **et al**., **2012** have studied the inhibitive action of grape pomace extract as green corrosion inhibitor against the corrosion of carbon steel in a 1 mol L^{-1} HCl solution using weight loss measurements. **Afia, et al**., **2014** have studied the inhibitive property of acid garlic essential oil as a green corrosion inhibitor in a 1 M HCl solution by weight loss method of monitoring corrosion rate.

Therefore, the present study of inhibition of kiwi juice on low carbon steel corrosion and the optimization of the independent variables is necessary, as well as important to the environment.

The experiments discussed in this work were designed to optimize the inhibition of low carbon steel by extracted kiwi juice where several variables, including temperature, inhibitor concentration and immersion time would influence the corrosion rate.

Design of experiment is a statistical procedure that can reduce significantly the number of experiment, keeping however, the reliability of the conclusions at high standard. The traditional experimental method, one factor at a time approach can hardly be used to establish relationships among all the experimental input factors and the output responses. Even though the traditional approach can be useful in finding predominate factors in this situation, it is difficult to observe the optimum value of the working parameters as no interaction among them is considered. To solve this problem and obtain a probable optimum, design of experiment (DOE) offers a better alternative to study the effect of variables and their responses with minimum number of experiments, **Giovanilton**, **et al**., **2011**, **Montgomery**, **2005**. A Box-Wilson is used to evaluate two or more factors simultaneously. The treatment is combination of level of the factors. The advantages of Box-Wilson design over one-factor-at-a-time experiment are that they are more efficient and they allow interactions to be detected. .

The aim of the present work is to investigate the influence of the operating parameters (temperature, inhibitor concentration of extracted kiwi juice and immersion time) on corrosion rate of low carbon steel alloy in hydrochloric acid solution under optimum conditions that are obtained by using Box-Wilson techniques, then estimation of the inhibition efficiency of extracted kiwi juice as green corrosion inhibitor in order to find a naturally, cheap and environmentally safe substance that could be used for inhibition purposes.

2. EXPERIMENTAL WORK

2.1 Metal Preparation

The material of working electrodes used in this study is low carbon steel in foil coupons of a tag shape were used as specimens. This material is cut of specimens by dimensions of (2×3×0.2 cm). Analysis of these specimens was carried out at National Center for Construction Laboratories and Research /Baghdad/Iraq. **Table 4** shows the nominal and the analytical chemical compositions of material used in this work. This analysis indicates that the main elements of material are within the standard limits.

2.2 Extraction of Inhibitor

Completely fresh ripe kiwi fruit weighing 2 kg was purchased from the local market (Baghdad-Iraq). The fruits washed in cold running tap water followed by distilled water, dried with clean tissue, and extracted the crust from it and then was squeezed mechanically to get corresponding juice. The resulting juice nomination in order to get a homogeneous solution. In this process, 1/2 liter of kiwi juice was obtained. The extracted juice was kept frozen at - 4 °C in glass graduated cylinder until further experiment. The concentrations of inhibitor were closer as 5, 15, 25, 35 and 45 cm^3/L kiwi juice concentration.

2.3 Box-Wilson Experimental Design (BWED) and Optimization of Variables

The running expense for each experiment is relatively high which leads to need of design of experiment. The design of experiment is a statistical tool which helps to minimize the number of experiments so that appropriate data will be collected, the minimum number of experiments will be performed to acquire the necessary technical information and suitable statistical methods will be used to analyze the collected data. The initial task of this stage is to find out the key process control parameters with their ranges and performance evaluation parameter (output) that is to be measured. The levels of each variable represent the range for which the effect of that variable is desired to be known.

Box-Wilson experimental design is easy to apply to many engineering situations, making it a powerful yet simple tool and a series of tests for characterizing a physical mechanism. These series of experiments have been developed which efficiently serve as a basic deriving the mathematical model of process, **Jeff**, and **Michael**, **2009**. For three variables, the quadratic polynomial equation can be represented as follows:

$$Y = B_0 + B_1X_1 + B_2X_2 + B_3X_3 + B_{11}X_1^2 + B_{22}X_2^2 + B_{33}X_3^2 + B_{12}X_1X_2 + B_{13}X_1X_3 + B_{23}X_2X_3 \quad (1)$$

A preliminary step is to set up the relationships between the coded level and the corresponding real variables, which are required in the determination of experimental range by the following equation.

$$X_{coded} = \frac{X_{real} - X_{center}}{\frac{X_{center} - X_{min}}{\sqrt{k}}} \quad (2)$$

The coded variables take the value between -2 and 2 in accordance with the central composite rotatable suggested by Tarantino, **Tarantino**, **2010**.

The range of real variables for the system could be represented in **Table 1**.

The expression of coded level for the system is estimated from Eq. (2)

$$X_1 = \frac{T - 45}{8.66} \quad (3)$$

$$X_2 = \frac{C - 25}{11.55} \quad (4)$$

$$X_3 = \frac{t - 3}{1.15} \quad (5)$$

Where:
T = Temperature of corroding medium (°C)
C = Inhibitor Concentration (cm^3/L)
t = Immersion Time (h)
Table 2 shows the relationship between the coded level and corresponding real variables.
The number of experiments that must be done shown in **Table 3**.

2.4 Experimentation

The cleaning procedure was as follows: The specimens were first degreased with analar benzene and acetone at 25 °C, and then annealed in a vacuum oven at 550 °C for 1.5 h and cooled to room temperature. Specimens were abraded in sequence under running tap water using emery paper of grade numbers 220,320,400 and 600, rinsed with running tap water followed by distilled water, dried with clean tissue, immersed in acetone and benzene, and kept in desiccator over silica gel bed until time of use. The specimens were completely submerged in 200 cm^3 corrosion solution at 2.5 M HCl, 30, 37.5, 45, 52.5 and 60 °C, and 5, 15, 25, 35 and 45 cm^3/L kiwi juice concentration for a period of time 1, 2, 3, 4 and 5 h. After each experiment the specimens were washed with running tap water followed by distilled water, dried with clean tissue, immersed in acetone and benzene, and kept in desiccators over silica gel bed to dry, then weighed by high accuracy electronic balance.

3. RESULTS AND DISCUSSION

The corrosion of low carbon steel in 2.5 M HCl solution containing various concentrations of inhibitor at different temperatures and immersion times was studied by weight loss measurments. The corrosion rate of low carbon steel was determined using the relation:

$$C.R = \frac{Weight\ loss\ (g)}{Area\ (m^2)\ x\ Time\ (day)} \quad (6)$$

$C.R$: Corrosion rate (g/m^2. day) (gmd)

The percentage inhibition efficiency (IE (%)) was calculated at optimum conditions using the relationship, **Alaneme**, and **Olusegun**, **2012**:

$$IE\% = \frac{W_{uninhibt} - W_{inhibit}}{W_{uninhibit}} \times 100 \quad (7)$$

Where $W_{uninhibt}$ and $W_{inhibit}$ are the corrosion rates in absence and presence of inhibitor respectively.

Table 5 will be first fitted through nonlinear regression analysis to estimate the coefficients of the proposed model. **Table 5** also shows the corrosion rate of the specimens that reached through the experimental work and the predicated corrosion rate, which are designed according to the central composite rotatable design method.

3.1 Response Surface Methodology:

Response Surface Methodology (RSM) can be regarded as a statistical technique for optimizing the objective functions through some mathematical methods. Basically, this involves doing several experiments. Using the result of one experiment, direction for what to do next is provided, **Lenth**, **2010**. The field of RSM consists of the experimental strategy for exploring the space of the process or independent variables, empirical statistical modeling to develop an appropriate approximating relationship between the yield and process variables and optimization methods for finding the values of process variables that produce desirable values of the response, **Acherjee**, **et al.**, **2009**. The main objective of RSM is to find the combination of factor levels to achieve the optimal response.

In the present work the RSM is used to study the parametric effect of process parameters on corrosion rate. The result of experiment is used to develop the regression model as discussed in the following section. The effect of temperature, inhibitor concentration and immersion time on corrosion rate is shown graphically in **Fig. 3** through **Fig. 5** by constructing the response surface and contour diagram.

Multiple regression analysis (MRA) is one of the most widely used statistical techniques for analyzing multifactor data, **Davim**, **et al.**, **2008**. In the present work a regression model is developed by establishment of correlation between the process control parameters such as temperature, inhibitor concentration and immersion time with the output parameter namely corrosion rate, one can use this relationship in various algorithms. A quadratic regression model for response corrosion rate ($C.R$) is developed based on experimental results using the coded data of the central composite rotatable design, **Table 6** the coefficients of the 2nd order polynomial were estimated by implementing nonlinear least squares regression analysis technique based on Rosenbrock and Quasi-Newton estimation method via the *STATISTICA* software of version 10.1 can be used for estimation of coefficients B_0, B_1,…., B_{23}. This model will help to predict the response as a function of independent variables and their interactions.

In order to obtain the second-order response surface model equation the following equation may be assumed:

$$Y = B_0 + \sum_{i=1}^{n} B_i X_i + \sum_{i=1}^{n} B_{ii} X_i^2 + \sum_{i<j}^{n} B_{ij} X_i X_j + e_i \quad (8)$$

Where Y is the predicted response, B_0 the intercept coefficient, B_i the linear terms, B_{ii} the squared terms, B_{ij} the interaction terms, X_i and X_j are coded levels of the process control variables, the residual, e_i measures the experimental error of the observation number and n is the total number of designed variables, **Jian-Ping**, **et al.**, **2007**, **Montgomery**, **2005**. The coefficients of the model for the corresponding response are estimated using multiple regression analysis technique included in RSM. The response surfaces of corrosion rate can be expressed by the following quadratic equation in terms of coded values and real units.

$$C.R_{weight\ loss\ (gmd)} = 70.41 + 8.73\,T - 18.44\,C + 10.42\,t + 10.24\,T^2 + 22.34\,C^2 + 12.56\,t^2 - 0.34\,T \times C + 7.42\,T \times t + 1.11\,C \times t \quad (9)$$

Where, T = Temperature (°C)
C = Concentration of Inhibitor (cm^3/L)
t = Immersion Time (h)

3.2 Statistical and Mathematical Analysis:

From **Table 5**:
$e_i = (C.R_E - C.R_P)$
An estimation of the experimental error variance (S_r^2) is obtained by dividing the residual sum of squares (e_i) by number of degree of freedom(γ); where:

$$\gamma = N_i - N_{\text{coff}} \quad (10)$$

Where:
N_i: No. of experiments
N_{coff}: No. of coefficients in the model

$$\gamma = 18 - 10 = 8 \quad (11)$$

$$S_r^2 = \sum e_i^2/\gamma \quad (12)$$

The estimated variance of coefficients (S_b^2) is then calculated by the following formula:

$$S_b^2 = S_r^2/\sum X^2 \quad (13)$$

The significant coefficient can be estimated by comparing the value of (B^2/S_b^2) to the critical value $F_{0.95(1,8)} = 0.29$ of the F-distribution at 95% level of confidence, **Jeff**, and **Michael**, **2009**. The results of these calculations are shown in **Table 7** for low carbon steel alloy. The final form of the proposed model was as follows:

$$C.R_{weight\ loss\ (gmd)} = 70.41 + 8.73\,T - 18.44\,C + 10.42\,t + 10.24\,T^2 + 22.34\,C^2 + 12.56\,t^2 + 7.42\,T \times t \quad (14)$$

The accuracy of an empirical model can also be done by means of statistical parameters, for example, correlation coefficient. The correlation coefficient (R^2) is a statistical measure of the strength of correlation between the predicted and measured values, **Devore**, **2005**. For the current problem, the following result is obtained: $R^2 = 0.895$. **Fig. 2** shows predicted corrosion rate by Eq. (14) against experimental one.

3.3 Inhibition Optimization Result and Estimating the Percentage Inhibition Efficiency:

According to Eq. (14), using *POLYMATH* software version 4.02 in terms of minimum corrosion rate, the optimum values were obtained. The optimum values of the studied variables in coded and real form are listed in **Table 8** below for low carbon steel alloy. A validation experiment was conducted at the specified optimized values and the results were used to calculate the response (corrosion rate). The practical value of the corrosion rate at the optimum conditions was comparable with the theoretical value and the result was closed.

The percentage inhibition efficiency at the optimum conditions can be calculated from the Eq. (7).

$$IE\% = \frac{0.1049 - 0.0041}{0.1049} \times 100 = 96.09\ \%$$

3.4 Influence of Process Parameters on Corrosion Rate:

The aim of this study was to find a corrosion rate whose features would have been previously defined from the operative conditions extracted from the quadratic mathematical model.
Because the direct exploitation of the equation was delicate, it was convenient to restore it under a graphic representation; while fixing one of the three factors of the survey, it was possible to represent the response surface materializing the surface of regression in a three-dimensional space. It was also possible to project the equation in a design under isoresponse curves, interpreted as card curves level.

A. Evolution of corrosion rate as a function of the temperature and the concentration of corrosion inhibitor:

Fig. 3 shows the evolution of the corrosion rate as a function of the temperature and the concentration of corrosion inhibitor (extracted kiwi juice). It can be seen that the inhibitor concentration has a strong influence on the tentative response. The minimal corrosion rate is obtained for an inhibitor concentration of 0.37 in coded variable, i.e., 29.29 cm^3/L in real variable. Considering simultaneous effects of temperature and inhibitor concentration is presented in **Fig. 3** contour plot. The figure shows, in high temperature (60 °C), the increase of corrosion rate is higher than in lower temperature (30 °C). This is also in close agreement with the research done by, **Da Rocha, et al., 2012**.

B. Evolution of corrosion rate as a function of the temperature and the immersion time:

Fig. 4 shows the synergism between the two factors: the temperature and immersion time in corrosion rate at inhibitor concentration 29.29 cm^3/L. It can be noted that the effect of the immersion time differed according to the corrosion rate's variation. This effect becomes positive and even more important when the corrosion rate is degraded (reduced). Analysis of corrosion rate as effects of interaction between temperature and immersion time is shown in **Fig. 4** contour plot. The model shows a decrease followed by growing of corrosion rate due to temperature and immersion time at the optimum condition of inhibitor concentration 29.29 cm^3/L and this in agreement with, **Alaneme**, and **Olusegun**, **2012**.

C. Evolution of corrosion rate as a function of the concentration of corrosion inhibitor and the immersion time:

Fig. 5 represents the evolution of the corrosion rate as a function of the inhibitor concentration and the immersion time. This figure shows that the corrosion rate initially decreased when the inhibitor concentration and immersion time increased. This evolution was however more accentuated up to a concentration of 29.29 cm^3/L kiwi juice until it reaches a minimum value of corrosion rate at 2.65 h, which contributes to the great tendency of corrosion protection causes decrease in corrosion rate then it begins to increase again with increasing the inhibitor concentration and immersion time. **Fig. 5** contour plot presents a polynomial surface response relating to effect of inhibitor concentration and immersion time on corrosion rate. It is shown that different corrosion rate is observed for inhibitor concentration and immersion time. Immersion time increased corrosion rate from 70-220 gmd along the immersion time setting (1-5

h). Concentration of inhibitor from 5-45 cm^3/L has decreased corrosion rate from 270-70 gmd. This is also in close agreement with the research done by, **Afia, et al., 2014**.

4. CONCLUSION

1. The results of experiment are extended to develop the second order polynomial regression model of the objective function (corrosion rate) in terms of three variables (i.e., temperature of corroding medium, inhibitor concentration and immersion time) using response surface methodology (RSM) gives Eq. (14), which adequately describes the behavior of the process throughout the studied range.
2. The three variables effect on the corrosion rate in following order:

   Inhibitor concentration > Immersion time > Temperature**.**
3. The green corrosion inhibitor made up the kiwi juice extract successfully reduced the corrosion rates of low carbon steel alloy in 2.5 M HCl solution.
4. The optimum conditions as predicted from Eq. (14) is 42.86 °C temperature of corroding medium, 29.29 cm^3/L inhibitor concentration and 2.65 h of immersion time for low carbon steel alloy.
5. Kiwi juice extract acts as a corrosion inhibitor of low carbon steel with inhibition efficiency of 96.09 % under the optimum conditions.
6. The corrosion rate of low carbon steel alloy in 2.5 M HCl solution in presence of kiwi juice extract, increases with increasing temperature and immersion time, and decreased with increasing concentration of inhibitor.
7. The analysis of statistical central composite rotatable Box–Wilson Experimental Design (BWED), generally, shows that the interaction effects on the corrosion rate by weight loss technique (within the studied range) is less pronounced compared with the main and square variables except the interaction effect of ($T \times t$) in presence of extracted kiwi juice.

ACKNOWLEDGEMENT

The author would like to thank National Center for Construction Laboratories and Research /Baghdad/Iraq for financial support.

5. REFERENCES

- Acherjee, B., Misra, D., Bose, D. and Venkadeshwaran, K., 2009, *Prediction of Weld Strength and seam Width for Laser Transmission Welding of Thermoplastic using Response Surface Methodology*, Optics & Laser Technology, No. 41, PP. 956-967.

- Afia, L., Benali, O., Salghi, R., Ebenso, E. E., Jodeh, S., Zougagh, M. and Hammouti, B., 2014, *Steel Corrosion Inhibition by Acid Garlic Essential Oil as a Green Corrosion Inhibitor and Sorption Behaviour,* Int J. Electrochem. Sci., Vol. 9, PP. 8392-8406.

- Alaneme, K. K. and Olusegun, S. J., 2012, *Corrosion Inhibition Performance of Lignin Extract of Sum Flower (Tithonia Diversifolia) on Medium Carbon Low Alloy Steel Immersed in H_2SO_4 Solution*, Leonardo Journal of Sciences, Vol. 20, No. 1-6, PP. 59-70.

- ASTM, Annual book, 2004, *Engineering Handbook-Technical Information*, 1st Edition, Huyett.

- Box, H. and Hunto, 2005, *Statistics for Experiments*, 2nd Edition, John-Wiley and Sons, Inc., New York, USA.

- Da Rocha, J. C., Ponciano Gemes, J.A.C., Delia, E., Gil Cruz, A. P., Cabral, L. M.C., Torres, A. G. and Monteiro, M. V. C., 2012, *Grape Pomace Extracts as Green Corrosion Inhibitors for Carbon Steel in Hydrochloric Acid Solutions*, Int. J. Electrochim. Sci., Vol. 7. PP. 11941-11956.

- Davim, J.P., Oliveira, C. and Cardoso, A., 2008 ,*Predicting the Geometric form of Clad in Laser Cladding by Powder Using Multiple Regression Analysis (MRA)*,Materials and Design, No.29, PP.554-557.

- Devore, P., 2005, *The Exploration and Analysis Data*, 5th Edition Thomson Learning, Belmont, USA.

- Dubey, A. K. and Sing, G., 2007, *Corrosion Inhibition of Mild Steel Using Brijj-30*, Portugaliae Electrochimica Acta, Vol. 25, PP. 205-219. http://dx.doi.org/10.4152/pea.200702205

- Ebenso, E.E., Eddy, N.O. and Odongenyi, A.O., 2009, *Inhibition of the Corrosion of Mild Steel by Methocarbamol*, Portugaliae Electrochimica Acta, Vol. 27, PP. 13-22.

- Ebenso, E.E., Eddy, N.O. and Odongenyi, A.O., 2008, *Corrosion Inhibitive Properties and Adsorption Behaviour of Ethanol Extract of Piperguinensis as a Green Corrosion Inhibitor for Mild Steel in* H2SO4, African Journal of Pure and Applied Chemistry, Vol. 4, PP. 107-115.

- El-Etre, A. Y., Abdallah, M. and El-Tantawy, Z. E., 2005, *Corrosion Inhibition of Some Metals Using Lawsonia Extract*, Corros. Sci., No. 47, PP. 389-395.

- El-Etre, A. Y., 2003, Corros. Sci., No. 45, P. 2485.

- Gazquez, J. L., 2006, *Quantum Chemical Study of the Inhibitive Properties of 2-Pyridyl-Azoles*, The Journal of Physical Chemistry, Vol. 110, PP. 8928-8934. http://dx.doi.org/10.1021/jp057143y

- Giovanilton, F. S., Fernando, L. C. and Andrea, L.O., 2011, *Application of Surface Methodology for Optimization of Biodiesel Production by Trans esterification of Soybeam Oil with Ethanol*, Fuel Processing Technology, Vol. 92, PP. 407-413. http://dx.doi.org/10.1016/j.fuproc.2010.10.002

- Jeff Wu, C. F. and Michael, S.H., 2009, *Experiments: Planning, Analysis and Optimization*, 2nd Edition, John-Wiley and Sons, Inc., New York, USA.

- Jian-Ping, W., Yong-Zhen, C., Xue-Wu G. and Han-Qing, Y., 2007, *Optimization of Coagulation-Flocculation Process for A Paper-recycling Wastewater Treatment Using Response Surface Methodology*, Colloids and surfaces A: Physicochem. Eng. Aspects, No. 302, PP.204-210.

- Keith, S., 2012, *Kiwi fruit Overview of Potential Health Benefits*, Nutrition and Food, Vol. 47, No. 3, PP.133-147.

- Khadom, A. A., Yaro, A. S., Al Taie, A. S. and Kadum, A. A. H., 2009, *Electrochemical, Activations and Adsorption Studies for The Corrosion Inhibition of Low Carbon Steel in Acidic Media*, Portug. Electrochim. Acta, Vol. 27, No. 6, PP. 699-712.

- Lenth, R. V., 2010, *Response-Surface Methods in R Using RSM*, Journal of Statistical Software, No.28, July.

- Montgomery, D.C., 2005, *Design and Analysis of Experiments*, 6th Edition, John Wiley and Sons, New York, USA.

- Musa, A. Y., Khadom, A. A., Kadhum, A. A., Mohamad, A. B. and Takriff, M. S., 2010, *Kinetic Behavior of Mild Steel Corrosion Inhibition by 4-Amino-5-Phenyl-4H-1,2,4-Trizole-3-Thiol*, J. Taiwan Inst. Chem. Eng., No.41, PP. 126-128.

- Noor, E. A., 2008, *Comparative Study of Corrosion Inhibition of Mild Steel by Aqueous Extract of Fenugreek Seeds and Leaves in Acidic Solution*, Journal of Engineering and Applied Sciences, Vol. 4, PP. 23-30.

- Oguzie, E. E., 2006, *Adsorption and Corrosion Inhibitive Properties of Azadirechtaindica in Acid Solution*, Pigment and Resin Technology, Vol. 35, PP. 334-340. http://dx.doi.org/10.1108/03699420610711335

- Perry, R.H. and Green, D.W., 2000, *Chemical Engineering Handbook*", 8th Edition, McGraw-Hill, United States.

- Raja, P. B. and Sethuraman, M. G., 2008, *Natural Products as Corrosion Inhibitor for Metals in Corrosive Media-A review*, Mater. Lett., Vol. 62, PP. 113-116.

- Roberge, P. R., 1999, *Corrosion Inhibitors, in: Handbook of Corrosion Engineering*, McGraw-Hill, New York, PP. 833-862.

- Tarantino, L., 2010, *Design and Analysis of Industrial Experiments*", 1st Edition, Tetra Pak.

- Yaro, A. S., Abdul Masih, N. Sh. and Khadom, A. A., 2000, *The Influence of Temperature on Corrosion Inhibition of Carbon Steel in Air –Saturated 7N H_3PO_4 by Potassium Iodide*, Iraqi, J. Chem. Petrol. Eng., No. 1, PP.83-87.

Table 1. The experimental range of variables.

Temperature (°C)	Inhibitor Concentration (cm^3/L)	Immersion Time (h)
30-60	5-45	1-5

Table 2. Real and coded of the independent variables used in RSM study.

Variables	Levels				
$X_1,\ X_2,\ X_3$	-2	-1	0	1	2
$X_1 = \text{Temperature (°C)}$	30	37.5	45	52.5	60
$X_2 = \text{Inhibitor Concentration } (cm^3/L)$	5	15	25	35	45
$X_3 = \text{Immersion Time (h)}$	1	2	3	4	5

Table 3. Sequence of experiments according to central composite rotatable experimental design.

Exp. No.	Coded Variables			Real Variables		
	X_1	X_2	X_3	Temp. (°C)	Inhibitor Conc. (cm^3/L)	Immersion Time (h)
1	-1	-1	-1	37.5	15	2
2	1	-1	-1	52.5	15	2
3	-1	1	-1	37.5	35	2
4	1	1	-1	52.5	35	2
5	-1	-1	1	37.5	15	4
6	1	-1	1	52.5	15	4
7	-1	1	1	37.5	35	4
8	1	1	1	52.5	35	4
9	-2	0	0	30	25	3
10	2	0	0	60	25	3
11	0	-2	0	45	5	3
12	0	2	0	45	45	3
13	0	0	-2	45	25	1
14	0	0	2	45	25	5
15	0	0	0	45	25	3
16	0	0	0	45	25	3
17	0	0	0	45	25	3
18	0	0	0	45	25	3

Table 4. A nominal, **Astm**, **2004** and analytical chemical composition (wt. %) of low carbon steel alloy.

Metal	Fe	C	Mn	Si	P	S	Cr	Mo	Ni	Al
Nominal	Rem.	0.02-0.13	0.3-0.6	0.002	0.004	0.005	0.024	0.0008	0.014	0.003
Analytical	Rem.	0.040	0.309	0.004	0.005	0.007	0.021	0.0009	0.010	0.004

Table 5. Two-level central composite rotatable experimental design of the independent variables with the observed, predicted values and experimental error for the response.

Exp. No.	Coded Variables			Real Variables			Exp. Corrosion Rate	Predicted Corrosion Rate	Corresponding residual
	X_1	X_2	X_3	Temp. (°C)	Inhibitor Conc. (cm^3/L)	Immersion Time (h)	$C.R_E$ (gmd)	$C.R_p$ (gmd)	$e_i = C.R_E - C.R_P$
1	-1	-1	-1	37.5	15	2	100.53	123.04	-22.51
2	1	-1	-1	52.5	15	2	125.88	126.33	-0.45
3	-1	1	-1	37.5	35	2	110.17	84.61	25.56
4	1	1	-1	52.5	35	2	111.45	86.54	24.91
5	-1	-1	1	37.5	15	4	130.44	126.81	3.63
6	1	-1	1	52.5	15	4	162.76	159.79	2.97
7	-1	1	1	37.5	35	4	121.82	92.83	28.99
8	1	1	1	52.5	35	4	175.49	124.45	51.04
9	-2	0	0	30	25	3	90.35	93.92	-3.57
10	2	0	0	60	25	3	103.87	128.84	-24.97
11	0	-2	0	45	5	3	219.09	196.64	22.45
12	0	2	0	45	45	3	71.89	122.87	-50.98
13	0	0	-2	45	25	1	100.33	99.82	0.51
14	0	0	2	45	25	5	112.44	141.49	-29.05
15	0	0	0	45	25	3	63.45	70.41	-6.95
16	0	0	0	45	25	3	65.32	70.41	-5.09
17	0	0	0	45	25	3	61.87	70.41	-8.54
18	0	0	0	45	25	3	62.45	70.41	-7.96

Table 6. The coefficient values of the predicted correlation.

Coeff.	B_0	B_1	B_2	B_3	B_{11}	B_{22}	B_{33}	B_{12}	B_{13}	B_{23}
Value	70.41	8.73	-18.44	10.42	10.24	22.34	12.56	-0.34	7.42	1.11
Correlation Coefficient (R^2)			0.895			Proportion of Variance			0.67	
Final Value of loss function			10042.18							

Table 7. Analysis of variance (ANOVA) for the fitted model.

Constant Estimated	ΣX^2	Estimated Coefficient (B)	Variance $Sb^2 = Sr^2/\Sigma X^2$	F-value $= B^2/Sb^2$	$F_{0.95(1,8)} = 0.29$
B_1	16	8.73	78.4539	0.97	S*
B_2	16	-18.44	78.4539	4.33	S
B_3	16	10.42	78.4539	1.38	S
B_{11}	16	10.24	78.4539	1.34	S
B_{22}	16	22.34	78.4539	6.36	S
B_{33}	16	12.56	78.4539	2.01	S
B_{12}	8	-0.34	156.9078	0.001	NS**
B_{13}	8	7.42	156.9078	0.35	S
B_{23}	8	1.11	156.9078	0.01	NS

(*) Significant
(**) Non-significant

Table 8. Optimum values of the process variables for minimum corrosion rate.

Variables	Optimum Values (low carbon steel alloy)	
	Coded	Real
X_1 = Temperature (°C)	-0.25	42.86
X_2 = Inhibitor Concentration (cm^3/L)	0.37	29.29
X_3 = Immersion Time (h)	-0.30	2.65
Function Minimum (Corrosion rate, gmd)	62.35	

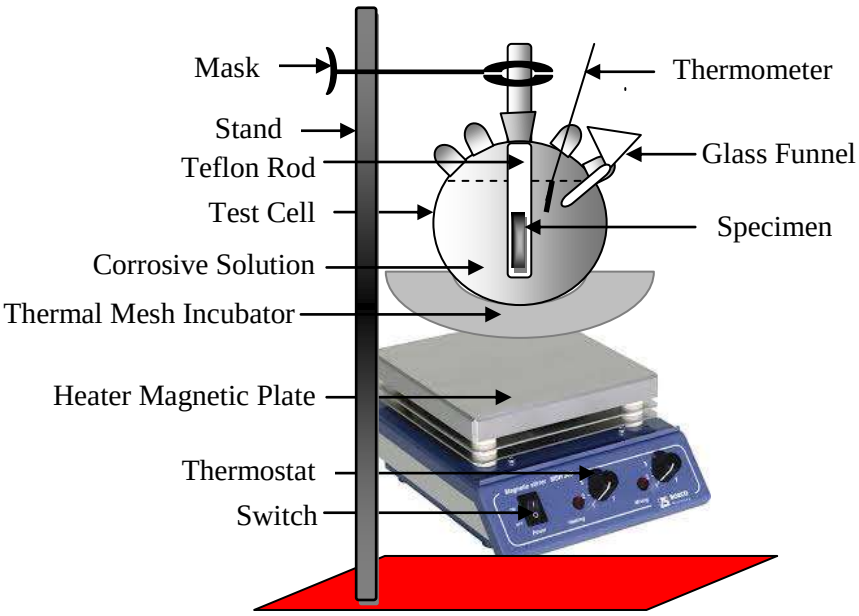

Figure 1. Experimental set-up for weight loss investigation.

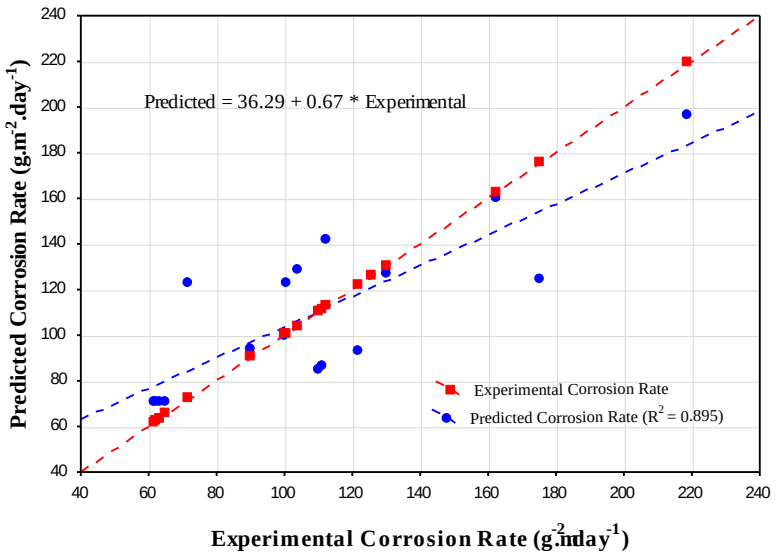

Figure 2. Predicted corrosion rate versus experimental corrosion rate.

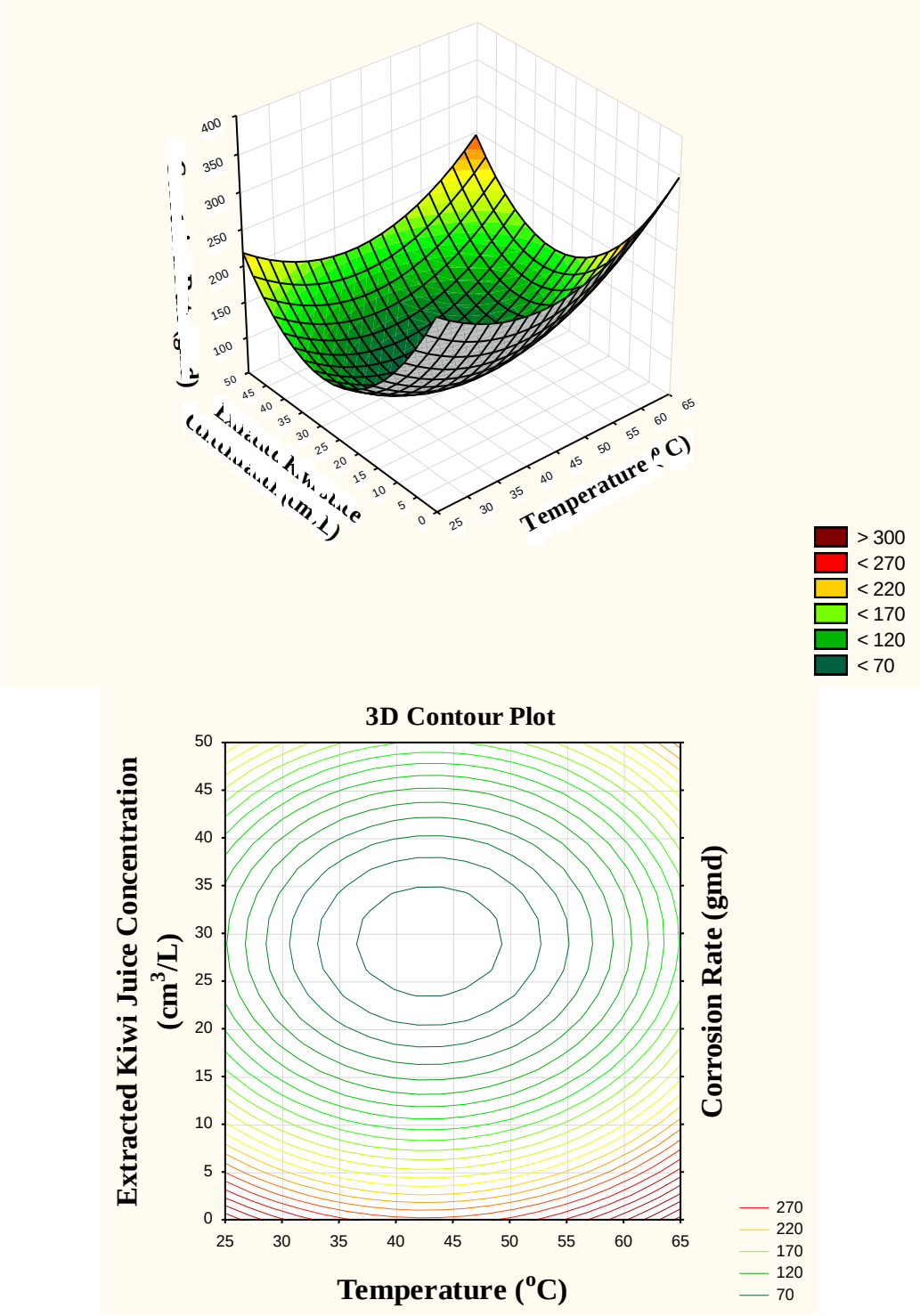

Figure 3. Response surface plot (top) and contour plot (bottom) showing the variation of corrosion rate as a function of the temperature and extracted kiwi juice concentration at the optimum value (2.65 h).

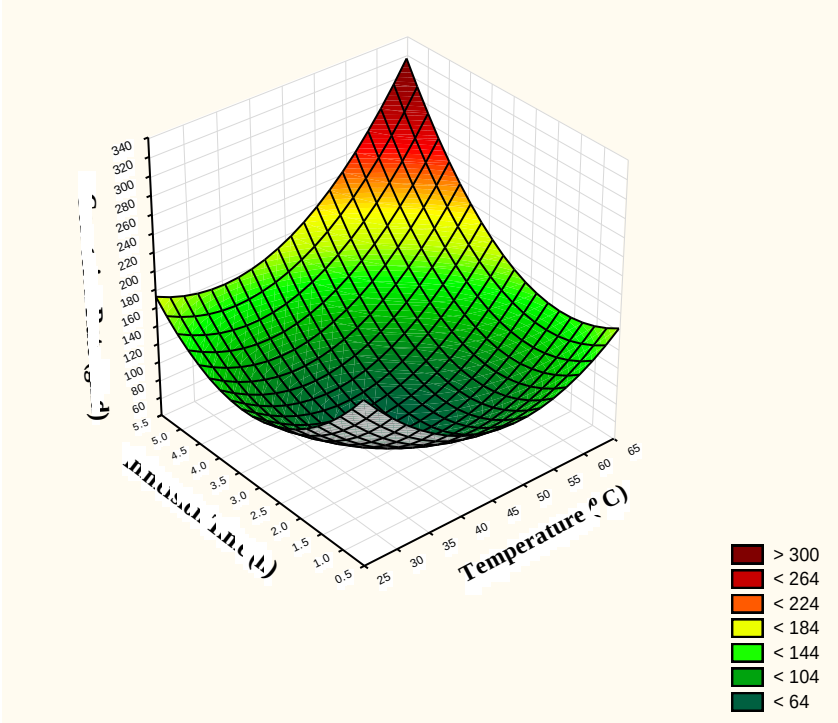

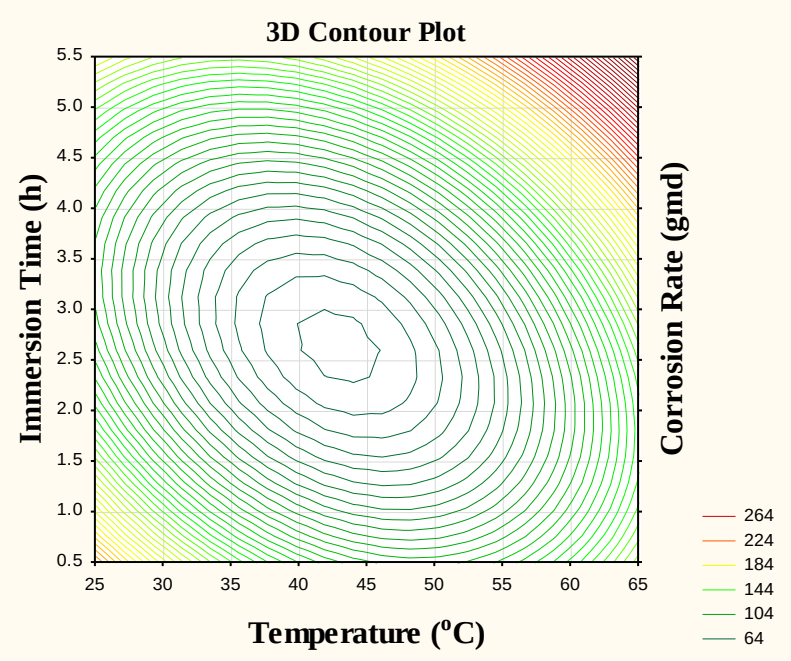

Figure 4. Response surface plot (top) and contour plot (bottom) showing the variation of corrosion rate as a function of the temperature and immersion time at the optimum value (29.29 cm^3/L).

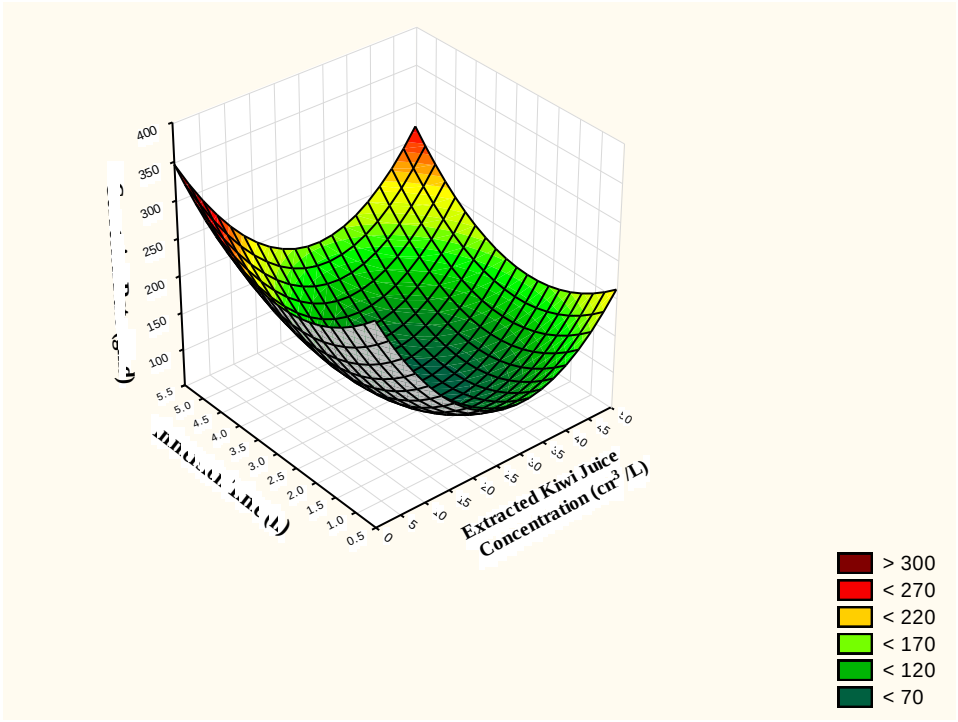

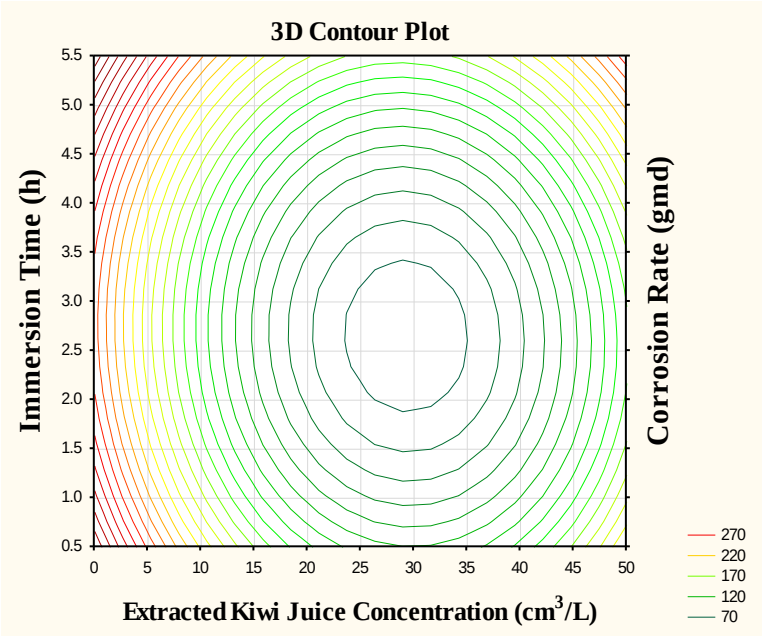

Figure 5. Response surface plot (top) and contour plot (bottom) showing the variation of corrosion rate as a function of the extracted kiwi juice concentration and immersion time at the optimum value (42.86 °C).

A Real-Time Fuzzy Load Flow and Contingency Analysis Based on Gaussian Distribution System

Asst. Prof. Dr. Hassan Abdullah Kubba
Electrical Engineering Department
College of Engineering/ Baghdad University
E-mail: hassankubba@yahoo.com

Yasser Falah Hassan
M.Sc. Electrical Engineering
Baghdad University
E-mail: **yasser.falah81@gmail.com**

ABSTRACT

Fuzzy logic is used to solve the load flow and contingency analysis problems, so decreasing computing time and its the best selection instead of the traditional methods. The proposed method is very accurate with outstanding computation time, which made the fuzzy load flow (FLF) suitable for real time application for small- as well as large-scale power systems. In addition that, the FLF efficiently able to solve load flow problem of ill-conditioned power systems and contingency analysis. The FLF method using Gaussian membership function requires less number of iterations and less computing time than that required in the FLF method using triangular membership function. Using sparsity technique for the input Ybus sparse matrix data gives reduction in overall computation time and storage requirements. The performance of the used methods had been tested on two typical test systems being the IEEE 14-bus and 30-bus systems in addition to the 362-bus Iraqi National Grid. All the obtained results under normal operating conditions show that the computation time of the fuzzy Load Flow (FLF) is less than the fast decoupled load flow (FDLF).

Keywords: Fast decoupled method, Fuzzy Load Flow, Fuzzy Contingency Analysis, Fuzzy Logic.

الحل اللحظي لمسألة سريان الحمل وتحليل الاضطرابات على اسس المنطق المضبب باستخدام دالة الكاوسين

أ.م. د. حسن عبدالله كبة
قسم الهندسة الكهربائية
كلية الهندسة/جامعة بغداد

ياسر فلاح حسن
قسم الهندسة الكهربائية
كلية الهندسة/جامعة بغداد

الخلاصة

تم في هذا البحث اقتراح طريقة لحساب مسألة سريان الاحمال و تحليل الاضطرابات أنيا في منظومات القدرة الكهربائية باستخدام نظرية المنطق المضبب. الطرق العددية غير كفؤة لحل مسألة سريان الاحمال و تحليل الاضطرابات وذلك لان شبكات القدرة الكهربائية اصبحت اكثر تعقيد. لذا, فأن استخدام نظرية المنطق المضبب للحل هي البديل الافضل وذألك لعدم اعتمادها على خصائص المسألة. تم اختبار الطريقة المقترحة على منظومة قدرة قياسية و تمت مقارنة النتائج المتحصلة مع نتائج الحل باستخدام الطرق العددية لحل مسألة سريان الاحمال بهدف التحقق من صحة وثوقيه الطريقة المقترحة للعمل على الشبكة الوطنية العراقية. اوضحت النتائج باستخدام الطريقة المقترحة خاصية الحل اللحظي بما يوصى باستخدامها في انظمة القدرة صغيرة و كبيرة الحجم بالإضافة الى الامكانية التطبيقية لظروف عمل اعتيادية و طارئة.

الكلمات المفتاحية: المنطق المضبب, حل مسألة سريان الاحمال و تحليل الاضطرابات باستخدام المنطق المضبب.

1. INTRODUCTION

The load flow problem is one of the basic problems in the field of power system engineering. The development of numerical methods to solve the load flow problem has been continuing for many years. One of the most common computational procedures used in power system analysis is the load flow calculations **Grisby, 2012**.

The mathematical model of load flow problem is a set of non-linear simultaneous equations. The solution for these equations can be implemented using iterative methods, the traditional methods of repeating the solutions became inefficient as need a lot of calculations at any iteration so that the computational time will be large **Kubba, 1987**.

Contingency Analysis behaves like a fictitious test performs on a list of postulated contingency cases (single or multiple outages). The most important simulation of contingency analysis is to give the operators an indication of what might happen to the power system if an event occurs. The contingency analysis is time consuming as it involves the computation of complete AC load flow calculations following every possible outage events like outages occurring at various generators and transmission lines **Mishra and Khardenvis, 2012**.

Uncertainty is one of the most important issues in power system planning when decisions are made regarding the future system expansion and operation. The uncertainties in the power system come from the errors in input data of the power systems due to error in measurements and errors in the load demand for the system load buses **Grisby, 2012**.

In trying to include uncertainty into the solution process, analysis have tried different approaches. A better solution would be to provide solutions over the range of uncertainties included, i.e., solutions that are sets of values instead of single points. Fuzzy systems have been increasingly used to develop more efficient schemes for the power system operation, planning, control, and management. Fuzzy systems rely on a set of rules. These rules allow the input to be fuzzy **Tomsovic, et al., 1995**.

A brief survey of solving the load flow problem and contingency analysis by the fuzzy logic theory,

J.G. Vlachogiannis, made a new FLF method based on fuzzy logic controller (FLC) to solve the load flow problem using triangular membership functions to represent the fuzzy input and fuzzy output signal of the FLC **Vlachogiannis, 2001**. P. K. Satpathy, et al., proposed the fuzzy set theory that has been implemented for performing the power flow analysis in a fuzzy environment. A trapezoidal fuzzy membership function has been selected for this purpose **Satpathy, 2004**. P.Gajalakshmi and S.Rajesh, proposed fuzzy logic based power flow method. The input signals are fuzzified into corresponding fuzzy signals and output fuzzy signals represented in triangular membership function **Gajalakshmi and Rajesh, 2007**. P. Acharjee and Kawsar Ali, proposed the decoupled fuzzy load Flow, the fuzzy load flow algorithm (FLF) has been built up considering the decoupling properties of the power flow variables. Both power mismatche and summation of power mismatche are taken as two inputs for fuzzy logic controller **Acharjee and Ali, 2011**. K. L Lo and A. K. I. Abdewlall, applied fuzzy logic on contingency selection for voltage ranking **Lo and Abdewlall, 2000**. A.Y.Abdelaziz, et al., presented Fuzzy logic based algorithm for contingencies ranking **Abdelaziz, et al., 2013**. A load flow solution and contingency analysis methods based on the fuzzy control theory is developed in this paper. The proposed method is demonstrated on the IEEE 14 buses and 30 buses typical test systems and Iraqi National Grid for different normal and contingent operating conditions.

2. FUZZY LOGIC

Most of our traditional tools for formal modeling, reasoning, and computing are crisp, deterministic, and precise in character. By crisp we mean dichotomous, that is yes-or-no-type rather than more-or-less type. In conventional dual logic, for instance, a statement can be true or false-and nothing in between. In set theory, an element can either belong to a set or not; and in optimization, a solution is either feasible or not. The traditional way of representing elements *u* of a set *A* is through the characteristic function. **Zimmermann, 1996** :

$\mu_A(u) = 1$ if *u* is an element of the set *A* (1)

$\mu_A(u) = 0$ if *u* is not an element of the set *A* (2)

In fuzzy sets, an object can belong to a set partially. The degree of membership is defined through a generalized characteristic function called the membership function:

$$\mu_A(u) : U \rightarrow [0,1] \quad (3)$$

Where *U* is called the universe, and *A* is a fuzzy subset of *U*. The values of the membership function are real numbers in the interval [0, 1], where 0 means that the object is not a member of the set and 1 means that it belongs entirely to the set **Lee, 2005**.

The main phases to solve any problem using the fuzzy logic approach are as follows:

1. Identifying the problem and choosing the type of fuzzy system which best suits the problem requirements.
2. Defining the input and output variables, their fuzzy values, and their membership functions.
3. Articulating the set of heuristic fuzzy rules.
4. Choosing the fuzzy inference method, fuzzification and defuzzification methods if necessary.

Experimenting with the fuzzy system prototype; drawing the goal function and output fuzzy variables; changing membership functions and fuzzy rules if necessary; tuning the system and validation of results **Zimmermann, 1996**.

3. SOLUTION OF THE LOAD FLOW PROBLEM

3.1 Fast Decoupled Load Flow (FDLF) Method

Fast decoupled load flow method, possibly the most popular method used by utilities, is well known for its speed of solution, reduced memory, and reliable convergence **Stott and Alsac, 1974**. The algorithm is simpler, faster and more reliable than Newton's method and has lower storage requirements. The fast decoupled load flow method is based on Newton's load flow method with the modifications of neglecting J_2 and J_3 Jacobian sub matrices due to the weak coupling between ″P-V″ and ″Q-δ″ quantities in power transmission system. Together with other approximations, the fast decoupled load flow equations become **Vlachogiannis, 1994**:

$$\left[\frac{\Delta P}{V}\right] = [B'][\Delta\delta] \quad (4)$$

$$\left[\frac{\Delta Q}{V}\right] = [B''][\Delta V] \quad (5)$$

4. PROPOSED FUZZY LOAD FLOW METHOD

The fuzzy power flow equations are derived from fast decoupled load flow set of equations, being Eq. (4) and (5) respectively. In Eq. (4), the state vector δ is updated but state vector V is fixed. Eq. (5) is used to update the state vector V while state vector δ is fixed. The whole calculation will terminate if the errors of both these equations are within the desired error tolerance.
The above system of equations can be expressed as

$$\Delta F = B * \Delta X \quad (6)$$

The last equation states that the correction of state vector ΔX at each bus of the system is directly proportional to the vector ΔF. The proposed fuzzy load flow method is based on the previous FDLF equation, but the repeated update of the state vector of the system is being performed using fuzzy logic control instead of using the classical load flow approach. This can be expressed by

$$\Delta X = fuz(\Delta F) \quad (7)$$

Where fuz represents a fuzzy logic function.
The FLF algorithm is illustrated schematically in **Fig. 1** that the power parameters ΔF_P and ΔF_Q are calculated and introduced to the $P-\delta$ fuzzy logic controller $FLC_{P\text{-}\delta}$ and the $Q-V$ fuzzy logic controller $FLC_{Q\text{-}V}$, respectively. The FLCs generate the correction of the state vectors ΔX namely, the correction of the voltage angle $\Delta\delta$ for the $P-\delta$ cycle and the correction of voltage magnitude ΔV for the $Q-V$ cycle.
The proposed fuzzy load flow controller (FLFC) has a structure that may be traced easily in **Fig.2** that comprises four principal components: a fuzzification interface, a rule base, process logic and a defuzzification interface. The fuzzification interface involves the following functions during iteration:
1. Calculate and per unit the power parameters ΔF_P and ΔF_Q at each bus of the system.
2. The above parameters are elected as crisp input signals. The maximum power parameter ($\Delta F_{P\max}$ or $\Delta F_{Q\max}$) determines the range of scale mapping that transfers the input signals into corresponding universe of discourse at every iteration.
3. The input signals are fuzzified into corresponding fuzzy signals ($\Delta F_{P\text{fuz}}$ or ΔFQ_{fuz}) with seven linguistic variables; large negative (LN), medium negative (MN), small negative (SN), zero (ZR), small positive (SP), medium positive (MP) and large positive (LP) **Vlachogiannis, 2001.** They are being represented in Gaussian membership function forms. **Fig.3** gives sketches of these membership functions. Each two points (width and center) are designed. These seven linguistic variables are designed by two points (width and center): LN : [$2\Delta F_m/3$, $-\Delta F_m$], MN : [$2\Delta F_m/3$, $-2\Delta F_m/3$], SN : [$2\Delta F_m/3$, $-\Delta F_m/3$], ZR : [$2\Delta F_m/3$, 0], SP : [$2\Delta F_m/3$, $\Delta F_m/3$], MP: [$2\Delta F_m/3$, $2\Delta F_m/3$], LP : [$2\Delta F_m/3$, ΔF_m].
The rule base involves seven rules tallying with seven linguistic variables:
Rule 1: if ΔF_{fuz} is LN then ΔX_{fuz} is LN, Rule 2: if ΔF_{fuz} is MN then ΔX_{fuz} is MN

Rule 3: if ΔF_{fuz} is SN then ΔX_{fuz} is SN, Rule 4: if ΔF_{fuz} is ZR then ΔX_{fuz} is ZR

Rule 5: if ΔF_{fuz} is SP then ΔX_{fuz} is SP, Rule 6: if ΔF_{fuz} is MP then ΔX_{fuz} is MP

Rule 7: if ΔF_{fuz} is LP then ΔX_{fuz} is LP

4. Design of these fuzzy rules is based upon two observations. The first of them is that when the computed value obtained in each iteration is far away from the specified one, it will require more compensation from the fuzzy logic controller. The second is that these fuzzy rules are consistent with the observation that corrective action to state vector ΔX is directly proportional to power vector ΔF Eq. (7) at every iteration **Lo K., et al., 1999**.

5. The fuzzy signals ΔF_{fuz} are sent to process logic, which generates the fuzzy output signals ΔX_{fuz} based on the previous rule base and are represented by seven linguistic variables similar to input fuzzy signals.

The output fuzzy signals ΔX_{fuz} are then sent to the defuzzification interface, which performs the following function: The maximum corrective action $\Delta X_{\max}$ of state variables determines the range of scale mapping that transfers the output signals into the corresponding universe of discourse at every iteration. The maximum correction of these variables can be calculated by:

$$\Delta X_{max} = \left(\frac{df_I}{dx_I}\right)^{-1} * \Delta F_{\max I} \quad (8)$$

Where F_I expresses the real or reactive power balance equations at bus-I with maximum real or reactive power mismatches of the system, X_I represents the voltage angle or magnitude at bus-I **Vlachogiannis, 2001**. Therefore, each two points (width and center) of the Gaussian membership functions of ΔX_{fuz} is designated in a similar way to **Fig.3** as may be shown in **Fig.4**. Hence, the output fuzzy membership classes are redesigned in similar way to **Fig.2** and are listed as:

LN : $[2\Delta X_m/3, -\Delta X_m]$, MN: $[2\Delta X_m/3, -2\Delta X_m/3]$, SN: $[2\Delta X_m/3, -\Delta X_m/3]$, ZR: $[2\Delta X_m/3, 0]$, SP: $[2\Delta X_m/3, \Delta X_m/3]$, MP:$[2\Delta X_m/3, 2\Delta X_m/3]$, LP : $[2\Delta X_m/3, \Delta X_m]$.

Finally, the defuzzifier will transform fuzzy output signals ΔX_{fuz} into crisp values ΔX for every bus of the network. The centroid-of-area (COA) defuzzification strategy is being adopted. This strategy finds the geometrical center *Zo* in the universe *C* of an output variable *Z*, which center ″balances″ the inferred membership function $\mu_C(z)$ as a fuzzy value for *Z*. The following formula is used **Ross, 2010**.

$$Zo = \frac{\sum_{i=1}^{n} \mu_c(Zi) * Zi}{\sum_{i=1}^{n} \mu_c(Zi)} \quad (9)$$

The second method is the Mean-of-Maxima (MOM), Sugeno method; this method finds the value *Zo* which has $\mu_C(z)_{\max}$ is the maximum membership degree according to the fuzzy output variable Z. The following formula is used

$$Zo = \sum_{i=1}^{n} \frac{\mu_c(Zi)max}{k} \quad (10)$$

and the state vector is being updated as

$$X^{i+1} = X^i + \Delta X \quad (11)$$

where the index *i* depicts the number of iterations. The number of Gaussian fuzzy-membership functions used and fuzzy rules are selected heuristically to minimize the overall computing time required for convergence.

5. IMPLEMENTATION RESULTS

The FLF method was implemented on the IEEE 14 buses shown in **Fig.5** and 30 buses typical test systems in for the following cases of normal operation and contingent operation. The power mismatches (active and reactive) are given for each case of operation as shown below:

1. Normal operating condition with power mismatch of (0.001 p.u, equivalent to 0.1 MW/MVAr).
2. Single-line, double-line, and triple-line outage with power mismatches of 0.001 p.u.
3. Single generator outage with power mismatches of (0.001 p.u.).
4. Overload of the active power demand of a load (PQ) bus in percentage of 125% of rated bus load demand with power mismatches of 0.001 p.u.
5. In addition to the cases mentioned above, the performance of the system was studied in the case of adding series capacitance to three branches of the system. Robustness of the proposed method is studied in the later step.

The obtained results are exhibited in the **Table.1** for 14 Buses IEEE Typical Test System, Power Mismatches (Active / Reactive) = 0.001per unit (0.1 MW/MVAr), Normal Condition.

For contingent conditions (Single, Double and Triple-lines out of the service) the required number of iterations and the total computation time increases by a considerable amount. The FLF solution using GMF at these types of contingent conditions is remained sufficient for on-line operation. In a single-line outage, the line connecting buses (1) and (5) was brought out-of-service. In double-lines outage case, the lines connecting buses (1) and (5), and buses (4) and (9) were brought-of-service. The last case of line outages is the triple-lines outage. In this case, lines connecting buses (2) and (4), (7) and (8), and (10) and (11) were the faulty lines in respective order.

Tables.2 through **4** shows the results of the FLF solutions with (single, double and triple) lines outage using GMF. The required number of iterations and the total computation time increases by a considerable amount for contingent conditions (Single, Double and triple-lines out of the service). The importance of these studies is to know whether the system voltage magnitudes and voltages phase angles cross their limits (±5%) or not, causing unstable operation of the system or not.

Table.5 shows the system′s performance when the FLF algorithm using GMF is implemented under contingent operation of single generator outage. In this step, generator at bus number 3 was brought out-of-service. A generator outage is meant that its voltage magnitude, voltage angle, generated active/ reactive powers are all set to zero. It is noted that even with the voltage magnitude and voltage angle set initially to zero for the faulty generator bus, the final values of the voltage magnitude and angle of the faulty bus after the load flow calculations are implemented include non-zero values in the both cases.

This may be explained by assuming that the system tries to compensate for the lost generator voltage to keep the normal operating point unchanged as possible. For a contingent operation of two generators outage, the solution diverged. It means that the system could not compensate for the lost of two generators voltage to keep the system in a stable condition. It can be seen that FLF algorithm using GMF is faster from the other.

To explore the performance of the FLF algorithm using GMF under conditions of over-loading bus, the active power demand of load bus number (13) was increased. In the first case, the active power demand was increased from 13.5 MW to 16.875 MW, i.e. an increment by 25% above the rated load. The test results of these studies are presented in **Table.6** for 14-bus IEEE system for the FLF algorithm.

The FLF success to solve ill-conditioned power systems by adding a series capacitor of capacitive reactance 0.04 p.u on the same bases to branches connecting buses (2) and (3), (4) and (7), as well as

(7) and (9).The results are show in the **Table.7**. The FLF based on GMF was converged without facing any problems.

From **Tables.1 to 7**, it is concluded that the total computing time for load flow solution is the least in case of normal operating condition. As well as the number of iterations for most contingent conditions is larger than the normal condition. But, the time per iteration for the latter cases is too much such that the overall computing time is more than the normal operating condition. These depend on the configuration of the network and the type and location of faulted elements. These were demonstrated from the tables.

Implementing the fuzzy load flow method on the 362 buses Iraqi National Grid(two main connection grids: 132 and 400 KV connection grids) gave satisfactory results for both voltage magnitudes and angles. For a power mismatch of 0.001, the total time required to obtain a solution was about 1.0628 seconds with an iteration number of 25. Due to huge tabulations of the Iraqi National Grid results, they are omitted and not shown in this paper.

The FLF method based on GMF is faster and more accurate than TMF for on-line applications, planning as well as control of electrical power systems. The total computing time and number of iterations of the FLF algorithm based on GMF are less than FLF algorithm based on TMF for load flow solutions under normal and contingent conditions.

Table.8 shows a comparison between fuzzy load flow″ FLF″ (Triangular and Gaussian membership functions), fast decoupled load flow ″FDLF″, and Newton-Raphson ″NR″ methods according to the following criteria; number of iterations and percentage computing time under normal conditions. From the table, it can be observed that FLF requires more iteration as compared to FDLF and NR methods for the tested systems. However, the total computation time is much less than FDLF and NR method. In the table, the % computation time is taken relative to NR method.

Table.9 illustrates the reduction in computational time and storage requirements for different power systems by using the proposed fuzzy load flow method using Gaussian function with sparsity technique. The reduction in computation time and storage requirements increases as the matrix density decreases. While the nodal admittance matrix is the main input data which is a sparse matrix.

Defuzzification interface is very important part of the FPF controller structure as it will transform fuzzy output signals ΔX_{fuz} into crisp values ΔX for all buses of the network. There are many defuzzification techniques but primarily only two of them are in common use, first the centroid-of-area (COA) defuzzification technique, secondly the Mean-of-Maxima Method (MOM) defuzzification techniques. These two defuzzification techniques are implemented. The comparison between them for major two criteria which are computational time and accuracy, are shown in **Table.10** shows that the defuzzification technique Mamdani-type (COA) is more accurate than the Mean-of-Maxima Method (MOM), Sugeno-type. The computing time required for both methods are comparably the same to providing the crisp output values.

6. CONCLUSION

A robust method based on the fuzzy logic controller to solving the load flow problem under normal and contingent conditions is presented and could be used as a base to incorporate all the modern power control strategies designed using fuzzy logic. All the obtained results show that the computation time of the Fuzzy Load Flow (FLF) is less than the Fast Decoupled Load Flow (FDLF) according to the following analysis.

Fuzzy Logic was used efficiently to solve the load flow problem due to its solution speed are simple and very fast, respectively. It simplifies the complexity of obtaining a solution by incorporating the uncertainties in input data processed. The proposed method provides faster solution; it can be implemented at real-time operation in electric power control centers having either small- or large-scale power system configurations on the IEEE 14 buses and 30 buses test system. In addition to the test system, the proposed method is tested on the 362 buses Iraqi National Grid to test its on-line characteristic.

The most important feature to mark is the capability of solving ill-conditioned cases of inserting series capacitors to certain lines of the transmission network. The FLF method using Gaussian membership function requires less number of iterations and slightly less computing time than that required in the FLF method using Triangular membership function due to the smoothly varying curve of the Gaussian function. The defuzzification strategy of the FLF method for both membership functions (Triangular and Gaussian) was implemented by using Center of Gravity (Centroid of Area) and the Mean-of-Maxima method, it is found that the first method is more accurate but the computing time is very slightly more. The reduction in overall computational time and storage requirements by using sparsity technique for the input sparse matrix data. All the points mentioned above recommend the use of the proposed method in power control centers.

REFERENCES

- Abdelaziz A.Y., Taha A., Mostafa M. and Hassan A., 2013, *Fuzzy Logic Based Power System*
- *Contingency Ranking*, International Journal of Intelligent Systems and Applications, February,
- pp. 1-12.

- Acharjee P. and Ali K., 2011, *Load Flow Analysis Using Decoupled Fuzzy Load Flow Under Critical Conditions"*, International Journal Engineering, Science and Technology, Vol. 3, No. 3.

- Gajalakshmi P. and Rajesh S., 2007, *Fuzzy Modeling of Power Flow Solution*, IEEE Telecommunications Energy Conference, Oct., pp. 923-927.

- Grisby L. L., 2012, *Power Systems*, CRC Press, Taylor and Francis Group, Book, Third Edition.

- Kubba H. A., 1987, *Comparative Study of Different Load Flow Solution Methods*, M.Sc. Thesis,
- Baghdad University, Engineering College, Electrical Engineering Department.

- Lee K. H., 2005, *First Course on Fuzzy Theory and Applications*, Springer, Book.

- Lo K. L., Lin Y. J. and Siew W. H., 1999, *Fuzzy Logic Method for Adjustment of Variable Parameters in Load-Flow Calculation*, IEE Proc. – Gener. Trans. Distrib., Vol. 146, No.3, pp. 276-282.

- Lo K. L. and Abdelaal A. K. I., 2000, *Fuzzy Logic Based Contingency Analysis*, International
- Conference on Electric Utility Deregulation and Restructuring and Power Technologies, London, April, pp. 499-504.

- Mishra. V. and Khardenvis M., 2012, *Contingency Analysis of Power System*, IEEE Conference,
- Electrical, Electronics and Computer Science (CEECS), 1-2 March.

- Ross T. J., 2010, *Fuzzy Logic with Engineering Applications*, A John Wiley and Sons, Ltd, Book, Third Edition.

- Satpathy P. K., Das D. and Dutta P., 2004, Power Flow Analysis Using Fuzzy Set Approach, IE
- Journal India, Vol. 85, June, pp. 55-59.

- Stott B. and Alsac O., 1974, *Fast decoupled load flow*, IEEE Transactions on Power Apparatus
- and Systems, Vol. PAS-93, May, pp. 859-869.

- Tomsovic K., Momoh J. and Xinwang M., 1995, *Overview and Literature Survey of Fuzzy Set*
- *Theory in Power Systems*, IEEE Transactions, Power Systems, Vol.10, No. 3, Aug, pp.1676-
- 1690.

- Vlachogiannis J.G., 2001, *Fuzzy Logic Application in Load Flow Studies*, IEEE Proceedings, Generation, Transmission and Distribution, Vol.148, Issue 1, Jan., pp. 34-40.

- Vlachogiannis J.G., 1994, *Control adjustments in fast decoupled load flow*, Electrical Power System Res., 31, pp. 18S-194

- Zimmermann H. J., 1996, *Fuzzy Set Theory and its Applications*, Book 3rd Edition, Kluwer Academic Publishers.

LIST OF SYMBOLS AND ABBREVIATIONS

ΔP: active power mismatch.
ΔQ: reactive power mismatch.
V : voltage magnitude
δ : voltage phase angle.
μ_A : membership function.
$\Delta\delta$: The correction of the voltage angle.
ΔV: The correction of voltage magnitude.
MOM: mean of maxima
FLFC: Fuzzy Load Flow Controller.
FLC : Fuzzy Logic Controller.
FLF : Fuzzy Load Flow
FDLF: Fast Decoupled Load Flow.
COA: Centroid of Area.

ΔF: real or reactive power mismatches per voltage magnitude vector
ΔX: correction of state vector (voltage angle or magnitude vector)
B': sparse-constant matrix of P- θ cycle
B'': sparse-constant matrix of Q- V cycle
B : represents either B' or B'' matrix

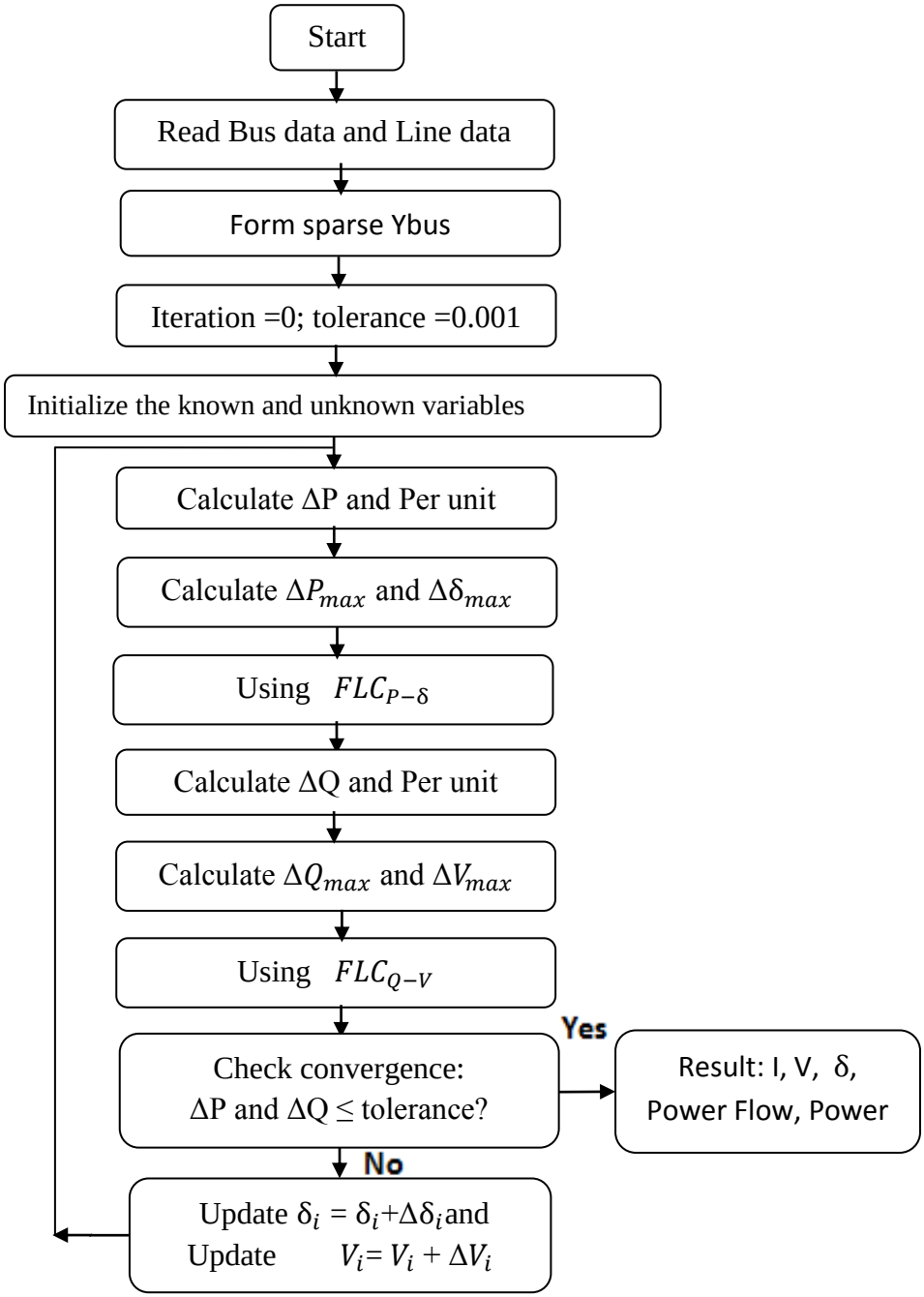

Figure1. Fuzzy Power flow algorithm.

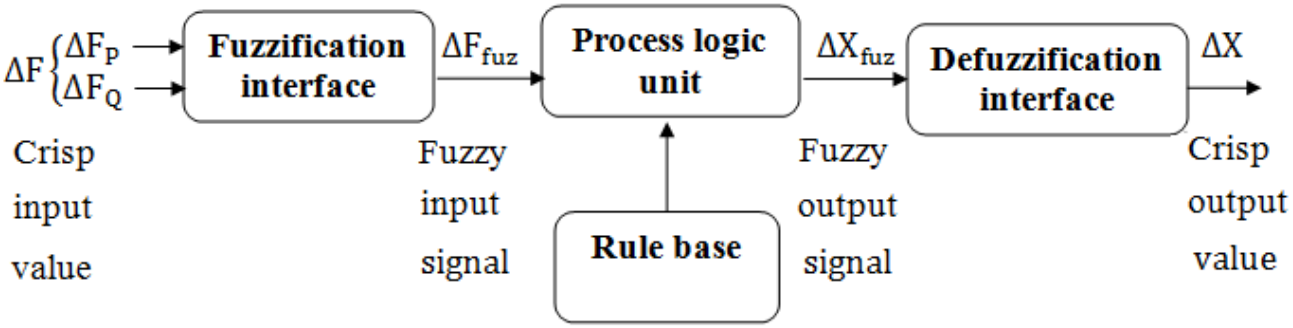

Figure2. Structure of the fuzzy load flow controller.

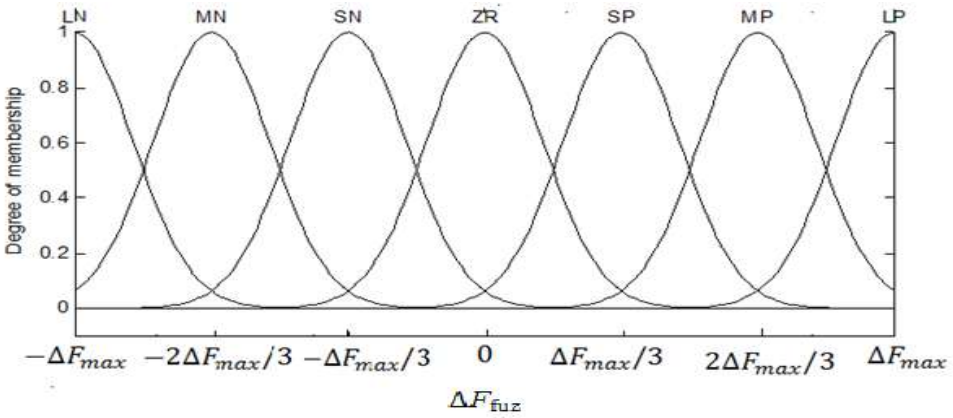

Figure3. Membership functions for input signals $\Delta F_{\text{fuz.}}$

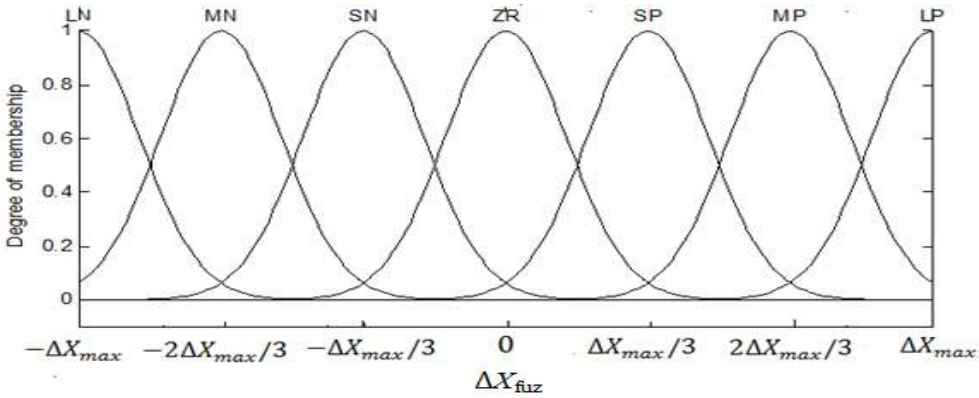

Figure4. Membership functions for output signals $\Delta X_{\text{fuz.}}$

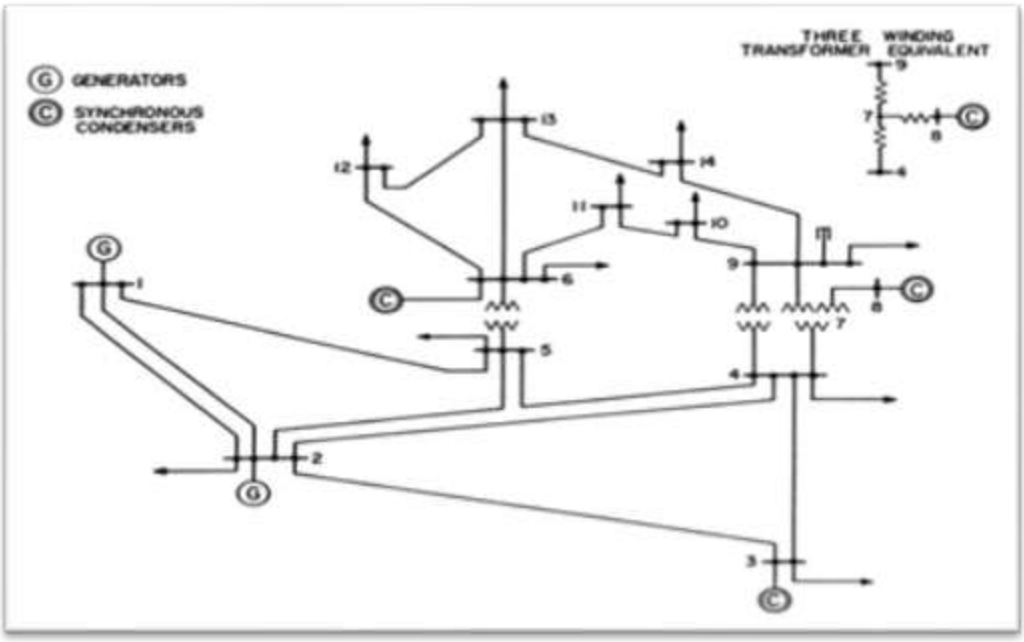

Figure5. Single-line Diagram of 14-Bus IEEE Test System.

Table1. Fuzzy load flow solution for 14 buses IEEE typical test system, power mismatches (Active / Reactive) = 0.001per unit (0.1 MW/MVAr), normal condition. Bus Type:(1: Stands for Slack bus; 2: Defines PV bus; 0: Defines PQ buses).

Bus Num.	Bus Type	Voltage Mag. (p.u.)	Voltage Angle (deg.)	ΔP (p.u)	ΔQ (p.u)
1	1	1.060	0.000	0.0	0.0
2	2	1.045	-3.734	0.000022	0.0
3	2	1.010	-9.929	0.000333	0.0
4	0	1.41	-8.341	0.000250	0.0009689
5	0	1.043	-6.156	0.000227	0.0009599
6	2	1.070	-5.836	0.000216	0.0
7	0	1.071	-6.691	0.000081	0.0004656
8	2	1.090	-6.424	0.000003	0.0
9	0	1.066	-8.390	0.000260	0.0000190
10	0	1.063	-6.823	0.000110	0.0001055
11	0	1.063	-7.406	0.000004	0.0000149
12	0	1.062	-7.543	0.000038	0.0000031
13	0	1.059	-6.994	0.000085	0.0000059
14	0	1.056	-6.433	0.000142	0.0000270
Number of iterations					9
Computation time					0.093410 sec

Table2. Fuzzy load flow solution for 14 buses IEEE typical test system, single-line outage.

Bus Num.	Bus Type	Voltage Mag.(p.u.)	Voltage Angle(deg.)	ΔP (p.u)	ΔQ (p.u)
1	1	1.060	0.000	0.0	0.0
2	2	1.045	-3.519	0.000003	0.0
3	2	1.010	-8.464	0.00025	0.0
4	0	1.037	-10.033	0.000219	0.000317
5	0	1.037	-9.761	0.000238	0.000950
6	2	1.070	-7.655	0.000236	0.0
7	0	1.073	-8.544	0.000110	0.000011
8	2	1.090	-8.456	0.000062	0.0
9	0	1.069	-10.661	0.000231	0.0000018
10	0	1.065	-8.745	0.000123	0.0000722
11	0	1.065	-8.634	0.000018	0.0000091
12	0	1.061	-9.888	0.000024	0.0000072
13	0	1.059	-9.149	0.000074	0.0000095
14	0	1.058	-8.204	0.000156	0.0000230
Number of iterations					10
Computation time					0.109894sec

Table3. Fuzzy load flow solution for 14 buses IEEE typical test system, double-lines outage.

Bus Num.	Bus Type	Voltage Mag. (p.u.)	Voltage Angle (deg.)	ΔP (p.u)	ΔQ (p.u)
1	1	1.060	0.000	0.0	0.0
2	2	1.045	-5.905	0.000021	0.0
3	2	1.010	-14.181	0.000187	0.0
4	0	1.035	-10.393	0.000188	0.000953
5	0	1.037	-10.390	0.000180	0.000974
6	2	1.070	-8.085	0.000184	0.0
7	0	1.072	-9.016	0.000133	0.000093
8	2	1.090	-8.587	0.000007	0.0
9	0	1.062	-10.807	0.000177	0.000015
10	0	1.063	-9.439	0.000153	0.000094
11	0	1.064	-9.773	0.000013	0.000060
12	0	1.061	-10.508	0.000048	0.000014
13	0	1.059	-9.742	0.000108	0.000064
14	0	1.056	-8.758	0.000155	0.000061
Number of iterations					11
Computation time					0.114429sec

Table4. Fuzzy load flow solution for 14 buses IEEE typical test system, triple-lines outage.

Bus Num.	Bus Type	Voltage Mag. (p.u.)	Voltage Angle (deg.)	ΔP (p.u)	ΔQ (p.u)
1	1	1.060	0.000	0.0	0.0
2	2	1.045	-6.685	0.000027	0.0
3	2	1.010	-14.327	0.000239	0.0
4	0	1.015	-12.175	0.000253	0.0009994
5	0	1.018	-14.287	0.000221	0.0001395
6	2	1.070	-12.706	0.000239	0.0
7	0	1.058	-13.951	0.000114	0.000032
8	2	1.090	-11.256	0.0	0.0
9	0	1.048	-11.152	0.000234	0.000023
10	0	1.054	-14.585	0.000118	0.000098
11	0	1.063	-15.410	0.000007	0.000008
12	0	1.050	-16.425	0.000031	0.000032
13	0	1.038	-15.174	0.000077	0.000031
14	0	1.041	-13.619	0.000152	0.000051
Number of iterations					12
Computation time					0.121348 sec

Table5. Fuzzy load flow solution for 14 buses IEEE typical test system, generator (3) outage.

Bus Number	Bus Type	Voltage Mag. (p.u.)	Voltage Angle (deg.)	ΔP (p.u)	ΔQ (p.u)
1	1	1.060	0.000	0.0	0.0
2	2	1.045	-4.425	0.000026	0.0
3	2	1.000	-0.000	0.000001	0.0
4	0	1.038	-10.844	0.000042	0.000285
5	0	1.040	-10.523	0.000009	0.000910
6	2	1.070	-9.436	0.000203	0.0
7	0	1.070	-9.797	0.000082	0.000068
8	2	1.090	-9.386	0.000005	0.0
9	0	1.065	-12.356	0.000189	0.000028
10	0	1.063	-9.124	0.000157	0.000085
11	0	1.062	-10.319	0.000055	0.000023
12	0	1.060	-11.118	0.000033	0.000015
13	0	1.058	-10.005	0.000097	0.000012
14	0	1.054	-9.747	0.000157	0.000006
Number of iterations					12
Computation time					0.128729 sec

Table6. FLF solution for 14 buses IEEE typical test system, 125% active power overloading.

Bus Num.	Bus Type	Voltage Mag. (p.u.)	Voltage Angle (deg.)	ΔP (p.u)	ΔQ (p.u)
1	1	1.060	0.000	0.0	0.0
2	2	1.045	-9.327	0.000008	0.0
3	2	1.010	-13.610	0.000426	0.0
4	0	1.030	-11.868	0.000264	0.000273
5	0	1.032	-13.216	0.000241	0.000847
6	2	1.070	-12.141	0.000213	0.0
7	0	1.064	-14.644	0.000083	0.000006
8	2	1.090	-13.855	0.000006	0.0
9	0	1.059	-16.505	0.000246	0.000016
10	0	1.055	-14.218	0.000120	0.000020
11	0	1.054	-14.653	0.000009	0.000016
12	0	1.061	-15.892	0.000025	0.000023
13	0	1.040	-13.651	0.000135	0.000024
14	0	1.049	-13.439	0.000144	0.000008
Number of iterations					9
Computation time					0.100163sec

Table7. FLF solution for 14 buses IEEE typical test system, Addition of Series Capacitance.

Bus Num.	Bus Type	Voltage Mag.(p.u)	Voltage Angle (deg.)	ΔP (p.u)	ΔQ (p.u)
1	1	1.060	0.000	0.0	0.0
2	2	1.045	-3.266	0.000038	0.0
3	2	1.010	-7.608	0.000213	0.0
4	0	1.039	-7.811	0.000210	0.000180
5	0	1.042	-6.683	0.000194	0.000992
6	2	1.070	-5.755	0.000216	0.0
7	0	1.072	-6.136	0.000133	0.000115
8	2	1.090	-5.928	0.000035	0.0
9	0	1.068	-7.945	0.000227	0.000047
10	0	1.065	-6.237	0.000135	0.000038
11	0	1.064	-7.030	0.000032	0.000411
12	0	1.061	-7.184	0.000037	0.000012
13	0	1.060	-6.580	0.000086	0.000031
14	0	1.058	-5.890	0.000156	0.000013
Number of iterations					16
Computation time					0.146616 sec

Table8. Comparison of fuzzy load flow and numerical methods according to number of iterations required & percentage computing time

Type of test system	No. of iterations required				% computing time			
	FLF GMF	FLF TMF	FDLF	N-R	FLF GMF	FLF TMF	FDLF	N-R
14-bus IEEE	9	16	3	4	8	19	32	100
30-bus IEEE	11	17	4	5	10	21	39	100
362-bus ING	28	34	7	8	12	22	51	100

Table9. Comparison of reduction in computation time and storage requirement for different power systems using the FLF with sparsity technique method

Type of power system	Matrix density of *[Y]*	%Reduction in Computational Time	%Reduction in Storage Requirement (FLF With sparsity technique)
14-bus IEEE	17.34%	38%	55%
30-bus IEEE	78.8%	56%	69%
362-bus ING	0.628%	84%	88%

Table10. Comparison of reduction in computational time and accuracy requirement for different defuzzification technique methods.

Type of power system at normal condition	Fuzzy Load Flow Controller Structure using Defuzzification technique COA		Fuzzy Load Flow Controller Structure Using Defuzzification technique MOM	
	Computational Time	% Accuracy	Computational Time	% Accuracy
14-bus IEEE	0.093410 sec	80%	0.087745 sec	76%
30-bus IEEE	0.108791sec	74%	0.101423sec	68%
362-bus ING	1.062819 sec	65%	1.017269 sec	59%

Applying Penman-Monteith Equation to Evaluate the Performance of Atmometer Apparatus in Greenhouse for Estimating Reference Evapotranspiration

Rafah Zuhair Dawood Al-Shaikh
Graduate Student
College of Engineering
Baghdad University
Email:rafah-z.al-shaikh@yahoo.com

Asst. Prof. Sabah A. Dawood Almasraf
Department of Water Resources Engineering
College of Engineering
Baghdad University
Email:sabah_dawood@yahoo.com

ABSTRACT

In this paper an atmometer apparatus were used in the greenhouses for estimating reference evapotranspiration values. Experimental work was conducted in the agriculture research center in the College of Agriculture-University of Baghdad west of the city of Baghdad. One atmometer was used in eggplant greenhouse and in cucumber greenhouse through the winter growing season 2013-2014. FAO Penman-Monteith equation was applied outside the greenhouse and used only 65% from the value of ET_o in the greenhouses for estimating the reference evapotranspiration in the greenhouse. Moreover, Penman-Monteith equation was applied in greenhouses for the evaluating the performance of the atmometer. The results show that the error analyses between FAO Penman-Monteith equation in greenhouse and the atmometer readings, the root mean square difference (RMSD), mean bias error (MBE) and relative error (RE) for eggplant and cucumber greenhouses were: 1.163mm/day, 0.933mm/day, 30.19%, and 0.688mm/day, 0.518mm/day and 22.93%, respectively. A fair agreement was found. While the error analyses between 65% from outdoor ET_o of FAO Penman-Monteith equation and the atmometer readings, the RMSD, MBE and RE for eggplant and cucumber greenhouses were: 0.930mm/day, 0.743mm/day, 24.27%, and 0.374mm/day, 0.289mm/day and 12.47%, respectively. A good agreement was found. The atmometer apparatus could be used successfully by researchers and farmers in estimation daily or weekly reference evapotranspiration in greenhouses as well as in low technology greenhouses.

Keywords: Greenhouse, reference evapotranspiration, atmometer, Penman-Monteith.

تطبيق معادلة بنمان-مونتيث لتقييم أداء جهاز الاتموميتر في البيوت الخضراء لتخمين الاستهلاك المائي الكامن

رفاه زهير داود الشيخ
طالبة ماجستير /قسم هندسة الموارد المائية
كلية الهندسة/ جامعة بغداد

أ.م.صباح أنور داود المصرف
قسم هندسة الموارد المائية
كلية الهندسة/ جامعة بغداد

الخلاصة

في هذا البحث تم أستخدام أجهزة الاتموميتر داخل البيوت الخضراء لتخمين قيم الاستهلاك المائي الكامن, حيث أجريت الدراسة العملية في المركز البحثي الزراعي التابع الى كلية الزراعة – جامعة بغداد غربي مدينة بغداد. أستخدم جهاز الاتموميترداخل البيوت الخضراء المزروعة بمحصولي الباذنجان والخيار وخلال الموسم الزراعي الشتوي 2013-2014. طبقت معادلة بنمان- مونتيث, وأستخدم منها فقط 65% من القيم المحسوبة للاستهلاك المائي الكامن. بالاضافة الى انه قد استخدمت معادلة بنمان – مونتيث داخل البيت الاخضر وبالاعتماد على المتغيرات الجوية المقاسة داخليا وذلك لتقييم أداء جهاز الاتموميتر. أظهرت التحليلات والمقارنات الاحصائية لقيم الاستهلاك المائي الكامن اليومية من جهاز الاتموميتر ومع مثيلاتها من معادلة بنمان – مونتيث المقاسة داخل البيت الاخضر لنبات الباذنجان والخيار بأن الجذر التربيعي لمعدل مربع الفرق, مطلق معدل الفرق والنسب المئوية للفروقات كانت على التوالي: 1.163 ملم\يوم و0.933 ملم\يوم و 30.19% و 0.688 ملم\يوم و 0.518 ملم\يوم و 22.93%. تشير النتائج الى توافق ضعيف. بينما أظهرت التحليلات والمقارنات الاحصائية لقيم الاستهلاك المائي الكامن اليومية من جهاز الاتموميتر مع مثيلاتها من قيم نسبة 65% من معادلة بنمان – مونتيث الخارجية للبيت الاخضر لنباتي الباذنجان والخيار بأن الجذر التربيعي لمعدل مربع الفرق, مطلق معدل الفرق والنسب المئوية للفروقات كانت على التوالي: 0.930 ملم\يوم و 0.734 ملم\يوم و 24.27% و 0.374 ملم\يوم و 0.289 ملم\يوم و 12.47%. حيث تشير النتائج الى توافق جيد. يمكن الاعتماد على القراءات اليومية أو الاسبوعية لجهاز الاتموميتر من قبل الباحثين والمزارعين لتخمين الاستهلاك المائي الكامن في البيوت الخضراء بالاضافة الى البيوت الخضراء واطئة التكنلوجيا.

الكلمات الرئيسية: البيوت الخضراء, الاستهلاك المائي المرجعي, الاتموميتر, بنمان-مونتيث

1. INTRODUCTION

Evapotranspiration (ET) is one of the major components of hydrological cycle. Accurate estimation of this parameter is essential for studies such as water balance, irrigation system design and management and water resources management. Greenhouses type materials and technology used are also effect on prediction of reference evapotranspiration values**. Fazlil, 2009**, used weighting lysimeter and atmometer apparatus in different types of greenhouses models (low, medium and high technology), and was found to be good reference evapotranspiration (ET_o) equipment in greenhouse which can give accurate measurement of crop (actual) evapotranspiration (ET_c). While FAO Penman model was recommended to calculate ET_o in low technology (plastic) and Hargreaves method in greenhouse with screen cover rather than

plastic one. Moreover, Stanghellini model was most accurate method in medium and high technology greenhouses. Reference evapotranspiration inside greenhouses was also estimated by using class A pan, a reduced pan and an atmometer, and another class A pan was installed outside the greenhouses. A good agreement relation was found between atmometer, class A pan and reduced pan, but fair agreement relations was found between class A pan, reduced pan and class A pan outside the greenhouses, **Ferrandes, et al., 2003**. Five methods were evaluated to estimate ET_c in greenhouse conditions and compared their performance in relation to the evapotranspiration directly determined from water balance measurement in an irrigated Lettuce crop during nine weeks. Daily values of the ET_o from class A pan, atmometer,and drainage lysimeter were used between 1993 and 2004 to measure ET_o inside a plastic greenhouse with a perennial grass in south-eastern of Spain. Different methodologies to calculate ET_o were checked against the measurements in the greenhouse with and without whitening. The results show that the performed best in terms of accuracy and statistics were: FAO Penman-Monteith with a fixed aerodynamic resistance, and FAO 24 Pan evaporation method with a constant value. Additionally the Hargreaves and the radiation equations were recommended for the calculation of greenhouse ET_o because of their simplicity, **Fernandez, et al., 2010**. Actual evapotranspiration ET_c for a crop can be found from ET_o and crop coefficient (K_c). **Fahkri, 2014**, predicted crop coefficient values for eggplant and maize in open field based on daily basis using watermark sensors measuring ET_c and atmometers measuring ET_o through the growing stages. The results indicted a good agreement in mid and late of seasons between the predicted, FAO and Russian study K_c values.

In this paper FAO Penman-Monteith equation in the greenhouses and 65% from outdoor ET_o of Penman-Monteith equation were applied in the greenhouses to evaluate the performance of the atmometer for estimating reference evapotranspiration (ET_o) in greenhouse. Weather parameters were measured outside and inside the greenhouse.

2. MATERIALS AND METHODS

2.1 Location of the Field Study

The research greenhouses field for this study was located within College of Agriculture – University of Baghdad in Abu-Ghraib Township, 30 km away from west part of city of Baghdad-Iraq. The site was located at (latitude: 33°12' N, longitude: 44°12'E, altitude: 32m). **Fig.1** shows Google map for the field site location. Two numbers of low technology greenhouses (no automatic ventilation system was available) were used; the approximated total area of the greenhouse was 250 m^2 for each. **Fig. 2** shows the interiors structure of the greenhouses. Eggplant and cucumber crops were used in the study for the winter growing season of 2013-2014. Trickle irrigation system was used in the greenhouses. The laboratory analyzes of the soil samples were conducted in the soil laboratories of College of Agriculture. The objective of the analysis was to verify the physical characteristics of the soil

in order to determine the texture of the soil and all physical properties. The soil textures for eggplant and cucumber greenhouses were loam and clay loam, respectively as shown in **Table 1**.

2.2 Devices and Equipment

The followings were specifications and description of apparatus and equipment were used in the study field work.

2.2.1 Atmometer or ETgage

An atmometer, the brand name (ETgage), has gained increasing popularity. It is one of the alternative tools that can be used to measures the amount of water evaporated to the atmosphere from a wet, porous ceramic surface. The atmometer consists of a canvas-covered ceramic evaporation plate mounted on a distilled water reservoir. The reservoir capacity is 300 mm as water depth. The fabric covering creates a diffusion barrier (resistance) that controls the evaporation rate and ranging from (112–294) s/m similar to that found in healthy leaves in a well-watered plant community. The green canvas cover that surrounds the ceramic plate mimics the crop albedo so that solar radiation absorption by the ETgage will be similar to the solar radiation received at the crop canopy. In the ETgage system, water is provided to the ceramic cup by suction through a glass or plastic supply tube and check valve consisting of a diaphragm mounted in a section of silicon tubing attached at the lower end of the glass supply tube. The shape of the evaporating surface also helped in easier fabric mounting and maintained better contact between the canvas cover and the ceramic plate. **Fig. 3** shows the main parts of the atmometer. Distilled water is always used in the ETgage reservoir to prevent accumulation of solutes in and on the plate that can reduce the porosity of the plate and affects the evaporation rate a sight glass on the water reservoir allows the water levels in the reservoir to be read manually. Accuracy of daily ET data by reading the plastic sight tube is limited. The ETgage is easy to install and requires little maintenance which is typically mounted on a wooden post with the evaporation surface approximately 1 m above the ground surface or according to the height of crop canopy. **Fig.4** shows the location of the atmometer in the greenhouses.

2.2.2 Hand weather station tool

Scientific Mini Environmental Quality Meter, hand movable weather station tool was used for measuring: air temperature, relative humidity and wind speed in the greenhouse. **Fig. 5** shows mini environmental quality meter.

2.3 FAO Penman-Monteith Model

FAO Penman-Monteith **(Allen, et al., 1998)** simulates a reference crop of 0.12 meter in height. This method estimates evaporation from an extensive surface of green grass cover of uniform height, actively growing, completely shading the ground and under non-limited soil water. The Penman-Monteith equation for the calculation of daily ET_o (mm/day) is as follow:

$$ET_o = \frac{0.408\,\Delta\,(R_n - G) + \gamma \frac{900}{T_{mean}+273} u_2 (es - ea)}{\Delta + \gamma\,(1 + 0.34 u_2)} \quad (1)$$

Where:

ET_o = Reference evapotranspiration, mm/day.
R_n = Net radiation at the crop surface, MJ m^{-2} day^{-1}.
G = Soil heat flux density, MJ. m^{-2}. day^{-1}.
T_{mean} = Mean daily air temperature at 2 meter height, °C.
u_2 = Wind speed at 2 meter height, m. s^{-1}.
es = Mean saturation vapour pressure, kPa.
ea = Mean actual vapour pressure, kPa.
es – ea = Vapour pressure deficit, kPa.
Δ = Slope vapour pressure curve, kPa $°C^{-1}$.
γ = Psychrometric constant, kPa $°C^{-1}$.

For day and ten-day periods, G is assumed to be zero **(Allen, et al., 1998).**

2.4 Statistical Analysis Methods

In this paper, comparison between estimated reference evapotranspiration from the atmometers, FAO Penman-Monteith equation in greenhouse and 65% from ET_o of FAO Penman-Monteith outdoor equation values **(Fernandez et al., 2010** and **Orgaz et al., 2005)** were conducted on the daily basis through the winter growing season of the eggplant and cucumber. For error analyses the following statistics were used:

$$RMSD = \sqrt{\frac{1}{n}\sum_{i=1}^{n}(y_i - x_i)^2} \quad (2)$$

$$RE = \frac{RMSD}{Xav} \times 100 \quad (3)$$

$$MAE = \frac{\sum_{i=1}^{n}|(y_i - x_i)|}{n} \quad (4)$$

Where:

RMSD = Root mean square difference.

RE = Relative error, %.
MBE = Mean bias error.
n = Number of daily observations.
x_{av} = Average values of estimated ET_o, mm/day
x_i = ET_o calculating value by using equations in the i^{th}.day, mm/day, and
y_i = ET_o measured by the atmometer in the i^{th}.day, mm/day.

3. RESULTS AND DISCUSSIONS

FAO-Penman-Monteith equation in the greenhouse conditions and 65% from outdoor reference evapotranspiration of FAO Penman-Monteith equation were applied; air temperature, relative humidity and wind speed were recorded daily in the greenhouses, while sun shine radiation, air temperature and all other parameters in the Penman-Monteith equation for the outdoor were provided daily through the winter growing season of eggplant and cucumber crops by the Ministry of Agriculture / Directorate of Planning & Pursuance / Project of Agricultural Weather Forecasting. The materials of the cover used for the greenhouse was white plastic hard sheet; the manufacturer company of the plastic sheet recommend that transmit of the sun shine through the sheet is about 89%. Therefore, the sun shines radiation outdoor will be multiply by 0.89 to get the value in greenhouses. Atmometers readings for eggplant and cucumber greenhouses were recorded on daily basis which represented reference evapotranspiration, starting from 17-2-2014 to 29-5-2014 and from17-2-2014 to 10-5-2014, respectively. **Figs. 6** and **7** shows the daily reference evapotranspiration estimated from atmometers recording, Penman-Monteith equation in greenhouses and 65% from outdoor ET_o for eggplant and cucumber greenhouses through the winter growing seasons of 2014, respectively. The statistical error analysis for comparison between atmometer readings and FAO Penman-Monteith equation in greenhouses for reference evapotranspiration in eggplant and cucumber greenhouses, the following parameters were calculated: RMSD, MBE and RE were: 1.163mm/day, 0.933mm/day, 30.19%, and 0.688mm/day, 0.518mm/day and 22.93%, respectively. The results indicated a fair agreement between the two values. On the other hands, the statistical error analyses for comparison between atmometer readings and 65% from FAO Penman-Monteith outdoor equation for reference evapotranspiration in eggplant and cucumber greenhouses, the following parameters were calculated: RMSD, RE and MBE were: 0.930mm/day, 0.743mm/day, 24.27%, and 0.374mm/day, 0.289mm/day and 12.47%, respectively. The results indicted a good agreement between the two values, especially in cucumber greenhouse. **Figs. 8, 9, 10** and **11** show the statistical error analyses to compare the performance of atmometer readings with the Penman-Monteith equation inside the

greenhouse and with the 65% of the outdoor ET_o for the two greenhouses. Comparison between the atmometer readings with the 65% from outdoor Penman-monteith equation, indicated that the atmometer apparatus could be used successfully in estimating the ET_o inside the low technology greenhouses, where no ventilation or automation systems technologies were available. The behavior of the atmometer could be affected by the environmental and weather parameters in greenhouse such as humidity, air temperature, sun shine and vapor pressure. Therefore some of the atmometer readings were higher in some days. Also, water management and quantities of application water could be effected on atmometer's performance.

4. CONCLUSIONS

The conclusions for this paper were:

1- Statistical error analysis from the comparison between atmometer readings and Penman-Monteith equation in greenhouse for reference evapotranspiration show a fair agreement. While, the statistical error analysis from the comparison between atmometer readings and 65% of the outdoor Penman-Monteith equation in greenhouse for reference evapotranspiration show a good agreement.
2- Atmometer apparatus could be used successfully in greenhouses for estimating reference evapotranspiration.
3- Atmometer could be used in a low greenhouse technology satisfactorily.
4- Different percentage values (60-80%) from outdoor Penman-Monteith equation were tested. no clear variation was noticed. The value of 65% was more suitable percentage represented the Penman-Monteith equation inside the low technology greenhouses.
5. A percentage of 65% from outdoor of the Penman-Monteith equation can be applied in greenhouse for estimating reference evapotranspiration using external weather parameters.

REFERENCES

- Allen, R.G., L.S. Pereira, D. Raes, and M. Smith., 1998,*Crop Evapotranspiration-Guidelines for computing crop water requirement*,.FAO Irrigation and Drainage Paper 56. Food and Agriculture Organization. Rome, Italy.
- Fakhri, E. H., 2014, *Evaluation of Atmometer (Evapotranspiration gage) under Iraqi Conditions"*, M.Sc. Thesis, Department of Water Resources Engineering, College of Engineering, University of Baghdad, 160 P.
- Fernandez M.D., S. Bonachela, F. Orgaz, R. Thompson, J.C. Lopez, M.R. Branados, M. Gallardo, and E. Fereres, 2010,*Measurement and Estimation of Plastic Greenhouse Reference Evapotranspiration in a Mediterranean Climate*, Irrigation Science, 28, pp: 497-509.
- Ferrandes, C. C, Jose Eduardo Cora, and Jairo Augusto Campos de Araujo, 2003, *Reference Evapotranspiration Estimation inside Greenhouses*. Sientia Agricola, Vol. 60, No. 3, PP: 591-594. July/Sept.
- Orgaz, F., Fernandez, M.D., Bonachela, S., Gallardo, M., Fereres, E., 2005. *Evapotranspiration of horticultural crops in an unheatedplastic greenhouse*. Agricultural Water Management. Vol. 72, PP. 81–96.
- Fazlil, W. F., 2009, *Evapotranspiration Models in Greenhouses*, M.Sc, Thesis, Agricultural and Bioresearch Engineering, Wageningen University, Netherlands.

NOMENCLATURE

ET_o = Reference evapotranspiration, mm/day.
ET_c = Crop evapotranspiration, mm/day.
K_c = Crop coefficient, dimensionless.
R_n = Net radiation at the crop surface, MJ m^{-2} day^{-1}.
T_{mean} = Mean daily air temperature at 2 meter height, °C.
u_2 = Wind speed at 2 meter height, m/s.
G = Soil heat flux density, MJ m^{-2} day^{-1}.
ea = Mean actual vapour pressure, kPa.
es = Mean saturation vapour pressure. kPa.
es – ea = Saturation vapour pressure deficit, kPa.
Δ = Slope vapour pressure curve, kPa.°C^{-1}.
γ = Psychrometric constant, kPa.°C^{-1}.
RMSD = Root mean square difference.
RE = Relative error, %.
MBE = Mean bias error.
n = Number of daily observations.

x_{av} = Average values of estimated ET_o, mm/day
x_i = ET_o calculating value by using equations in the i^{th}.day, mm/day and
y_i = ET_o measured by the atmometer in the i^{th}.day, mm/day.

Figure1. Google map for the field study area.

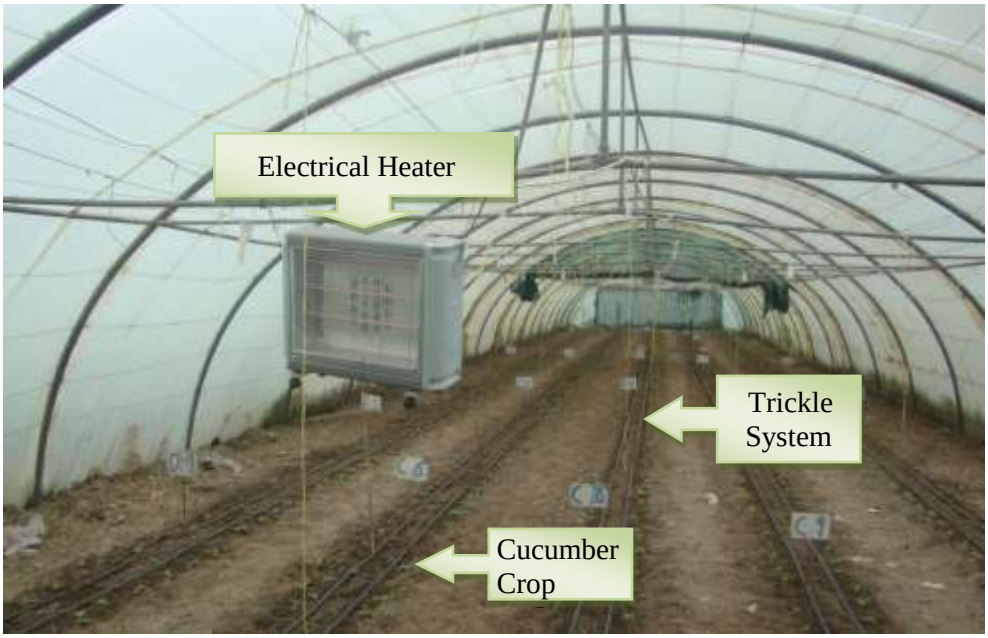

Figure2. Interior structure of the greenhouse.

Table 1. Physical properties for the soil of eggplant and cucumber greenhouses.

Types of test	Specifications of the soil	
	Eggplant greenhouse	Cucumber greenhouse
Bulk (apparent) density (gm/cm^3)	1.245	1.237
Soil texture	Loam	Clay loam
Water content at field capacity (% by volume)	29.30	29.49
Water content at permanent wilting point (% by volume)	15.90	17.01

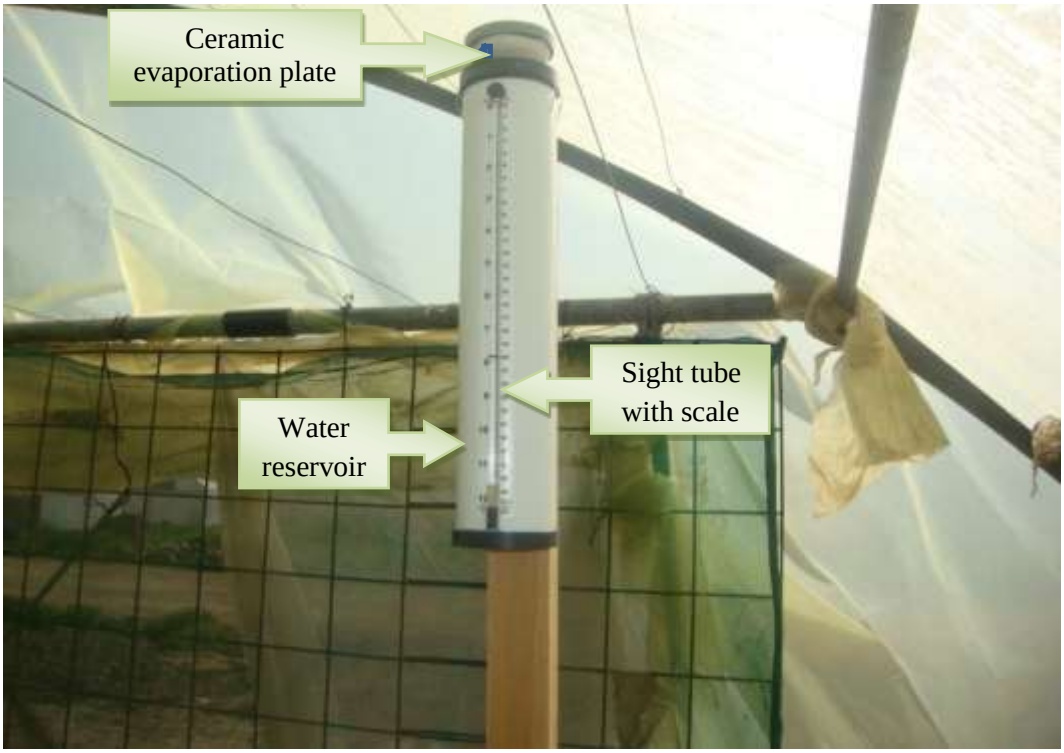

Figure 3. Main parts of the atmometer.

Figure 4. Location of the atmometer in the greenhouses.

Figure 5. Mini environmental quality meter.

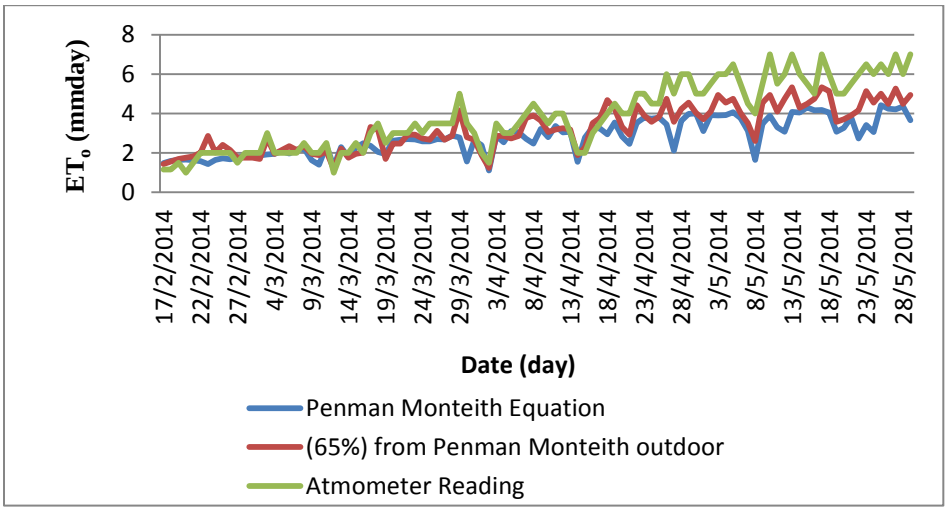

Figure 6. Daily reference evapotranspiration estimated from atmometers readings, Penman-Monteith equation in greenhouses and 65% from outdoor ET_o for eggplant through the winter growing season 2014.

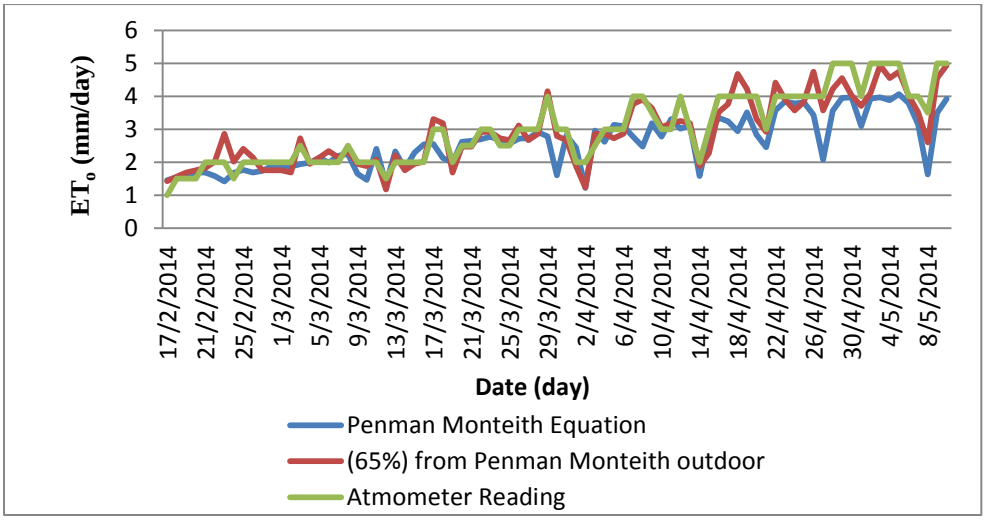

Figure 7. Daily reference evapotranspiration estimated from atmometers readings, Penman-Monteith equation in greenhouses and 65% from outdoor ET_o for cucumber through the winter growing season 2014.

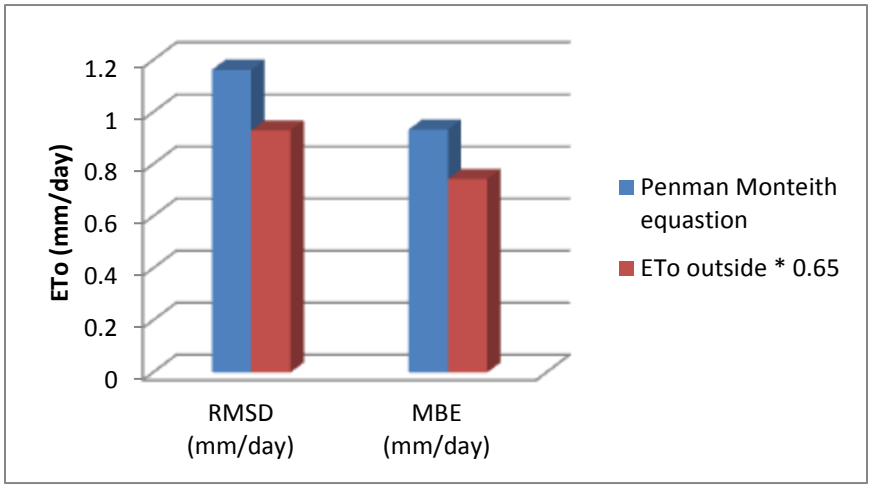

Figure 8. RMSD and MBE error analyses for eggplant greenhouse.

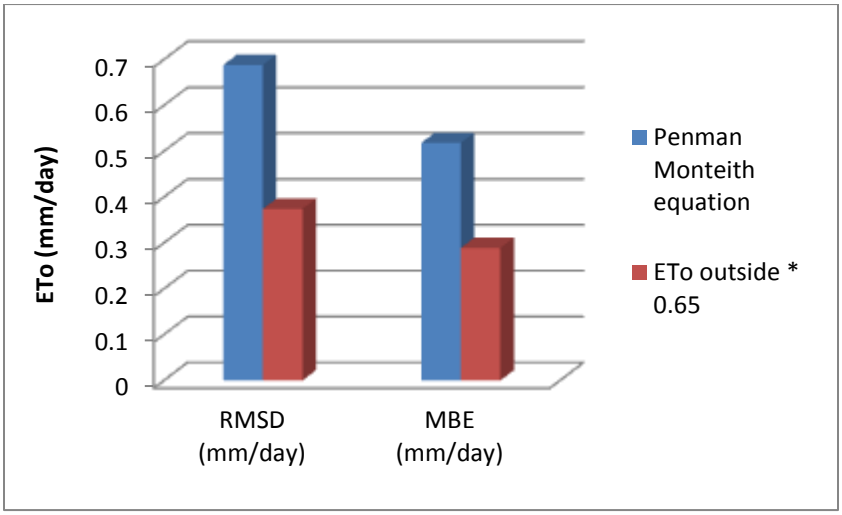

Figure 9. RMSD and MBE error analyses for cucumber greenhouse.

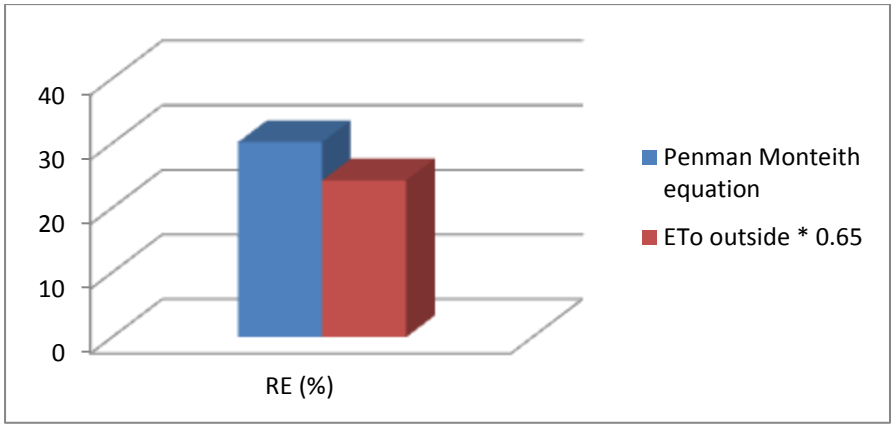

Figure 10. Relative error analyses for eggplant greenhouse.

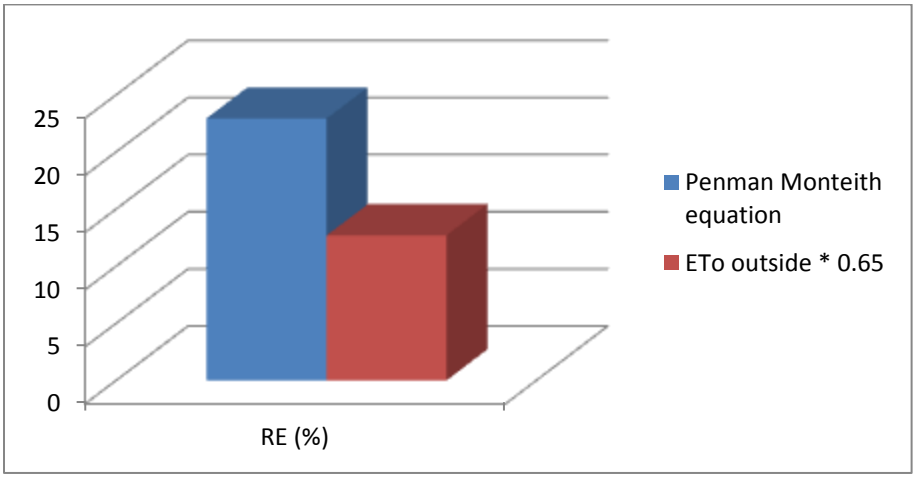

Figure 11. Relative error analyses for cucumber greenhouse.

تحسين انتاجية المقطر الشمسي التقليدي احادي التاثير مزدوج الميل بواسطة تعديل بسيط في التصميم

وسام حميد عليوي
مدرس
مركز التدريب والمعامل - الجامعة التكنولوجيه
Wissam_772005@yahoo.com

الخلاصة

البحث الحالي هو دراسة تجريبية لتحسين اداء المقطر الشمسي البسيط احادي التاثير مزدوج الميل وذلك عن طريق اجراء تغيير بسيط في التصميم للمقطر الشمسي التقليدي يوفر زيادة في عملية التكثيف بدون استخدام اي وسيلة مساعدة للتكثيف. انجز ذلك من خلال تكبير ابعاد المقطر نسبة لحوضه وهذا يوفر زيادة اضافية في مساحة سطح التكثيف فضلا عن امكانية ربط الواح عاكسة للاشعة الشمسية مع قاعدة المقطر تقوم بعكس جزء من الاشعة الشمسية الساقطة عليه والمساهمة في التسخين الاضافي لحوض التقطير. تم لهذا الغرض تصنيع مقطريين شمسيين، احدهما بالتصميم التقليدي والاخر بالتصميم المقترح. فحصت المقطرات الشمسية خلال الفترة الممتدة بين شهري شباط وتموز من عام 2009 وتحت الضروف المناخية المختلفة لمدينة البصرة (جنوب العراق). بينت النتائج التجريبية امكانية تحسين انتاجية المقطر الشمسي التقليدي مزدوج الميل بمقدار (18-24%).

الكلمات المفتاحية: انتاجية، المقطرات الشمسية، المقطر الشمسي التقليدي

Improving the productivity of single effect double slope solar still by simple modification

Wissam H. Alawee
Lecture
Center of truuing-Univ. of tecnology

ABSRTACT

The present paper is an experimental study to improve the productivity of the conventional solar still. This done by modifying conventional still in a way that the distilled basin is larger than distillation basin, thus providing an increase in the condensation surface and speeding up the condensation process. Moreover, increase in the dimensions of the distilled base helps coupling reflective panels to the distilled base to reflect incident solar radiation to the distillation basin. For this purpose , two solar stills were made, one conventional designand another made according to the proposed design. The two solar stills were tested during the period from February to July 2009 under varying weather conditions of Basra, Iraq (latitude of 33.33 and longitude of 44.43). Experimental results showed that the modified still gives about 18%-24% higher distillate than the conventional still for the same basin condition.

Keywords: Distilled water productivity; solar still; productivity; conventional solar still

1. المقدمة

من المعروف ان تحلية المياه المالحة باستخدام انظمة تعمل بالطاقة الشمسية ومنذ فترة طويلة تعتبر حل عملي لانتاج الماء الصالح للشرب وخاصة في المناطق النائية التي تعاني من شحة في المياه الصالحة للشرب بسب ضعف البنية التحتية وعدم اتصال الكثير منها بالشبكة الرئيسية الوطنية للماء، بالمقابل ممكن لمنظومة تقطير صغيرة ان تكون حل عملي واقتصادي للطلب الحالي والمستقبلي للمياه الصالحة للشرب مع توفر موارد المياه وكمية اشعاع شمسي كبيرة في تلك المناطق النائية، لذلك يتعين بحث العوامل المؤثرة في انتاجية وكفاءة المقطرات الشمسية ومحاولة تحسينها وايجاد طرق تؤدي الى زيادة انتاجيتها.

قام العديد من الباحثين في شتى انحاء العالم بدراسات عديدة تهدف الى تحسين تكنولوجيا تحلية المياه بالطاقة الشمسية، من خلال تقييم تاثير بعض العوامل الهامة على اداء النظام مثل تاثير المناخ والظروف التشغيلية والموقع الجغرافي على انتاجية المياه [Al-Hinai, 2002][Akash and Naifeh, 2000]. نشرت نتائج جيدة من قبل بعض الباحثين في مجال تحسين أداء منظومات تحلية المياه بالطاقة الشمسية [Bochekima, 2003] [Joseph, 2005]. من الطرق المتبعة لتحقيق هذا الهدف هو زيادة عملية التكثيف باستخدام الاساليب المختلفة [Ahmed, 1988] [Abbas, 2005]. من المناطق التي تعاني من شحة المياه العذبة ومشكلة ارتفاع نسبة الملوحة في العراق وبالتحديد ناحية السيبة التابعة لقضاء الفاو جنوب البصرة، لذلك أُخذت هذه المنطقة كمثال واقعي لتشغيل وفحص أداء منظومة التقطير الشمسية المستخدمة في هذا البحث. خاصة اذا علمنا ان العراق بشكل عام ومحافظة البصرة بشكل خاص من مناطق العالم الغنية بالطاقة الشمسية وان اشعة الشمس متوفرة على مدار السنة وبحدود 3600 ساعة سنويا [Alawee, 2008].

هدف البحث الحالي هو دراسة لمنظومة تقطير شمسي مزدوجة الميل بعد اجراء تغيير في التصميم التقليدي بهدف الحصول على زيادة في انتاجية الماء المقطر، تم ذلك من خلال تكبير ابعاد المقطر نسبة لحوضه وهذا يوفر زيادة اضافية في مساحة سطح التكثيف فضلا عن امكانية ربط الواح عاكسة للاشعة الشمسية مع قاعدة المقطر تقوم بعكس جزء من الاشعة الشمسية الساقطة عليه والمساهمة في التسخين الاضافي لحوض التقطير

2. وصف المنظومة

اساس عمل المقطر الشمسي بسيط جدا، حوض التقطير يعمل كلوح ماص للطاقة الشمسية التي بدورها تقوم بتسخين المياه المالحة او القليلة الملوحة داخله وبالتالي فالماء فقط هو الذي يتبخر تاركا الملوثات والمعادن الصلبة الذائبة التي ليس لديها القدرة على ان تتبخر، بخار الماء يبدأ بلارتفاع نتيجة لخلق قوة دافعة (تيارات الحمل الحراري) بسب اختلاف درجات الحرارة بين الماء والزجاج، بخار الماء عندما يكون في تماس مع السطح الزجاجي (سطح التكثيف) الابرد نسبيا فانه سوف يبدأ بالتكثف في قطرات مختلفة الحجم من الماء المقطر، تحرك القطرات المتكثفة وبفعل الجاذبية على طول اللوح الزجاجي المائل. واخيرا يتم جمع الماء المتكثق من خلال قناة تجميع. من اجل موثوقية النتائج تم تصنيع اثنين من المقطرات الشمسية واختبارها بصورة متزامنة. الاول مقطر ماء شمسي شمسي بالتصميم المقترح (هذف الدراسة) ونرمز له بالرمز (A) تم تصنيعه بما يوفر مساحة سطحية اكبر لسطح التكثيف بالمقارنه مع مقطر شمسي اعتيادي له نفس مساحة حوض التقطير، تساهم زيادة مساحة سطح التكثيف بلاسراع من معدل التكثيف بما يوازي معدل التبخير، المقطر الثاني ونرمز له بالرمز (B) وهو مقطر ماء شمسي تقليدي له نفس المساحة السطحية لحوض التقطير للمقطر (A). الجدول رقم (1) يمثل مواصفات المقطرات الشمسية المصنعة.

جدول رقم 1: موصفات المقطرات الشمسية المستخدمة في البحث

ت	المقطر A (المقترح)	المقطر B (التقليدي)
1	حوض التقطير مصنوع من صفائح من الحديد المغلون بسمك (1 mm) بمساحة ($0.75\ m^2$) لحوض التقطير ومساحة مقدارها ($1.375\ m^2$) لقاعدة المقطر الداخلية.	حوض التقطير مصنوع من صفائح من الحديد المغلون بسمك (1 mm) بمساحة ($0.75\ m^2$) لحوض التقطير وبنفس مساحة قاعدة المقطر الداخلية ومقدارها ($0.75\ m^2$).
2	غطاء من الزجاج الاعتيادي بسمك (4 mm) وبمساحة كلية مقدارها ($1.8\ m^2$)	غطاء من الزجاج الاعتيادي بسمك (4 mm) وبمساحة كلية مقدارها ($1m^2$)
3	غُلفت قاعدة المقطر وجدارنه الداخلية بصفائح ورقية عاكسة من الالمنيوم لتقوم بعكس قسم من الاشعة الشمسية الساقطة والمساهمة في التسخين الاضافي لحوض المقطر.	قاعدة المقطر هي نفسها حوض التقطير، اي لا توجد مسافة بين حوض المقطر وقاعدته
4	ارتفاع الحافات الجانبية للمقطرات الشمسية تؤثر بنفس المقدار على كلا المقطرين	

لتركيز الطاقة الشمسية على حوض المقطر تم طلاء الطبقة السطحية لحوض التقطير بطلاء اسود داكن غير لماع من صنع شركة الاصباغ الحديثة العراقية، له امتصاصية مقدارها (0.96) وانبعاثية مقدارها (0.81). استعملت الواح من الزجاج الاعتيادي بسمك (4mm) لتكوين سطح التكثيف وتم امالتها بزاوية مقدارها (20^o) [Radwan, 2009]. ثُبتت الالواح الزجاجية باحكام باستخدام شريط معدني وطبقة من السليكون المطاط لاسناد الالواح الزجاجية من الاعلى اما من الاسفل فقد تم تثبيت الالواح الزجاجية مع حافة الحوض ايضا باستخدام مادة السليكون المطاط لمنع تسرب البخار الى الخارج. للحفاظ على مستوى ثابت للماء داخل حوض المقطر وحسب العمق المطلوب استّعملت طوافة من النوع الدقيق تم تصنيعها بصورة خاصة من اجل البحث. تم عزل جهاز التقطير بمادة الصوف الزجاجي بسمك (70 mm) من الاسفل ومن الجوانب. غلف جهاز التقطير بطبقة من الحديد المغلون بسمك (0.3 mm) وصندوق خشبي بسمك (10 mm) لغرض حفظ واحتواء المقطر والمادة والعازلة علاوة على اعتباره مادة عازلة اضافية. استخدم خزان رئيسي بسعه (40 L) لتجهيز الماء المالح. الشكل رقم (1) يمثل مخطط توضيحي للمقطرات الشمسية المستخدمة في البحث والاشكال (2) و (3) تمثل صور فوتوغرافية لهما. استخدمت لقياس درجات الحرارة للمقطرات الشمسية مزدوجات حرارية نوع (T) تم توصيلها من خلال مفتاح انتقائي (Selector switch) يحتوي على عشرون نقطة الى محرار رقمي (Digital thrmometer). درجة حرارة المحيط الخارجي تم قياسها بواسطة محرار زئبقي معزول عن عن الاشعة

الشمسية والمؤثرات الجوية وموضوع داخل صندوق خاص به وعلى ارتفاع متر واحد من سطح الارض. كمية الماء المتجمعة تم قياسها بواسطة وعاء سعته الكلية (2 liter) وقياس اصغر تدريج فيه هو (100 mm).

3. طريقة الفحص

تم اجراء عدد من التجارب العملية على المقطرات الشمسية تحت الظروف المناخية المختلفة لمدينة البصرة (خط طول 48.36 شرقا وخط عرض 30.34 شمالا). استخدمت عينات من الماء المالح لمنطقة (السيبة) التابعة لقضاء الفاو، جنوب البصرة. نفذت التجارب بشكل متزامن لكلا المقطرين (A) و (B)، كل تجربة تعاد اربع مرات لكل شهر من اشهر الاختبار وذلك للتاكد من موثوقية النتائج. التجارب التي تغيرت فيها اعماق المياه داخل حوض التقطير اجريت ايضا بصورة متوالي لضمان قدر الامكان ظروف عمل متشابهه لاجل المقارنه مع كل عمق من اعماق المياه المستخدمة في التجربة. تبدا جميع التجارب (بعد التاكد من نظافة الاغطية الزجاجية) من الساعة الثامنة صباحا بمعدل ثمان او عشر ساعات لكل اختبار وحسب الموسم للفترة الممتدة بين شهري شباط وتموز من عام 2009.

خلال جميع التجارب التي اجريت تم تسجيل المتغيرات التالية لكل ساعة: الانتاجية (كمية الماء المقطر)، معدل درجة حرارة الماء في حوض التقطير، درجة حرارة المياه التعويضية الداخلة الى حوض المقطر، درجة حرارة الغطاء الزجاجي، درجة حرارة المحيط الخارجي. كمية الاشعاع الشمسي فقد تم حسابها رياضيا باستخدام المعادلات المستخدمة من قبل الباحث [Hadi, 1984]. سرعة الرياح مؤثرة على كلا المقطرين بنفس المقدار لذلك لم يتم قياسها وكذلك لا يوجد ماء مستنزف من حوض المقطر.

4. النتائج والمناقشة

تم اجراء عدد من التجارب العملية لكلا المقطرين المستخدمين في البحث للفترة الممتدة بين شهري شباط وتموز من عام 2009، كانت جميع التجارب متشابهة تقريبا من حيث السلوك الحراري لذلك تم اختيار بعض التجارب ليتم تمثيلها بيانيا:

4.1 تاثير التصميم الحالي على انتاجية وكفاءة المقطر الشمسي

تم في البداية تثبيت عمق المياه داخل حوض المقطر عند (1 cm) واجراء التجارب بصورة متزامنة وتحت نفس الضروف المناخية لكلا المقطرين (A) و (B). من خلال جميع التجارب التي اجريت وجد ان التصميم الحالي يوفر مساحة اكبر لسقوط الاشعاع الشمسي من خلال الصفائح العاكسة التي تقوم بعكس الاشعاع الساقط على قاعدة المقطر وتؤدي الى زيادة تسخين المياه في حوض التقطير فضلا عن زيادة مساحة سطح التكثيف، مما له تاثير واضح في زيادة كمية الماء المنتج بالمقارنة مع المقطر الشمسي الاعتيادي وهذا بسب ما يوفره التصميم الحالي من توازن بين زيادة معدل الماء المتبخر والمساحة السطحية الكافية لتكثف الماء.

الشكل رقم (4) يمثل الانتاجية الساعية من الماء المقطر لكلا المقطرين تحت شدة اشعاع شمسي مقداره (31.9 MJ/day) خلال ساعات الاختبار (من الثامنة صباحا الى الخامسة مساءا)، نجد ان هناك زيادة في الانتاجية مقدارها (18%–24%) يحققها المقطر المعدل (A) بالمقارنة مع المقطر التقليدي (B) في جميع التجارب التي اجريت وهي بدون الانتاج اليلي.

يمثل الشكل رقم (5) معدل الانتاجية اليومية خلال النهار مع شدة الاشعاع الشمسي لاشهر مختلفة من السنة ومقارنة النتائج مع القطر (B) تحت نفس الضروف المناخية ومن خلاله نلاحظ الزيادة الواضحة في الانتاجية وللاسباب المذكوره اعلاه.

الشكل رقم (6) يمثل مقارنة المقطرين من حيث الكفاءة الساعية خلال فترة الاختبار، اما الشكل رقم (7) فيوضح تغيير الكفاءة اليومية مع شدة الاشعاع الشمسي خلال الاشهر المختلفة من السنة، حيث وجد ان كفاءة المقطر (A) الساعية واليومية تزداد بصورة ملحوضة في جميع الاختبارات التي اجريت وهذه بسب زيادة كمية الماء المنتج لنفس كمية الاشعاع الشمسي التي يتعرض لها المقطرين، اذ ان التسخين الاضافي الناتج من الاشعة المنعكسة من قاعدة المقطر ساهم بشكل كبير في تحسين الاداء، وهذا ايضا ما يوضحه الشكل رقم (8) الذي يمثل تاثير اضافة الصفائح العاكسة الى قاعدة المقطر على الانتاجية، وجد ان هناك زيادة في الانتاجية مقدارها تقريبا (14%) في حالة اضافة الصفائح العاكسة الى قاعدة حوض المقطر.

4.2 فحص المقطر باعماق مياه مختلفة وتاثير العمق على انتاجية وكفاءة المقطر

من اجل التحقق من فعالية التصميم الحالي (A) تم في هذا الجزء من التجارب فحص اربع اعماق مختلفة للمياه داخل حوض التقطير وهي (5 mm, 10 mm, 2mm, 3mm) لاربعة ايام متوالية. تسجل لكل عمق قرائتين، الاولى للمقطر (A) والثانية للمقطر (B). بينت النتائج ان هناك افضلية في الانتاجية يحققها المقطر(A) في كل اعماق المياه المستخدمة في البحث وبنسبة تتراوح (18%-24%)، كذلك بينت النتائج بان عمق المياه داخل حوض التقطير له تاثير كبير على الانتاجية حيث ان الانتاجية تزداد كلما قل عمق المياه داخل حوض التقطير بشكل طردي مع زيادة معدل التبخير. الاشكال رقم (9) و (10) تمثل النتائج التي تم الحصول عليها خلال ساعات النهار (بدون الانتاج الليلي) لكلا المقطرين، اذ اعطى استخدام العمق الاقل للماء (5 mm) زيادة في الانتاجية مقدارها (10%) بالمقارنه بالمقارنة مع العمق (10 mm) واعطى نسبة زيادة مقدارها (17%) بالمقارنة مع العمق (2 mm) و ايضا اعطى زيادة مقدارها (19%) بالمقارنة مع العمق (3 cm). هذه الزيادة هي بسب زيادة معدلات انتقال الحرارة كلما قل سمك الماء داخل حوض التقطير وبالتالي زيادة معدل التبخير ومن جهه اخرى توفر المساحة الكافية للتكثيف الذي يعطيه التصميم الحالي للمقطر. الاشكال رقم (11) و (12) توضح تغير الكفاءة الساعية لكلا المقطرين لاعماق مختلفة من المياه داخل حوض التقطير. يتم حساب الكفاءة اليومية من العلاقة التالية: $\eta_h = (P.L_h)/I_T$ ونلاحظ من خلالها كيفية زيادة الكفاءة مع نقصان عمق المياه داخل حوض التقطير. كفاءة المقطر (A) هي (15%-57%) بينما كانت كفاءة المقطر (B) هي (-14% 51%) لنفس العمق (0.5 cm).

4.3 تاثير التصميم الحالي على فرق درجات الحرارة (Tw-Tg)

النتائج التي ذكرت في الفقرات السابقة بينت حصول زيادة في الانتاجية يحققها التصميم المعدل (المقطر A) الذي يسهل من اضافة الواح عاكسة تساعد في زيادة درجة حرارة الماء في حوض التقطير. الشكل رقم (13) يمثل فرق درجات الحرارة بين الماء في حوض التقطير والغطاء الزجاجي (Tw-Tg)، حيث تم الحصول على (10 $^{\circ}$C) فرق في درجات بالنسبة للمقطر (A) وعلى (4 $^{\circ}$C) بالنسبة للمقطر (B). ان زيادة فرق درجات الحرارة بين الماء في حوض التقطير والغطاء الزجاجي (Tw-Tg) هو بسب التاثير الكبير للسطوح العاكسة المضافة الى قاعدة المقطر والتي ساهمت في التسخين الاضافي لحوض التقطير. في جميع التجارب التي اجريت كانت قياسات درجات الحرارة متشابه من حيث السلوك الحراري لكنها مختلفة في القيم حسب نوع التجارب

والظروف التشغيلية، الشكل رقم (14) يمثل نتائج قياسات درجات الحرارة (درجة حرارة الماء، درجة حرارة الغطاء الزجاجي، درجة حرارة الهواء الخارجي) لعينة اخرى مختارة من الاختبارات.

5. الاستنتاجات

1. بينت النتائج العملية امكانية تحسين انتاجية المقطر الشمسي الاعتيادي باستخدام اسلوب مبسط يتضمن زيادة حجم المقطر نسبة لحوضه وهذا زيادة واضحة في مساحة التكثيف وكذلك التسخين الاضافي للماء داخل حوض التقطير باستخدام صفائح عاكسة.

2. ان اضافة الصفائح العاكسة للاشعاع الشمسي تساهم في التسخين الاضافي لحوض المقطر وبالتالي تؤدي الى زيادة فرق درجات الحرارة بين الماء والغطاء الزجاجي مما يزيد من معدل التكثيف.

3. ممكن زيادة الانتاجية من خلال تقليل اعماق المياه داخل حوض التقطير، اذ اعطى العمق الاقل للماء (0.5 cm) زيادة في الانتاجية مقدارها (10%) بالمقارنه بالمقارنة مع العمق (1 cm) واعطى نسبة زيادة مقدارها (17%) بالمقارنة مع العمق (2 cm) و ايضا اعطى زيادة مقدارها (19%) بالمقارنة مع العمق (3 cm) وبلامكان زيادة هذه النسب خلال فترة غياب الاشعاع الشمسي نتيجة لارتفاع درجة حرارة طبقة المياه داخل حوض المقطر

4. ان الموقع الجغرافي لاجراء التجارب والمتمثل بمدينة البصرة () له اثار ايجابية كبيرة على الانتاجية نظرا لما يتمتع به من شدة اشعاع شمسي عالي على مدار السنة.

المصادر

- Khalifa, A. H., 1984, Water distillation using a cooling tower and a flat plate solar collector, M.Sc Thesis, University of technology, Baghdad, Iraq,.
- Wisam H. A., 2008 "A simple Design Solar Water Heater" Al-Taqani Journal, 21, 27-38
- AL-Hinai H., AL-Nassiri M.S., and Jubran B.A., Parametric investigation of a double effect solar still in comparison with a single-effect solar still, Desalination, Vol.150, 2002, 75-83
- Akash B., Naifeh W., and Mohsen M., 2000, Energy Conversion and Mgmt, Vol.41, 883
- Bchiar Bouchekima, 2003, A small solar desalination plant for the production of drinkable water in remote arid areas of southern Algeria, Desalination, Vol. 159, 197-204.
- Joseph, I. and Saravanan, S., 2005, Study of single solar distillation system for domestic application, Desalination, Vol. 173, , 77-82
- Abbas K. I., 2005, Solar water distillation using a combind solar water heater distillater, M.Sc Thesis, University of technology, Baghdad, Iraq,.
- Radwan, S. M., Hassanain, A.A., 2009, Single slope solar still for sea water distillation." World applied science Journal, 7(4), 485-497.
- Ahmed S. T. , 1988, Study of single-effect solar still with an internal condenser, Solar and wind tech. vol 5 no.6 pp. 637-643,

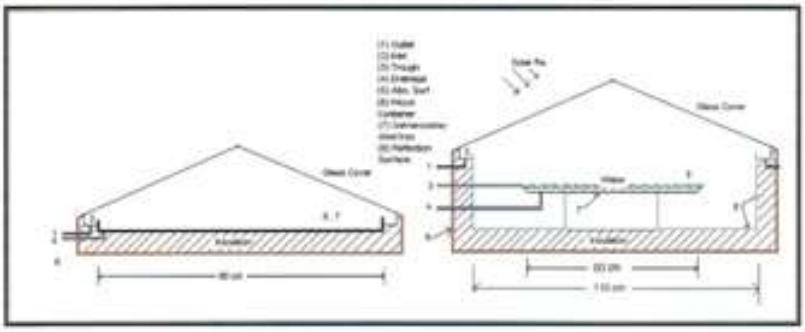

الشكل (1): يمثل مخطط موضح فيه الشكل العام للمقطرات المستخدمة فى البحث

الشكل (2): صورة فوتوغرافية توضح الشكل العام للمقطر (A)

الشكل (3): صورة فوتوغرافية توضح الشكل العام للمقطر (B)

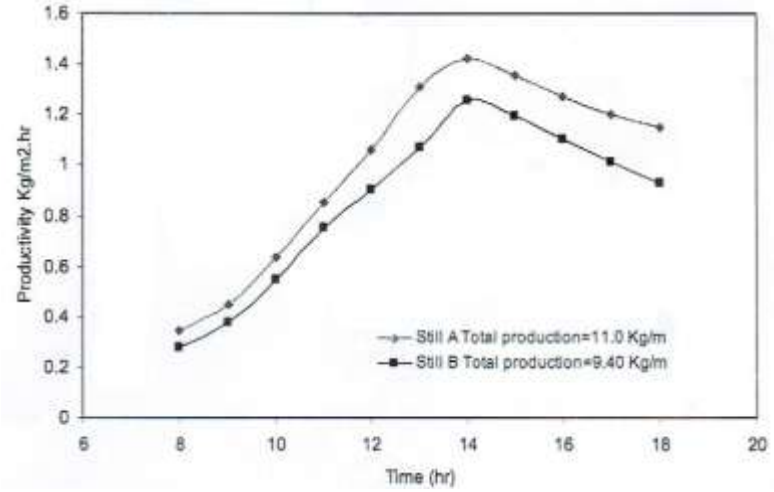

الشكل (4): تغير الانتاجية اليومية مع ساعات النهار لكلا المقطرين لعمق (1 cm)

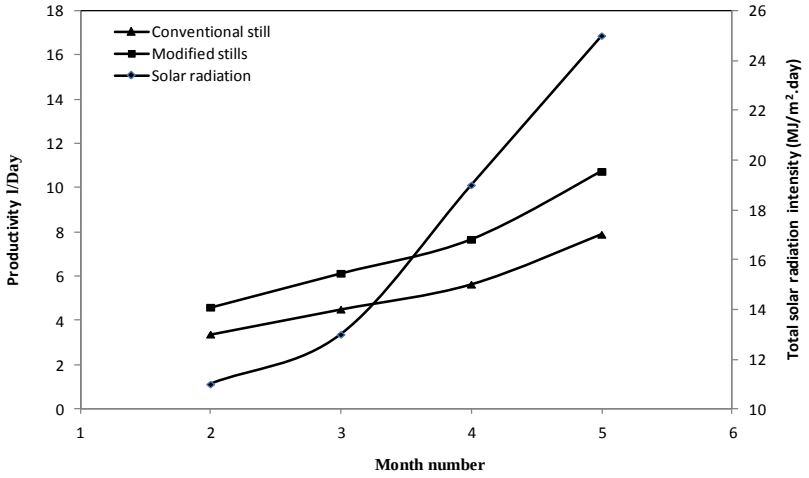

الشكل (5) : تغير الانتاجية اليومية مع شدة الاشعاع الشمسي لاشهر مختلفة من السنة

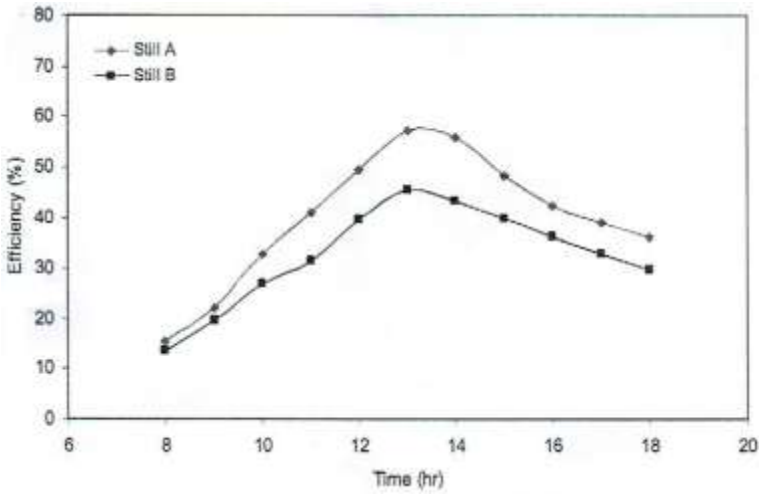

الشكل (6) : تغير الكفاءة الساعية مع ساعات النهار لكلا المقطرين لعمق (1cm)

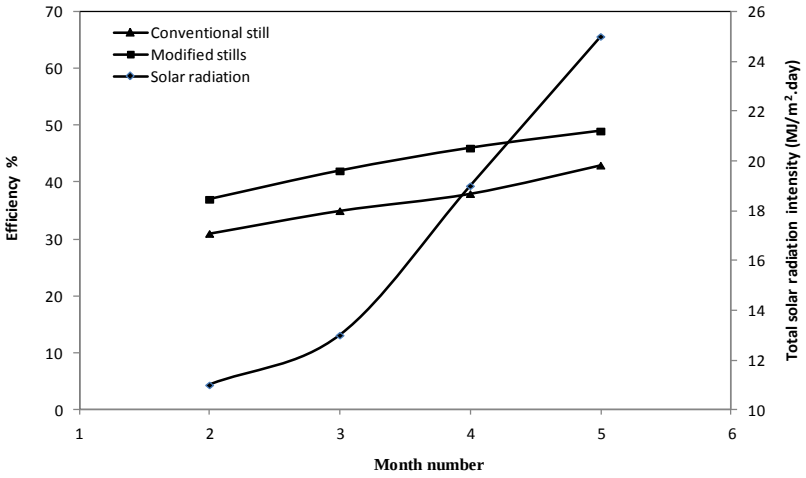

الشكل (7): تغير الكفاءة اليومية مع الاشعاع الشمسي لكلا المقطري لاشهر مختلفة من السنة

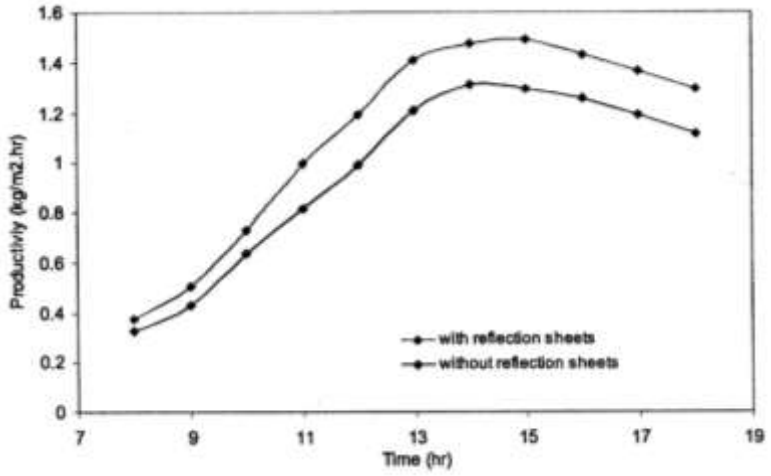

الشكل (8): تاثير اضافة صفائح عاكسة للاشعاع الشمسي على الانتاجية الساعية

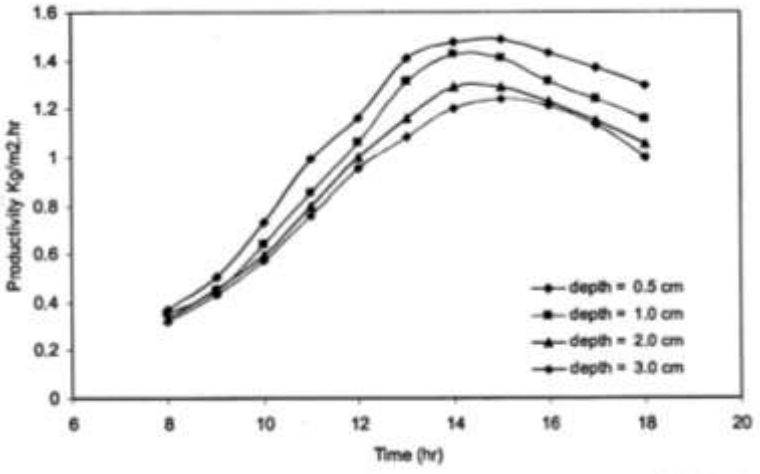

الشكل (9): تغير الانتاجية مع ساعات النهار لاعماق مختلفة من المياه للمقطر (A)

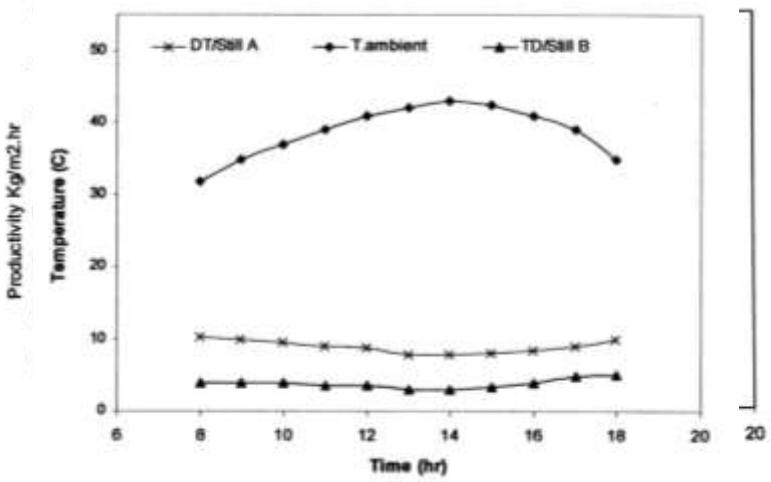

الشكل (10): تغير الانتاجية مع ساعات النهار لاعماق مختلفة من المياه للمقطر (B)

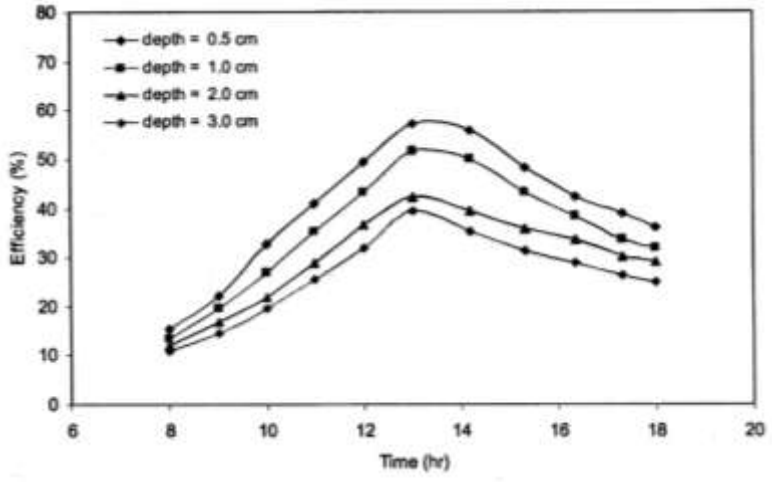

الشكل (11): تغير الكفاءة مع ساعات النهار لاعماق مختلفة من المياه للمقطر (A)

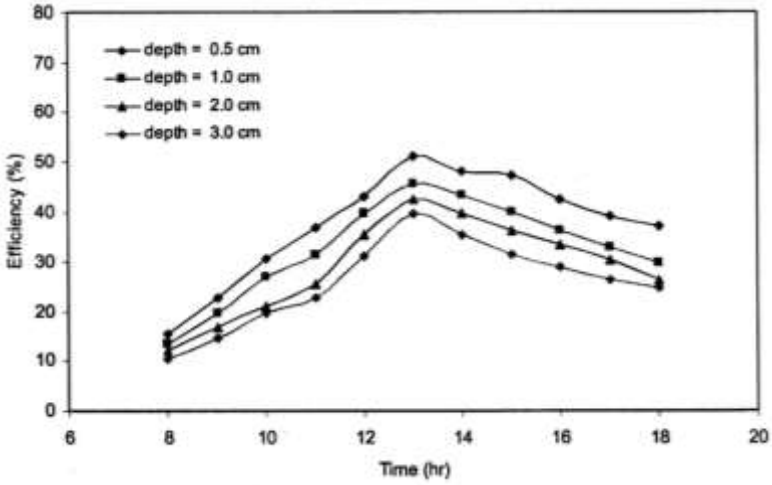

الشكل (12): تغير الكفاءة مع ساعات النهار لاعماق مختلفة من المياه للمقطر (B)

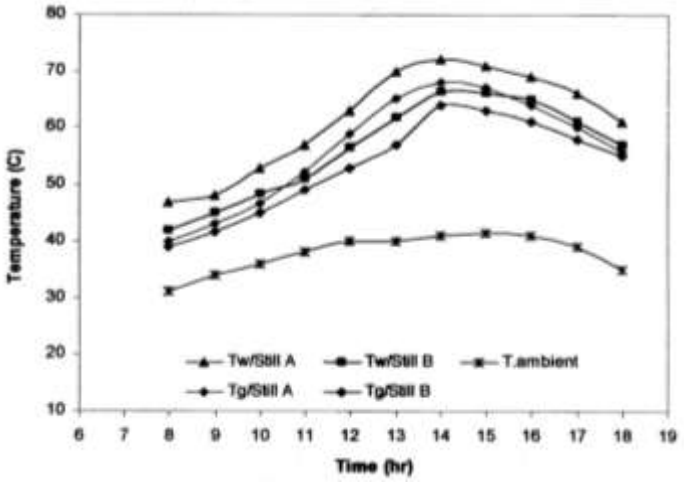

الشكل (13): يمثل تغير درجات الحرارة للماء المقطر والغطاء الزجاجي والهواء الحارجي مع الزمن لكلا المقطرين لعمق (1 cm)

An Investigation into Thermal Performance of Closed Wet Cooling Tower for Use with Chilled Ceilings in Buildings

Asst. Prof. Dr. Najim Abid Jassim
Department of Mechanical Engineering
College of engineering
University of Baghdad
Email: najmosawe@yahoo.com

Athraa Hameed Turki
Department of Mechanical Engineering
College of engineering
University of Baghdad
Email: Msc_mechanic@yahoo.com

ABSTRACT

Chilled ceilings systems offer potential for overall capital savings. The main aim of the present research is to investigate the thermal performance of the indirect contact closed circuit cooling tower, ICCCCT used with chilled ceiling, to gain a deeper knowledge in this important field of engineering which has been traditionally used in various industrial & HVAC systems. To achieve this study, experimental work were implemented for the ICCCCT use with chilled ceiling. In this study the thermal performances of closed wet cooling tower use with chilled ceiling is experimentally and theoretically investigated. Different experimental tests were conducted by varying the controlling parameters to investigate their effects on the ICCCCT characteristics such as tower cooling capacity, chilled ceiling cooling capacity, tower saturation efficiency, mass transfer coefficient and heat transfer coefficient. The following controlling parameters are varied during experiments: spray water flow rate (90 to 150 kg/hr), ambient air wet bulb temperature (12 to 18 ^{o}C), and also changing chilled ceiling flow rate (2 to 6 l/min).

KEY WORDS: Cooling tower, chilled ceiling, Droplet trajectory, Two-phase flow, Computational fluid dynamics

دراسة الأداء الحراري لبرج تبريد من النوع المغلق ذي الإتصال غير المباشر مع السقوف المبردة

أ.م.د. نجم عبد جاسم
قسم هندسة الميكانيك
كلية الهندسة / جامعة بغداد

م.م. عذراء حميد تركي
قسم هندسة الميكانيك
كلية الهندسة / جامعة بغداد

الخلاصة

توفر انظمة السقوف المبردة الطاقة بكفاءة كبيرة.إنَ الهدف الرئيسي من هذا البحث هو دراسة الأداء الحراري لبرج تبريد ذي النوع المغلق والإتصال غير المباشرالمستخدم مع انظمة السقوف المبردة, للحصول على معرفة اعمق في هذا المجال الهندسي المهم الذي يستخدم بكثرة في كثير من التطبيقات الصناعية وفي تكييف الهواء. لتحقيق هذه الدراسة، فلقد تم إجراء إختباراتٍ عملية لبرج التبريد المذكور.في هذه الدراسة قد تم التحقق من الأداء الحراري ابراج لتبريد الرطبة المغلقة المستخدمة مع السقوف المبردة نظريا وعمليا.تم إجراء عدد من الإختبارات العملية عن طريق تغيير العوامل الحاكمة في أداء برج التبريد لتحري تأثيراتها على خصائص البرج مثل السعة الحرارية للبرج،السعة الحرارية للسقف المبرد, معامل الأداء، كفاءة الإشباع، معامل إنتقال الكتلة، معامل إنتقال الحرارة. تم إجراء الإختبارات العملية بتغيير الظروف الآتية:معدل تدفق ماء الرش بِمَدى(90 إلى 150 كلغ/ساعة)، درجة حرارة البصلة الرطبة للهواء الخارجي بِمَدى(12 إلى 18 م^{o})، وكذلك تم تغيير معدل تدفق السقف المبرد(2 إلى 6 لتر/ثانية) من أجل تحري تأثير ذلك على هبوط ضغط الهواء.

1. INTRODUCTION

Chilled beam means a cooled element or cooling coil situated in, above or under a ceiling which cools convectively using natural or induced air flows. The cooling medium is usually water. Chilled beam systems are used mostly in the nonresidential buildings. These are commercial buildings, offices, hotels, banks, universities, schools and hospitals.

Inside a CWCT, three fluids flow: cooling water, spray water and air. The cooling water is the fluid to be cooled, which flows inside tubes arranged in rows inside the tower. Spray water, injected on the tubes surface, re-circulates in a closed circuit, which makes it an intermediate fluid in the heat transfer process. Heat carried away from the building by the cooling water transfers to the spray water through the tube walls. From the spray water, heat transfers to air by both sensible heat and latent heat. The latter makes the major contribution and is caused by the evaporation of a small amount of the spray water into the air stream. The use of the closed type of cooling towers, which is indirect contact equipment, permits high level of cleanliness of the piping resulting in effective internal heat transfer surface, reduced maintenance costs and longer operational life.

A system consisted of a CWCT and chilled ceilings when used for cooling of buildings will result in a low cost, CFC free and environmentally clean system. The initial and running costs of the system are low when compared with traditional vapor-compression cooling systems. The low energy consumption results in higher coefficient of performance and lower CO_2 emissions.

The cooling rate is affected by the heat transfer from the water inside tubes to the spray water and then to the air. Hence, the optimum performance of a cooling tower depends on the number and arrangement of tube coils and on the uniformity and effectiveness of the water distribution as well as the cooling capacity of ambient air and the distribution of air velocity through the coils. An unsatisfactory distribution of water over coils would lead to a reduced evaporative cooling surface and increased air flow and flow resistance in areas devoid of water flow. A non-uniform distribution of air would increase flow resistance in areas of high local velocities and decrease heat transfer in areas of low velocities. Simultaneous occurrence of non- uniform distributions of air and water would further degrade the performance of the tower.

Chilled beam systems are based on dry cooling principle. Therefore these systems are applied in the premises where humidity of air is controlled by means of dehumidification of primary air and limitation or control of infiltration through the enclosing structures. In other words the building should meet standards of air tightness. Condensation on surface of chilled beam exchanger should be prevented via control of water temperature.

Research dealing with the application of cooling towers as the sole free cooling source in air-water systems, i.e. systems comprising chilled ceilings or chilled beams for cooling, is however limited. The earliest found is by **,Niu and Kooi 1993. and ,Niu et al. 1995**. Their work consisted of measurements of chilled ceilings in a laboratory and development of a simulation program, ACCURACY, with the aim of studying the performance of chilled ceilings. In their work, they also studied the performance of chilled ceilings in connection with an evaporative cooling tower.

Koschenz 1995. presented an analytical model for CWCT to be used with chilled ceilings. He made two assumptions: first, constant spray water temperature along the tower and second that the spray water temperature was equal to the outlet cooling water temperature. However, spray water temperature is variable inside the tower and if, the heat loss from the spray water piping outside the CWCT casing is ignored, spray water temperature will be equal in the tower's inlet & outlet.

Almadari et al 1998. reported the test performed by BRE (Building Research Establishment, London UK) where an office room was equipped with a chilled ceiling connected to a cooling tower. At a sensible heat gain of 60 W/m^2, a maximum indoor air temperature of 25.2°C was registered.

Gan and Riffat 1999. used computational fluid dynamic CFD calculations to predict the thermal performance of a CWCT for chilled ceiling system. They used CFD package, FLUENT, to simulate the two-phase flow of gas and water droplets in a 2D simulation. The Eulerian approach was used for the gas phase flow using standard k-ε model to represent the effect of turbulence while the Lagrangian approach was used for the water droplet phase flow, with two-way coupling between the two phases with the assumption of uniformly distributed volumetric heat generation from the tubes of the heat exchanger. The gas phase equations were solved numerically using a control volume technique embodied in the SIMPLE algorithm for the coupling between the pressure and the velocity fields. The computational results showed an increase of cooling water temperature for the lower tube rows in the tower. This behavior was attributed to the assumption of uniform heat flux generation. In reality, heat flux is higher for the upper rows because of the higher inlet cooling water temperature. The CFD technique was validated by comparing the predicted cooling performance with measurement. The predicted maximum decrease in the coil temperature is also in good agreement with the measured result for the water temperature.

Sprecher and Tillenkamp 2003. published an investigation on a system with a closed evaporative cooling tower and a water circuit embedded in the concrete slab. They used the simulation program TRNSYS for investigating such a system. Sprecher and Tillenkamp processed dynamic simulations of a large shopping centre, 10 000 m^2, in Lucerne, Switzerland, with internal heat gain from people and lighting at 42 W/m^2. During the warmest weak of the year, the indoor air temperature was kept below 26°C.

Hasan et al. 2007. uses a simulation tool (IDA-ICE) to find out the best performance of a cooling tower combined with chilled ceiling, serving a four storey residential building. The highest yearly mean COP achieved was 8,3.

It can be concluded that there are few published data concerning the resulting indoor climate in buildings equipped with chilled ceilings connected to an evaporative cooling tower, especially where the cooling tower is the sole provider of chilled water. The available data indicate the possibility to achieve an indoor thermal. In this work, a new application of already established cooling techniques is investigated under Iraqi climate conditions. The application comprises the use of a cooling tower, as the sole provider of chilled water, in conjunction with a hydronic cooling system with chilled ceiling.

2. EXPERIMENTAL WORK

The system that used in the experimental tests is a (WL 320 Demo cooling tower, made by Gunt Company in Germany). It was an open circuit direct contact counter flow forced draft cooling tower. This cooling tower was modulated to be used as an indirect contact closed type cooling tower by adding several components such as a bare-tube heat exchanger & the cooling water circuit The heat exchanger was designed and then manufactured according to the procedure that presented by (Kern in 1978). It was consisted of 8 mm outside copper tube diameter with 6 rows and 12 columns in an inline arrangement. The experimental apparatus consists generally of the cooling column, cooling water circuit, spray water circuit, the air circuit& test room. A schematic diagram & a photograph of the experimental apparatus are shown in Figures (1) & (2), respectively.

Typical experiments were conducted with the following procedure:

1) Experiment of Changing Chilled Ceiling & Tower Flow Rate:

After all the measured parameters were stabilized at the desired level, the tower let to operate with 2 l/min chilled ceiling & tower flow rate. It was noticed that after about 30 minutes all the measured values were stabilized. At this moment all the measured values were collected and recorded and then chilled ceiling & tower flow rate was increased 1 l/min, for each test, and so on until chilled ceiling & tower flow rate reached 6 l/min recording the measured values at each test.

2) Experiment of Changing Spray Water Flow Rate:

After all the measured parameters were stabilized at the desired level, the tower let to operate with 90 l/hr spray water flow rate. It was noticed that after about 30 minutes all the measured values were stabilized. At this moment all the measured values were collected and recorded and then spray water flow was increased 15 l/hr, for each test, and so on until spray flow rate reached 150 l/hr recording the measured values at each test.

3) Experiments of changing The Inlet Air Wet Bulb Temperature:

After turning on the fan and pumps and heating the cooling water, the dry bulb temperature and the relative humidity of the inlet air were changed by the use of the humidifier and the dehumidifier. The wet bulb temperature was taken then from a computer program for psychometric chart according to the measured values of dry bulb temperature and relative humidity. After few minutes the air stabilized at the desired wet bulb temperature and then measurements were recorded. This experiment was started with 12 ^{o}C wet bulb temperature increasing it 2 ^{o}C at each time until it reached 18 ^{o}C.

3. Analysis of the Experimental Data

The cooling capacity of the cooling tower was calculated according to the following equation by **Hasan & Serin (2002)**:

$$Q_{C.T}=\dot{m}_{cw}C_{p,\ cw}dT_{cw} \qquad (1)$$

Where dT_{cw} is the cooling water range defined as:

$$dT_{cw}=T_{cw,in}-T_{cw,out} \qquad (2)$$

The coefficient of performance of the tower was calculated from the following equation by **Hasan & Serin (2002)**:

$$COP_{C.T}=\frac{Q_{C.T}}{W_{tot}} \qquad (3)$$

Where, W_{tot} is the total power consumption by the air fan and spray water pump defined as:

$$W_{tot}=W_f+W_{sp} \qquad (4)$$

Where, W_f is the fan power (W) while W_{sp} is the spray water pump power (W).

Another important variable in a cooling tower performance is the saturation efficiency which refers to how much the discharged air is saturated with water vapor. The

saturation efficiency, ε, for the closed circuit cooling towers was calculated from the following equation by **Yeon Yoo et al. 2010.**

$$\varepsilon=\frac{T_{cw,in}-T_{cw,out}}{T_{cw,in}-WBT_{in}} \qquad (5)$$

The calculation of the experimental mass transfer coefficient of water vapor between spray water film and air, and the calculation of the experimental heat transfer coefficient between tube external surface and spray water film are important part of the presented work because it permits to comparison with the other works.

Olivera & Facao (2002) presented a procedure to determine the mass transfer coefficient after experimental measurements by using an enthalpy balance by the following equation:

$$G\left(h_{air,out}-h_{air,in}\right)=\alpha_m \; A \; LMhD \quad (6)$$

where, α_m is the mass transfer coefficient for water vapor between spray water film and air (kg/m^2 s), A is the surface area of the heat exchanger equal to 0.226 m^2 , and LMhD: logarithmic mean enthalpy difference (kJ/kg) defined as:

$$LMhD=\frac{h_{air,out}-h_{air,in}}{\ln\frac{h_{sat,Ti}-h_{air,in}}{h_{sat,Ti}-h_{air,out}}} \qquad (7)$$

Where $h_{sat,Ti}$ is the specific enthalpy of the saturated air at the interface temperature (kJ/kg).

The average of spray water temperatures was taken as the interface temperature according to **Olivera & Facao (2002)** as well as **Stabat & Marchio (2004)** while the inlet and outlet air enthalpies were taken from the psychrometric chart according to the measured data.

The overall heat transfer coefficient, U_o, between water inside tubes and the interface based on the outer area of the tube. U_o is calculated as follows:

$$Q_{C.T}=\dot{m}_{cw}C_{p,cw}dT_{cw}=U_o \; A \; LMTD \qquad (8)$$

Where LMTD: is the logarithmic mean temperature difference (^oC) defined as:

$$LMTD=\frac{T_{cw,out}-T_{cw,in}}{\ln\frac{T_{cw,out}-T_{sp,ave}}{T_{wc,in}-T_{sp,ave}}} \qquad (9)$$

Where $T_{sp,ave}$ is the average spray water temperature (^oC) according to **Olivera & Facao (2002)** as well as **Stabat & Marchio 2004**.

After the overall heat transfer coefficient was calculated from the two equations above, it used to calculate spray heat transfer coefficient between the tubes external surface & spray water film:

$$\frac{1}{U_o}=\frac{1}{\alpha_w}\frac{D}{d}+\frac{D}{2k_{tube}}\ln\frac{D}{d}+\frac{1}{\alpha_s} \quad (10)$$

The coefficient of spray heat transfer which takes place between tubes external surface and spray water film was calculated as follows which was presented by **Olivera & Facao (2002)**.

$$\alpha_s=\left[\frac{1}{U_o}-\frac{1}{\alpha_w}\frac{D}{d}-\frac{D}{2k_{tube}}\ln\frac{D}{d}\right]^{-1} \quad (11)$$

Where α_w is the heat transfer coefficient for water inside the tubes ($W/m^2\ ^oC$) and it was calculated according to **Stabat & Marchio 2004.** by the following equation:

$$\alpha_w=0.023\frac{k_{cw}}{d}Re^{0.8}\ Pr^{0.3} \quad (12)$$

Where Reynolds number and Prandtl number were taken for the water inside tubes.

The cooling capacity of the chilled ceiling was calculated according to the following equation:

$$Q_{ceiling}=\dot{m}_{ceiling}C_{p,\ cw}dT_{ceiling} \quad (13)$$

Where dT_{cw} is the cooling water range of the chilled ceiling defined as:

$$dT_{ceiling}=T_{ceiling,out}-T_{ceiling,in} \quad (14)$$

4. RESULT AND DISCUSSION

Figures (3) to (8) indicate the effect of inlet air wet bulb temperature and chilled ceiling flow rate on the cooling tower performance and test room represented by cooling capacity, coefficient of performance, saturation efficiency, spray heat transfer coefficient, mass transfer coefficient, and chilled ceiling cooling capacity respectively.

As it seen in **Fig. 3**, wet bulb temperature affects the tower cooling capacity greatly. This figure shows that as the wet bulb temperature increases, cooling capacity decreases significantly. The increasing in inlet air wet bulb temperature means increasing in both the dry bulb temperature & the humidity of the inlet air and this decreases the transfer of heat both by convection & evaporation. It is also decrease when coil flow rate decrease with constant spray water flow rate.

When air wet bulb temperature reduces the tower cooling capacity, it reduces the tower coefficient of performance by the same rate as for cooling capacity because the wet bulb temperature has no effects on the power consumption of the equipment, this clear in **Fig. 4** and it decreases when chilled ceiling flow rate decreases too because the tower coefficient of performance depended on cooling capacity.

The wet bulb temperature of air has also influence on the tower efficiency as shown in **Fig. 5**. The efficiency increases slightly with the wet bulb temperature. If the wet bulb temperature increases, the difference between the inlet cooling water temperature & the inlet

wet bulb temperature in the denominator of Eq. (5) is decreased with a rate more than the rate of decreasing cooling water range so that the saturation efficiency is increased with increasing the wet bulb temperature. Also the efficiency is increased when coil flow rate decreases due to the increasing of the difference between the inlet cooling water temperature & outlet cooling water temperature.

When the wet bulb temperature increases, the spray heat transfer coefficient decreases, as expected, and as shown in **Fig. 6**. This is simply because of that the decreasing in the cooling capacity, as wet bulb increases, leads to decrease the overall heat transfer coefficient and thus the spray heat transfer coefficient decreases. It's also decrease with decreasing the chilled ceiling flow rate due to the decreasing in the cooling capacity, as wet bulb increases.

When the inlet air wet bulb temperature increases, mass transfer coefficient increases slightly as shown in **Fig. 7**. It is clear as the wet bulb temperature increases the difference between the outlet and inlet air enthalpy, Δh_{air}, is decreased with a rate less than that in the logarithmic mean enthalpy difference, LMhD, causing an increasing in mass transfer coefficient. Also it's decrease with decreasing the chilled ceiling flow rate due to the increase in cooling water range that is lead to decrease the difference between the outlet and inlet air enthalpy, Δh_{air},.

As it seen in **Fig. 3**, the wet bulb temperature has effect on the tower cooling capacity consequently on the chilled ceiling cooling capacity as it seen in **Fig. 8**. This figure shows that as the wet bulb temperature increases, cooling capacity of the chilled ceiling decreases significantly and also its decrease when chilled ceiling flow rate decrease.

Generally, air wet temperature has effect on the performance of cooling towers as it dictates the physical phenomena that take place inside it. It decreases the heat transfer; on the other hand it increases the efficiency of the tower & mass transfer.

Figures (9) to (13) indicate the effect of the spray water flow rate and chilled ceiling flow rate on the cooling tower performance represented by cooling capacity, coefficient of performance, saturation efficiency, spray heat transfer coefficient and mass transfer coefficient, respectively and **Fig. 14** indicates the effect of spray water flow rate and chilled ceiling flow rate on the test room performance represented by chilled ceiling cooling capacity.

Fig. 9 indicates that the cooling capacity of the cooling tower depends greatly on the spray water flow rate and it increases approximately linearly as the spray water flow rate increases. This is mainly because that when spray water flow rate increases, the rate of evaporation is augmented causing more heat transferred from the cooling water. For a spray water flow rate more than 135 kg/hr it is seen that the increasing rate in cooling capacity becomes rather less and this is partially attributable to the fact that this flow rate is sufficient to achieve completely wetting of the outer surface of the heat exchanger tubes. The evaporation of the water droplet at this flow rate can't continue that smoothly. When the mass flow rate of the spray water increased, the heat transfer increased and thus the heat absorbed by the air both by convection and evaporation was increased causing in increasing the cooling capacity. This means that the air flow rate becomes sufficient to absorb moisture at the interface between the air and the spray water film by the evaporative cooling, but as the spray water flow is constant so the absorption of moisture will not still to increase in the same rate when the air flow rate becomes high. Also the cooling capacity of chilled ceiling increase when the chilled ceiling flow rate increase.

The variation of the coefficient of performance of the experimental apparatus with respect to the variation of spray water flow rate and constant chilled ceiling flow rate is

shown in **Fig. 10**. It is clear that the coefficient of performance increases as spray water flow rate increases. When the flow rate of spray water increases both the cooling capacity & the power of the spray water pump, which are shown in table (1), increase but the increasing in the cooling capacity is much larger than that in pump power and this makes COP to increase with the increasing in spray water flow rate. The coefficient of performance for a cooling tower is the ratio of the cooling capacity to the total power consumption of the fan and the spray water pump and it is calculated according to Eq. (4). For example, when spray water mass flow rate increases, for the case with chilled ceiling flow rate equal to 6 l/min, from 90 to 150 kg/hr, then the cooling capacity increases with a ratio of 1.55 from 378 to 588 Watt while the spray water pump power increases with a ratio of 1.05 from 448 to 426 Watt and the fan power constant equal to 134 Watt because no changing in air fan power and this causing in increasing COP from 0.65 to 1.03 and it's also increase when chilled ceiling flow rate increase.

The effect of the spray water mass flow rate on tower efficiency can be seen in **Fig. 11**. An increase in spray flow rate increases cooling range and this increases the tower efficiency up to a certain level. Above a rate of about 135 kg/hr, an increase in spray flow rate does not significantly improve tower performance because the tube surface is almost completely wet as discussed in **Fig. 9** and this conforms well to the results of Riffat et al.

We studied the effects of the operating parameters on the thermal efficiency of the tower defined as Eq. (5) we observations were that: $T_{cw,in}$ had a very little influence on tower efficiency , increase of spray water flow rate resulted in an increase in tower efficiency and increased with the increase of air mass flow rate and decreased with the increase of coil mass flow rate. And it's also increase when chilled ceiling flow rate increase.

Fig. 12 shows spray water heat transfer coefficient, α_s, as a function of spray water flow rate. It indicates that the heat transfer coefficient increases with increasing spray water flow rate. This can be explained by Eq. (8). When spray water increases, the cooling capacity increases too leads to increase the overall heat transfer coefficient, U_o, and then α_s increases according to Eq. (10). From the other side, when spray water flow rate increases then cooling water range increases leading to increase the logarithmic mean temperature difference, LMTD in Eq. (8), although α_s increases and this is because that the increasing rate in LMTD is less than that of cooling capacity and this needs U_o as well as α_s to increase. For example, when spray water flow rate increases, for the case with chilled ceiling flow rate equal to 6l/min, from 90 to 150 kg/hr, then the cooling capacity increases from 378 to 588 Watt with a ratio of 1.55 while LMTD increases from 2.6 to 3.05 ^oC with a ratio of 1.17 and this makes both U_o & α_s increase.

Fig. 13 indicates that the mass transfer coefficient is influenced by spray water flow rate. As spray flow increases mass transfer coefficient increases too. This mainly because that the increasing in spray flow means there is a large amount of water droplet could be evaporated and transferred to the air stream.

When spray water flow rate reduces the tower cooling capacity, that lead to reduces the cooling capacity of the test room by the same rate as for cooling capacity because the tower cooling capacity effects on the test room cooling capacity, this clear in **Fig. 14**.

Generally, spray water flow rate affects ICCCCT characteristics and it leads to enhance the performance of the tower. The heat transfer coefficient improved better with spray flow.

3.COMPARISON BETWEEN THE PRESENT WORK AND OTHER WORKS

Some of the present experimental results, for the common case when the ICCCCT operates with chilled ceiling, are compared in this section with other previous experimental

works. The comparison is a qualitative comparison and it is not a quantitive comparison, i.e. the agreement was attained in the behavior of the characteristics and the tendency of the curves but there is no agreement in the values with the previous works and this was shown in Figures. (15) to (19).

Fig. 15 shows a comparison between the present experimental results including cooling capacity with respect to inlet air wet bulb temperature for different cooling water flow rate (the right panel of figure) and the experimental results (the left panel of figure) presented by **Sarker 2007**. Sarker studied an investigation on the optimum design of a heat exchanger in a hybrid closed circuit cooling tower of 1RT rated capacity and staggered arrangement heat exchanger of the relevant design parameters were selected based on the typical East Asian meteorological constrains for the year-round smooth operation of the cooling tower. Sarker is evident from figure, the cooling capacity increases with increasing of the cooling water flow rate but decreases with the increase of WBT as well as by the decrease of the cooling water flow rate. The difference in the amount of cooling capacity between the two studies belongs to the difference in dimensions of the tower & the heat exchanger between the two experimental apparatus but both results having the same behavior.

Fig. 16 shows compares the presented experimental results of the range of cooling water with respect to variable inlet wet-bulb temperature (WBT) and results represented by **Sarker el at. 2009.** From this figure it is clear that the temperature drop of the cooling water decreases with increasing of inlet wet-bulb temperature. This is because when the inlet WBT increases, the temperature difference between inlet cooling water and air decreases. Therefore, the rate of evaporation of spray water flowing at the outer surface of the pipes decreases so that the falling of temperature of cooling water flowing inside the tubes deceases.

Fig. 17 compares the presented experimental results of the temperature drop and cooling capacity and presented by **Sarker el at. 2009.** with respect to spray water volume flow rate are shown at the left and right axes, respectively. As it is clear in this figure, that both tower's cooling capacity & temperature drop increase linearly as spray flow rate increases. This result coincides well to the experimental results of the presented work.

In **Fig. 18** the experimental results of the presented work for the influence of the difference of inlet and the outlet temperatures of the cooling water with respect to the ratio of cooling water to air mass flow rate (on the right panel of figure) are compared with that presented by **Sarker et al. 2005.** (on the left panel of figure). This figure shows a qualitative agreement between the presented work and that presented by **Sarker et al. (2005)**in the experimental behavior of cooling water range with respect to the ratio of cooling water to air mass flow rate shows the same behavior between results presented by **Sarker et al. (2005**) and present results.

Fig. 19 shows the experimental effect of spray water flow rate on both cooling capacity & saturation efficiency, (on the right panel of figure). It is compared with the results presented by **Yeon Yoo et al. 2010.**, (on the left panel of figure). **Yeon Yoo et al. 2010** xpressed, in the experimental behavior of both cooling capacity & saturation efficiency with respect to the spray water flow rate shows the same behavior between results presented by **Yeon Yoo et al. 2010**. and present results.

4. CONCLUSIONS

The following conclusions are valid only for the given parameters of the heat exchanger, configuration and the other operational conditions of the present work:

1. All the characteristics of the performance of the ICCCCT increases with respect to chilled ceiling flow rate, spray water flow rate, inlet air wet bulb temperature and provided

heat load but performance of chilled ceiling increases with respect to chilled ceiling flow rate, spray water flow rate, and decreases with respect to inlet air wet bulb temperature and provided heat load.

Tower cooling capacity increases with a ratio of 1.55 for the case with chilled ceiling flow rate equal to 6 l/min and spray water flow rate varying from 90 to 150 kg/hr, COP increase from 0.65 to 1.03, while LMTD increases from 2.6 to 3.05 ^{o}C with a ratio of 1.17 and this makes both U_o & α_s increase. But higher tower cooling capacity, higher coefficient of performance, higher saturation efficiency and higher chilled ceiling cooling capacity can be obtained with low gas to liquid flow ratio. For example, when G/L increases from 1.4179 to 2.3633, with constant chilled ceiling flow rate equal to 6l/min, the cooling capacity decreases from 588 to 378 Watt, coefficient of performance decreases from 1.0103 to 0.6494, the tower efficiency decreases from 11.3821 % to 9.375 % and chilled ceiling cooling capacity decreases from 462 to 252 Watt, respectively. This mostly because when G/L increases for constant mass air flow rate, then the spray water flow rate decreases and becomes insufficient to accomplish the same transfer of heat especially by evaporation and this causing reducing of the cooling water range leading to decrease these characteristic keeping G constant and varying L.

2. The tower coefficient of performance is influenced greatly by the cooling capacity and little by the total power consumption of air fan and spray water pump, it increases as the cooling capacity increases. From another perspective, the better COP can be obtained at about 6l/min chilled ceiling flow rate & 150 kg/hr spray flow rate as the increasing rate in cooling capacity above these values becomes less while the power consumption increases approximately linearly.
3. Spray flow rate has the greatest influence on spray heat transfer coefficient, α_s, but it is also a function of the air flow rate and the spray water temperature.
4. Both air and spray water flow rate affect the mass transfer coefficient, α_m, but the great effect belongs to the air flow rate.
5. Inlet air wet bulb temperature has a great influence on the all characteristics of the tower. Tower Cooling capacity, COP, chilled ceiling cooling capacity and spray heat transfer coefficient are decreased while saturation efficiency and mass transfer coefficient are increased with wet bulb temperature varying from 12 to 18 ^{o}C.

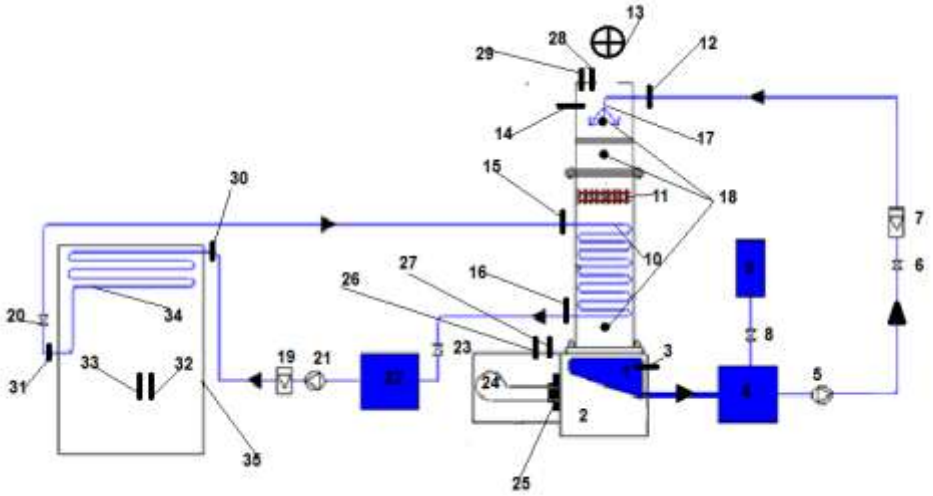

1	Drain	19	Cooling Water Flow Meter
2	Air Chamber	20	By-Pass Valve
3	Outlet Spray Water Temp. Sensor	21	Cooling Water Pump
4	Spray Water Tank	22	Cooling water Tank
5	Spray Water Pump	23	Controlling Valve
6	Controlling Valve	24	Fan
7	Spray Water Flow Sensor	25	Butterfly Valve (Damper)
8	Controlling Valve	26	Inlet Air Temp. Sensor
9	Make-Up Water Tank	27	Inlet Air Moisture Sensor
10	Heat Exchanger	28	Outlet Air Temp. Sensor
11	Fill Packings	29	Outlet Air Moisture Sensor
12	Inlet Spray Water Temp. Sensor	30	Inlet Cooling Water Temp. Sensor
13	Anemometer	31	Outlet Cooling Water Temp. Sensor
14	Combined Temp. /Moisture Sensor	32	Inlet Room Temp. Sensor
15	Inlet Cooling Water Temp. Sensor	33	inlet Room Moisture Sensor
16	Outlet Cooling Water Temp. Sensor	34	Chilled Ceiling
17	Spray Water Nozzle	35	Test Room
18	Holes for Sensing Pressure Drop		

Figure.1 system components.

Figure. 2 Photograph of the experimental apparatus.

Table.1 the measured electrical power consumptions of the spray water pump and air fan at a voltage of 220 volt.

Spray water pump power consumption

Spray water flow rate	kg/hr	90	105	120	135	150
The measured current	Amp.	1.936	1.97	1.97	2.01	2.03
The power consumption	Watt	426	433	437	442	448

Air fan power consumption

Air Velocity*	m/s	10.5
The measured current	Amp.	0.6
The power consumption	Watt	134

* The values of air velocity are measured at the outlet air section.

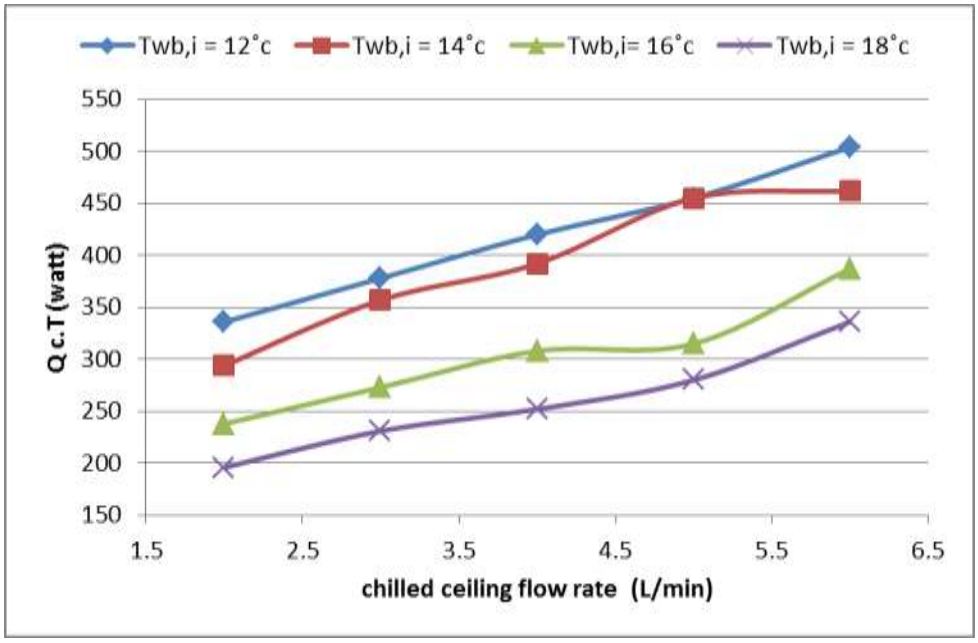

Figure. 3 Influence of the chilled ceiling flow rate on cooling capacity for different inlet air wet bulb temperature

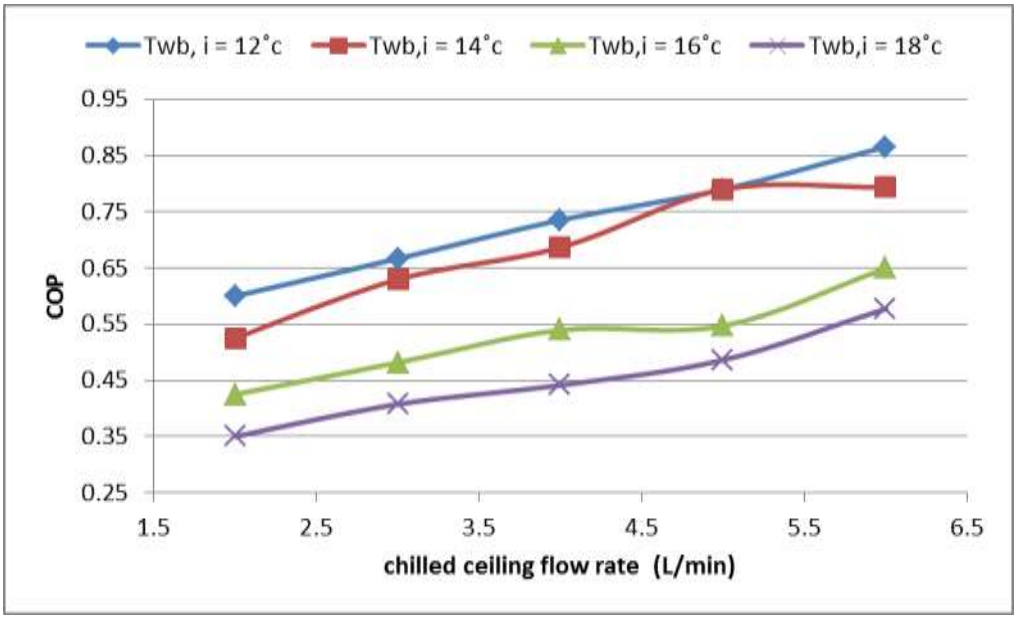

Figure. 4 Influence of the chilled ceiling flow rate on the coefficient of performance for different of the inlet air wet bulb temperature

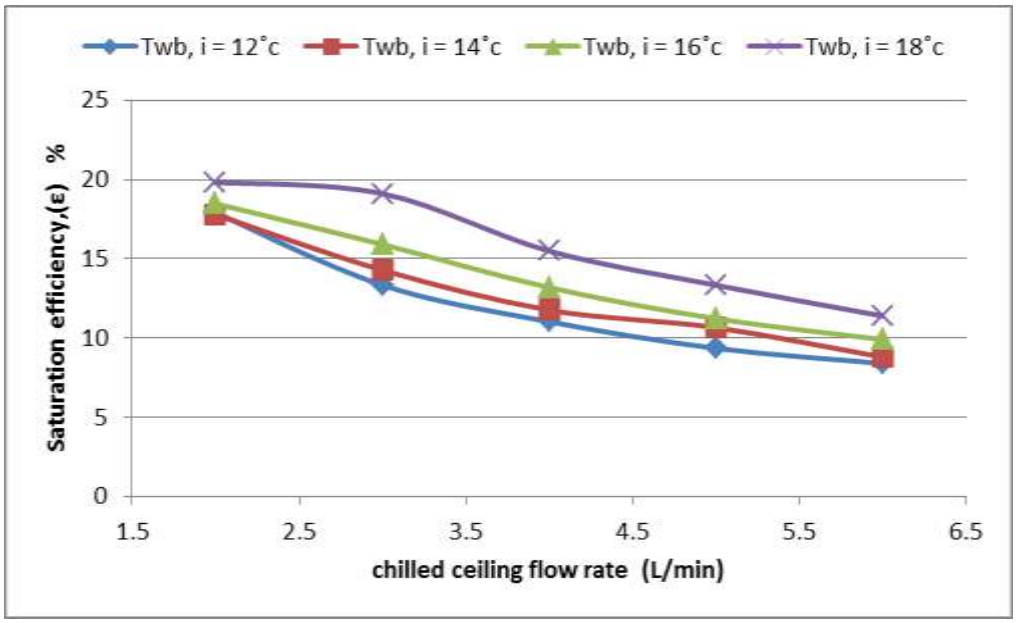

Figure. 5 Influence of the chilled ceiling flow rate on saturation efficiency for different of the inlet air wet bulb temperature

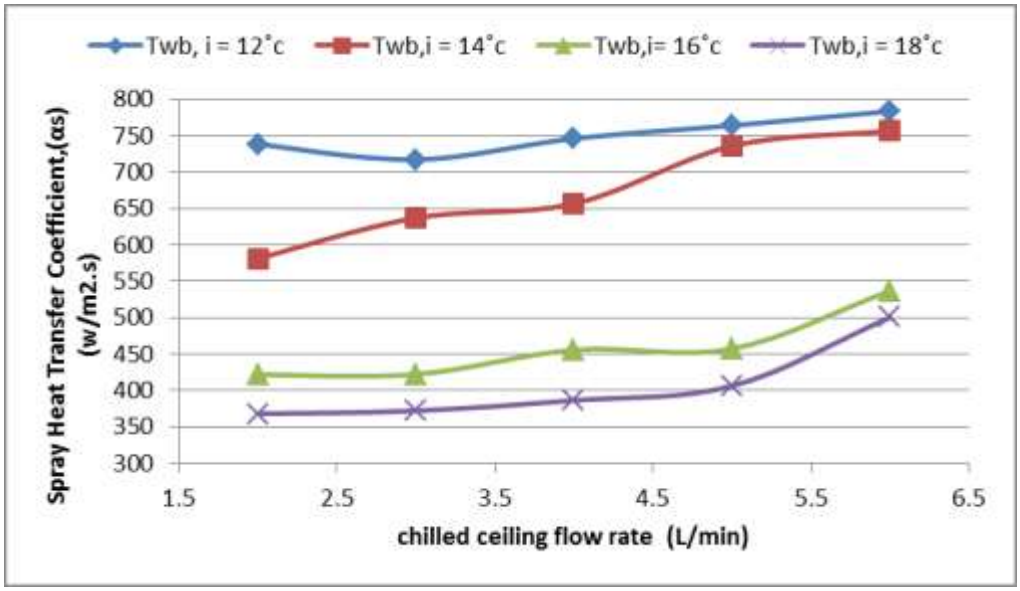

Figure. 6 Influence of the chilled ceiling flow rate on spray heat transfer coefficient for different of the inlet air wet bulb temperature

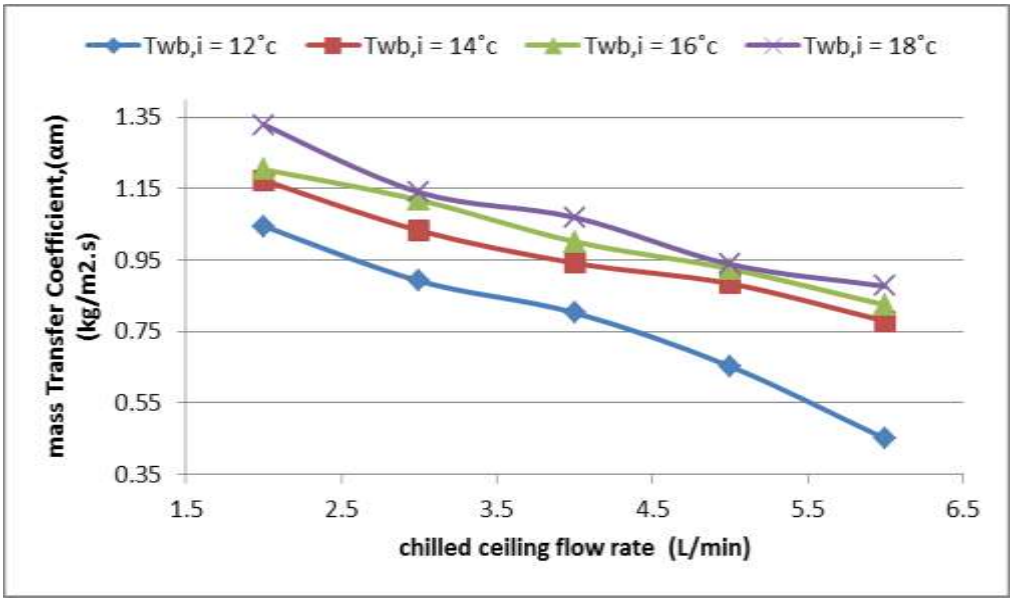

Figure. 7 Influence of the chilled ceiling flow rate on mass transfer coefficient for different of the inlet air wet bulb temperature

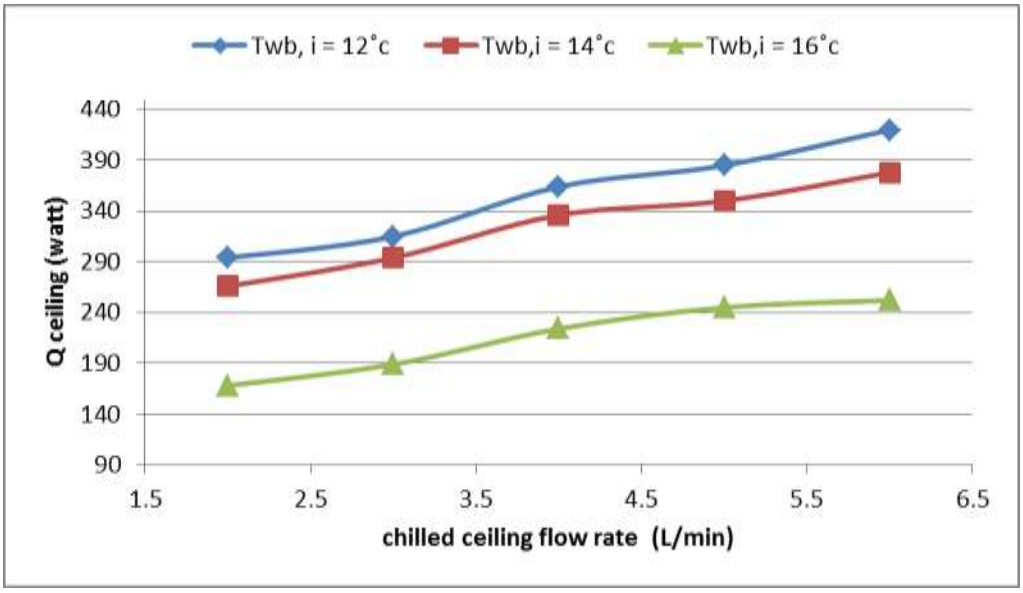

Figure. 8 Influence of the chilled ceiling flow rate on chilled ceiling cooling capacity for different of the inlet air wet bulb temperature

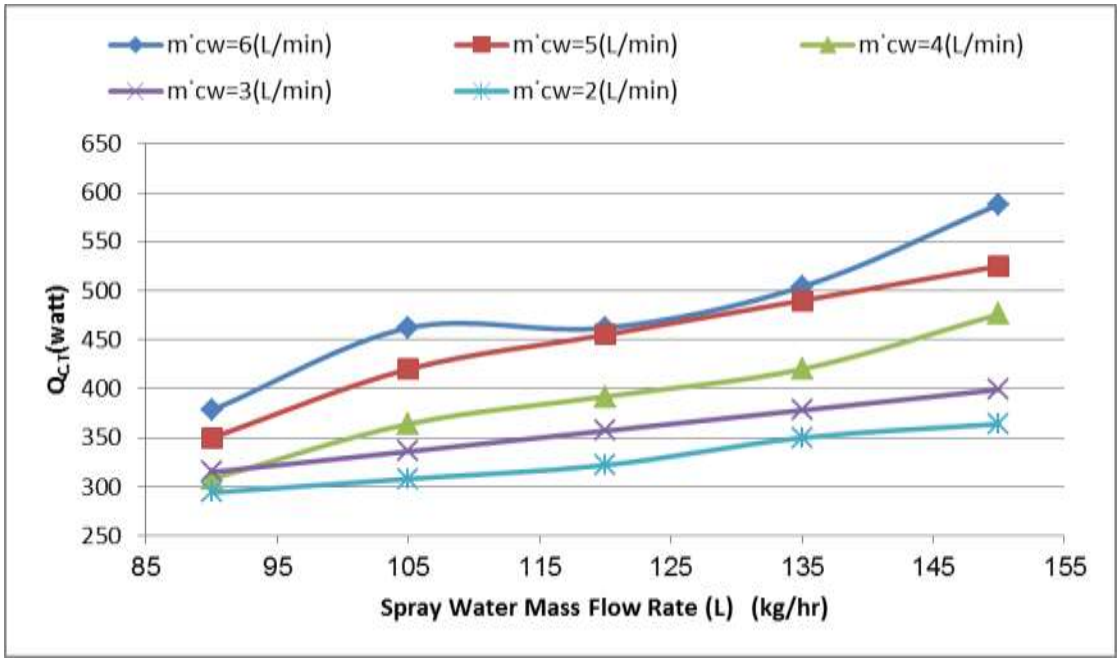

Figure. 9 Influence of the spray water mass flow rate on tower cooling capacity

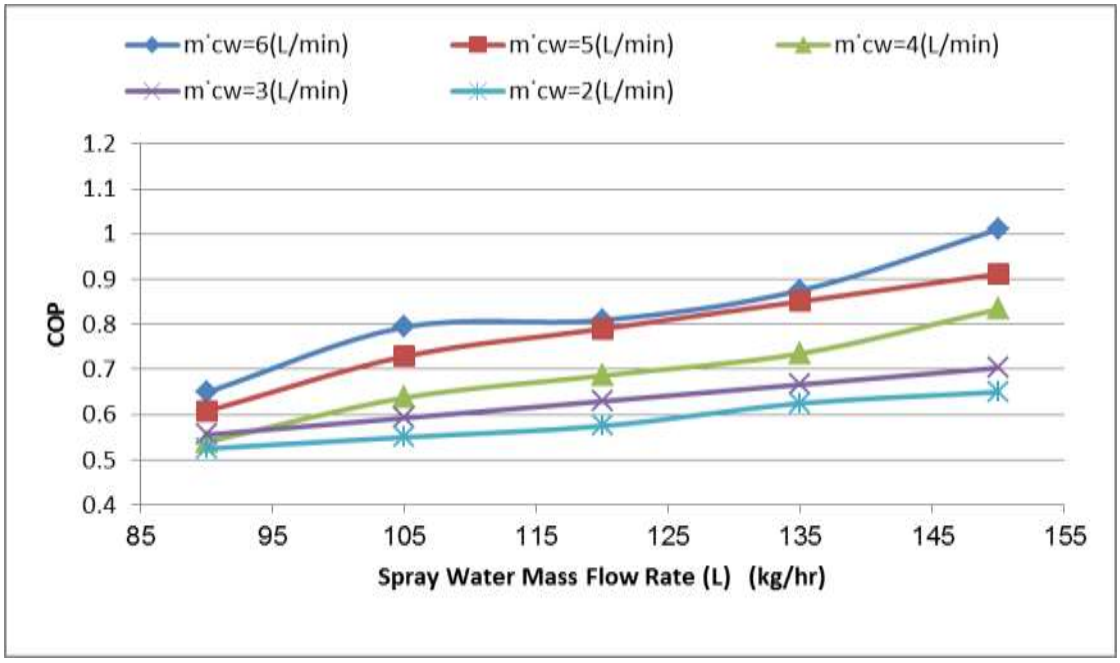

Figure. 10 Influence of the spray water mass flow rate on the coefficient of performance

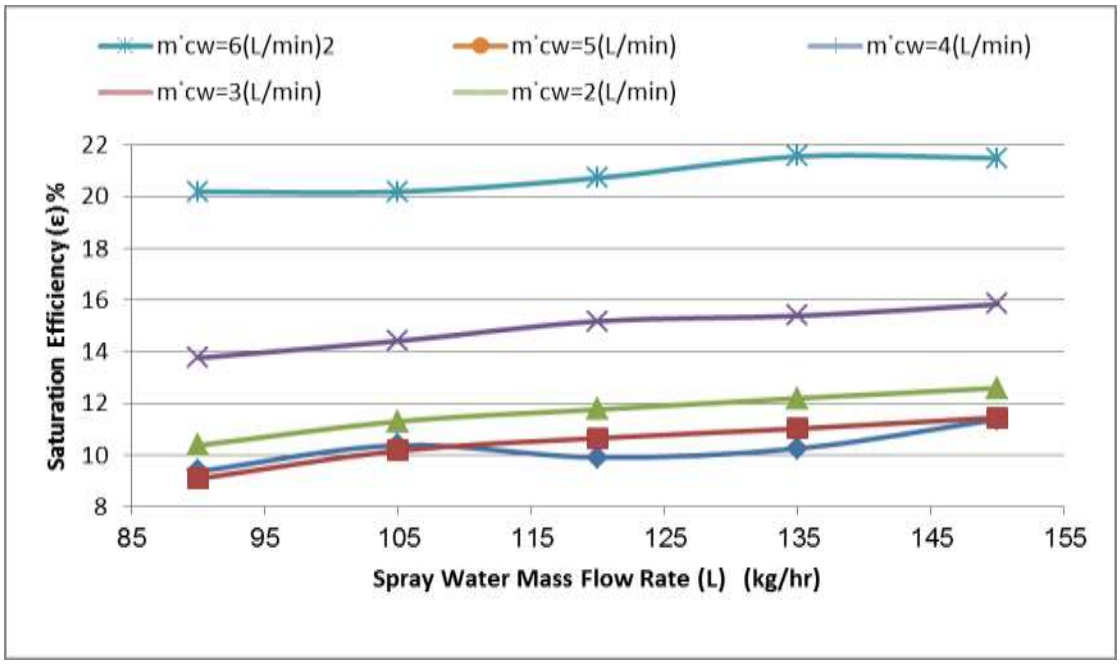

Figure. 11 Influence of the spray water mass flow rate on saturation efficiency

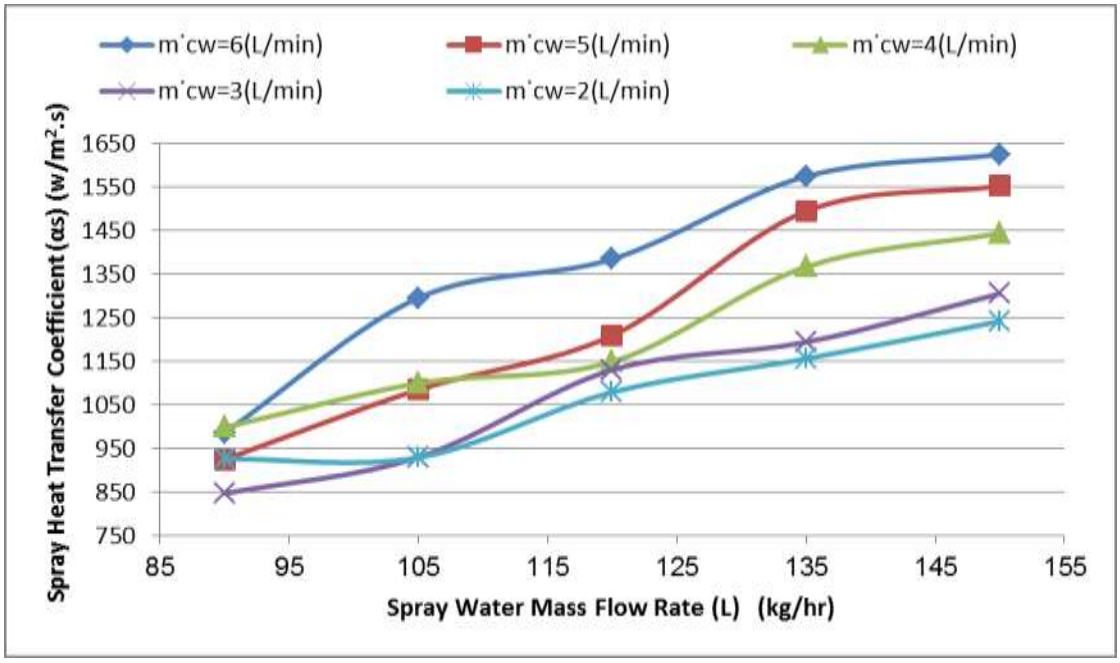

Figure. 12 Influence of the spray water mass flow rate on spray heat transfer coefficient.

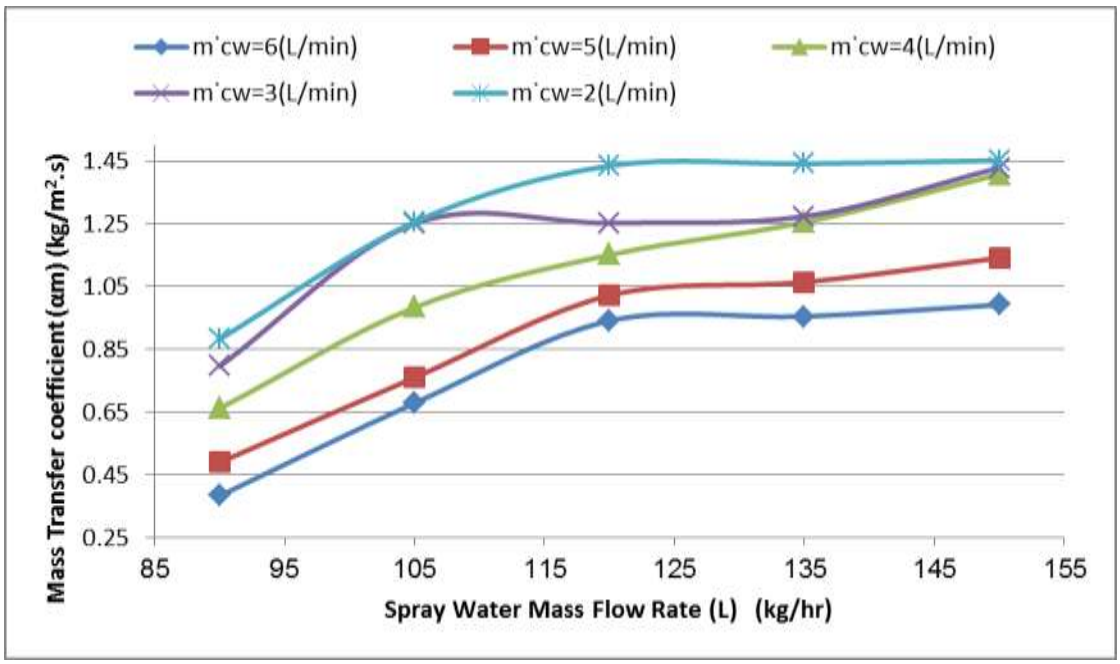

Figure. 13 Influence of the spray water mass flow rate on mass transfer coefficient.

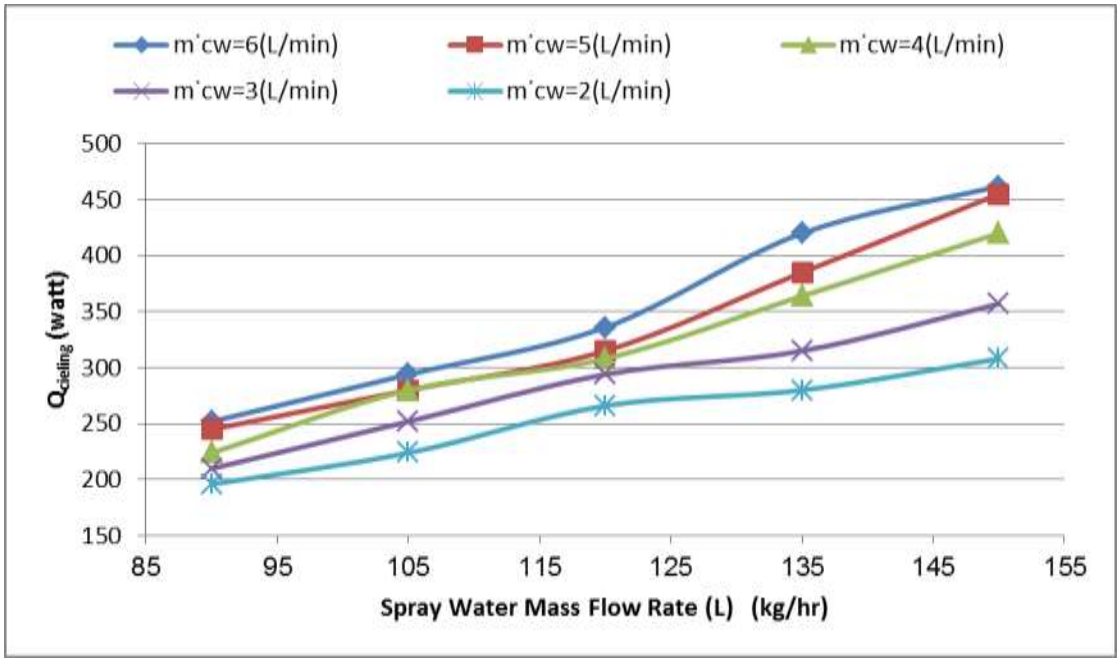

Figure. 14 Influence of the spray water mass flow rate on chilled ceiling cooling capacity

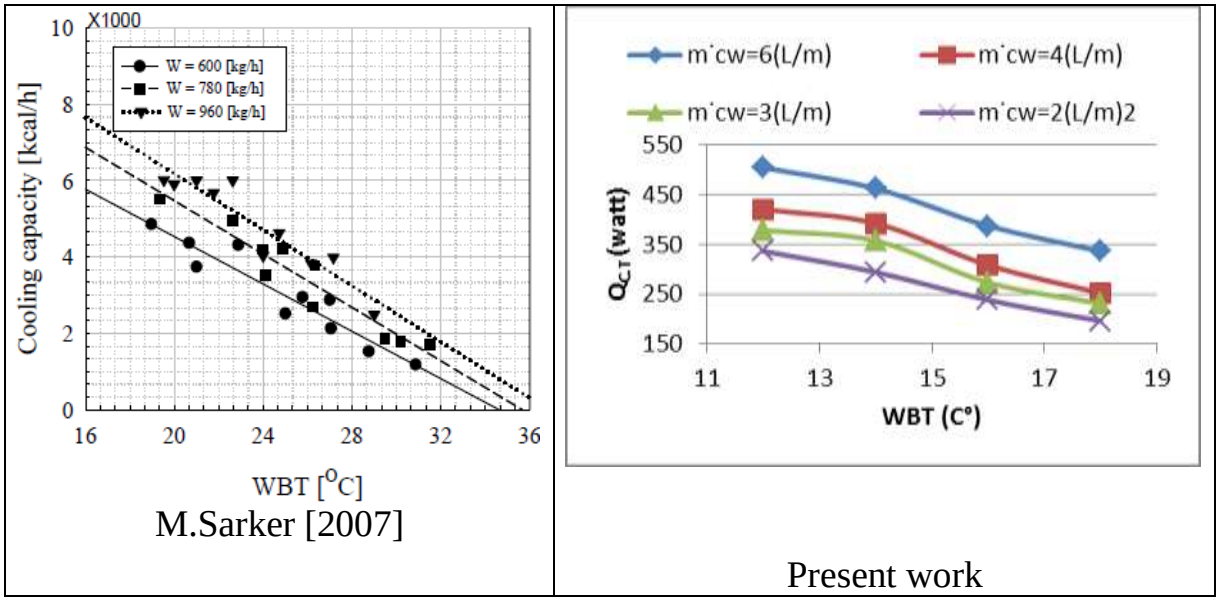

Figure. 15 Comparison of the concluded effect of inlet air wet bulb temperature on cooling capacity with other works

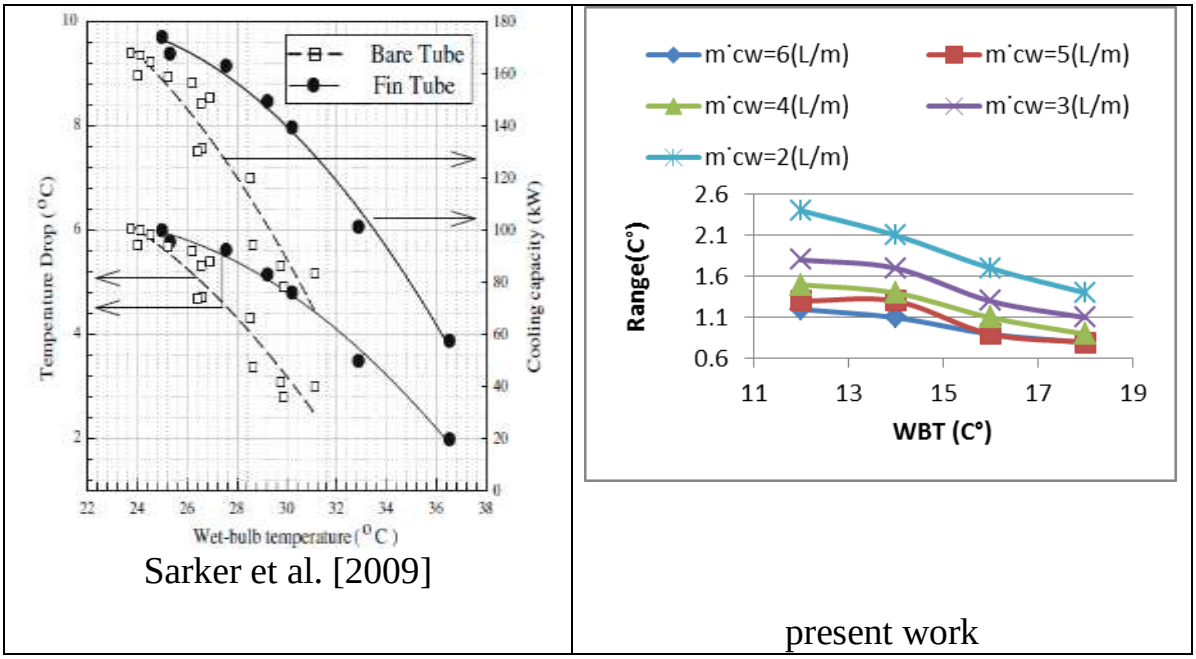

Sarker et al. [2009]

present work

Figure. 16 Comparison of the concluded effect of inlet air wet bulb temperature on cooling water range with other works

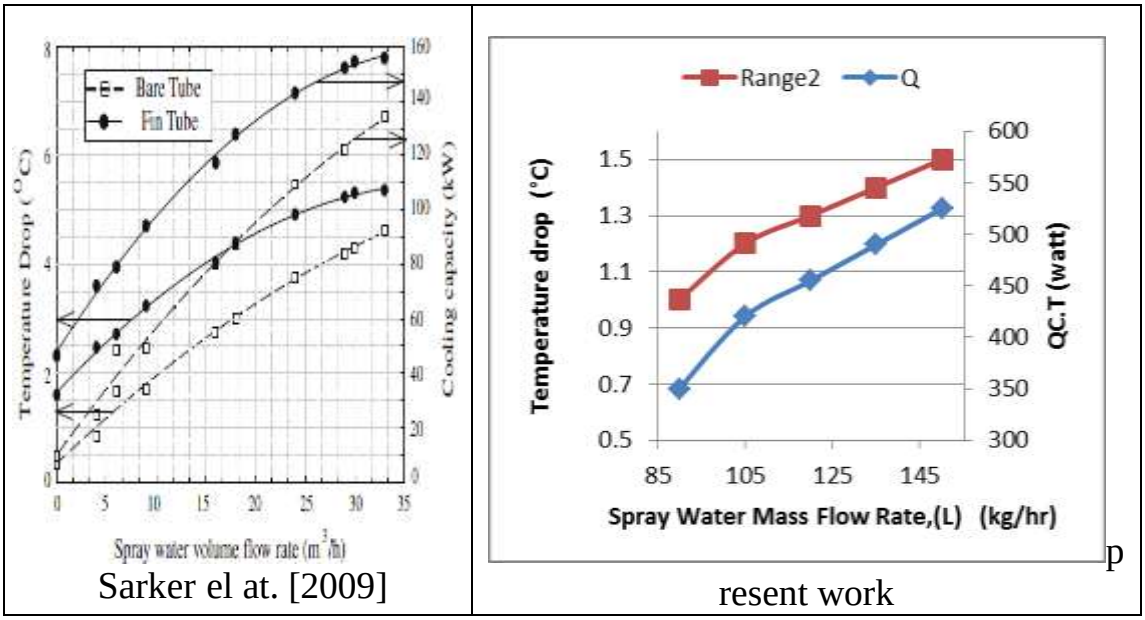

Sarker el at. [2009]

present work

Figure. 17 Comparison of the concluded effect of spray water flow rate on both cooling capacity & temperature drop with other work

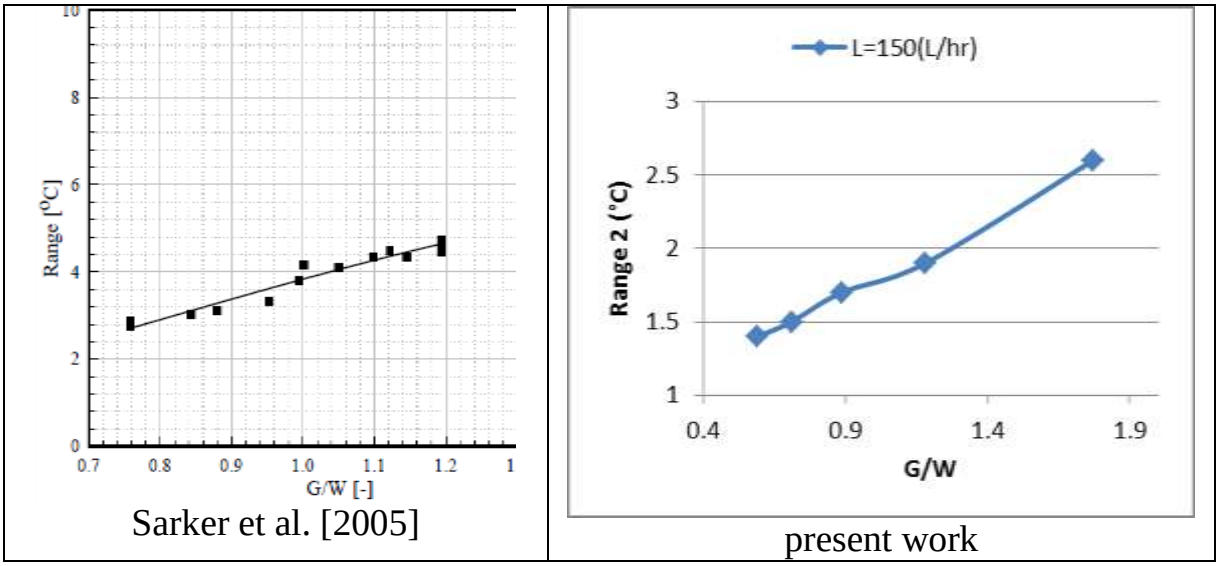

Figure. 18 Comparison of the concluded effect of (air mass flow rate to cooling water ratio) on cooling water range with other work

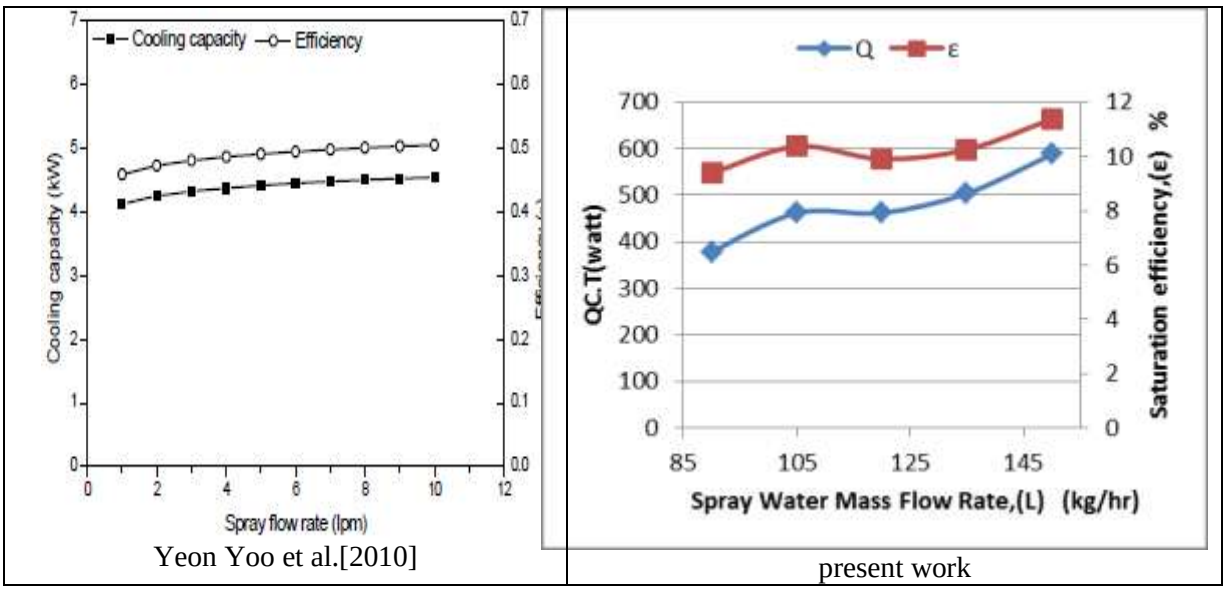

Figure. 19 Comparison of the concluded effect of spray water flow rate on both cooling capacity & saturation efficiency with other work

REFERENCES

- Niu J., and Kooi J.V.D., 1994, *Indoor climate in rooms with cooled ceiling systems*, Building and Environment, Vol. 29 (3), pp 283-290.
- Niu, J., Kooi, J. and Ree, H. 1995, Energy *saving possibilities with cooled-ceiling systems*, Energy and Buildings, Vol. 23 (2), pp 147-158.
- Koschenz M.,1995, *Model for closed circuit evaporative cooling tower in: building simulation*, Madison, WI, 14-16 August.
- Imanari.T, and Omori T., Bogaki K., 1999, *Thermal comfort and energy consumption of the radiant ceiling panel system: comparison with the conventional all-air system*, Energy and Buildings, Vol. 30, pp 167-175
- Gan G., Riffat S.B., 1999, *Numerical simulation of closed wet cooling towers for chilled ceiling systems*, Applied Thermal Engineering, Vol. 19, pp 1279-1296.
- Sprecher P., Borth J., and Niessen R., 2000, The energy conservation in Buildings research, pilot and demonstration program of the Swiss Federal Office of Energy.
- Hasan A., Vuolle M., Sirén K., Holopainen R., and Tuomaala P., 2007, *A cooling tower combined with chilled ceiling: system optimization*, International Journal of Low Carbon Technologies vol. 2 (3), pp 217-224.
- Hasan A., and Serin G., 2002, *Simplification of analytical models and incorporation with CFD For The Performance Predication Of Closed Wet Cooling Towers*, International Journal Of Energy Research, Vol. 26, pp 1161-1174.
- Yeon Yoo S., Kim J.H., and Han K.H., 2010, *Thermal performance analysis of heat exchanger for closed wet cooling tower*, Journal of Mechanical Science and Technology, Vol. 24(4), pp.893-898.
- Oliveira A., and Facão J., 2002, *Heat and mass transfer correlations for the design of small indirect contact cooling tower*, 1st International Conference on Heat, Fluid Mechanics an Thermodynamics, South Africa.
- Stabat P., and Marchio D., 2004, *Simplified model for indirect-contact evaporative cooling-tower behavior*, Applied Energy, Vol. 78, pp. 433-451.
- Facão J., and Oliveira A., 2000, Thermal behavior of closed wet cooling tower for use with chilled ceilings, Applied Thermal Engineering, Vol. 20, pp 1225-1236.
- Sarker M. M. A., Moon C. G., and Yoon J. I., 2007, " Investigation on the optimum design of heat exchangers in a hybrid closed circuit cooling Journal of Mechanical Engineering, Vol.37, pp.52-57.
- Sarker M. M. A., Moon C. G., and Yoon J. I., 2009, *Enhancement of cooling capacity in hybrid closed circuit cooling tower*, Applied thermal engineering, Vol. 29, pp.3328-3333.
- Sarker M. M. A., Moon C. G., and Yoon J. I., 2005, *The Cooling Capacity And Pressure Drop In A Hybrid Closed Circuit Cooling*. Proceeding of The International Conference On Mechanical Engineering, Dhaka, Bangladesh.

NOMENCLATURE

A	Area (m^2)
Cp	Specific heat at constant pressure (kJ/kg ^oC)
D	Outer tube diameter (m)
d	Inner tube diameter (m)
G	Air mass flow rate (kg/hr)
$\dot{G}$	Air mass velocity based on minimum Section = ρ v ($kg/m^2.s$)
h	Specific enthalpy (kJ/kg)
k	Thermal conductivity (W/m ^oC)
L	Spray water mass flow rate (kg/hr)
$\dot{m}$	Mass flow rate (kg/hr)
Q	Cooling capacity (Watt)
Pr	Prandtl number
Re	Reynolds number
T	Temperature (^oC)
U_o	Overall heat transfer coefficient ($W/m^2\ ^oC$)
V	Velocity (m/s)
WBT_{in}	inlet wet bulb temperature (^oC)

Greek letter

α_m	Mass transfer coefficient for water vapor, between spray water film and air (kg/m^2 s)
α_s	Heat transfer coefficient between tube surface and spray water film ($W/m^2\ ^oC$)
α_w	Heat transfer coefficient for water inside the tubes ($W/m^2\ ^oC$)
Γ	Spray water mass rate per length of tube (kg/m s)
ρ	Density (kg/m^3)

Sub-Script

ave	Average
air	Air flow (a)
cw	Cooling water
in	Inlet
out	Outlet
i	Interface between spray water film & air
f	Saturated air-spray water film
sat	Saturation properties
sp	Spray water (w)

Abbreviations

CFC	Chlorofluorocarbon
LMhD	Logarithmic mean enthalpy difference (kJ/kg)
LMTD	Logarithmic mean temperature difference (^oC)
CWCT	Closed wet cooling tower
ICCCCT	Indirect contact closed circuit cooling tower
HVAC	Heating ventilation air conditioning

Stability and Dynamic Analysis of Laminated Composite Plates

Assist. Prof. Dr. Widad I. Majeed
Department of Mechanical Engineering
College of Engineering
Baghdad University
Email:wedad_majeed@yahoo.com

Firas H. Tayeh
Department of Mechanical Engineering
College of Engineering
Baghdad University
Email:firas_frs_drsf@yahoo.com

ABSTRACT

Buckling and free vibration analysis of laminated rectangular plates with uniform and non uniform distributed in-plane compressive loadings along two opposite edges is performed using the Ritz method. Classical laminated plate theory is adopted. The static component of the applied in-plane loading are assumed to vary according to uniform, parabolic or linear distributions. Initially, the plate membrane problem is solved using the Ritz method; subsequently, using Hamilton's variational principle, linear homogeneous algebraic equations in terms of unknown are generated, the set of linear algebraic equations can be solved as an Eigen-value problem. Buckling loads for laminated plates with different combinations of boundary conditions are obtained and their effect on the natural frequencies of plate are also investigated. The proposed method is verified by comparing results to data obtained by the finite element method (FEM) using ANSYS program, from experimental program and that obtained by other researchers. Analytical results are also presented to bring out the effects of aspect ratio, boundary conditions, lamination angle, and loading type on the critical buckling load and natural frequency.

Key words: Vibration, stability, anisotropic plates, classical laminated plate theory, Ritz method

تحليل الإستقرارية و الديناميكة لصفائح مركبة طبقية

أ.م.د. وداد ابراهيم مجيد
قسم هندسة الميكانيك
كلية الهندسة / جامعة بغداد

فراس حميزة تايه
قسم هندسة الميكانيك
كلية الهندسة -جامعة بغداد

الخلاصة

أجري في هذا البحث تحليل الانبعاج و الاهتزاز الحر لصفائح طبقية مستطيلة معرضة لأحمال ضاغطة موزعة بشكل منتظم أو غير منتظم على حافتين متعاكستين باستخدام طريقة Ritz. النظرية الكلاسيكية للصفائح الطبقية قد اختيرت لإجراء هذه الدراسة. أختير المكون الساكن للأحمال المسلطة ضمن المستوي ليكون موزع بثلاثة أشكال: منتظم, خطي, و منحني على شكل قطع مكافئ. بدايةً, تم استخدام طريقة Ritz لحل مسألة الصفيحة و الحصول على معادلات خطية جبرية متجانسة كدوال لمجاهيل باستخدام المبدأ التغييري لـ Hamilton ; يتم حل هذه المعادلات كمسألة Eigen-value. تم إيجاد حمل الانبعاج للصفائح الطبقية و التي تكون مثبتة بحدود مختلفة و دراسة تأثير هذه الاحمال على التردد الطبيعي. تم التحقق من النتائج بمقارنتها بنتائج عددية مستحصلة باستخدام برنامج ANSYS و بنتائج مختبرية تجريبية, و كذلك مقارنتها ببعض النتائج المقدمة بواسطة باحثين آخرين. النتائج التحليلية قدمت لدراسة تأثير نسبة الطول الى العرض, حدود التثبيت, زاوية التصفيح, و نوع التحميل على حمل الانبعاج الحرج و التردد الطبيعي.

الكلمات الرئيسية: اهتزاز, استقرارية, صفيحة متباينة الخواص, النظرية الكلاسيكية للصفائح الطبقية, طريقة Ritz.

1. INTRODUCTION

Thin plates of various shapes used in naval and aeronautical structures are often subjected to normal compressive and shearing loads acting in the middle plane of the plate (in-plane loads). Under certain conditions such loads can result in a plate buckling. In many cases, a failure of thin plate elements may be attributed to an elastic instability and not to the lack of their strength. Therefore, plate buckling analysis presents an integral part of the general analysis of a structure, **Ventsel and Krauthammer, 2001**. It is important to note that a plate leading from the stable to unstable configuration of equilibrium always passes through the neutral state of equilibrium, which thus can be considered as a bordering state between the stable and unstable configurations. In the mathematical formulation of elastic stability problems, neutral equilibrium is associated with the existence of bifurcation of the deformations. According to this formulation, the critical load is the smallest load at which both the flat equilibrium configuration of the plate and slightly deflected configuration are possible , **Ventsel and Krauthammer, 2001**. The composite structures whether used in civil, marine or aerospace are subjected to dynamic loads during their operation. Therefore, there exists a need for assessing the natural frequency. Therefore, for assessing the natural frequency of the laminated composite plate structures, the accurate mathematical model is required, **Reddy, et al., 2013**. There are many applications on buckling and stability of composite materials structures in the present industry such as ship hull, crown of the hat-stiffened panel, blended wing body (BWB) Aircraft. Many researchers have studied the stability of composite plates subjected to buckling loads, each one with his own perspective. **Matsunaga, 2000,** analyzed natural frequencies and buckling stresses of cross-ply laminated composite plates by taking into account the effects of shear deformation, thickness change and rotatory inertia. **Leissa and Kang, 2002,** investigated exact solutions for the free vibration and buckling of rectangular plates having two opposite edges simply supported and the other two were clamped, with the simply supported edges subjected to a linearly varying normal stress. **Craciun and Simionescu–Panait, 2004,** considered the internal and superficial instability of a prestressed fiber reinforced orthotropic elastic composite. **Jana and Bhaskar (2007)** examined the effect of a non-uniform distribution of the applied edge loads on their net critical value with in-plane lateral restraint. **Amabili, et al., 2010,** presented an investigation to laminate composite rectangular plates with different boundary conditions subjected to an external point force. **Tang and Wang**, **2011**, investigated the buckling analysis of symmetrically laminated rectangular plates with parabolic distributed in-plane compressive loadings along two opposite edges using the Rayleigh–Ritz method. In the present work, the stability and buckling analysis of laminated composite plate under uniaxial uniform and non-uniform distributed load is performed. Classical laminated plate theory is adopted. Buckling loads for laminated plates with different combinations of boundary conditions are obtained and their effect on the natural frequencies of plate are also investigated.

2. THEORY

This study is based on classical laminated plate theory (CLPT) and used Hamiltons principles to derive the equation of motion. Ritz method is used to solve the principle of minimum potential energy as an Eigen-value problem to get the critical buckling load and natural frequency for different considerations (boundary conditions, aspect ratios, mechanical properties, lamination systems).

2.1 Classical Laminated Plate Theory

The simplest laminated plate theory is the classical laminated plate theory (or CLPT), which is an extension of the Kirchhoff (classical) plate theory to laminated composite plates. It is based on the displacement field, **Reddy, 2004**.

$$u(x,y,z,t) = u_o(x,y,t) - z\frac{\partial w_o}{\partial x}$$

$$v(x,y,z,t) = v_o(x,y,t) - z\frac{\partial w_o}{\partial y}$$

$$w(x,y,z,t) = w_o(x,y,t) \quad (1)$$

where (u_o, v_o, w_o) are the displacement components along the (x, y, z) coordinate directions, respectively, of a point on the midplane (i.e., z = 0). The displacement field implies that straight lines normal to the xy-plane before deformation remain straight and normal to the midsurface after deformation. The Kirchhoff assumption neglects both transverse shear and transverse normal effects; i.e., deformation is due entirely to bending and in-plane stretching.

2.2 Total Mechanical Energy

The first law of thermodynamics or the principle of conservation of energy serves as the foundation for energy-based methods employed in the analysis of structures, including plates. The total mechanical energy (defined as the sum of its potential and kinetic energies) of a particle being acted on by only conservative forces is constant, **Brown, 2007**.

$$E = E_c + \Pi = Constant \quad (2)$$

where E is the total mechanical energy; E_c is the total kinetic energy; Π is total potential energy. The kinetic energy E_c is written as the following form taking in account the transverse deformation only on the vibration frequencies, **Berthelot, 2010**:

$$E_c = \frac{1}{2}\omega^2 \iint I_o w_o^2 dx\, dy \quad (3)$$

where ω is the natural frequency of the plate vibrations and I_o is the moment of inertia of the laminate at point (x, y) given below:

$$I_o = \int_{-h/2}^{h/2} \rho dz = \sum_{k=1}^{L} \rho_k (z_k - z_{k-1}) \quad (4)$$

Where L is the total number of layers in the laminate; k denotes the layer number; h is the thickness of the laminate; z_k and z_{k-1} are distances from the reference plane of the laminate to the two surfaces

of the *kth* ply **Fig. 1** .The total potential energy, Π, consists of the strain energy of internal forces, *U*, and the work of external forces, Ω, i.e. **Reddy, 2004**,

$$\Pi = U + \Omega \tag{5}$$

The strain energy for an anisotropic material is written as, **Kollar, and Springer, 2003**:

$$U = \frac{1}{2}\int_0^b \int_0^a \begin{Bmatrix} k_x \\ k_y \\ k_{xy} \end{Bmatrix}^T \begin{bmatrix} B_{11} & B_{12} & B_{16} & D_{11} & D_{12} & D_{16} \\ B_{21} & B_{22} & B_{26} & D_{21} & D_{22} & D_{26} \\ B_{61} & B_{62} & B_{66} & D_{61} & D_{62} & D_{66} \end{bmatrix} \begin{Bmatrix} k_x \\ k_y \\ k_{xy} \end{Bmatrix} dx\, dy \tag{6}$$

where κ_x, κ_y, and κ_{xy} are the curvatures of the reference plane of the plate defined as:

$$k_x = -\frac{\partial^2 w_o}{\partial x^2}\,, \qquad k_y = -\frac{\partial^2 w_o}{\partial y^2}\,, \qquad k_{xy} = -\frac{2\partial^2 w_o}{\partial x \partial y} \tag{7}$$

[B] and [D] are the coupling and bending stiffness matrices, respectively. The elements of these matrices are (i, j = 1, 2, 6) given as functions of the transformed reduced stiffness matrix elements $\bar{Q}_{ij}$

$$B_{ij} = \frac{1}{2}\sum_{k-1}^{L}\left(\bar{Q}_{ij}\right)_k (z_k^2 - z_{k-1}^2)\ , D_{ij} = \frac{1}{3}\sum_{k-1}^{L}\left(\bar{Q}_{ij}\right)_k (z_k^3 - z_{k-1}^3) \tag{8}$$

By using the relationships between the curvatures and the deflections, the expression of the strain energy for a symmetric layup is as follows:

$$U = \frac{1}{2}\int_0^b \int_0^a \left[D_{11}\left(\frac{\partial^2 w_o}{\partial x^2}\right)^2 + D_{22}\left(\frac{\partial^2 w_o}{\partial y^2}\right)^2 + D_{66}\left(\frac{2\partial^2 w_o}{\partial x \partial y}\right)^2 + 2\left(D_{12}\frac{\partial^2 w_o}{\partial x^2}\frac{\partial^2 w_o}{\partial y^2} + D_{16}\frac{\partial^2 w_o}{\partial x^2}\frac{2\partial^2 w_o}{\partial x \partial y} + D_{26}\frac{\partial^2 w_o}{\partial y^2}\frac{2\partial^2 w_o}{\partial x \partial y}\right)\right] dx\, dy \tag{9}$$

The potential energy is related only to the in-plane distributed loads N_x applied uniaxially to the edges *x=0, a*, and is written as

$$\Omega = -\frac{1}{2}\iint \left[N_x \left(\frac{\partial w_o}{\partial x}\right)^2 \right] dx\, dy \tag{10}$$

N_x is assumed to be distributed load (uniform and not uniform) taking the forms as derived **Fig. 2**:

$$N_x = -N_o\ , N_x = -\frac{4N_o y}{b}\left(1 - \frac{y}{b}\right)\ , N_x = -N_o\left(1 - \frac{y}{b}\right) \tag{11}$$

where N_o is the maximum intensity of the compressive force at the edges $x=0$ and $x=a$.

2.3 Boundary Conditions

The approximate solution is sought in the usual form of a double series in separate variables **Berthelot, 2010**:

$$w_o(x,y) = \sum_{m=1}^{M}\sum_{n=1}^{N} A_{mn} X_m(x) Y_n(y) \tag{12}$$

where M and N are the numbers of half-waves used in the x and y directions, respectively, of a mode shape. The functions $X_m(x)$ and $Y_n(y)$ must constitute functional bases and are chosen so as to satisfy the boundary conditions along the edges $x = 0$, $x = a$, $y = 0$, and y = b. The coefficients A_{mn} are determined by the stationarity conditions:

$$\frac{\partial U}{\partial A_{mn}} = 0 \tag{13}$$

where $m = 1, 2, \ldots, M$ and $n = 1, 2, \ldots, N$. To select an expression for the deflection w_o, the functions $X_m(x)$ and $Y_n(y)$ are selected to satisfy the geometrical boundary conditions for the studied cases:

a- For the case of a simply supported (**SSSS**) plate, the boundary conditions functions along the edges are as follows, **Reddy, 2004**:

$$X_m(x) = sin\frac{m\pi x}{a}\,, \qquad Y_n(y) = sin\frac{n\pi y}{b} \tag{14}$$

b- For the case of a built in (**CCCC**) plate, the functions of the transverse deflection w_o can be taken as follows **Berthelot, 2010**:

$$X_m(x) = cos\,\lambda_m\frac{x}{a} - cosh\,\lambda_m\frac{x}{a} - \gamma_m\left(sin\lambda_m\frac{x}{a} - sinh\lambda_m\frac{x}{a}\right)$$
$$Y_n(y) = cos\,\lambda_n\frac{y}{b} - cosh\,\lambda_n\frac{y}{b} - \gamma_n\left(sin\lambda_n\frac{y}{b} - sinh\lambda_n\frac{y}{b}\right) \tag{15}$$

where $\lambda_m, \lambda_n, \gamma_m,$ and γ_n are constants given in **Table (1)**.

c- In the case where two opposite edges are clamped along $x=0$ and $x=a$ and the other two edges are simply supported along $y=0$ and $y=b$, that can be sampled as (**CSCS**), the transverse deflection w_o functions are as follows **Berthelot, 2010**:

$$X_m(x) = cos\,\lambda_m\frac{x}{a} - cosh\,\lambda_m\frac{x}{a} - \gamma_m\left(sin\lambda_m\frac{x}{a} - sinh\lambda_m\frac{x}{a}\right), \qquad Y_n(y) = sin\frac{n\pi y}{b} \tag{16}$$

d- For the case where the edges along *x=0* and *x=a* are simply supported and the edges along *y=0* and *y=b* are free that can be sampled as (**SFSF**), the functions that satisfy these boundary conditions can be taken as follows **Berthelot, 2010**:

$$X_m(x) = sin\frac{m\pi x}{a}, Y_1(y) = 1\,, Y_2(y) = \sqrt{3}\left(1 - 2\frac{y}{b}\right),$$
$$Y_n(y) = cos\,\lambda_n\frac{y}{b} + cosh\,\lambda_n\frac{y}{b} + \gamma_n\left(sin\lambda_n\frac{y}{b} + sinh\lambda_n\frac{y}{b}\right) \quad (17)$$

The values of λ_n and γ_n are reported in **Table (1)**.

e- When the plate is taken clamped along two opposite edges where *x=0* and *x=a* and free along the others where *y=0* and *y=b* that can be sampled as (**CFCF**), and the functions will be combined as shown below **Berthelot, 2010**:

$$X_m(x) = cos\,\lambda_m\frac{x}{a} - cosh\,\lambda_m\frac{x}{a} - \gamma_m\left(sin\lambda_m\frac{x}{a} - sinh\lambda_m\frac{x}{a}\right),$$
$$Y_1(y) = 1\,, Y_2(y) = \sqrt{3}\left(1 - 2\frac{y}{b}\right)\,, Y_n(y) = cos\,\lambda_n\frac{y}{b} + cosh\,\lambda_n\frac{y}{b} + \gamma_n\left(sin\lambda_n\frac{y}{b} + sinh\lambda_n\frac{y}{b}\right) \quad (18)$$

where $\lambda_m, \lambda_n, \gamma_m,$ and γ_n are constants given in **Table (1)**.

2.4 Weak Forms

The Ritz method can be used to determine an approximate solution to the bending, buckling, and natural vibrations of symmetric laminates. The weak form or the statement of the principle of minimum total potential energy for buckling and natural vibration problems is given below, **Reddy, 2004**:

$$0 = \int_0^b \int_0^a \left\{ D_{11}\frac{\partial^2 w_o}{\partial x^2}\frac{\partial^2 \delta w_o}{\partial x^2} + D_{12}\left(\frac{\partial^2 w_o}{\partial y^2}\frac{\partial^2 \delta w_o}{\partial x^2} + \frac{\partial^2 w_o}{\partial x^2}\frac{\partial^2 \delta w_o}{\partial y^2}\right) + D_{22}\frac{\partial^2 w_o}{\partial y^2}\frac{\partial^2 \delta w_o}{\partial y^2} \right.$$
$$+4D_{66}\frac{\partial^2 w_o}{\partial x\partial y}\frac{\partial^2 \delta w_o}{\partial x\partial y} + 2D_{16}\left(\frac{\partial^2 w_o}{\partial x\partial y}\frac{\partial^2 \delta w_o}{\partial x^2} + \frac{\partial^2 w_o}{\partial x^2}\frac{\partial^2 \delta w_o}{\partial x\partial y}\right) + 2D_{26}\left(\frac{\partial^2 w_o}{\partial x\partial y}\frac{\partial^2 \delta w_o}{\partial y^2}\right.$$
$$\left. \left. + \frac{\partial^2 w_o}{\partial y^2}\frac{\partial^2 \delta w_o}{\partial x\partial y}\right) + N_x\frac{\partial w_o}{\partial x}\frac{\partial \delta w_o}{\partial x} - \omega^2(I_o w_o \delta w_o)\right\} dx\,dy \quad (19)$$

where ω denotes the frequency of natural vibration. For buckling analysis, all terms involving frequency of vibration are set to zero, while N_x is eliminated for natural vibration.

2.4.1 Buckling of a simply supported plate

Consider a simply supported rectangular plate made of an orthotropic laminate, the material directions of which coincide with the plate directions. This plate is subjected to uniaxial uniform in-plane compressive forces N_x along the edges $x = 0$ and $x = a$. The total potential energy can be written in the following expression:

$$\Pi = \frac{1}{2}\int_0^b \int_0^a \left[D_{11}\left(\frac{\partial^2 w_o}{\partial x^2}\right)^2 + D_{22}\left(\frac{\partial^2 w_o}{\partial y^2}\right)^2 + 4D_{66}\left(\frac{\partial^2 w_o}{\partial x \partial y}\right)^2 + 2\left(D_{12}\frac{\partial^2 w_o}{\partial x^2}\frac{\partial^2 w_o}{\partial y^2} + D_{16}\frac{\partial^2 w_o}{\partial x^2}\frac{2\partial^2 w_o}{\partial x \partial y} + D_{26}\frac{\partial^2 w_o}{\partial y^2}\frac{2\partial^2 w_o}{\partial x \partial y}\right) + N_x\left(\frac{\partial w_o}{\partial x}\right)^2 \right] dx\, dy \quad (20)$$

The transverse displacement (w_o) is written as mentioned in section 2.3 in the following form:

$$w_o = A_{mn} sin\frac{m\pi x}{a} sin\frac{n\pi y}{b}, \;\; m = 1, 2, \dots, M \text{ and } n = 1, 2, \dots, N \quad (21)$$

Assume a plate of a symmetric layup subjected to uniaxial compression; for a simple case, consider m=n=1:

$$w_o = A_{11} sin\frac{\pi x}{a} sin\frac{\pi y}{b} \quad (22)$$

substituting w_o Eq. (22) in Eq. (20) and performing the differentiation and integration processes, and then by using Eq. (19) , the following representation of the critical buckling load N_{cr} can be obtained:

$$N_{cr} = (9.869D_{11}b^4 + 9.869D_{22}a^4 + 19.739D_{12}a^2b^2 + 39.478D_{66}a^2b^2)/a^2b^4 \quad (23)$$

when *m* and *n* are more than 1, the critical load N_{cr} is determined by solving Eigen value problem. For different arbitrary boundary conditions and *m & n* are greater than 1, the solution becomes more difficult and needs computer programming to determine the critical buckling load.

2.4.2 Vibration of simply supported plate

For vibration problem, the total mechanical energy is written as:

$$E = \frac{1}{2}\int_0^b \int_0^a \left[D_{11}\left(\frac{\partial^2 w_o}{\partial x^2}\right)^2 + 2D_{12}\frac{\partial^2 w_o}{\partial x^2}\frac{\partial^2 w_o}{\partial y^2} + D_{22}\left(\frac{\partial^2 w_o}{\partial y^2}\right)^2 + 4D_{66}\left(\frac{\partial^2 w_o}{\partial x \partial y}\right)^2 + 2\left(D_{12}\frac{\partial^2 w_o}{\partial x^2}\frac{\partial^2 w_o}{\partial y^2} + D_{16}\frac{\partial^2 w_o}{\partial x^2}\frac{2\partial^2 w_o}{\partial x \partial y} + D_{26}\frac{\partial^2 w_o}{\partial y^2}\frac{2\partial^2 w_o}{\partial x \partial y}\right) - I_o\omega^2 w_o^2 \right] dx\, dy \quad (24)$$

The natural frequancy ω is obtained using the same procedure to be as below:

$$\omega = \pm\frac{9.869}{a^2b^2}\,(D_{22}a^4 + D_{11}b^4 + 2D_{12}a^2b^2 + 4D_{66}a^2b^2)^{0.5}/I_o \quad (25)$$

In case of finding the natural frequency under the action of critical buckling force N_{cr}, the total mechanical energy is written as:

$$E=\frac{1}{2}\int_0^b\int_0^a\left[D_{11}\left(\frac{\partial^2 w_o}{\partial x^2}\right)^2+2D_{12}\frac{\partial^2 w_o}{\partial x^2}\frac{\partial^2 w_o}{\partial y^2}+D_{22}\left(\frac{\partial^2 w_o}{\partial y^2}\right)^2+4D_{66}\left(\frac{\partial^2 w_o}{\partial x\partial y}\right)^2+2\left(D_{12}\frac{\partial^2 w_o}{\partial x^2}\frac{\partial^2 w_o}{\partial y^2}\right.\right.$$
$$\left.\left.+D_{16}\frac{\partial^2 w_o}{\partial x^2}\frac{2\partial^2 w_o}{\partial x\partial y}+D_{26}\frac{\partial^2 w_o}{\partial y^2}\frac{2\partial^2 w_o}{\partial x\partial y}\right)+N_{cr}\left(\frac{\partial w_o}{\partial x}\right)^2-I_o\omega^2 w_o^2\right]dx\,dy \qquad (26)$$

The natural frequency under that critical buckling load is found to be:

$$\omega=\pm\frac{1.637}{a^2b^2\sqrt{I_o}}(36.322D_{11}b^4+36.322D_{22}a^4+72.644D_{12}a^2b^2+145.289D_{66}a^2b^2$$
$$+3.680N_{cr}a^2b^4)^{0.5} \qquad (27)$$

The natural frequency given in Eq. (25) and Eq. (27) is the fundamental natural frequency where it occurs at *m=n=1* **Reddy, 2004**.

3. EXPERIMENTAL WORK

The experimental work is performed on a plate composed of Polyester as a matrix reinforced with E-Glass fibers.

3.1 Mold Preparation and Mechanical Properties

Two flat wood panels are shaped as square panels of 35 cm*35 cm, with proper thickness to carry moderate loads; they are used as base and cover of the mold to prepare the desired models. One of the panels is used as the base where the materials are molded up, and the other one is the cover that transferes the pressure from up surface to the surface of the desired plate molded on the base. After weaving a layer of E-glass fibers, the catalyzed resin mixture with hardener must be applied to the fibers carefully to prevent distortion in them during the brushing process until the fibers saturate with the risen. Brushes and rollers are used to diffuse the mix over the fibers, and blades are used to take the air bubbles out of the laminate layers **Fig. 3**. Then the mold is left for a day in room temperature for curing after that we cut the model to the desired dimensions by a proper diamond impregnated wheel, cooled by running water. Before starting the experimental work, the fiber, matrix, and then composite densities are measured see **Table (2)**. Then, the fiber volume fraction is measured experimentally to be 0.323. Tensile test is performed to find the composite mechanical properties. D3039 ASTM is used to formulate the tested specimens. The tensile test led to the mechanical properties of E-Glass/Polyester laminated composite plate listed in **Table (2)**.

3.2 Buckling Test

For buckling test, tow models of E-Glass/Polyester laminated plates are prepared. One of the models is (20 cm*20 cm*0.25 cm, $[0/90]_s$) where the aspect ratio (a/b) is equal to 1, and the other one is (40 cm*20 cm*0.2 cm, $[0/90]_2$) where $a/b = 2$. The models are placed vertically between the testing device jaws, where the machine is of 100 KN capacity. The boundary conditions of the tested plates are simply supported along the top and bottom edges while the left and right edges are left free. The compression is exerted on the upper edge by moving stiff head with a speed of 2 mm/min while the lower head is fixed. For determination of the buckling load, load-displacement

method is used **Fig. 4**. Analytical and Numerical results are determined for the tested models and are presented to verify the found experimental results which are listed in **Table (3)**.

3.3 Experimental Modal Analysis

For free vibration test, a model specimen is manufactured with dimensions of (30 cm*30 cm*0.37 cm) and lamination of $(0/90)_2$. The plate is placed in a structure **Fig. 5.a**, where the boundary conditions are simply supported along the four edges and the real tested area is (25 cm* 25 cm) where the edges of the structure are designed to prevent the plate from moving in z-direction. Calibration operation is performed before the test to ensure that the result from the test is right with less error. The plate is placed in the structure that is already manufactured for this purpose where the boundary conditions are kept to be simply supported. The oscilloscope is viewing the response of the specimen that is loaded with hit by an impact hammer which is connected to the oscilloscope and generates the input load to the specimen. The accelerometer is connected to the charge amplifier which will reduce the frequency noise by filters were built to limit the frequency range to the range of interest. The signal goes from the amplifier to the oscilloscope to analyze it and then present it as wave with tops that will give the frequency of the modes. The hit exerted by the impact hammer on the plate. The FFT solution generated **Fig. 5.b** captured from the oscilloscope monitor in purple color wave. The natural frequency ω_o of the first mode taken from the wave is found to be 0.0331 rad/sec. The non-dimensional natural frequency is calculated as below:

$$\bar{\omega} = \frac{\omega_o a^2}{h}\sqrt{\frac{\rho_c}{E_2}} = \frac{0.0331 * 0.25^2}{0.0037}\sqrt{\frac{1369}{5.881}} = 8.529 \quad (28)$$

The analytical result is found to be $\bar{\omega} = 7.832$ so that the error is 8.9%, and that is an accepted error if some conditions are taken in account such as movement of the structure, accuracy of the devices, and the molding process, etc.. **Fig. 5.b** shows the response wave of the plate in yellow color.

4. RESULTS AND DISCUSSION

This study investigates mainly the effect of the critical buckling load that a composite materials plate can hold on its natural frequency. The results are determined analytically and numerically, and study the effect of boundary conditions, aspect ratio, lamination angle, and type of applied edge load.

4.1 Investigation of Critical Buckling Load

The critical buckling load is studied under some considerations. The load is obtained as the non-dimensional load ($\bar{N}$).

a- Effect of Boundary Conditions

Assume a square symmetric cross-ply [0 90 0] laminate (E_1/E_2 =10, G_{12}=0.6E_2, υ_{12}=0.25) is subjected to uniaxial edge loads. **Table (4)** shows the Nondimensionalized buckling load ($\bar{N} = \frac{N_{cr}b^2}{E_2 h^3}$) that the plate can hold. It shows that the clamped plate along two or four edges can hold buckling load more than plate with simply supported boundary

conditions, especially for the case where the plate is SFSF. In the case where the plate is simply supported or mixed with free edges, it is weak to hold large loads compared with clamped plates. From **Table (4)**, it is observed that the critical buckling load for SFSF decreases by 80.28% compared with CCCC for uniformly loaded plate, 74.6% for parabolic load, and 86.28% for linear load.

b- Effect of aspect ratio

Assume a plate (E_1/E_2 =10, G_{12}=0.6E_2, υ_{12}=0.25) with various aspect ratios. From **Fig. 6.a**, it is observed that the Nondimensionalized buckling load ($\bar{N} = \frac{N_o b^2}{\pi^2 D_{22}}$) for clamped plated decreases rapidly with the increase of the aspect ratio until the aspect ratio is 1.6 where $\bar{N}$ starts to increase again for the three types of loading; but for SFSF which is the weaker case, the plate buckles with close values of loads for larger aspect ratios than 1.6 with no increasing in buckling load. Hence, the increasing of aspect ratio decreases buckling load as verified with **Reddy, 2004, Hu, and Abatan, 2003**. **Fig. 6.b** shows the Nondimensionalized buckling load ($\bar{N}$) for a simply supported plate laminated as $[0/90]_2$ and subjected to uniform distributed load in x direction, the plot is compared with that presented by **Reddy, 2004** as a verification. It shows that $\bar{N}$ decreases very slowly with increasing aspect ratio after a/b=1.3 especially when a/b=2.3 where the difference in the load starts to be very small, and observing that the buckling occurs rapidly with increasing aspect ratio.

c- Effect of lamination angle

Assume a square plate (E_1/E_2 =40, G_{12}=0.5E_2, υ_{12}=0.25) subjected to distributed loads in x direction and has the lamination $[-\theta/\theta]_2$. From **fig. 7**, it is observed that the plot is symmetric about $\theta = 45^o$ and the buckling load is maximum for SSSS conditions (verified with **Reddy, 2004**). But for other boundary conditions, the load decreases with the increase of lamination angle.

d- Effect of Loading Type

Table (5). shows dimensionless critical buckling load ($\bar{N} = \frac{N_{cr} b^2}{E_2 h^3}$) of a simply supported and clamped plates (E_1/E_2=10, G_{12}=0.6E_2, υ_{12}=0.25, [0/90/0]) subjected to different loading types. It shows that uniformly loaded plate buckles earlier than the others, while the linearly loaded plate buckles with higher loads which means that the plate will retain more load than plate subjected to uniform load. The critical linear loads for the two boundary conditions are twice the critical uniform loads.

4.2 Investigation of Natural Frequency of Free Vibration

The natural frequency is investigated with and without the action of buckling where the critical buckling load applied to the plate is precalculated from the previous section. Several considerations are presented to investigate the natural frequency which is calculated as dimensionless form ($\bar{\omega} = \frac{\omega_o a^2}{h}\sqrt{\frac{\rho_c}{E_2}}$). In case of buckling action, a ratio (d) of critical load is applied. The effect of the load ratio (d) is studied to present the behavior of the plate and its frequency.

a- Effect of Boundary Conditions

In this analysis, a square plate (E_1/E_2=10, G_{12}=0.6E_2, υ_{12}=0.25, [0/90/0]) with various boundary conditions is taken to calculate the dimensionless natural frequency. From **Table (6**), it is found that the clamped plate vibrates with natural frequency higher than the other boundaries because of the high stiffness due to boundary. In other hand, the natural frequency for the SFSF plate is minimum due to low stiffness. The same investigation is repeated in **Table (6**) for the same plate subjected to parabolic load (load ratio d=0.5), and it is clear that the natural frequency is less than that found without loading.

b- Effect of aspect ratio

The increasing aspect ratio decreases the natural frequency, till a/b=2, where the frequency starts to converge with higher aspect ratio. **Fig. 8** shows this behavior for a $[0/90]_2$ simply supported laminate (E_1/E_2=10, G_{12}=0.6E_2, υ_{12}=0.25) with and without the action of buckling for parabolic load. It is obvious that natural frequency with buckling is lower than that without buckling.

c- Effect of lamination angle

Assume a square plate (E_1/E_2=10, G_{12}=0.6E_2, υ_{12}=0.25) but with different lamination systems and boundary conditions. From **Table (7),** it is obvious that $[45/-45]_2$ plate has the same frequency of $[45\ -45]_s$ plate, but for SFSF plate under buckling action, it is greater in symmetric than unsymmetric laminates. For the other laminates, the frequency is equal for symmetric and unsymmetric in the cases of SSSS and CCCC conditions while it is unequal for the other conditions for the same laminate. It can be seen for the two cases that the natural frequency for symmetric laminates $[0\ 90]_s$ is greater than that for unsymmetric laminates $[0/90]_2$. Oppositely; for laminates $[60\ 30]_s$, the natural frequency is less than that for unsymmetrical laminates $[60\ 30]_2$.

d- Effect of loading type and ratio

The natural frequency under buckling is almost equal for different loading types in analytical solution, where the difference is very infinitesimal, while the frequency determined by numerical solution differs with very small error, but for case of parabolic load, the discrepancy is greater than other loading cases which may reach 7% for d=0.75 of clamped plate. **Table (8)** shows the dimensionless natural frequency of a laminated plate (E_1/E_2=10, G_{12}=0.6E_2, υ_{12}=0.25, [0/90/0]) under buckling of different load functions. It is obvious that the natural frequency ($\bar{\omega} = \frac{\omega_o b^2}{\pi^2}\sqrt{\frac{\rho_c h}{D_{22}}}$) is inversely proportional to the load ratio, where the increasing in load ratio decreases the frequency.

4.3 Verification Study for Buckling and Vibration of Laminated Plate

The numerical results are obtained using programming software (ANSYS) to verify the analytic derivation. The programming in ANSYS is stepped as follows:

1- Choosing the element type (shell 281).
2- The material properties as (E_1/E_2=10, G_{12}=0.6E_2, υ_{12}=0.25).
3- The layers angles and their thicknesses ([0/90/0]).
4- Creating the model as a square plate (a/b=1).
5- Meshing the area with different sizes for convergent result.
6- Choosing the analysis type with prestress option.

7- Define the boundary conditions and loads.
8- Solving the model.
9- Reading and plotting the results.
10- Finishing the solution.

Assume two simply supported and clamped plates subjected to different loads at edges x=0, a. **Table (5)** showed the numerical and analytical dimensionless critical buckling loads ($\bar{N} = \frac{N_{cr} b^2}{E_2 h^3}$). The comparison shows a good agreement between the analytical and numerical results, where the higher discrepancy is 4% for CCCC plate under parabolic load buckling. As investigated in section 4.1, it is obvious that the buckling occurs earlier for uniform load than other loading types.

The Nondimensionalized natural frequency of the same plates found numerically for SSSS conditions to be ($\bar{\omega} = \frac{\omega_o a^2}{h}\sqrt{\frac{\rho_c}{E_2}} = 10.643$) while analytic result is ($\bar{\omega} = 10.645, discrepancy = 0.01\%$). It is clear that a high agreement between the analytical and numerical results was obtained. The numerical natural frequencies of a plate under buckling action of different loads are listed in **Table (9).** The analytical result is ($\bar{\omega} = 7.530$) for a simply supported plate subjected to the three load types. From the comparison between the results, high agreement is produced where the discrepancy does not exceed 2.8% for parabolic buckling case.

5. CONCLUSIONS

The buckling and vibration results lead to the following conclusions:

1- The number of half wavelengths affects the critical buckling load, where the increasing of aspect ratio requires larger number (half-waves number) to get more accurate results.
2- The aspect ratio affects the buckling load and natural frequency reversely. The buckling load decreases rapidly with increasing aspect ratio till it is about 1.5, after that it takes constancy or close values for higher aspect ratios. The natural frequency, decreases with high percentage until aspect ratio a/b=2, then it takes the constancy for higher ratios.
3- The boundary conditions affect the critical buckling load and fundamental natural frequency. Clamped edges conditions offer high stiffness, results in high critical buckling load and natural frequency. It is obvious for highly constrained edges, the stiffness increases which causes the plate to sustain high load and frequency. The results grade from higher to lower values as CCCC-CSCS-CFCF-SSSS and then SFSF.
4- The lamination angle has clear effect on the buckling load of the laminate, where the critical load of a simply supported plate is directly proportional to the angle under 45^o where the maximum load occurs, and then it is reversely proportional to the increasing in lamination angle. For other boundary conditions, the load is reversely proportional to the angle.
5- The plate subjected to buckling linear load can hold larger load than other loading types; the uniform load buckles the plate earlier than others. The effect of load type is very small on the natural frequency.
6- The natural frequency changes indirectly with buckling load ratio.

REFERENCES

- Amabili1, M., Karagiozis1 K., Farhadi, S., and Khorshidi K. , 2010, Nonlinear Vibration of Plates with Different Boundary Conditions using Higher Order Theory, Chaos, 3rd Chaotic Modeling and Simulation.

- Berthelot, J., 2010, Mechanics of Composite Materials and Structures, ISMANS, Institute for Advanced Le Mans, Materials and Mechanics, France.

- Brown, R. G., 2007, Introductory Physics I: Elementary Mechanics, Duke University Physics Department.

- Craciun, E.M. and Simionescu-Panait, O., 2004, Instability Critical Loads of The Fiber Reinforced Elastic Composites, Ovidius Constanta, Vol. 12(2), PP. 99-108.

- Hu, H., Badir, A., and Abatan, A., 2003, Buckling Behavior of a Graphite/Epoxy Composite Plate under Parabolic Variation of Axial Loads, International Journal of Mechanical Sciences 45, PP. 1135–1147.

- Jana, P. and Bhaskar, K., 2007, Analytical Solutions for Buckling of Rectangular Plates under Non-Uniform Biaxial Compression or Uniaxial Compression with In-Plane Lateral Restraint, International Journal of Mechanical Sciences 49, PP. 1104-1112.

- Kollar, L. A. and Springer, G. S., 2003, Mechanics of Composite Structures, Cambridge University Press.

- Kumar, M. M., Jacob, C. V., Lakshminarayana N., Puneeth, B. M., and Nagabhushana, M., 2013, *Buckling Analysis of Woven Glass Epoxy Laminated Composite Plate*, American Journal of Engineering Research (AJER), Vol. 2, Issue-7, PP. 33-40.

- Leissa, A. W. and Kang, J. , 2002, Exact Solutions for Vibration and Buckling of an SS-C-SS-C Rectangular Plate Loaded by Linearly Varying In-Plane Stresses, International Journal of Mechanical Sciences 44, PP. 1925–1945.

- Matsunaga, H., 2000, Vibration and Stability of Cross-Ply Laminated Composite Plates According to a Global Higher-Order Plate Theory, Composite Structures 48, PP. 231-244.

- Reddy, B. S., Reddy, M. R., and Reddy V. N., 2013, Vibration Analysis of Laminated Composite Plates Using Design of Experimentspproach, International Journal of Scientific Engineering and Technology, Vol. No.2, Issue No.1, PP. 40-49.

- Reddy, J.N., 2004, Mechanics of Laminated Composite Plates and Shells: Theory and Analysis, CRC Press LLC, 2nd ed..

Tang, Y. and Wang, X., 2011, *Buckling of Symmetrically Laminated Rectangular Plates under Parabolic Edge Compressions*, International Journal of Mechanical Sciences 53, PP. 91-97.

Ventsel, E. and Krauthammer, T.,2001, *Thin Plates and Shells: Theory, Analysis, and Applications*, The Pennsylvania State University, University Park, Pennsylvania.

NOMENCLATURE

A_{mn}= coefficients in the assumed series for deflection, dimensionless.
a, b= Plate length and width, m.
B_{ij}= coupling stiffness matrix elements, N.
D_{ij}= bending stiffness matrix elements, N.m.
d= Load ratio, dimensionless.
E= total mechanical energy, N.m.
Ec= total kinetic energy, N.m .
E_1,E_2= modulus of elasticity in 1 and 2 directions respectively, GPa.
G_{12}= shear modulus in plane 1-2, GPa.
h= thickness of the laminate, m.
I_o= moment of inertia of the laminate at point (*x, y*), Kg/m^2.
k= layer number.
$\kappa_x, \kappa_y, \kappa_{xy}$= curvatures of the reference plane of the plate, dimensionless.
L= total number of layers in the laminate.
M, N= upper limits of double series, dimensionless.
m, n= numbers of half wavelengths, dimensionless.
N_x= in-plane force in x direction, N/m.
$\overline{N}$= nondimensionalized buckling load, dimensionless.
N_{cr}= critical buckling load, N/m.
N_o= load intensity of distributed load, N/m.
N_o= Load intensity of distributed load, N/m.
$\overline{Q}_{ij}$= transformed reduced stiffness matrix elements, N/m.
U= strain energy of internal forces, N.m.
u, v, w= displacements in x, y, z directions, m.
u_o, v_o, w_o= displacement components along the (*x, y, z*) coordinate directions, m.
v_f= fiber Volume fraction, dimensionless.
$X_m(x)$, $Y_n(y)$= functional bases for boundary conditions, dimensionless.
zk and *zk-1*= distances from the reference plane of the laminate to the two surfaces of the *kth* ply, m.
γ, λ= constants of boundary conditions functions, dimensionless.
δ= variation of a amount, dimensionless.
θ= Angle of layer lamination, Degree.
υ_{12}= poisson ratio in plane 1-2, dimensionless.
Π= total potential energy, N.m.
ρ= density of material, Kg/m^3.
ρ_c, ρ_f, ρ_m= densities of the composite, fiber, and matrix respectively, Kg/m^3.
Ω= work of external forces, N.m.

ω= natural frequency of the plate vibrations, Hz.
$\bar{\omega}$= nondimensionalized natural frequency, dimensionless.

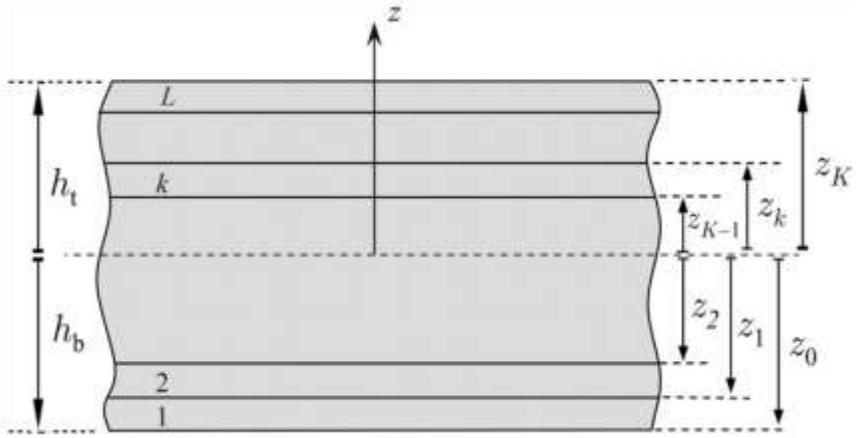

Figure 1. Distances from the reference plane.

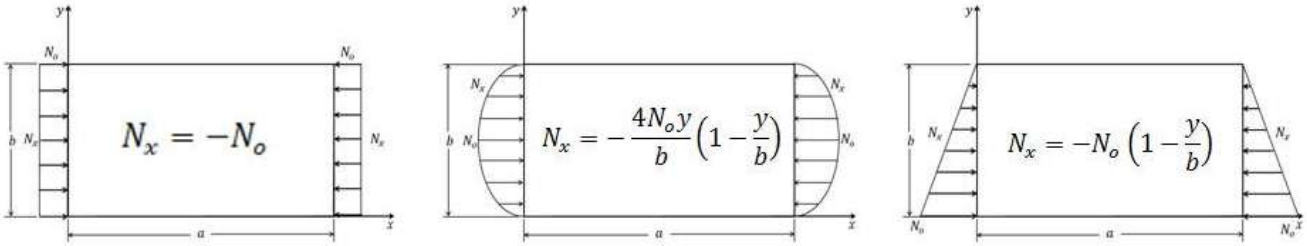

Figure 2. Plates subjected to distributed loads.

Figure 3. Specimen molding process

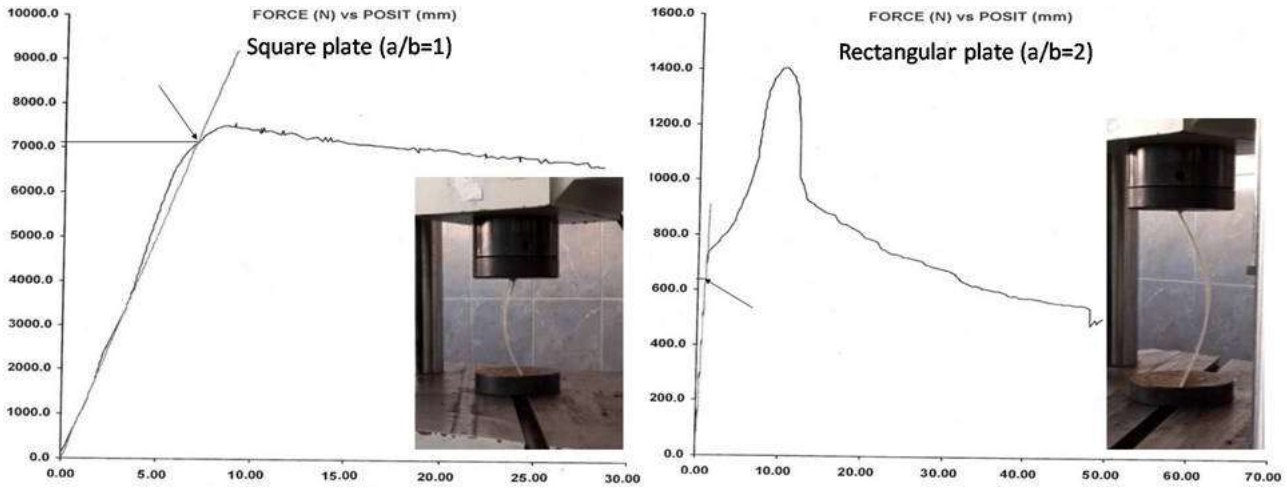

Figure 4. Load displacement curves of the Buckled plates.

(a) **(b)**

Figure 5. a) Free vibration test setup; (1) Power supply, (2) Impact hammar, (3) Testing structure, (4) weights, (5) Tested plate, (6) Accelerometer, (7) Charge amplifier for Accelerometer, (8) Oscilloscope; **b)** Generated response and FFT wave.

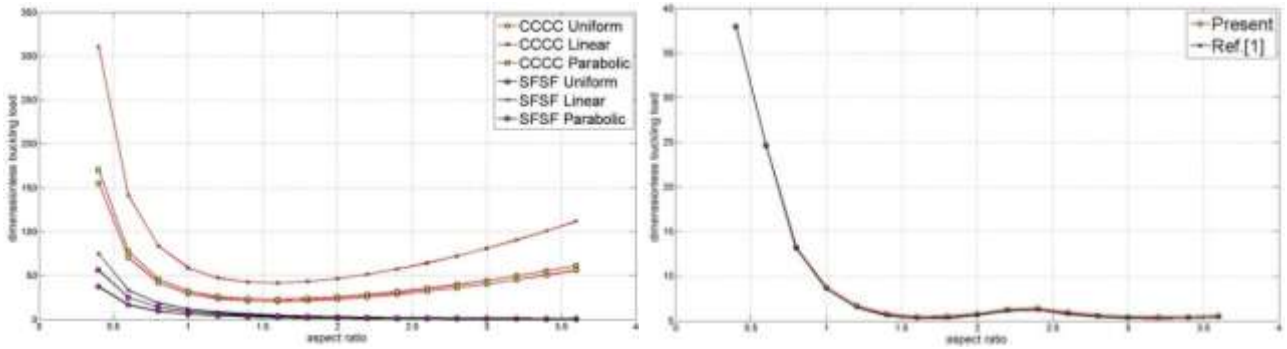

(**a**) **(b)**

Figure 6. Nondimensionalized buckling load ($\bar{N}$) versus aspect ratio for: **a)** CCCC and SFSF; **b)** SSSS orthotropic plates $[0/90]_2$.

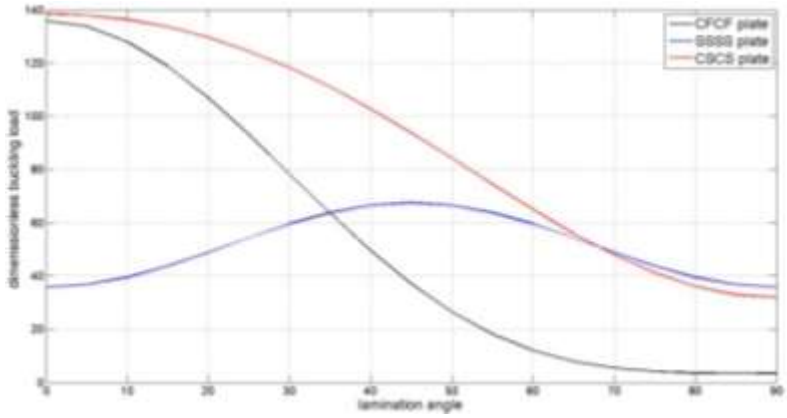

Figure 7. Nondimensionalized buckling load ($\bar{N} = \frac{N_{cr}b^2}{E_2h^3}$) versus lamination angle (θ) of antisymmetric angle-ply square laminates under uniaxial uniform compression.

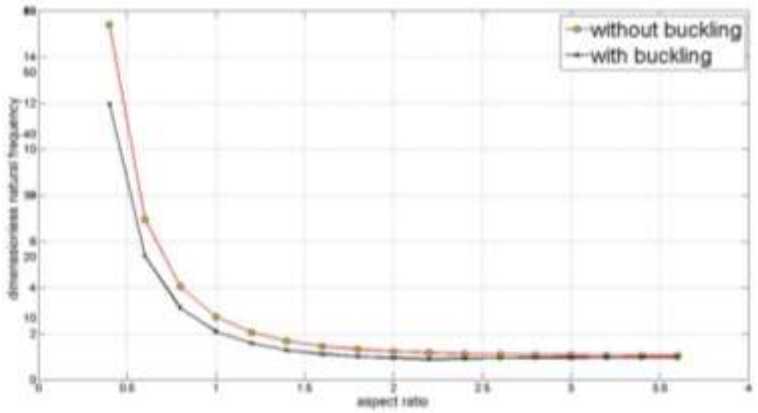

Figure 8. Nondimensionalized fundamental frequency ($\bar{\omega} = \frac{\omega_o b^2}{\pi^2}\sqrt{\frac{\rho_c h}{D_{22}}}$) versus aspect ratio of SSSS symmetric laminates subjected to parabolic load.

Table 1. Values of the constants λ_i and γ_i of the plate functions in the case of clamped and free ends of the plate.

m=n=i	λ_i		γ_i	
	Clamped	Free	Clamped	Free
1	4.7300	0	0.9825	
2	7.8532	0	1.0007	
3	10.9956	4.730	0.9999	–0.9825
4	14.1371	7.853	1.0000	–1.0008
5	17.2787	10.996	0.9999	–1.000
6	20.4203	14.137	1.0000	–1.000
7	23.5619	17.279	1.0000	–1.000
8	26.7035	20.420	1.0000	–1.000

Table 2. Experimental mechanical properties of E-glass/Polyester composite plate.

Physical and Mechanical Property	Obtained Result
$\rho_f(Kg/m^3)$	2360
$\rho_m(Kg/m^3)$	970
$\rho_c(Kg/m^3)$	1369
E_1(GPa)	26.285
E_2(GPa)	5.882
G_{12}(GPa)	2.213
ν_{12}	0.25
V_f	0.323

Table 3. Experimental non-dimensional critical buckling loads $\frac{N_{cr}b^2}{E_2h^3}$ of the tested plates.

Plate Geometry (cm)	20×20×0.25	40×20×0.2
Aspect Ratio a/b	1	2
Angle Ply Orientations	$[0/90]_s$	$[0/90]_2$
Experimental Result	3.097	0.538
Analytical Result	3.398	0.575
Discrepancy%	8.8	6.4

Table 4. Nondimensionalized buckling load ($\bar{N}$) of a square plate laminated as (0/90/0) and subjected to uniaxial edge loads (The results between the brackets represent the numerical results for comparison. The subscript refers to (m=n)).

Type of applied load	**Type of boundary conditions**				
	$SSSS_1$	$CCCC_1$	$CSCS_1$	$SFSF_3$	$CFCF_1$
Uniform load	11.491 (11.559)	40.507 (40.777)	36.255 (36.276)	7.991 (8.018)	32.982 (32.968)
Parabolic load	13.219 (13.694)	44.395 (46.207)	41.705 (42.83)	11.279 (11.638)	49.473 (46.462)
Linear load	22.983 (22.838)	81.015 (80.11)	72.510 (70.481)	11.120 (11.327)	65.964 (64.391)

Table 5. Nondimensionalized buckling load ($\bar{N}$) of a SSSS and CCCC square plate laminated as (0/90/0) and subjected to uniaxial edge loads.

Type of Load	**Boundary Conditions**					
	SSSS			**CCCC**		
	Analytical Result	Numerical Result	discrepancy	Analytical Result	Numerical Result	discrepancy
Uniform	11.491	11.6	0.9%	40.507	40.8	0.7%
Parabolic	13.219	13.7	3.6%	44.395	46.2	4%
Linear	22.983	22.8	0.7%	81.015	80.1	1.1%

Table 6. Nondimensionalized fundamental frequency of a symmetric cross-ply square plate of various boundary conditions (the results between the brackets refer to the Nondimensionalized fundamental frequency of the same plate subjected to parabolic load of load ratio d=0.5).

Boundary Conditions	**Analytical results**	**Numerical results**	**Discrepancy%**	**Other Researches**
SSSS	10.649 (7.530)	10.645 (7.613)	0.03 (1.1)	10.650[Reference 1]
CCCC	22.323 (15.785)	22.310 (16.237)	0.05 (2.8)	————
CSCS	21.119 (14.933)	21.115 (15.256)	0.01 (2.1)	21.118[Reference 1]
SFSF	8.886 (5.973)	8.875 (5.774)	0.1 (3.3)	————

Table 7. Nondimensionalized fundamental frequency ($\frac{\omega_o b^2}{\pi^2}\sqrt{\frac{\rho h}{D_{22}}}$) of a square plate of various laminations and boundary conditions (d=0.5 for buckled plate).

Angle Ply		**Type of boundary conditions**				
		SSSS	CCCC	CSCS	SFSF	CFCF
$[0\ 90]_s$	Without Buckling	2.556 (2.555)	5.358 (5.312)	4.914 (4.913)	1.988 (2.041)	4.632 (4.630)
	With Buckling	1.807 (1.755)	3.788 (3.603)	3.475 (3.569)	1.688 (1.631)	3.275 (3.095)
[0 90 0 90]	Without Buckling	1.588 (1.601)	3.330 (3.398)	2.606 (2.586)	0.956 (1.002)	2.266 (2.317)
	With Buckling	1.123 (1.146)	2.355 (2.237)	1.842 (1.766)	0.801 (0.950)	1.602 (1.577)
$[60\ 30]_s$	Without Buckling	1.877 (1.815)	3.242 (3.101)	2.391 (2.287)	0.781 (0.711)	1.441 (1.491)
	With Buckling	1.327 (1.397)	2.292 (2.131)	1.691 (1733)	0.846 (0.873)	1.019 (0.971)
[60 30 60 30]	Without Buckling	2.240 (2.318)	3.869 (3.633)	3.146 (3.358)	0.869 (0.912)	2.266 (2.199)
	With Buckling	1.584 (1.501)	2.735 (2.613)	2.225 (2.399)	1.010 (1.138)	1.602 (1.423)
$[45\ -45]_s$	Without Buckling	2.517 (2.728)	4.125 (4.492)	3.397 (3.152)	1.070 (0.910)	2.267 (1.986)
	With Buckling	1.780 (1.694)	2.916 (3.089)	2.402 (2.495)	1.187 (1.036)	1.602 (1.554)
[45 -45 45 -45]	Without Buckling	2.517 (2.311)	4.125 (4.016)	3.397 (3.248)	0.486 0.441)	2.267 (2.252)
	With Buckling	1.780 (1.701)	2.916 (3.052)	2.402 (2.258)	0.711 (0.730)	1.602 (1.523)

Table 8. Dimensionless natural frequency of a laminated plate under buckling of different load functions and ratios (superscripts refer to the first letter of the load type).

d	Type of boundary condition				
	SSSS	CCCC	CSCS	SFSF	CFCF
0	10.649 (10.645)	22.323 (22.310)	21.119 (21.115)	8.886 (8.875)	20.143 (20.133)
0.25	9.223 $(9.231)^{U}$ $(9.275)^{P}$ $(9.218)^{L}$	19.332 $(19.353)^{U}$ $(19.530)^{P}$ $(19.305)^{L}$	18.290 $(18.352)^{U}$ $(18.451)^{P}$ $(18.259)^{L}$	7.443 $(7.403)^{U}$ $(7.322)^{P}$ $(7.501)^{L}$	17.444 $(17.121)^{U}$ $(17.988)^{P}$ $(17.673)^{L}$
0.5	7.530 $(7.544)^{U}$ $(7.613)^{P}$ $(7.522)^{L}$	15.785 $(15.785)^{U}$ $(16.219)^{P}$ $(15.638)^{L}$	14.933 $(15.040)^{U}$ $(15.256)^{P}$ $(14.947)^{L}$	5.973 $(5.877)^{U}$ $(6.212)^{P}$ $(5.834)^{L}$	14.243 $(14.405)^{U}$ $(13.899)^{P}$ $(14.011)^{L}$
0.75	5.324 $(5.379)^{U}$ $(5.583)^{P}$ $(5.378)^{L}$	11.161 $(11.013)^{U}$ $(11.948)^{P}$ $(11.282)^{L}$	10.559 $(10.66)^{U}$ $(11.115)^{P}$ $(10.685)^{L}$	3.995 $(3.910)^{U}$ $(4.197)^{P}$ $(3.980)^{L}$	10.071 $(9.901)^{U}$ $(10.100)^{P}$ $(10.227)^{L}$

Table 9. Nondimensionalized natural frequency ($\bar{\omega}$) of a SSSS and CCCC square plate laminated as (0/90/0) and subjected to uniaxial edge loads.

Type of Load	SSSS	Discrepancy	CCCC	Discrepancy
No Load	10.643	0.01%	22.310	0.05%
Uniform Load	7.546	0.2%	15.839	0.3%
Parabolic load	7.621	1.2%	16.235	2.8%

Reducing of Manufacturing Lead Time by Implementation of Lean Manufacturing Principles

Prof. Dr. Hussein Salem Ketan
Engineering College-Baghdad University
Email: hussket@yahoo.com

Fatimah Mutashar Yasir
Engineering College-Baghdad University
Email: Fatimah.my89@yahoo.com

ABSTRACT

Many organizations today are interesting to implementing lean manufacturing principles that should enable them to eliminating the wastes to reducing a manufacturing lead time. This paper concentrates on increasing the competitive level of the company in globalization markets and improving of the productivity by reducing the manufacturing lead time. This will be by using the main tool of lean manufacturing which is value stream mapping (VSM) to identifying all the activities of manufacturing process (value and non-value added activities) to reducing elimination of wastes (non-value added activities) by converting a manufacturing system to pull instead of push by applying some of pull system strategies as kanban and first on first out lane (FIFO). ARENA software is used to simulate the current and future state. This work is executed in the state company for electrical industries in Baghdad. The obtained results of the application showed that implementation of lean principles helped on reducing of a manufacturing lead time by 33%.

Key words: Manufacturing Lead Time, Lean Manufacturing System, Value Stream Mapping, Pull System.

تقليل وقت التصنيع بتطبيق مفاهيم التصنيع النحيف

الاستاذ د. حسين سالم كيطان
جامعة بغداد - كلية الهندسة

فاطمة مطشر ياسر
جامعة بغداد- كلية الهندسة

الخلاصة

تهتم العديد من المؤسسات مهتمة بتطبيق مفاهيم التصنيع النحيف التي تمكنها من حذف الخسائر لتقليل وقت التصنيع. هذا البحث يركز على زيادة المستوى التنافسي للشركة في الأسواق العالمية و تحسين الإنتاجية والمرونة بتقليل وقت التصنيع. ولتحقيق هذا الهدف يتم استخدام الأداة الرئيسية التي هي مخطط مسار القيمة لتحديد كل فعاليات العملية التصنيعية (التي تضيف والتي لا تضيف قيمة) لتقليل و حذف الخسائر (الفعاليات التي لا تضيف قيمة) بتحويل نظام التصنيع من نظام دفع إلى نظام سحب باستخدام بعض إستراتيجيات نظام السحب مثل نظام السحب حسب الطلب (Kanban) و انجاز الطلب الداخل أولا (FIFO). استخدمت برمجية (ARENA) المحاكاة الحالة الواقعية والحالة المستقبلية المقترحة لعملية التصنيع. وهذا العمل تم تنفيذه في الشركة العامة للصناعات الكهربائية في بغداد. وقد أظهرت النتائج التي تم الحصول عليها من التطبيق تقليل وقت تصنيع المنتج بنسبة 33%.

الكلمات الرئيسية: وقت التصنيع, نظام التصنيع النحيف, مخطط مسار القيمة, نظام السحب.

1- INTRODUCTION

Nowadays, the success of any company is identified by its ability to quickly respond to the market changes, so the companies pay more effort to reducing their manufacturing lead times, **Yadav, et al., 2012**. Reductions in manufacturing lead time can generate numerous benefits, including lower work in process and finished goods inventory levels, improved productivity, lower costs. More importantly, reductions in manufacturing lead time increase flexibility and reduce the time required to respond to customer orders, **Samad, et al. 2013**. Manufacturing Lead Time refers to the total time it takes to complete the manufacturing process of a product. It is the time from when an order is ready to start on the production line to when it becomes a finished good, **Hari, et al. 2013**. A lead time is the period of time between the initiation of any process of production and the completion of that process, **Karunesh, and Thotappa, 2013**.

2- LEAN MANUFACTURING

The origins for initiatives of the lean manufacturing are traced to the Toyota Production System (TPS) and were started by Ohno (1978) and Shingo (1989) at TPS with its focus on the systematic and efficient use of the resources through level of scheduling. The term "lean manufacturing" as Ohno (1978) states, is providing a way to do more and more with less and less inventory, less human effort, less movement of material , less equipment and less time while coming closer to supplying the customers with what they want exactly, **Ravet, 2011.** Lean manufacturing means eliminating wastes by identifying non value added activities thorough out the supply chain. The five fundamental Lean principles are to specify value from the point of view of customer, identify the value stream, make the identified value flow, set the pull system which means only make as needed and finally perfection in producing what the customer wants and by when it is required in the right quantity with minimum waste**, Sambathkumar, and Vijayanand, 2013.**

3- VALUE STREAM MAPPING (VSM)

Value stream mapping is a mapping tool that helps on representing material and information flows of manufacturing process and also that signal and control the material flows. This representation facilitates the process of identify the value adding activities in a value stream of manufacturing process and eliminating the non value added activities, or wastes through implementation of lean principles, **Romero, and Chavez, 2011**. VSM is a visualization tool oriented to the version of TPS for lean manufacturing. It helps people to understand and identifying the work processes and then implementing of Toyota Production System tools and techniques, **Thorsen, 2004**. The value stream mapping (VSM) suite of tools can be used to map the current state of a production line and design a desired future state. , they provide a roadmap for how VSM can provide necessary information for analysis of equipment replacement decision problems encountered in lean manufacturing implementation, **Dighe, and Kakirde, 2014**. The focus of VSM is on a product “value stream” (all actions required to transform raw materials into a finished product) for a given “product family” (products that follow the same overall production steps). In applying VSM, waste is identified at a high level along the value stream in the form of all elements that prohibit or hamper flow and in the form of inventory (raw materials, work-in-process (WIP) and finished goods). In future state design, major issues that create waste in the process are addressed, **Romero, and Chavez, 2011**.

4- METHODOLOGY

To achieve the Research objectives the following steps will be applying:

1-Identifying a product and studying a manufacturing process of the product in details.

2-Draw flow diagram of the manufacturing process.

3-Documenting a list of activities flow for manufacturing process with the number of workers and the time required for each activity to identify a waste (non-value added activities) in the process.

4-Draw the value stream mapping for the current state of manufacturing process by using Visio Software.

5-Identify the areas of waste in current state and eliminating all non-value added activities to adding the requisite improvement (kaizen) by applying some of pull strategies as kanban, supermarkets and FIFO strategies to make a system pull instead of push to reducing long waiting time, overproduction and other wastes to reducing lead time.

6-Developing a future state of a process and an action plan after implementation of lean principles to achieve a high efficiency and lead time reduction.

7- Simulation of current and future state by using ARENA software to calculating a lean measurements and comparison the results.

4- THE MEASUREMENTS OF LEAN MANUFACTURING SYSTEM

The main measures of lean manufacturing are calculated as follows:

1- Manufacturing cycle time (CT), **Hopp, et al. 1990.**

$$CT=LT= T_w + T_s + T_p + T_i \quad (1)$$

Where:

T_w= waiting time, T_s= set up time, T_p= processing time, T_i= inspection time and LT= lead time.

2- Throughput (TH) (part/hour), **Standridge, 2004.**

$$TH = \frac{WIP}{CT} \quad (2)$$

Where:

WIP = work in process (unit) and CT= manufacturing cycle time (hour).

3- Value added ratio (VAR), **Karunesh, and Thotappa, 2013**.

$$VAR = \frac{VAT}{CT_t} \quad (3)$$

Where:

VAT= value added time (min) and CT_t= total cycle time (min).

4- Production capacity per week (Pc), **Dinesh, and Prabhukarthi, 2013.**

$$Pc = Wt \times P \quad (4)$$

Where:

Wt= available work time per week (hour) and P= Production rate (unit per hour).

5- SELECTING OF THE PRODUCT AND IMPLEMENTATION

To implementing a methodology of the research a product which is selected is the rotor of air coolant motor consist of three parts: rotor, shaft and sleeve as shown in **Fig. 1**, also studying a manufacturing process of the product in details including total cycle time, value added time, number of workers for each activity identifying all types of activities in manufacturing process (value added, non-value added and non-value added but necessary). The stages of product manufacturing process and their cycle times for patch production of (100 rotor) are shown in **Table 1**. and **Fig. 2** show the flow diagram of manufacturing process.

The next step after identifying the activities and flow diagram of manufacturing process is draw a current state value stream mapping as shown in **Fig. 3, Fig. 5** and **Fig. 7** to identifying the areas of waste by kaizen (continuous improvement) to solve the problems of the manufacturing process by application of pull system strategies in proposed future state value stream mapping as shown in **Fig. 4, Fig. 6 and Fig. 8** to improving the productivity and reducing a manufacturing lead time.

ARENA software (version 14.50) is used to simulate the current and future state of rotor manufacturing process as shown in **Fig. 9** to simulate a research problem and estimate a various performance parameters of lean manufacturing system as shown in **Table 2**. which show the simulation results. Also **Fig. 10** show the percentages of production activities type in current and future state of manufacturing process.

CONCLUSIONS

1- Implementation of lean manufacturing principles help on reducing a production lead time and improving of productivity and efficiency of production process.

2-Value stream mapping can be a valuable and an effective tool for identifying and eliminating the wastes and it also suggests ways to reducing non value added times in a manufacturing process.

3- By applying lean principles, the lead time of rotor manufacturing process is reducing by 33% and also value added ration (VAR) is increasing by 66%.

4- After the improving and reducing of a manufacturing lead time the future state will become current state, in that still more new developments and improvements can be added and this process will be repeated to obtain better results until an ideal state is established.

REFERENCES

- Dighe, S. B. and Kakirde, A., 2014, *Lean Manufacturing Implementation Using Value Stream Mapping: A Case study of Pumps Manufacturing Company,* International Journal of Science and Research, Vol. 3, No. 6, PP. 2492- 2498.

- Dinesh, J., Prabhukarthi, A., 2013, *Reduction of Lead Time Using Value Stream Mapping in Pump Manufacturing Industry*, Proceedings of the National Conference on Manufacturing Innovation Strategies & Appealing Advancements, College of Technology, Coimbatore, India, PP. 1-6.

- Hari, G., Sandeep, N. and Doss, K., 2012, *Manufacturing Lead Time Reduction of Gear Box Side Frame Using Lean Principles*, SASTECH, Vol. 11, No. 1, PP. 25-32.

- Hopp, W. J., Spearman, M. L., Woodruff, D. L., *1990, Practical Strategies of Lead Time Reduction*, Manufacturing Review, Vol. 3, No. 2, pp.78-84.

- Karunesh, G. and Thotappa, C., *2013, Lead Time Reduction in Order Execution of Horizontal Slurry Pumps Using Lean Concepts for Mining Equipments Manufacturing Company*, International Journal of Scientific & Engineering Research, Vol. 4, No. 3, PP. 1-15.

- Ravet, D., *2011, Lean Production and Agile Organization: The Link Between Supply Chain and Sustainable Development,* Dorich House Group « Developing Sustainability » Area: Material Manufacturing and Design, https://hal.archives-ouvertes.fr .

- Romero, D. and Chavez, Z., *2011, Use of Value Mapping Tools for Manufacturing Systems Redesign,* Proceedings of the World Congress on Engineering, Vol. I.

- Samad, M. A., SaifulAlam, M. D. and Tusnim N., 2013, *Value Stream Mapping to Reduce Manufacturing Lead Time in a Semi-Automated Factory* **,** Asian Transactions on Engineering , Vol. 02, No. 06, pp. 2221- 4267.

- Sambathkumar, R., Vijayanand, V., 2013, *Implementing Lean Tools in Centrifugal Pump Manufacturing Industry*, Manufacturing Innovation Strategies & Appealing Advancements.

- Standridge, C. R., *2004, How Factory Physics Helps Simulation,* Proceedings of the Winter Simulation Conference, pp. 1103-1108.

- Thorsen, W. C., 2004, *Value Stream Mapping & VM,* General Motors Corporation's Worldwide Facilities Group.

- Yadav, R. , Shastri, A. and Rathore, M., *2012, Increasing Productivity by Reducing Manufacturing Lead Time through Value Stream Mapping*, International Journal of Mechanical and Industrial Engineering, Vol. 1, No. 3, PP. 31-35.

NOMENCLATURE

List of Symbols and Abbreviations

Symbol	***Description***
CT_t	Total Cycle Time
CT	Cycle Time
FIFO	First in First Out
LD	Lead Time
TH	Throughput
T_i	Inspection Time
T_p	Processing Time
TPS	Toyota Production System
T_s	Set up Time
T_w	Waiting Time
VAR	Value-Add Ratio
VAT	Value-Add Time
VSM	Value Stream Mapping
WIP	Work-in-Process

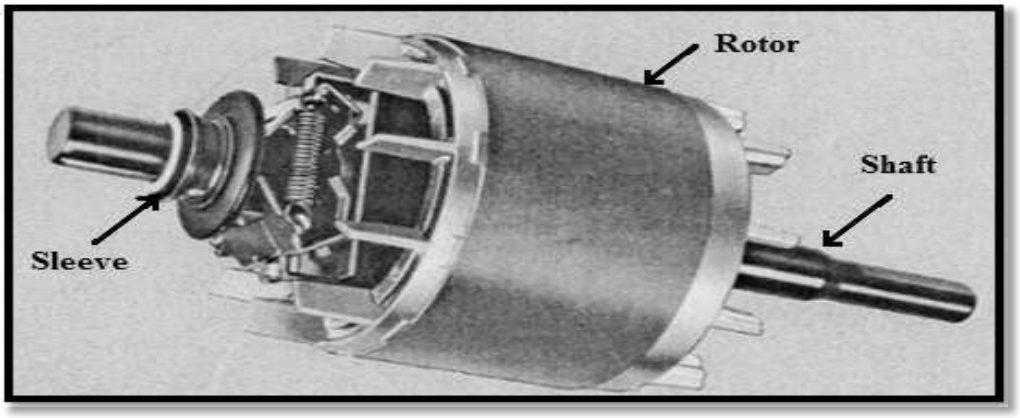

Figure 1. A Selected Product (Rotor of Air Coolant Motor).

Table 1. Operations Sequence of Product Manufacturing Process.

part	Operation	Cycle Time (min)
Rotor	Cutting process of laminations	60
	Annealing process	240
	Stacking process	55
	Casting process	50
	Cutting process	25
	Turning process	75
Shaft	Turning process of the shaft	50
	Cleaning process of the shaft	10
	Initial grinding process	75
	Final grinding process	75
	Milling process	68
	Chemical coating process of the shaft	125

Sleeve	Turning process of the sleeve	65
	Cleaning process of the sleeve	75
Assembly Process	Assembly process of rotor with shaft	71
	Assembly process of rotor with sleeve	60
	Painting process	30

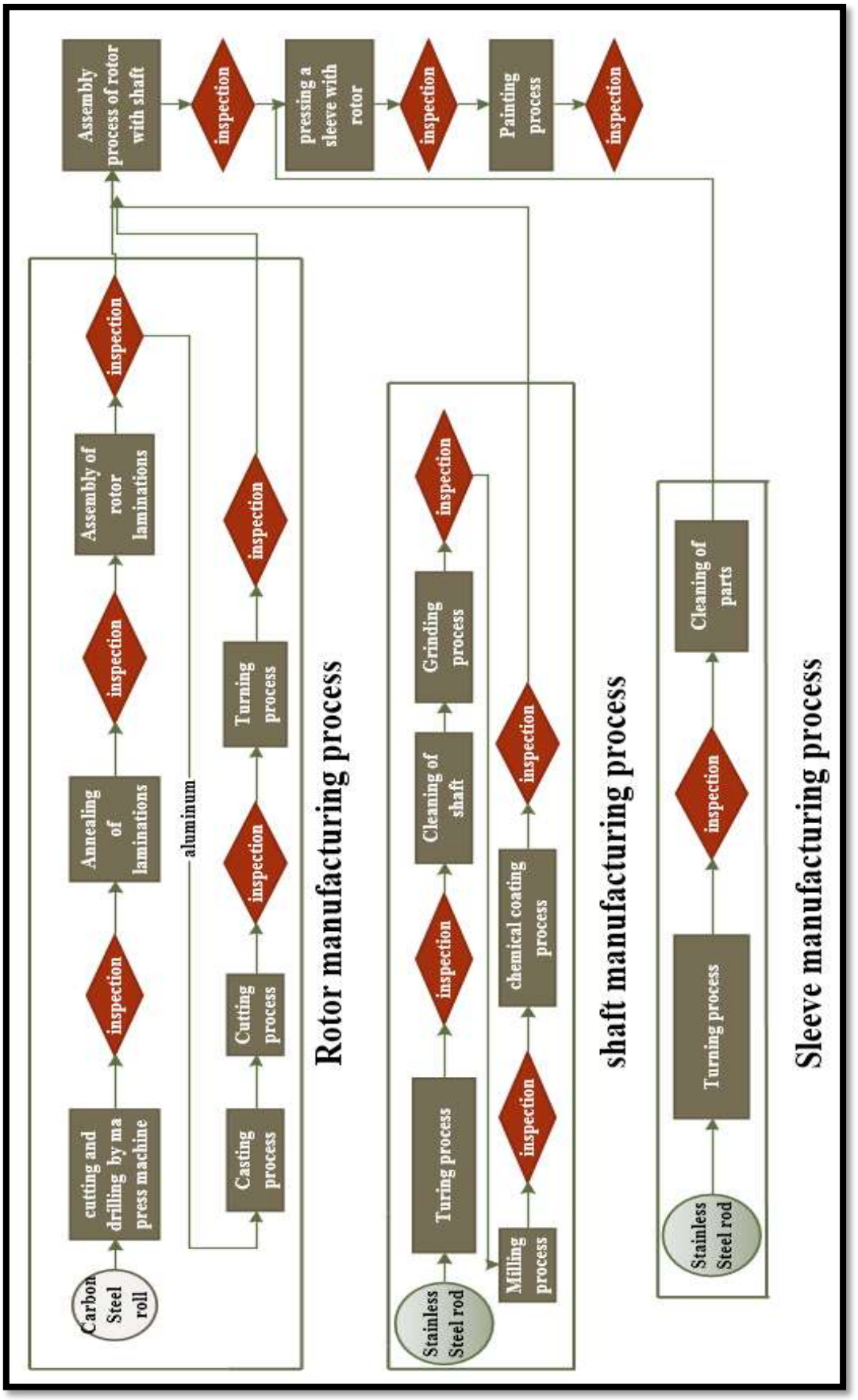

Figure 2. Flow Diagram of Rotor Manufacturing Process

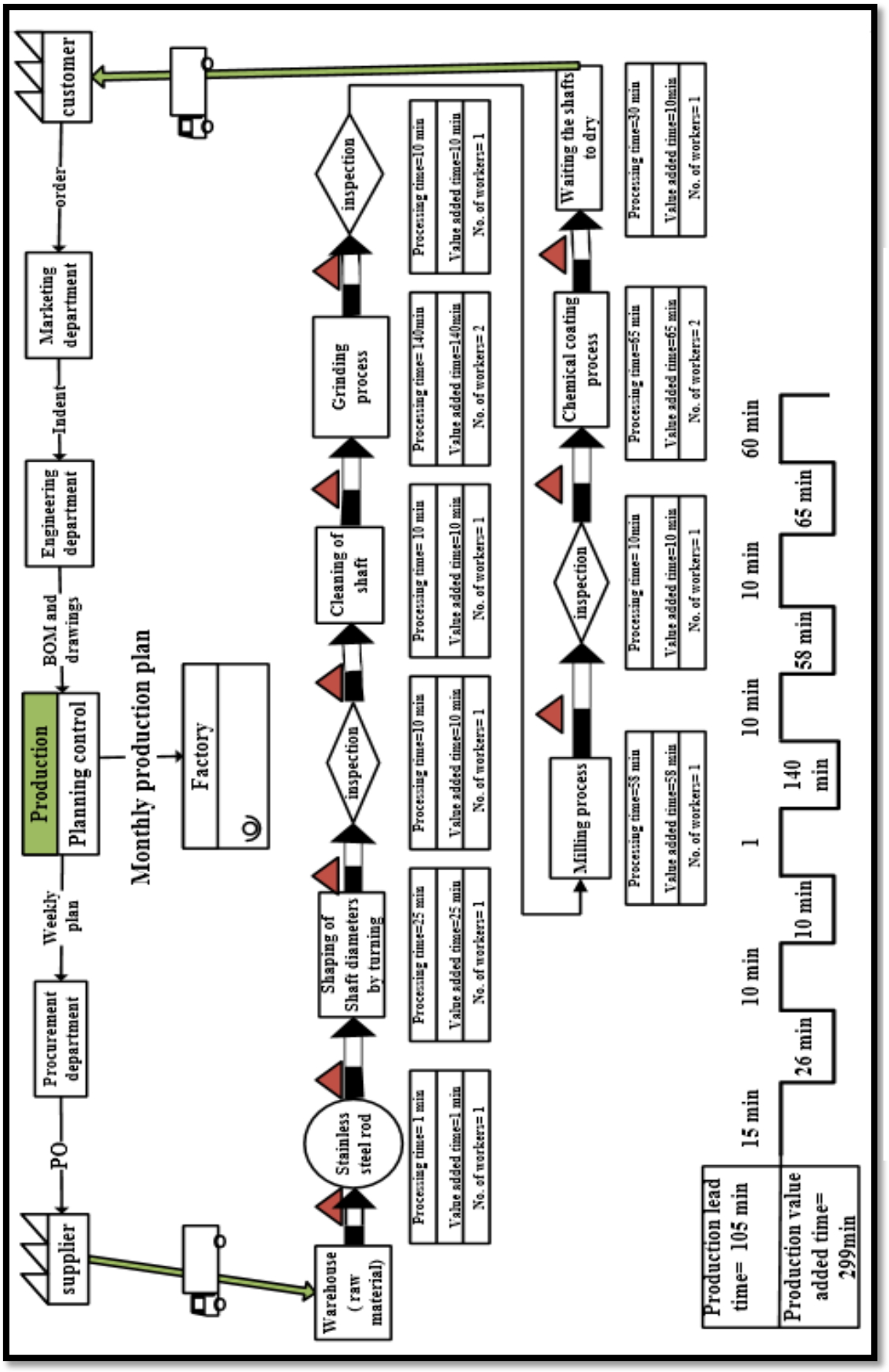

Figure 3. Current state value stream mapping of rotor manufacturing process

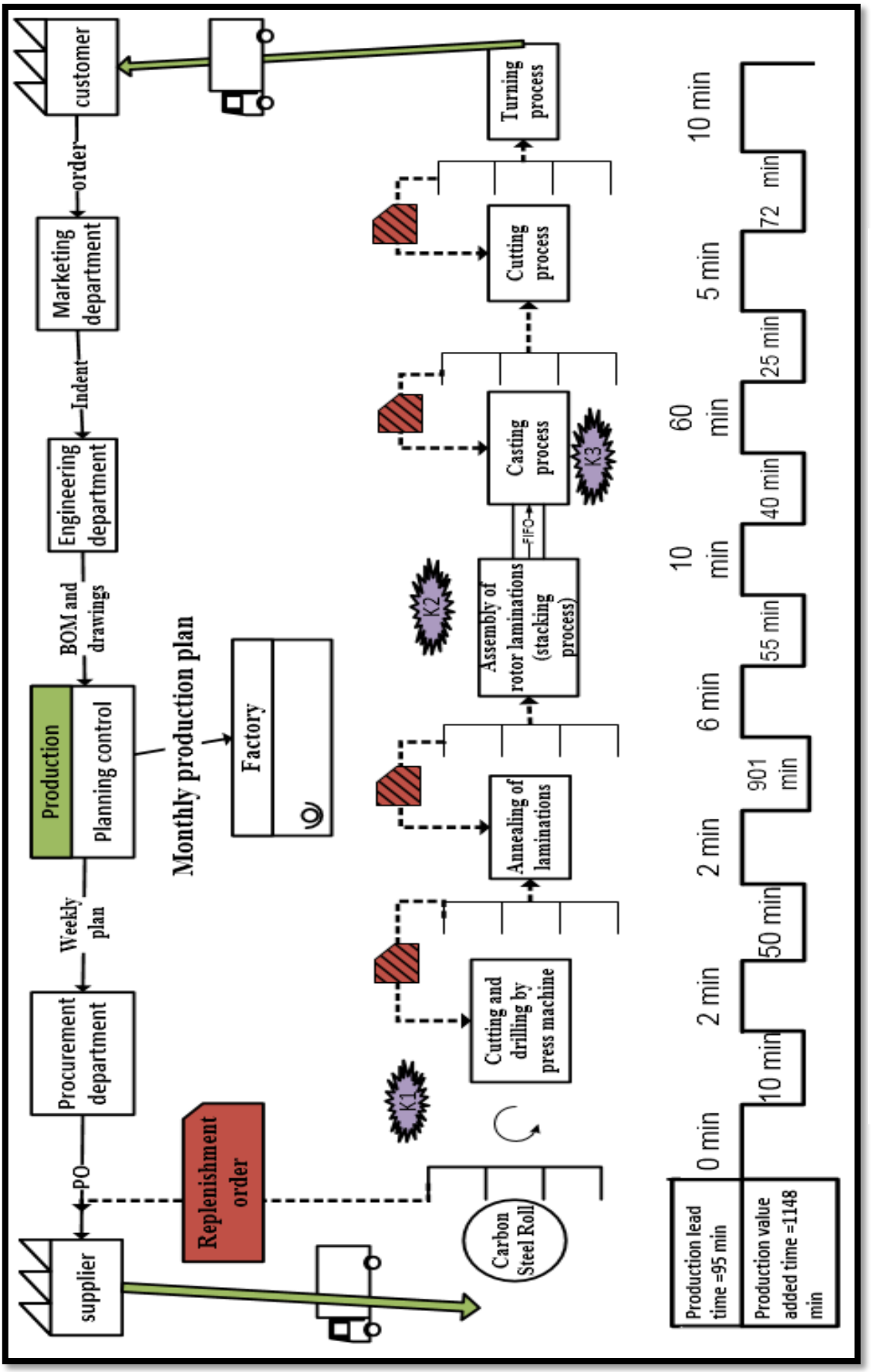

Figure 4. Future state value stream mapping of rotor manufacturing process

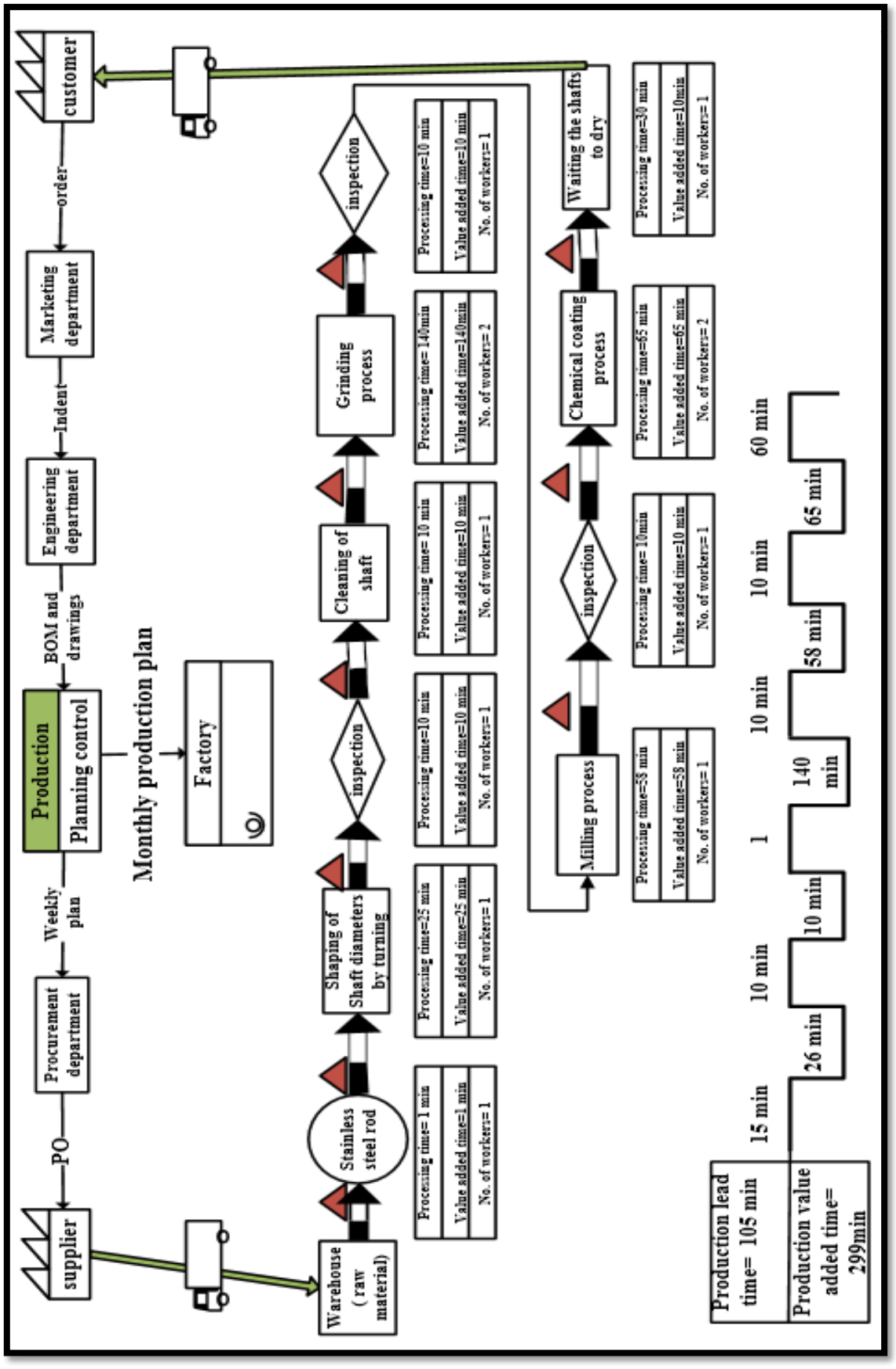

Figure 5. Current state VSM of the shaft manufacturing process

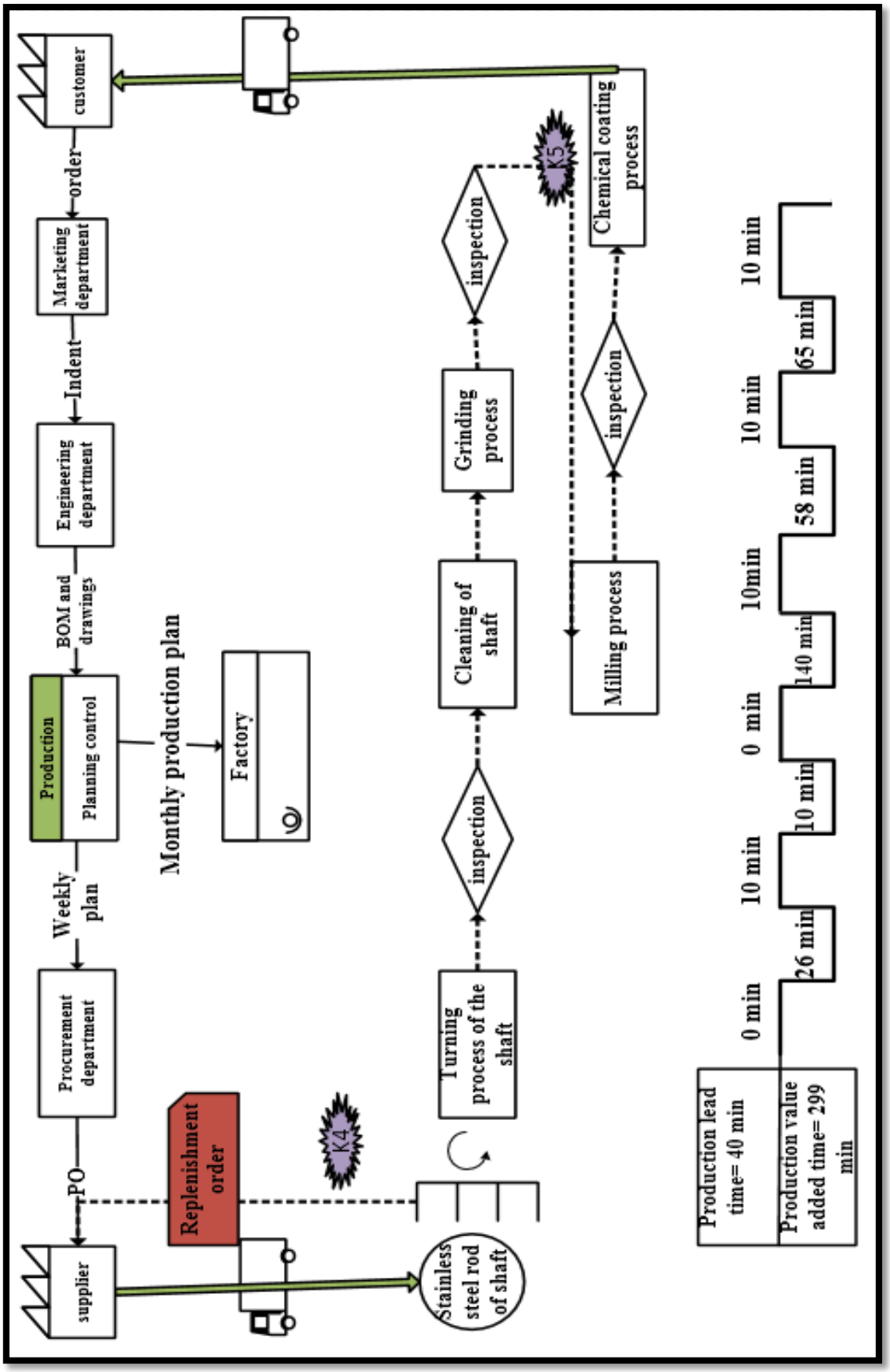

Figure 6. Future state VSM of the shaft manufacturing process

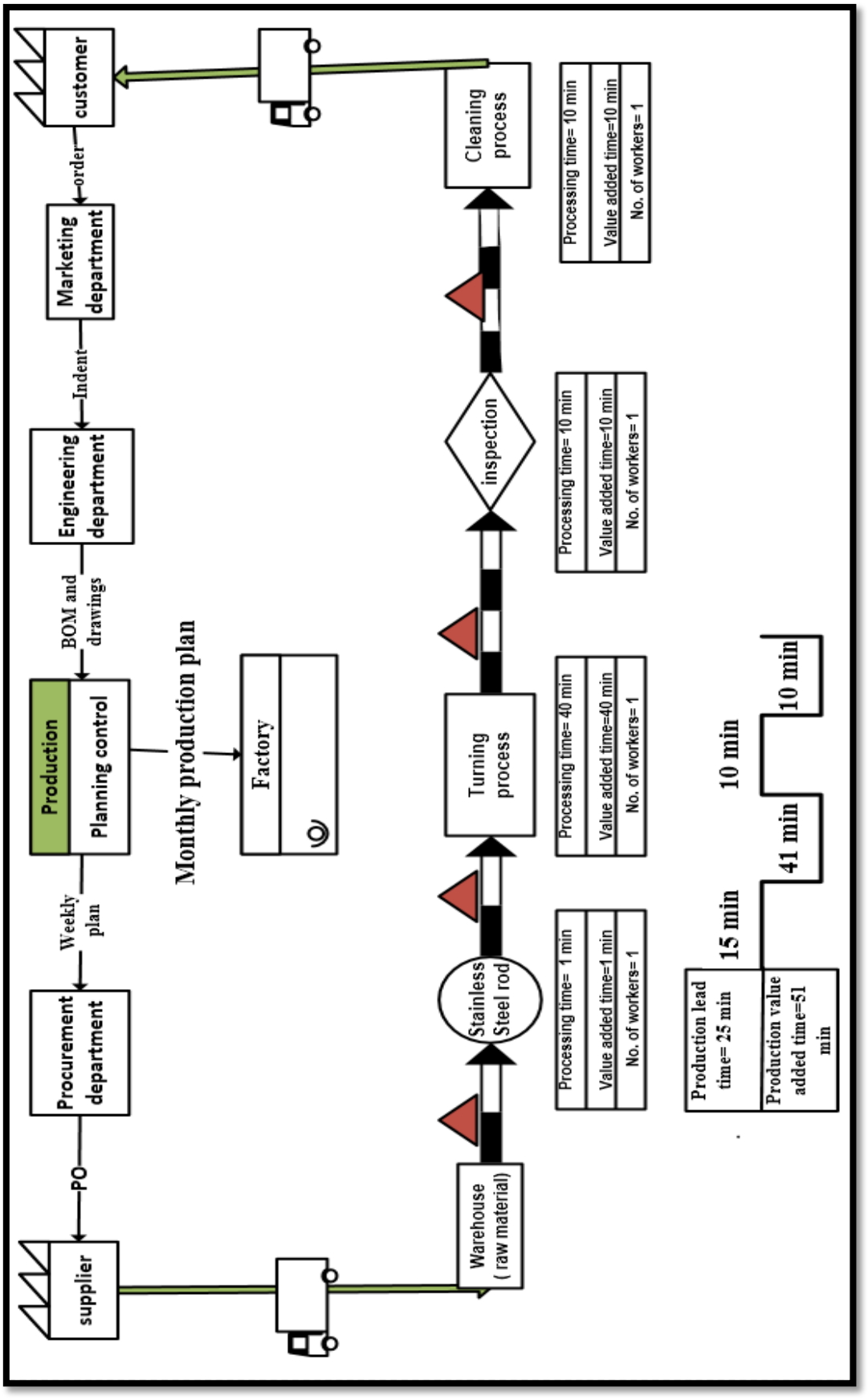

Figure 7. Current state VSM of the sleeve manufacturing process

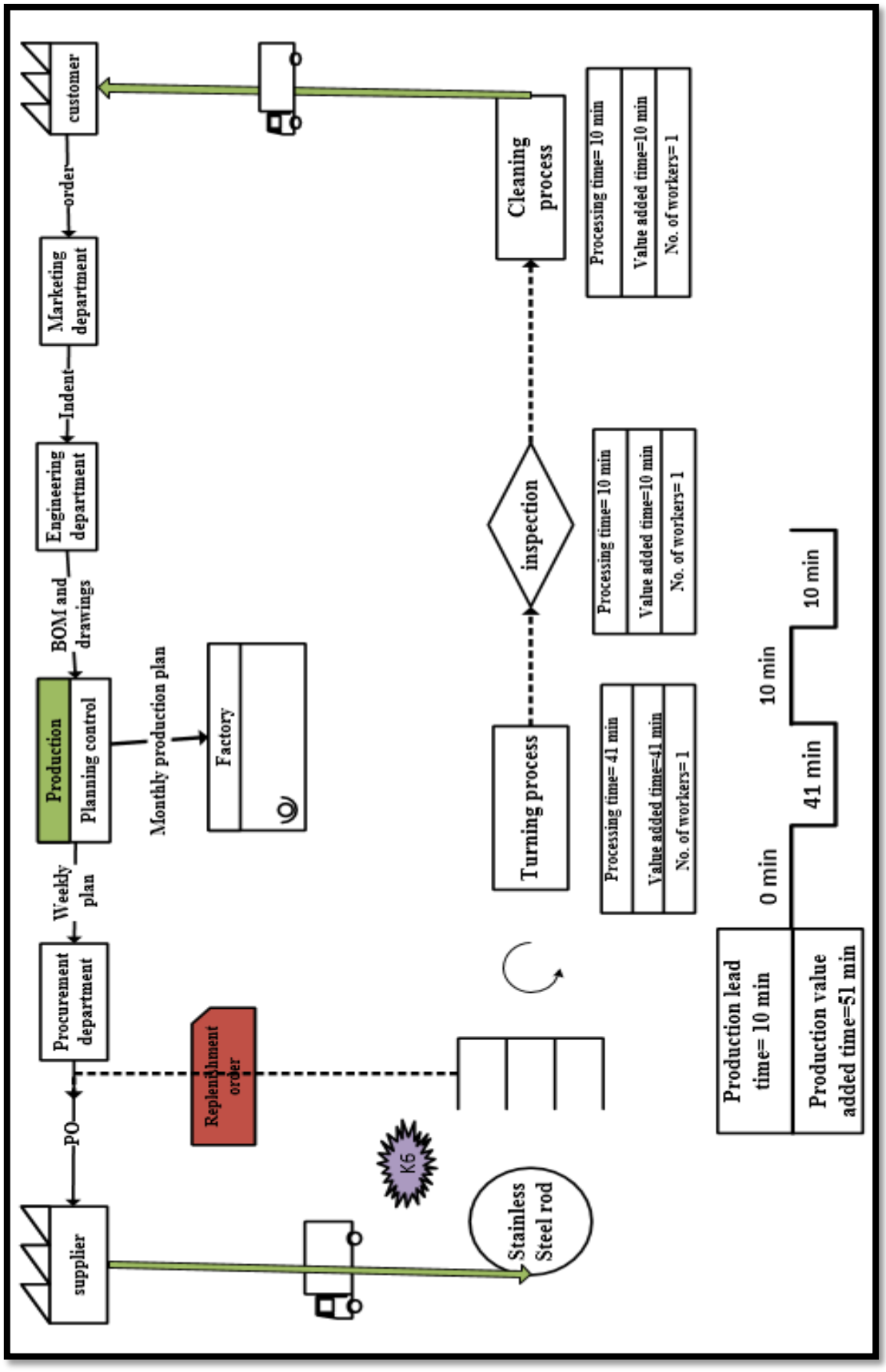

Figure 8. Future state VSM of the sleeve manufacturing process

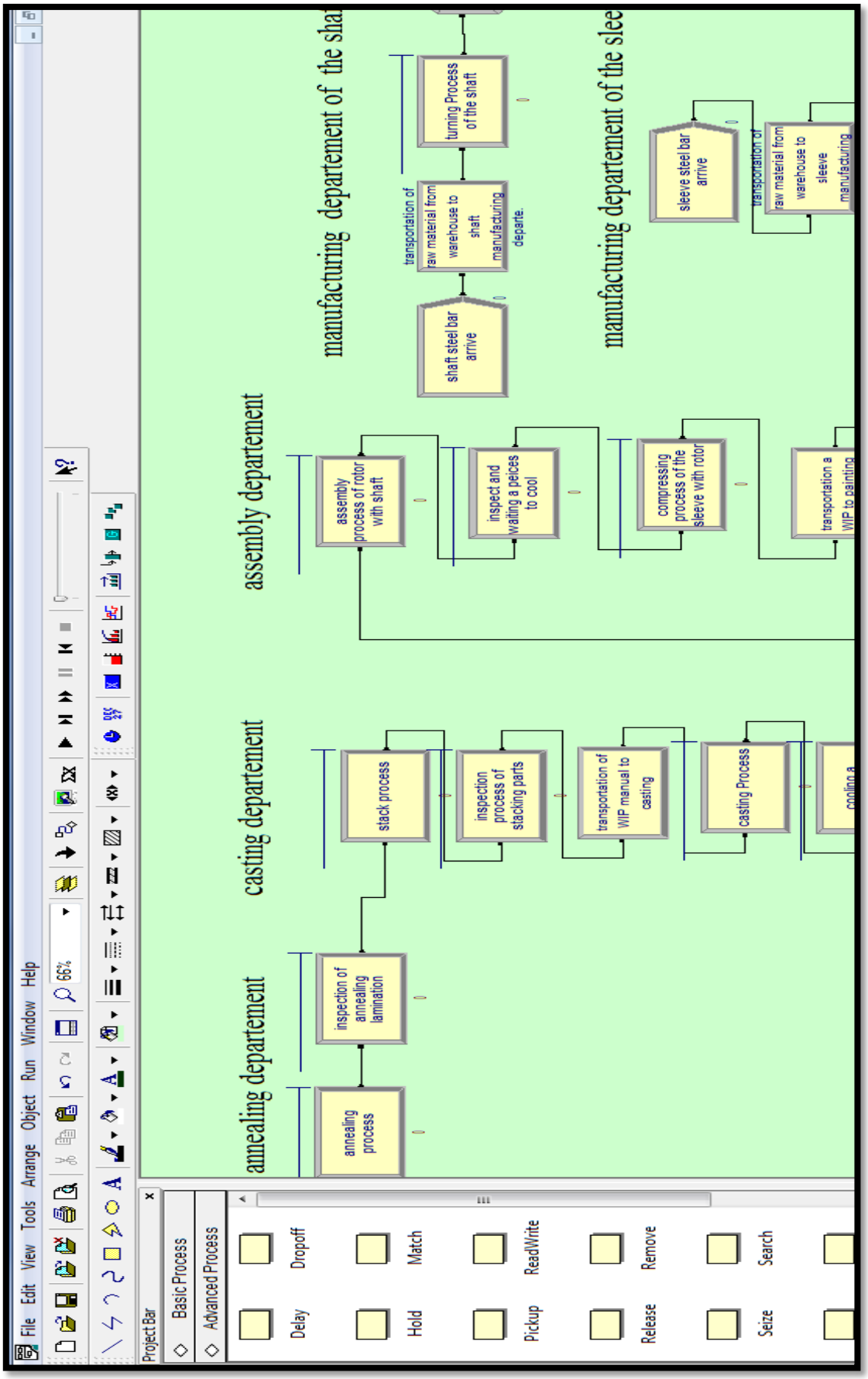

Figure 9. Simulation model of current and future state VSM

Table 2. Summary of simulation results for current and future state.

Measurement	Current state	Future state	Improvement ratio %
Production lead time (LT) (min)	2847	1920	33 %
Waiting time (T_w) min	1474	900	34%
Work in process (WIP) (unit)	12	10	16%
Throughput (TH)	72 unit per hr	88 unit per hr	22 %
Value added time (min)	848	927	10%
Non-value added time (min)	448 min	90 min	80 %
Value added ratio (VAR)	29%	48%	66%
Production capacity (Pc)	400 units per week	500 units per week	0.25 %

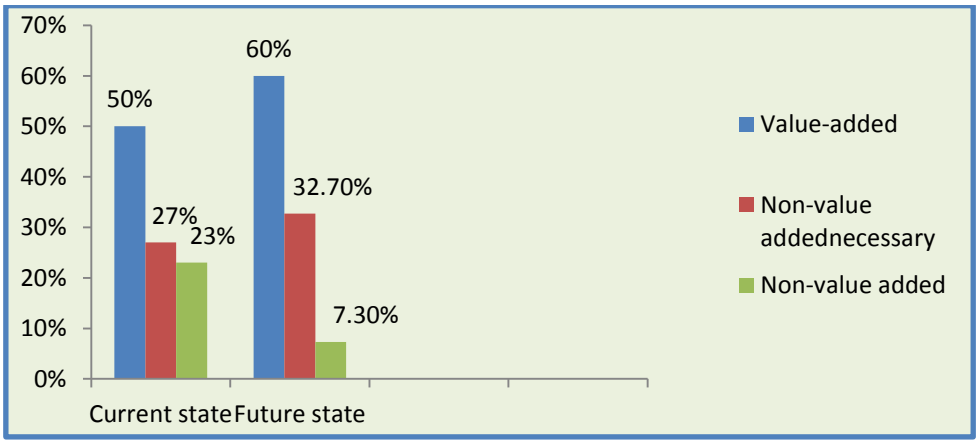

Figure. 10 The percentages of production activities type in current and future state .

Choosing Appropriate Distribution by Minitab's 17 Software to Analysis System Reliability

Asst. Prof. Dr. Ahmed Abdulrasool Ahmed
Department of Mechanical Engineering
College of Engineering
Baghdad University
Email: aa.alkhafaji@yahoo.com

B.Sc. Layla khudheir Jadwa
Department of Mechanical Engineering
College of Engineering
Baghdad University
Email: laylaalhamd@yahoo.com

ABSTRACT

This research aims to choose the appropriate probability distribution to the reliability analysis for an item through collected data for operating and stoppage time of the case study.

Appropriate choice for .probability distribution is when the data look to be on or close the form fitting line for probability plot and test the data for goodness of fit .

Minitab's 17 software was used for this purpose after arranging collected data and setting it in the theprogram.

The program results gave the best or well-fitting distribution among four of default probability distributions, that will use in order to estimate the distribution parameters values, for reliability determination and analysis. From probability plot can estimate time that designates the percent of the item's failure.

Key words: Reliability, Life data analysis, Probability distribution, Exponential distributions, Simple Weibull

اختيار التوزيع المناسب باستخدام برنامج (Minitab's 17 software) لتحليل معولية منظومة

ا.م.د. احمد عبد الرسول الخفاجي
فسم الهندسة الميكانيكية
كلية الهندسة / جامعة بغداد

ر. م: ليلى خضير جدوع
فسم الهندسة الميكانيكية
كلية الهندسة / جامعة بغداد

الخلاصة

هذا البحث يهدف الئ اختيار التوزيع الاحتمالي المناسب لتحليل المعولية لمعدة من خلال بيانات مجمعة لاوقات اشتغال وتوقف معدة قيد الدراسة ,الاختيار الافضل للتوزيع الاحتمالي يكون للبيانات التي على او قريبة من الخط المستقيم الرابط للبيانات في مخطط الاحتمالية و اختبار البيانات لجودة التوفيق.

وظف برنامج (Minitab`s 17) لهذا الغرض بعد ترتيب البيانات المجمعة وادخالها الى البرنامج.

نتائج البرنامج اعطت التوزيع الاحتمالي الصحيح من بين اربعة من التوزيعات الاحتمالية المفترضة والذي يستخدم في تخمين قيم متغيرات التوزيع لايجاد وتحليل المعولية, ومن مخطط الاحتمالية يمكن تخمين الوقت الذي يمثل النسبة المئوية لفشل المعدة .

الكلمات الرئيسيه: معولية, تحليل بيانات العمر, التوزيع الاحتمالي, التوزيع الاسي, توزيع ويبل البسيط.

1. INTRODUCTION

The increasing in complexity of equipment and systems lead to failures and as a result for the aspects of reliability, maintainability and availability have appeared into forefront. The failure of machineries and equipment causes interruption in production as a resulting from a loss of availability **Bose, et al., 2013**. Design for reliability is an important research area **Soleimania and Mohammad, 2014.** In life data analysis, statistical distribution represents the failure behavior of the equipment population through time, and subsequently it is possible to calculate the reliability indices of the equipment **Iqbal Ridwan, et al., 2010**. The term life data refers to the measurements of the lifetime of the equipment, whether in hours, years or cycles **Rausand , and Hoylanc, 2004** The repair of a system will initially sound like replacing a failed part with another one **Manortey, 2006.** the most common metric used to represent the reliability of repairable systems is Mean Time Between Failures" MTBF or "Average Run Life", that is used to characterize "life span" **MichelleI , 2011**, which is calculated by adding all the operating hours of all the systems and dividing by the number of failures. The popularity of the MTBF metric is due to its simplicity and its skill to supply to the one number syndrome, but MTBF hides information by not accounting for any trends in the appearance of failures and treating machines of all ages as coming from the same population

The probability plot represents the sum of the frequencies from the lowest value up to the considered point. The cumulative curve is the integral of the density function **Venkataramana.,et al., 2013**

2. THEORY OF RESEARCH

The theoretical population models used to describe unit lifetimes are known as Lifetime Distribution Models **Venkataramana.,et al., 2013**. The model selection tests were applied based on statistical analysis **Bose,2013.**

Minitab's 17 software used for the Distribution Identification and as a good tool can help to find the distribution that best fits the data.

A lifetime distribution model can be any probability density function (PDF) *f(t)* defined over the range of time from $t = 0$ to $t =$ infinity. The corresponding cumulative distribution function (CDF) $F(t)$ is a very useful function, as it gives the probability that a randomly selected

1. $F(t)$ = the area under the PDF $f(t)$ to the left of t.

2. $F(t)$ = the probability that a single randomly chosen new unit will fail by time t.

3. $F(t)$ = the proportion of the entire population that fails by time t. **Iqbal Ridwan,et al., 2010,Venkataramana.,et al., 2013**

PDF $f(t)$ has only non-negative values and eventually either becomes 0 as t increases, or decreases towards 0, The CDF $F(t)$ is increasing and goes from 0 to 1 **Ronniger, C. 2012** as t approaches infinity, in other words, total area under the curve is always 1.**Iqbal Ridwan,2010**

Probability plots are simple visual ways of summarizing reliability data by plotting CDF estimates vs. time on specially constructed probability paper **Venkataramana, P. 2013**.

2.1 Anderson Darling

The Anderson-Darling (AD) statistic measures how well the data follow a particular distribution.

For a specified data set and distribution, the better the distribution fits the data, the smaller this statistic will be, Goodness of Fit (GOF) test to determining how well a given curve can be modeled by a distribution.

In statistics, there is GOF measure including AD (used in this paper) which may give powerful test of fit **MichelleI P, 2011**, GOF test was evaluated and also whether the data was come from the same probability distributions was checked. The analysis based on AD criteria, Minitab calculates the AD statistic using either (maximum likelihood estimation method or least squares estimation) **Engmann, S .2011**

2.2 The Exponential Distribution

The exponential distribution is a continuous distribution that is used to represent the constant failure rates. It is characterized by the parameter λ which represents the failure rate of the item The failure rate λ of the exponential distribution is constant with respect to time **Rausand , M.2004,MichelleI P., 2011.**

θ = The distribution mean

λ = 1/θ = The failure rate (1)

λ= 1 / MTBF

The exponential reliability function is

$$R(x) = e^{-\frac{t}{\theta}} = e^{-\lambda t} \quad , t \geq 0 \qquad (2)$$

The cumulative distribution function

$$F(t) = 1 - e^{-\lambda t} \qquad (3)$$

The exponential probability density function is

$$\boldsymbol{f(x) = \frac{1}{\text{MTBF}} e^{\frac{-t}{\theta}} = \lambda e^{-\lambda t}} \qquad \mathbf{t \geq 0} \qquad (4)$$

Where: $\text{MTBF} = \frac{1}{\lambda} = \theta$

The exponential hazard function is constant

$$h(x) = \frac{f(t)}{R(t)} = \frac{1}{\theta} = \lambda \qquad (5)$$

2.3 The Weibull Distribution

Weibull distribution is one of the most widely used life distributions in reliability analysis, very flexible and can through parameters, models many types of failure rate behaviors so it's known with two parameters **,mIqbal Ridwan,et al., 2010, Ronniger , 2012.**

- Scale parameter $\eta > 0$
- Shape parameter $\beta > 0$

Survival Function

$$R(t)= pr\ (t > 0\ ) = e^{-\left(\frac{t}{\eta}\right)^{\beta}} \quad (6)$$

Cumulative Distribution Function

$$F(x) = 1 - \ e^{-\left(\frac{t}{\eta}\right)^{\beta}} \qquad t \geq 0:\ \beta > 0 \quad (7)$$

Probability density function

$$f(t) = \frac{\beta(t)^{\beta-1}}{\eta^{\beta}}\ e^{-\left(\frac{t}{\eta}\right)^{\beta}} \quad (8)$$

Hazard Function

$$h\ (t)= \frac{\beta(t)^{\beta-1}}{\eta^{\beta}} \qquad t \geq 0:\ \beta > 0 \quad (9)$$

$\beta = 1$ Failure rate is constant

$\beta > 1$ Failure rate function is increasing

$\beta < 1$ h (t) is decreasing **(Bose, et al., 2013)**.

$\beta = 2$ The resulting distribution is known as (Rayleigh Distribution) (**Venkataramana, P., 2013).**

3. APPLICATION

Fig. (1) indicated the methodology for research to reach its aim. The following steps for analysis data indicated the used path to find the suitable probability distribution to fit life data and estimate the parameters of distributions.

1. The reliability was studied through a compressor of Gasoline Reformer unit in Daura Refinery in Baghdad, this has helped to optimize the schedule for preventive maintenance.
2. The exact failure time data was collected for a part under study measured the time by hours that included operating and stoppage time for six years from (2005 to 2010).
3. Table (1) life data was sorting and arranged to be suitable to use in Minitab's 17 software application, included [From , To, TTR] in [hr.] as columns.
4. Data, table (1) was input to Minitab's 17 software for Reliability and Distribution analysis, this would discover which distribution that the recorded time to failure utilizing "Distribution ID Plot" function **Fig. (2)** shows the worksheet of Minitab's 17 software included the menus for software.
5. Output of Minitab's 17 software were, four probability distributions **Fig. (3)** as identical distributions (ID), (notice the software is able to analysis eleven probability distributions) and Session window with table of statistics **Fig. (4),** was summarized in **table (2).**
6. According to resultes the Weibull and Exponential distributions were good, and it is really the Exponential distribution is a special case of the Weibull distribution with shape parameter $\beta = 1$ but for constant failure rate .

From **Fig . (3)**:

- Distribution: four Distributions to select which plot has a majority of the data points closest to the line (representing the specific distribution trend).
- Anderson-Darling statistic measures for Goodness-of-Fit was shown how well the data follow a particular distribution, the better the distribution fits the data, the smaller this statistic will be, use the Anderson-Darling statistic to compare the fit of several distributions to see which one is best or to test whether a sample of data comes from a population with a specified distribution.
- Mean, MTTFs allow seeing how conclusions may change with different distributions, from session window **Fig. (3).**

4. RESULTS

For Weibull distribution the Minitab analysis provides displays of the future prediction of failures data behavior, to obtain equations those represent the Survival (reliability) function Cumulative failure probability function, Probability density function, and Hazard function, equations using the shape value of 1.45234 and scale value of 5681.08 hr. those were estimated by the maximum likelihood in **Fig.(5**) as substitutions for β and η respectively, the formulas were determined equations 6,7,8,9, and Minitab's 17 software was used to calculate Probability density, Cumulative distribution , and Hazard functions, .

Percentiles split the data set into parts, nth percentile has n% of the observations lower than it, and (100-n) % of observations higher than it. Percentiles divide a data set into 100 parts (data set arrange into an ascending order in Session window included the output Percentiles values of 1 5 10 50.

Confidence Interval for MTBF for 95%, which means acceptable risk of error $\alpha = 0.05$ lower and upper with standard error for means.

The exponential distribution functions **Fig.(6**) were determined by using equations 2, 3,4,5, with the estimated mean of distribution that equal 5110.37 hr. and the formulas values calculated by using Minitab's 17 software

5. DISCUSSION

- Life data analysis is able to provide the information on the reliability indices such as reliability, unreliability, mean time between failure and failure rate**.**
- The estimate MTBF of distribution was 5110.37 hr. equal to calculate mean for Exponential distribution but not equal for Weibull
- All calculations are computed for Weibull and Exponential distribution. Comparing the various results show that the Weibull distribution for upper phase .and Exponential distribution is suitable for lower phase of data life.
- **Fig.(6)** Probability density function (PDF): It is exponentially decreasing curve shows that the likelihood for item to have increasing time to failure values for the beginning time to failure in comparison to the probability of having less time to failure values for the last times to failure .
- **Fig. (6)** Survival (Reliability) Plot: This curve as the (PDF) showing that the proportion of surviving time for item decreases exponentially with time.
- **Fig. (6)** Hazard plot: As is the case here, for an Exponential distribution, the Hazard function displaying the instantaneous time failure rate is constant.

- **Fig. (5)**, for (PDF) and Survival plots for the Weibull distribution may be identical to the Exponential distribution except of the Hazard plot.
- **Fig. (5)** Hazard plot: For a Weibull distribution the Hazard function can take many shapes, and in this case, the trend is .the hazard rate is increasing over time, which means that the item was more likely to fail as it age.
- η is the value in time by which 63.2% of all failures will have occurred. In this sense, η is one point on the time scale, providing some standard measure of the distribution of times to failure.

REFERENCE

- Bose, D. Ghosh, G. Mandal,K. Sau S.P. and Kunar, S, 2013 *Measurement and Evaluation of Reliability, Availability and Maintainability of a Diesel Locomotive Engine* International Journal of Engineering Research and Technology, ISSN 0974-3154 Vol. 6, No. 4, pp. 515-534.
- Engmann, S and Cousineau, D. 2011, *Comparing Distribution: The Two-Sample. Anderson Darling Test as an Alternative to The Kolmogorov- Smirnoff Test* Journal of Applied Quantitative Methods Vol. 6 No. 3.
- Iqbal Ridwan, M, Kerk, L Y, Musa, A, Yunus, B ,(2010)., *Application of Life Data Analysis for the Reliability Assessment of Numerical Over current Relays* , International
    - Journal of Electrical, Robotics, Electronics and Communications Engineering Vol. 4 No:12, pp.45 -51.
- Manortey, S. O. 2006, *Life Data Analysis of Repairable Systems. A Case study on Brigham Young University Media Rooms*, (Master of Science Brigham Young University).
- MichelleI P, 2011, "*Electrical Submersible Pump Survival Analysis* Master's Degree Candidate.
- Rausand , M. and Hoylanc, A., (2004) *System Reliability Theory*, Models and Statistical Methods Second Edition, Wiley Series in Probability and Statistics, A John Wiley & Sons, INC., Publication,
- Soleimania, M and -Mohammad, M, P, 2014, *Design for Reliability of Complex System with Limited Failure Data; Case Study of a Horizontal Drilling Equipment* Probabilistic Safety Assessment and Management PSAM 12
- Venkataramana, P., Gurumahesh G..,and Ajay V. 2013, *Reliability Evaluation of Repairable Complex Systems an Analyzing Failure Data* , Int. J. Mech. Eng Vol. 2, No. 1.
- Ronniger, C. 2012 *Reliability Analyses with Weibull* www.crgraph.com.

Notation and Acronyms

AD Anderson-Darling
CDF Cumulative distribution function
From Start time, hr.
GOF Goodness-of-fit
ID Identical distribution
MTBF Mean time between failures, hr
PDF Probability density function
TTR Time to repair, hr.
α Acceptable risk of error= 1- Confidence Level
$\mathcal{B}$ Shape parameter
R Reliability
θ The distribution mean
η Scale parameter, hr.
λ The failure rate 1/hr.

Table 1. Operation time for compressor

From [hr.]	To [hr.]	TBF[[hr.]	TTR [hr.]
0.0000	1175	1175	0.5
1175.5	4887.5	3712	0.5
4888	9931	5043	2
9933	22953.5	13020.5	26.5
22980	25544.25	2564.25	24
25568.25	30715.75	5147.5	1.5

Table 2. Summarized outputs from Minitab 's 17 software.

Distribution	AD	Mean	Fitness	Notes
Smallest Extreme Value	2.567	4647.35	Bad	Estimated Mean≠ Calculated Mean
Normal	2.479	5110.38	Bad	Estimated Mean = Calculated Mean
Weibull	2.220	5149.56	Best fitness Smallest AD	Estimated Mean≠ Calculated Mean
Exponential	2.384	5110.37	Good	Estimated Mean = Calculated Mean

Table 3. Functions estimation values for Weibull distribution.

Time [hr]	R(t) w	F(t).	PDF.	h(t)
0	1.000	0.000	0.0000E+00	0.0000E+00
500	0.971	0.029	8.2571E-05	8.5022E-05
1000	0.923	0.077	1.0744E-04	1.1640E-04
2000	0.803	0.197	1.2798E-04	1.5937E-04
2500	0.738	0.262	1.3019E-04	1.7633E-04
3000	0.673	0.327	1.2898E-04	1.9152E-04
3500	0.610	0.390	1.2524E-04	2.0538E-04
4000	0.548	0.452	1.1968E-04	2.1820E-04
4500	0.490	0.510	1.1285E-04	2.3016E-04
5000	0.436	0.564	1.0520E-04	2.4142E-04
7000	0.258	0.742	7.2573E-05	2.8119E-04
8000	0.193	0.807	5.7688E-05	2.9873E-04
10000	0.103	0.897	3.3997E-05	3.3053E-04
13000	0.036	0.964	1.3323E-05	3.7226E-04

Table 4. Functions estimation values for exponential distribution

Time[hr.]	R (t) Exp.	F(t)	PDF	h(t).
0	1.0000	0.0000	1.9568E-04	1.9568E-04
500	0.9068	0.0932	1.7744E-04	1.9570E-04
1000	0.8223	0.1777	1.6090E-04	1.9570E-04
2000	0.6761	0.3239	1.3231E-04	1.9570E-04
2500	0.6131	0.3869	1.1997E-04	1.9570E-04
3000	0.5560	0.4440	1.0879E-04	1.9570E-04
3500	0.5041	0.4959	9.8652E-05	1.9570E-04
4000	0.4572	\0.5428	8.9457E-05	1.9570E-04
4500	0.4145	0.5855	8.1119E-05	1.9570E-04
5000	0.3759	0.6241	7.3558E-05	1.9570E-04
7000	0.2542	0.7458	4.9736E-05	1.9570E-04
8000	0.2090	0.7910	4.0896E-05	1.9570E-04
10000	0.1413	0.8587	2.7651E-05	1.9570E-04
13000	0.0786	0.9214	1.5373E-05	1.9570E-04

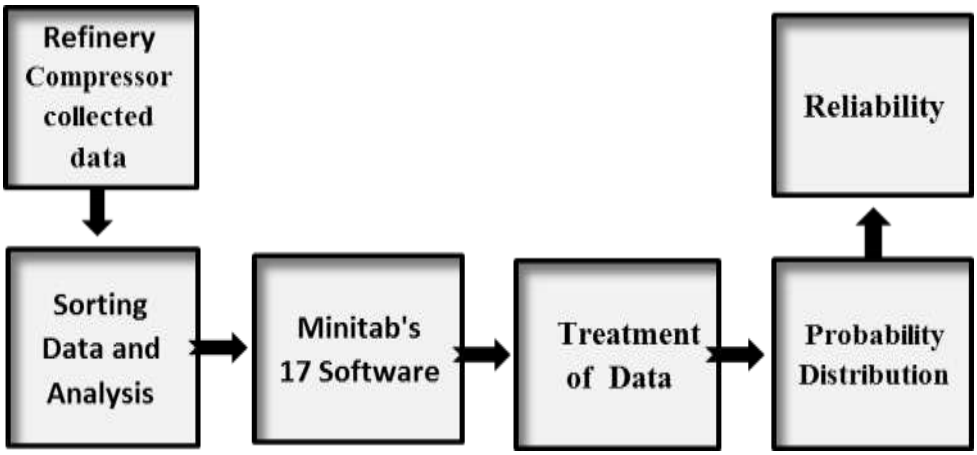

Figure 1. Steps for analysis.

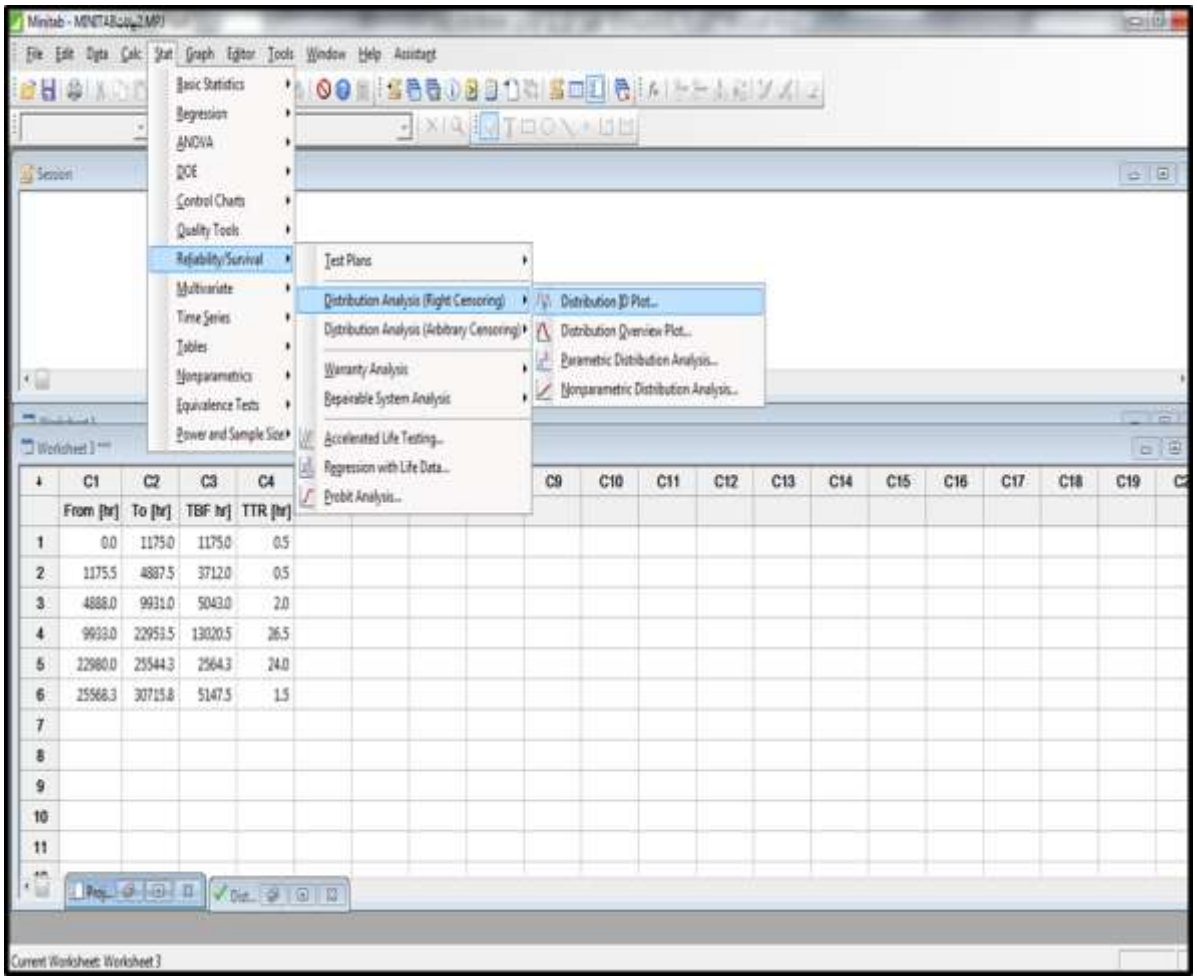

Figure 2. Worksheet for reliability analysis for system.

Results for: Worksheet 3

Distribution ID Plot: TBF hr]

Goodness-of-Fit

Distribution	Anderson-Darling (adj)
Smallest Extreme Value	2.567
Normal	2.479
Weibull	2.220
Exponential	2.384

Table of Percentiles

Distribution	Percent	Percentile	Standard Error	95% Normal CI Lower	Upper
Smallest Extreme Value	1	-13231.1	6805.64	-26569.9	107.753
Normal	1	-3722.67	2984.08	-9571.35	2126.01
Weibull	1	239.716	264.196	27.6421	2078.85
Exponential	1	51.3610	20.9680	23.0745	114.323
Smallest Extreme Value	5	-5987.35	4827.95	-15450.0	3475.26
Normal	5	-1135.07	2377.66	-5795.20	3525.07
Weibull	5	735.870	570.892	160.855	3366.41
Exponential	5	262.128	107.013	117.764	583.465
Smallest Extreme Value	10	-2788.34	3989.58	-10607.8	5031.09
Normal	10	244.377	2091.88	-3855.64	4344.39
Weibull	10	1207.59	769.412	346.400	4209.78
Exponential	10	538.432	219.814	241.896	1198.48
Smallest Extreme Value	50	5583.73	2144.37	1380.85	9786.62
Normal	50	5110.38	1550.10	2072.23	8148.52
Weibull	50	4414.69	1463.37	2305.40	8453.84
Exponential	50	3542.24	1446.11	1591.39	7884.60

Table of MTTF

Distribution	Mean	Standard Error	95% Normal CI Lower	Upper
Smallest Extreme Value	4647.35	2299.40	140.60	9154.1
Normal	5110.38	1550.10	2072.23	8148.5
Weibull	5149.56	1476.19	2936.03	9031.9
Exponential	5110.37	2086.30	2295.89	11375.1

Distribution ID Plot for TBF [hr.]

Figure 3. Session window included the output of program.

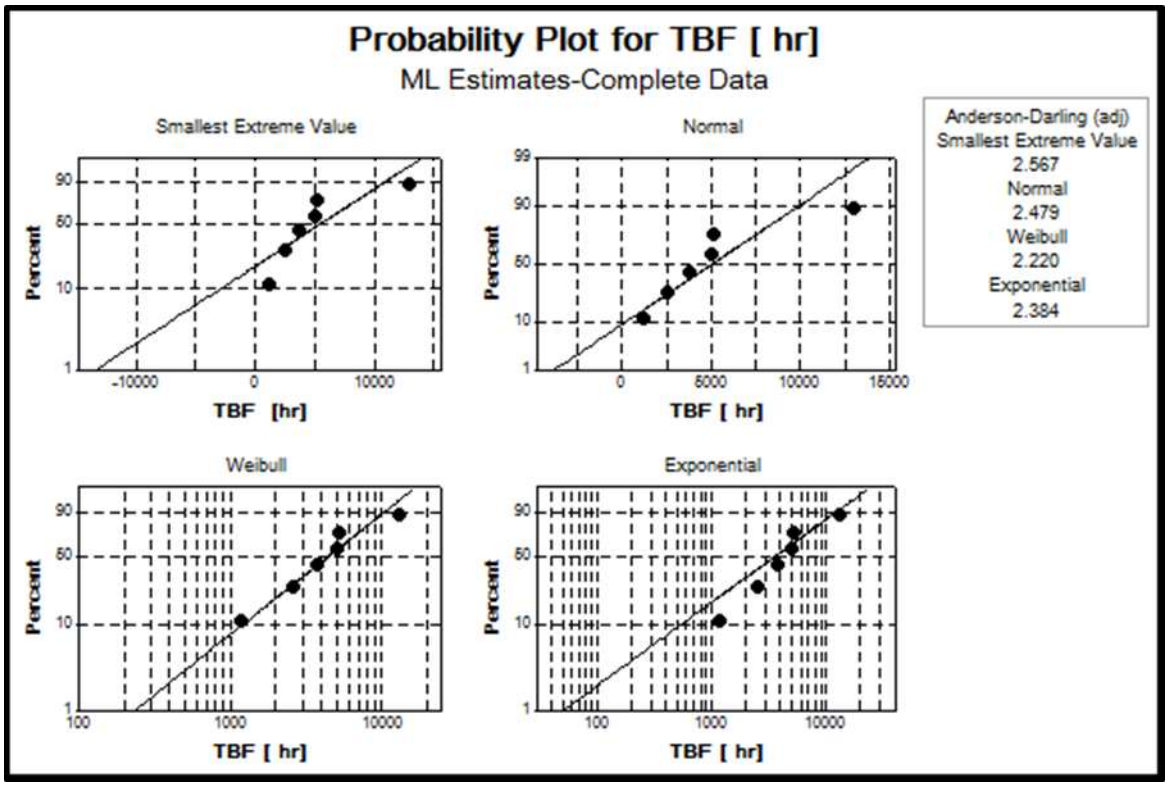

Figure 4. Probability Plot of the Failures and the values of Anderson Darling.

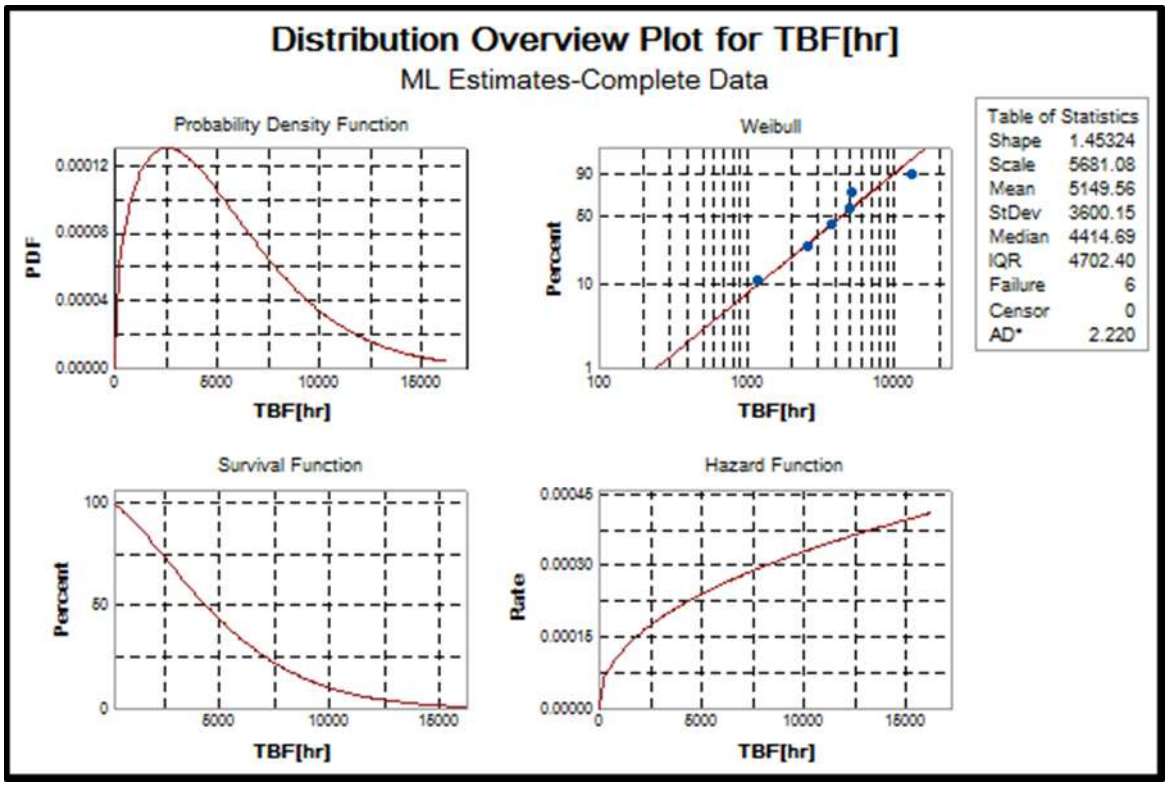

Figure 5. Weibull Distribution overview plot of the failures via Minitab of compressor.

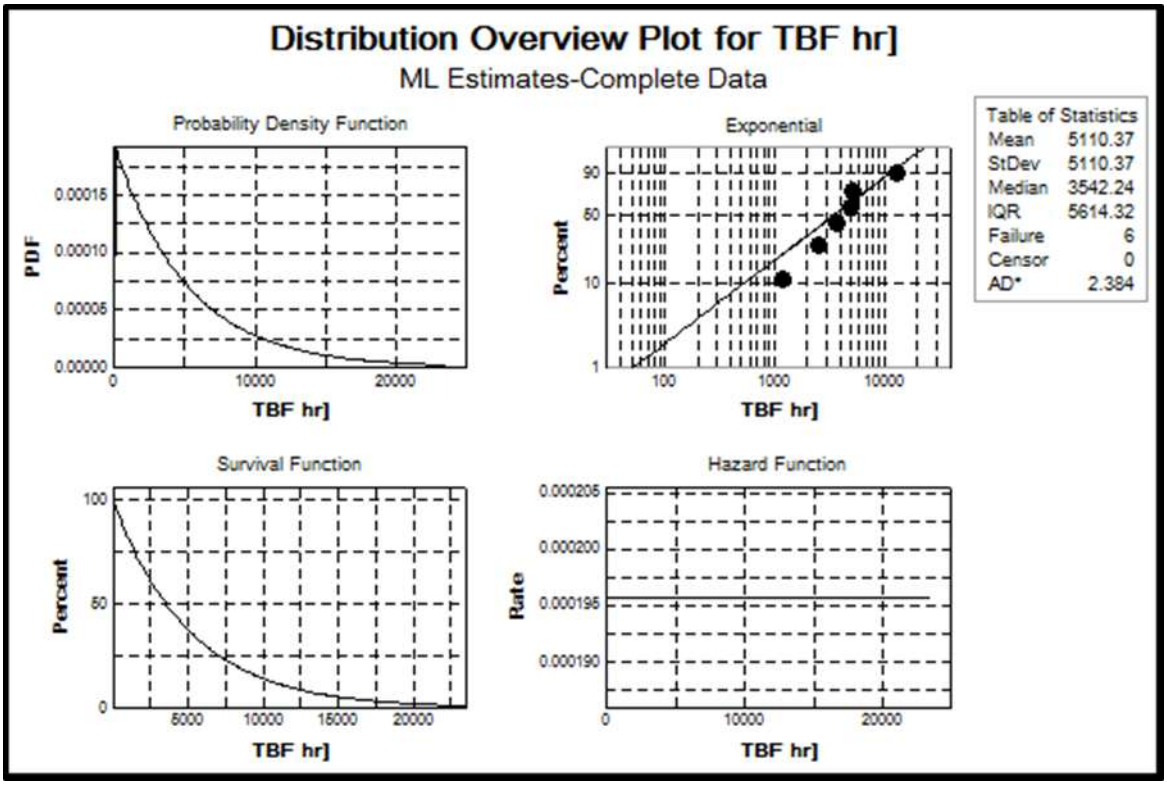

Figure 6. Exponential Distribution overview plot of the failures via Minitab of compressor.

Analytical Approach for Load Capacity of Large Diameter Bored Piles Using Field Data

Mr. Alaa Dawood Salman
University of Baghdad

Dr. Ali Hamoudi
University of Baghdad

ABSTRACT

An analytical approach based on field data was used to determine the strength capacity of large diameter bored type piles. Also the deformations and settlements were evaluated for both vertical and lateral loadings. The analytical predictions are compared to field data obtained from a proto-type test pile used at Tharthar –Tigris canal Bridge. They were found to be with acceptable agreement of 12% deviation.

Following ASTM standards D1143M-07e1,2010, a test schedule of five loading cycles were proposed for vertical loads and series of cyclic loads to simulate horizontal loading .The load test results and analytical data of 1.95m in diameter test pile proved efficiently to carry a working load of 450 tons. The calculated lateral displacements based on a specified coefficient of subgrade reaction are compared to the measured values from dial gauges and strain gauges placed at various locations along the length of the pile.

Keyword :bored piles, lateral displacement ,horizontal loads, vertical loads.

الاسلوب التحليلي لقوة التحمل لركائز الحفر ذات الأقطار الكبيرة باستعمال البيانات الحقلية

الخلاصة

تم تقديم تصور تحليلي مستنداً إلى نتائج فحوصات حقلية لتقييم قوة التحمل لركائز الحفر ذات الأقطار الكبيرة وكذلك تم تقييم الانحرافات والهبوطات بتأثير الأحمال العمودية والجانبية وتم مقارنة النتائج التحليلية مع نتائج الفحوصات الحقلية التي تم الحصول عليها من فحص الركيزة كاملة القياس والتي تم استخدامها في جسر كيلو 50الواقع على قناة الثرثار- دجلة . لقد وجد أن توافقاً مقبولاً في النتائج بانحراف في حدود12%.

إن برنامج الفحص وفقاً للمواصفة العالمية بخمس مراحل (ASTM standards D1143M-07e1, 2010) تمت للأحمال العمودية وسلسلة من دورات التحميل لمحاكات الأحمال الجانبية. ان النتائج التحليلية ونتائج فحص التحميل لركيزة قطرها 1,95 اثبتت كفاءتها لتحمل قوة خدمية مقدارها 450 طن وقد تم مقارنة نتائج الانحرافات الجانبية مع القياسات المأخوذة من مؤشرات الانفعال والانحراف المثبتة في نقاط مختلفة على طول الركيزة .

الكلمات الرئيسية : ركائز الحفر ,الإزاحات العرضية ,الاحمال الافقية ,الاحمال العمودية .

1. INTRODUCTION

Large diameter bored piles are non - displacement piles which are commonly used to transfer large vertical loads with or without horizontal loads and flexural bending moments to the surrounding subgrade. The preference of this type of deep foundation is economy per unit of load as compared to other types. Another advantages are early completion of the foundation construction even before land grading is experienced and elimination of pile caps ,also problems of cobbles and small boulders encountered in sub-strata have small effect in addition to smaller amounts of reinforcement .However the use of bored type piles is extremely affected by delay due to bad wet weather, building code restrictions and poor quality control or in adequate construction equipment . **Lee,1987**.

In-situ concrete piles with diameters of 0.3 m up to 3.0 m are referred to as large diameter bored piles. For their construction hollow spaces are made in the soil by means of drilling equipment. Depending on soil conditions the excavation is carried out under the protection of a casing or without casing. Subsequently the drilling holes are filled with concrete; according to static requirements a rebar cage is placed before concreting. **Poulos,1980**.

Large-diameter bored piles have a broad scope of application as foundation elements for carrying vertical building loads, foundation elements for retaining walls, temporary building pit walls components of the final structure, protection against uplift and for taking up tension loads slope security and energy piles. **Tomlinson, 1994**

2.Testing Program

2.1 Soil Investigation

Even though this type of pile requires careful and through exploration as compared to other types, limited soil investigation was done for this work .Few borings were drilled to check continuity of sub - strata and undisturbed soil samples. Two bore holes were drilled. The geological subgrade soil profile was (5-6) m of hard crested loamy clay resting on sandy layers with different gravel contents to a depth of 45m below G.L. A thick layer of sand stone was encountered at a greater depth **. Fig . 1** and **Fig.2** show standerad penetration test (SPT) results for B.H. No.1 near the test pile Cone Penetration Test(CPT) for Tharthar Tigris Canal Bridge Project KM 50, **Table 1.** Results of Atterberg Limits, Specific Gravity & Grain size. **Bowles, 1981.**

2.2 Test Pile Construction

The test pile was one of the series of piles used to support the abutments of a bridge at KM 50 Tharthar Tigris canal. All piles were drilled using Terra drill (80CA) mounted on a crawler crane (38RB).A bucket 1.5m in diameter was used with hinged reamer for 2m segmental drilling .At various levels during drilling of the pile shaft, soil samples were taken for testing in the laboratory .The hole walls were stabilized using bentonite slurry to keep them from collapsing and closing the hole particularly in the cohesionless layers .In order to avoid

soil caving and keeping risk to minimum a standard pipe 14mm thick was used as a casing in each pile hole .It was driven to a depth of 15m below G.L. The reinforcement cage was then lowered into the hole . The cage extended to the entire length of the pile .A ready mix concrete was transported by a rotary drum trucks and was placed into the holes using a tremi tube. Three control cube specimens of (200×200×200) mm were taken for compressive strength tests in the laboratory,**Das,2004.** and **Head,1984.**

3.CHARACTERISTICS OF TEST PILES

The test pile was 1.95 m in diameter and total length of 25.5 m. The reinforcement cage consisted of (45—Ø32 mm) diameter bars extended to length of 14.5m below G.L. The longitudinal reinforcement was reduced to (30—Ø32 mm) diameter to the remainder length of the pile. The lateral reinforcement were 12mm diameter ties spaced at 200 mm on center spacing .The tension piles were designed to receive the loading reactions .They were 1. 5 m in diameter and 25.5 m total length. They were reinforced longitudinally with (24—Ø32 mm) diameter and laterally with 12mm diameter ties at 200 mm on center spacing. Details of the piles reinforcement are shown in **Table 2** . The concrete used in both the test pile and the tension piles had a compressive strength of 28 MPa cube strength at 28 days with the maximum slump of 100 mm.

3.1 Expressions of the Strength Capacity and Settlement of Bored Piles:

R.D.Mindlin of Colombia presented a solution based on elasticity for a single force acting on a semi- infinit media . Mindlin took into account the transition effect of a body force in media of constant tensile strength and Young ′s modulus **,Mindlin,2007**. The equilibrium equations in Cartesian form are:

$$\frac{\partial \sigma x}{\partial x} + \frac{\partial \tau yx}{\partial y} = w_x \quad (1)$$

$$\frac{\partial \sigma y}{\partial y} + \frac{\partial \tau xy}{\partial x} = w_y \quad (2)$$

Where w_x and w_y are the body force per unit volume in x and y directions. The equation of compatibility including effect of time and volumetric strain is:

$$\frac{\partial u}{\partial t} = (k_x \frac{\partial^2 u}{\partial x^2} + k_y \frac{\partial^2 u}{\partial y^2}) * \frac{1}{\gamma} + \frac{\partial V}{\partial t} \quad (3)$$

Considering the pile as a linear elastic and the soil to follow modified cam clay model ,**Pestana ,et.al., 2002** suggested that utilizing Eq,(1) and Eq.(2) toghter with Eq. (3) that mean effective stress (σ') and deviatoric effective stress (q') are :

$$\sigma' = \frac{1}{2}(\sigma_x + \sigma_y) \quad (4)$$

$$q' = \frac{1}{\sqrt{2}}\{(\sigma_x - \sigma_y)^2 + \tau^2_{xy}\}^{0.5} \quad (5)$$

The pile load transfer is governed by the stresses induced initially in the soil, according to Mindlin′ s theory and the surface behaviour of the pile shaft with the surrounding soil .Therefore the pile strength capacity Q_u can be stated as the superposition of resistance at base of pile Q_B and resistance along pile shaft Q_F , **Mindlin,2007** where :

$$Q_F = \pi D_p L(\propto \tau'') \quad (6)$$

$$Q_B = \frac{\pi}{4} D_p^2 (0.75 q_u) \quad (7)$$

$$Q_u = Q_B + Q_F \quad (8)$$

The value of Q_B is related to the bearing area and pressure at base while Q_F is related to the traction and surface area of pile shaft. The parameters soil cohesion (τ') , effective stress (q'), shaft adhesion factor ($\propto$) and unit weight of soil (γ) are determined from lab tests .These parameters controlled the bearing capacity evaluation **,Bowles,1981.**and **Das,2004.**

3.2 Lateral Load Resistance :

The effects of lateral loading and or applied bending moments either on the supporting soil or flexural resistance in terms of over stressing the pile shaft .The problem of displacement compatibility is complex to simulate a rigorous analysis of ultimate soil resistance, particularly beyond elastic behaviour of soil.

Broms, 1995. suggested based on tests, that the ultimate lateral resistance (q_u) of cohesive soil could be related to ultimate shear resistance (τ_u) from triaxial compression test based on undrained conditions ($q_u = 9\,\tau_u$). The governing beam differential equation is :

$$EI\,(d^4u/dx^4) + K_x = 0 \quad (9)$$

And for a constant soil modulus (K_s) ,it can be shown that expressions for pile moment resistance (M) and lateral displacement of pile head (u), are: **Bowles,1981.**and **Das,2004.**

$$M = H_L R A_m + M_L B_m \quad (10)$$

$$u = H_L \frac{R^3}{EI} A_u + M_L \frac{R^2}{EI} B_u \quad (11)$$

E_cI_c : flexural stiffness of pile, A_m and B_m are moment coefficients ,taken 0.7 and 0.8 respectively at point of maximum moment , A_u and B_u are lateral displacement coefficients

,taken as 2.5 and 1.5 respectively at pile head ,R = $\sqrt[4]{\frac{EI}{K}}$ is the stiffness factor and K_s is soil modules (K= $\frac{1}{2}$ k_u L) ,where $k_u = 67\tau_u$ **Bowles, 1981.**

E_c : Young $'s$ modules for concrete.
I_c : Moment of inertia of pile section .

4. SETTLEMENT ANALYSIS

Short term elastic settlement was considered in this investigation rather than long term which could be small because of slow development of base resistance. Hence effects of creep of concrete and stress transfer from skin friction to the base was ignored. The ultimate skin friction (f_u)is :

$f_u = \propto \tau'$ (12)

where $\propto$ is the shaft adhesion coefficient ,varies from (0.3 - 0.45) and $\tau' = 0.75\ F_u$

The settlement Δ_b at pile base was assumed to be related to the pressure at pile base, size of base and soil properties.

$$\Delta_b = \frac{(1-\upsilon 2)\ q\ D_b}{E} \quad (13)$$

Where q was the average pressure at pile base which could be taken as the nominal vertical stress from triaxial test. The soil Young $'s$ modulus (E) is:

$$E = \frac{\frac{1}{2}(\sigma_1 - \sigma_3)}{\epsilon_1} \quad (14)$$

The elastic shortening and pile due to applied loads was calculated from:

$$\Delta_e = \frac{(P_b + \lambda\ P_s)}{A_p\ E_c} L \quad (15)$$

5. TESTING PROCEDURE

The top of pile was prepared by bedding a steel plate (38 mm thick) in cement mortar as a capping .The reaction loads were carried from the test pile through main beams and the sub- beams and tension bars to the four reaction piles .The vertical loads had been applied using four electrically operated hydraulic jacks which work together to a total capacity of 12000kN.The measurement of the testing loads were recorded by a pressure gauge attached to the oil pump. The pressure gauge was calibrated in advance.

Following the **ASTM D1143-o7e, 2010** , a schedule of five loading cycles has been set .The test was carried out with four cycles up to twice the working load of the test pile as shown in **table 3**.The fifth cycle included an addition of 4400kN to compensate the frictional resistance of pile shaft above scour level .This was due to the fact that testing load had been applied at ground level and before excavating around the pile .

Deflection dial gauges with accuracy of 0.02 mm and a stroke of 75 mm were used to measure deformations of the test pile and reaction piles during testing .Four dial gauges were attached at the top of the test pile and one dial gauge on each of the four tension piles. All the values used in the analysis were the average of the 4 readings.

The two reference beam used in the testing rig for vertical loadings were checked for any undesirable settlements. Two targets were fixed to them, observations had been done by using a level 20 m away from the target points. It was assumed that ground level at that point had not been by the testing altered by the testing operation. There was no movement recorded during the test and hence, no adjustments were required for the settlements of test pile measured by the dial gauges.

The lateral loads were applied by a 2000 kN capacity hydraulic jack which was operated electrically. The reaction loads had been taken by a transverse beam to the two non-working reaction pile. Measurements of the applied loads were taken by 3000kN proving ring which was calibrated before testing. Details of the horizontal loading rig are shown in **Fig. 3** and **Fig. 4**.

A number of cycle loading with increments of 50 kN had been conducted for the horizontal load testing . The first 2 cycles were up to 150 kN followed by 3 cycles 300 kN then 3 cycles to 450 kN and finally the last 3cycles to 650 kN which was kept for half an hour .Unloading to zero load was then done and readings were taken after 24 hours . Five dial gauges were attached to the test pile and one dial on each of the two reaction piles as shown in **Fig. 4**.All dials were fixed to the reference beam and pieces of glass were used to provide smooth surface for indicator tips. Details of the loading rig is shown in **Fig. 5**.

5.1 Examination of Results

The effective vertical stress of soil (F_u) was calculated to be 182 kN/m^2 based on an average shear reduction factor (α = 0.55) for sandy gravel base and an ultimate shear strength (τ_u) of soil supporting the pile equal 320 kN/m^2 which was an average value obtained from the in - situ cone penetration resistance and standard penetration tests. The Meyerhof ′ s bearing capacity factor N_q was 155 based on frictional angle ∅ =32°. The previous parameters led to the ultimate bearing capacity q_u of supporting soil stratum equal 14100 kN/m^2. With the allowable value of 4700 kN/m^2.Using Eq.(7) and Eq.(8) led to strength capacity for the test pile of 14010 kN/m^2 with a working load value of 4666 kN based on factor of safety = 3 .

The design strength of the test pile having (45- ∅32mm) longitudinal bars with yield strength = 350 MPa and concrete compressive stress $f_c^{'}$ = 28MPa, cube strength was calculated to be 12662 kN and casing strength was considered 890 kN. The effect of soil negative skin traction came to 935 kN from Eq. (7) .

Theoretical considerations that most settlements of a single pile occurred immediately after load application .Based on that Young′s modules for soil was interpreted from cone point resistance as 350 $\tau^{'}$ and was found = 63700 kN/m^2. The settlements at pile base $\Delta_b$was evaluated from Eq.(13) ,considering Poisson′s ratio for soil = 0.4, bearing coefficient R_c = 12 for dense

cohesionless soil. These parameters gave maximum base settlements = 41 mm. The deformation of the pile head due to elastic shorting Δe and due to shaft resistance were calculated from Eq.(15) based on shaft load influence factor $\lambda = 0.33$ and concrete modules of elasticity for deformation calculation E_c =1122800 kN/m^2 .The value came to 37 mm based on P_s = 935 kN and P_b = 4666 kN .

The value of (Δe) at twice the working load was 69 mm .Hence the total calculated settlement of pile head at working load was 78mm and at twice the working load was 110mm. The values of calculated and averaged measured value at pile head are shown in **Fig. 6** .The problem of displacement compatibility is complex to simulate a rigorous analysis Eq. (9) for lateral loading ,since soil behaviour is the problem .Hence maximum lateral displacement is at pile head and diminishes some where at two-third pile length below that point. The lateral displacement was calculated from Eq.(11),based on ($k = 25 \times 10^4$ kN/m^3) and soil modulus ($K_s = 1.063 \times 10^6$ kN/m^2),hence the lateral displacement coefficient related to lateral loads is 2.0 and vanishes at a distance 8.5m below pile head . The calculated and measured lateral displacement is shown in **Fig.7**.

6. CONCLUSION

1- The design strength capacity of large diameter bored type piles could be predicted using eqs.(6,7 and 8) to within 15% accuracy. The (1.95m) diameter test pile was sufficient to carry the 4666 kN working load based on a safety factor 3.0 .

2-The pile strength to horizontal loads showed adequacy to resist a design load of 350 kN based on a safety factor 2.0 .

3-The values of soil parameters based on laboratory control tests were acceptable ,since lateral displacement and settlement were 20 % less than measured values .It was related to the proper Young's moduli Ec and E for deformation calculations .Also it could be concluded that predicted values of the cefficient of horizontal subgrade reaction Ks was within the acceptable value .

4-The load- settlement curve at the pile head was close to linear particularly at early stage of loading .At higher loads, the curve shifted from linearity ,hence it could be considered as segments of straight lines with different slopes .

5-The calculated settlements increased 3 times when the load was doubled and no effect of heave at the surface was noticed even with time delay of loading .

6- There was no cracking observed at the tension piles even during the application of maximum uplift force during testing.

REFERENCES

- American Standards for Testing Materials,2010.
- Bowles,J.E. 1981 , Engineering Properties of Soils &Their Measurement, McGraw-Hill, Inc.
- Broms, B.B, 1995 **,** Design of lateral loaded piles**,** Proc.ASCE,Vol.91,No.3.
- Cook,P.K.and Davis,T.G. 2006 **,** Axially and laterally loaded single piles embedded in a non-homogenous Soils **,** Journal of Geotechnique Engineering,Vol.29,No.2, pp 113-147.
- Das, B.M.,2004 **,** Principle of Geotechnical Engineering , 5th edition: Thomson Learning, USA.
- Head, K.H. 1984 **,**Manual of Soil Laboratory Testing, Pentech Press, London, Vol.1, 2 &3.
- Mindlin,R.D.,2007 ,An Introduction to the Mathematical Theory of Vibrations of Elastic Plates, edited by Jiashi Yang, World Scientific.
- Lee,S.L.,Kog Y.C. and Karunaratne,G.P, 1987 **,** Axially loaded piles in layered soil **,** Journal of Geotechnical Engineering,Vol.113,No.4, pp 366-381.
- Pestana,J.M,Hunt,C.E. and Bray,J.D, 2002 ,Soil deformation and excess pore pressure field around a closed-ended pile, Journal of Geotechnical and Geoenvion mental Engineering,Jan., Vol.128,No.1, pp 1-12.
- Poulos, H.G. and Davis, E.H., 1980, Pile Foundation Analysis and Design, John Wiley & Sons, New York.
- Tomlinson, M. J., 1994, Pile Design and Construction Practice, Fourth edition, E &FN Spon Publishing Company.

NOTATION

A_m , B_m : moment coefficients.
A_u , B_u : lateral displacement coefficients.
D_p :diameter of pile .
E_c : modulus of elasticity of concrete .
f_c' : compressive strength of concrete at 28 days.
f_y :yield strength of reinforcement .
F_u : ultimate skin friction at pile shaft .
G.L: ground level .
Gs: Specific Gravity.
H_L : horizontal load resistance .
I_c : moment of inertia of pile section with it reinforcement .
K_s : soil modulus.
K_u : ultimate coefficient of soil reaction.
K_x : soil modulus at depth x of pile.
L : length of pile.
LL: Liquid limit.
M_L : moment resistance .
PI: Plasticity index.
PL: Plastic limit.
P_b : force acting at base of pile.
P_s : force acting along shaft of pile.
q : allowable effective stress.
q' : deviatoric effective stress.
Q_B : maximum strength of pile base.
Q_F : maximum strength of pile shaft.
Q_u : ultimate strength capacity of pile.
R : stiffness factor.
u : lateral displacement of pile head .
USCS: Unified Soil Classification System.
w_x , w_y : components of dead load in x and y directions.
$\propto$: shaft adhesion factor .
γ : unit weight of soil.

ε_1: axial soil strain.
Δ_b: settlement of pile base.
Δ_e : elastic shortening of pile .
σ_x , σ_y : components of normal stress in x and y directions.
τ': allowable shear traction along pile.
τ_{xy} , τ_{yx} :shearing stress components.
λ: influence factor for safety .
υ : Poisson′s ratio for soil.

Table 1. Results of Atterberg Limits, Specific Gravity & Grain size.

Depth (m)	Layer thick (m)	Gs	Atterberg Limits			Sieve & Hydrometer				USCS
			LL	PL	PI	Gravel %	Sand %	Silt %	Clay %	
0-3	3	2.66	22	NP	NP	9	55	36	0	SM
3-5	2	2.64	20	NP	NP	11	59	26	4	SM
5-6	1	2.74	42	23	19	2	3	30	65	CL
6-12	6	2.64	20	NP	NP	12	58	25	5	SM
12-17	5	2.74	40	22	12	13	55	7	25	SC
17-22	5	2.65	24	NP	NP	9	60	31	9	SM
22-29	7	2.66	NP	NP	NP	12	53	27	8	SM

Table 2. Details of the test pile and the tension piles.

Type of test	Diameter (m)	Length (m)	Reinf.	Lateral reinf.
Test piles	1.5	25.5	45 ϕ 32mm 30 ϕ32mm	ϕ 12mm@20cm .c/c with 14mm thick,15m long casing
Tension pile	1.95	22.5	24 ϕ 32mm	ϕ 12mm@20cm .c/c No casing

Table 3. Details of the four previously propose cycles.

1st cycle (1/2 Working load)		2nd cycle (2/2 Working load)		3rd cycle (3/2 Working load)		4th cycle (4/2 Working load)	
Load (kN)	Time (hrs)	Load (kN)	Time (hrs)	Load (kN)	Time (hrs)	Load (kN)	Time (hrs)
0	0	0	0	0	0	0	0
1100	1:00	2200	0:20	2200	1:00	2200	1:00
2200	1:00	3300	2:00	4400	1:00	4400	1:00
1100	0:20	4400	2:00	5500	2:00	5500	1:00
0	0.20	3300	0:20	6600	2:00	6600	2:00
		2200	0:20	5500	1:00	7700	2:00
		1100	0:20	4400	1:00	8800	1:00
		0	0:20	3300	1:00	6600	1:00
				2200	1:00	5500	1:00
				1100	1:00	4400	0:20
				0	1:00	2200	0:20
					1100	0:20	
					0	0:20	

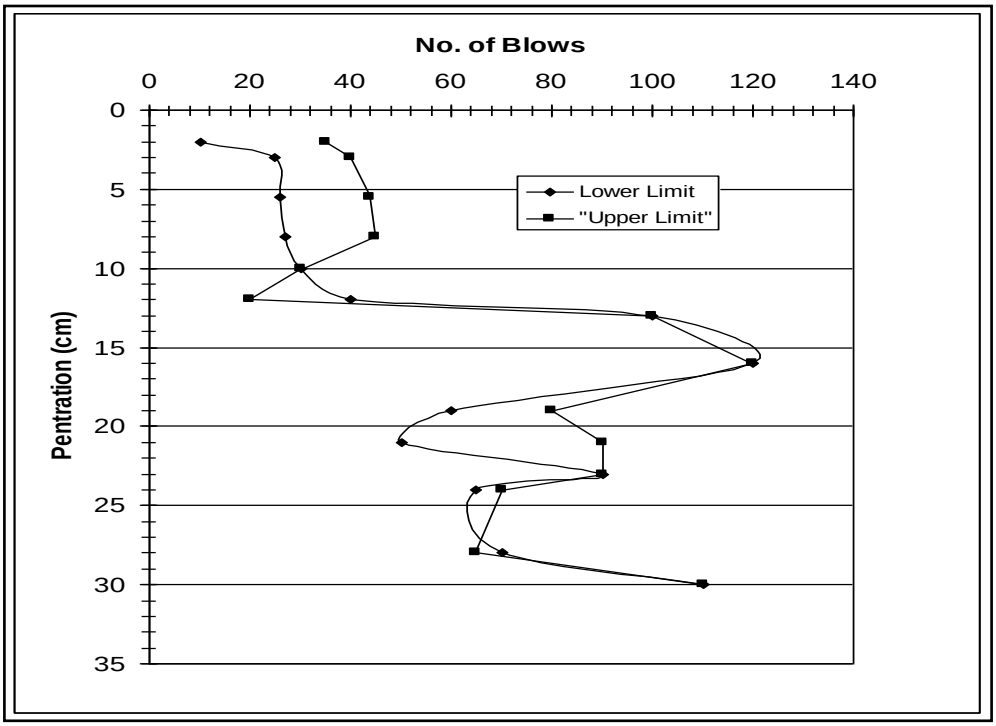

Figure 1. SPT results for B.H. no.1 near the test pile.

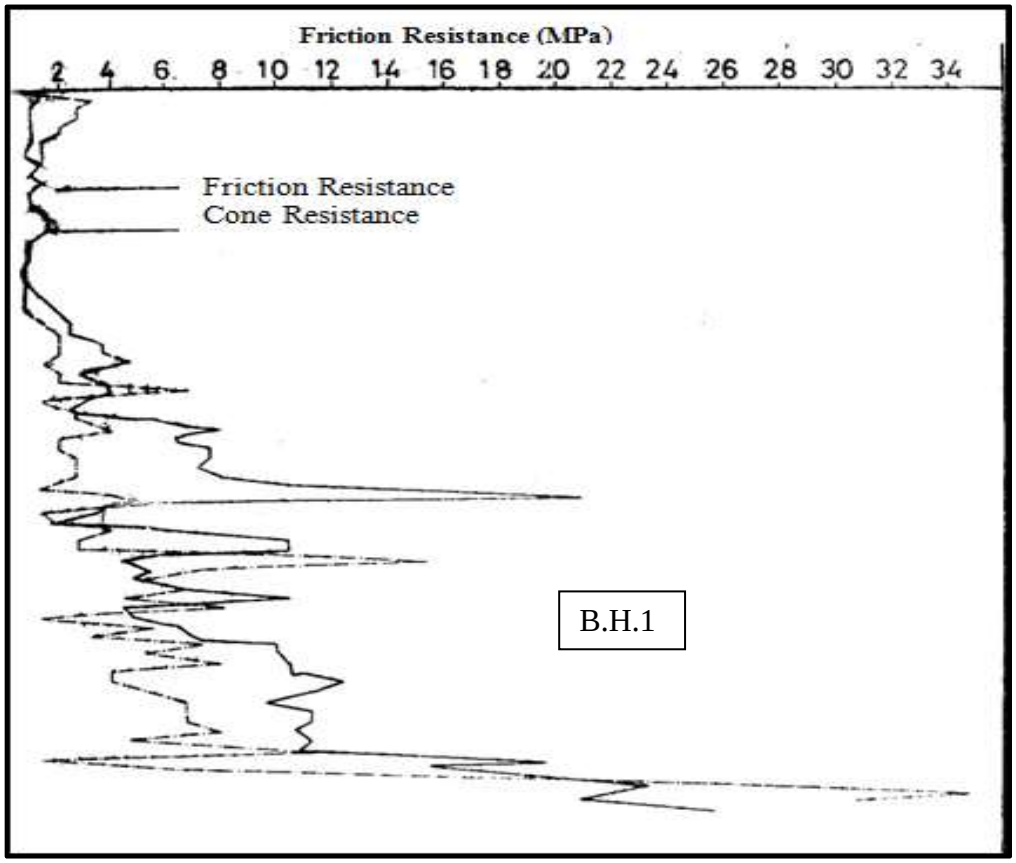

Figure 2. Cone Penetration Test(CPT) for Therthar Tigris canal bridge project KM 50.

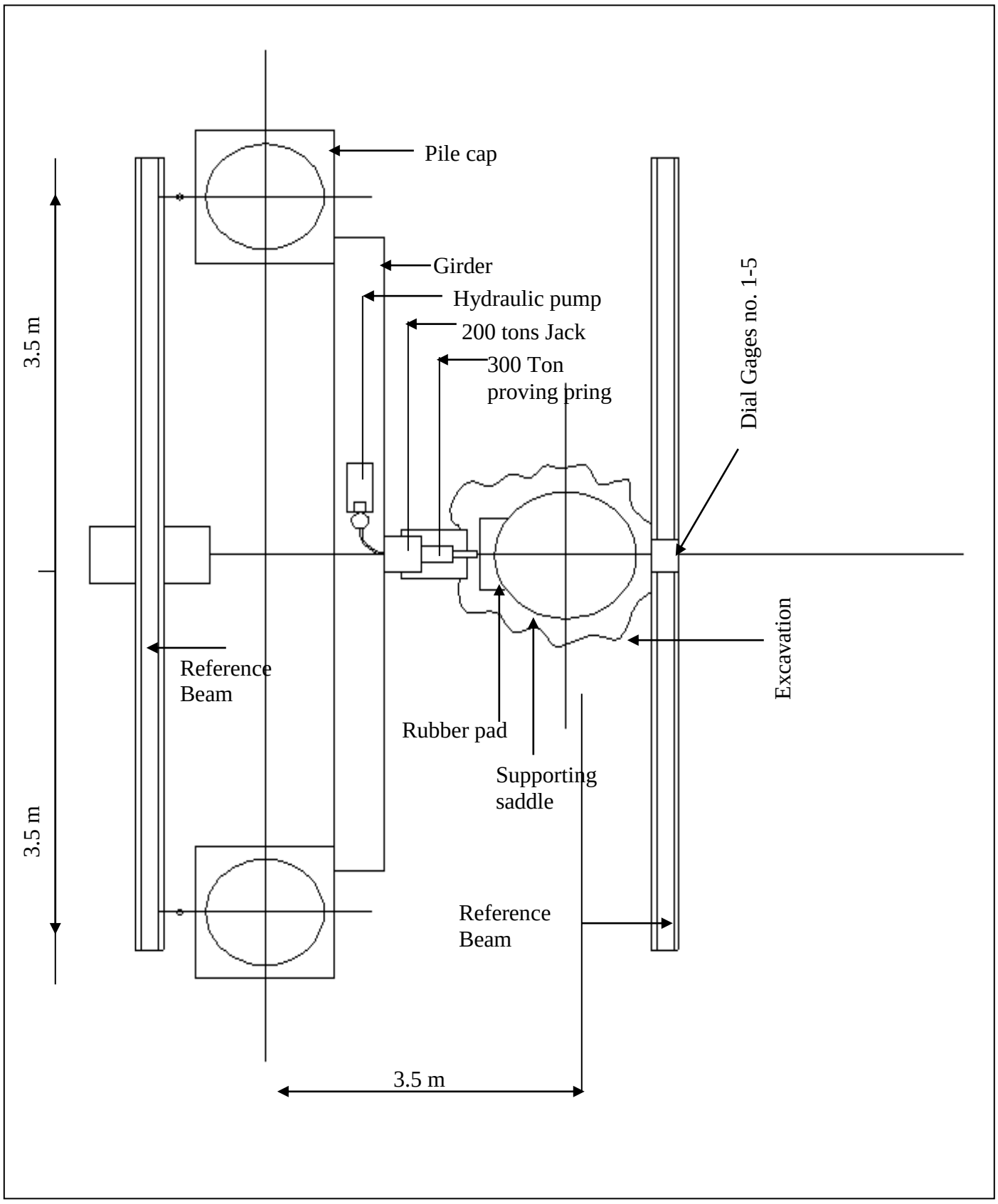

Figure3. Lateral testing insulation (Plan).

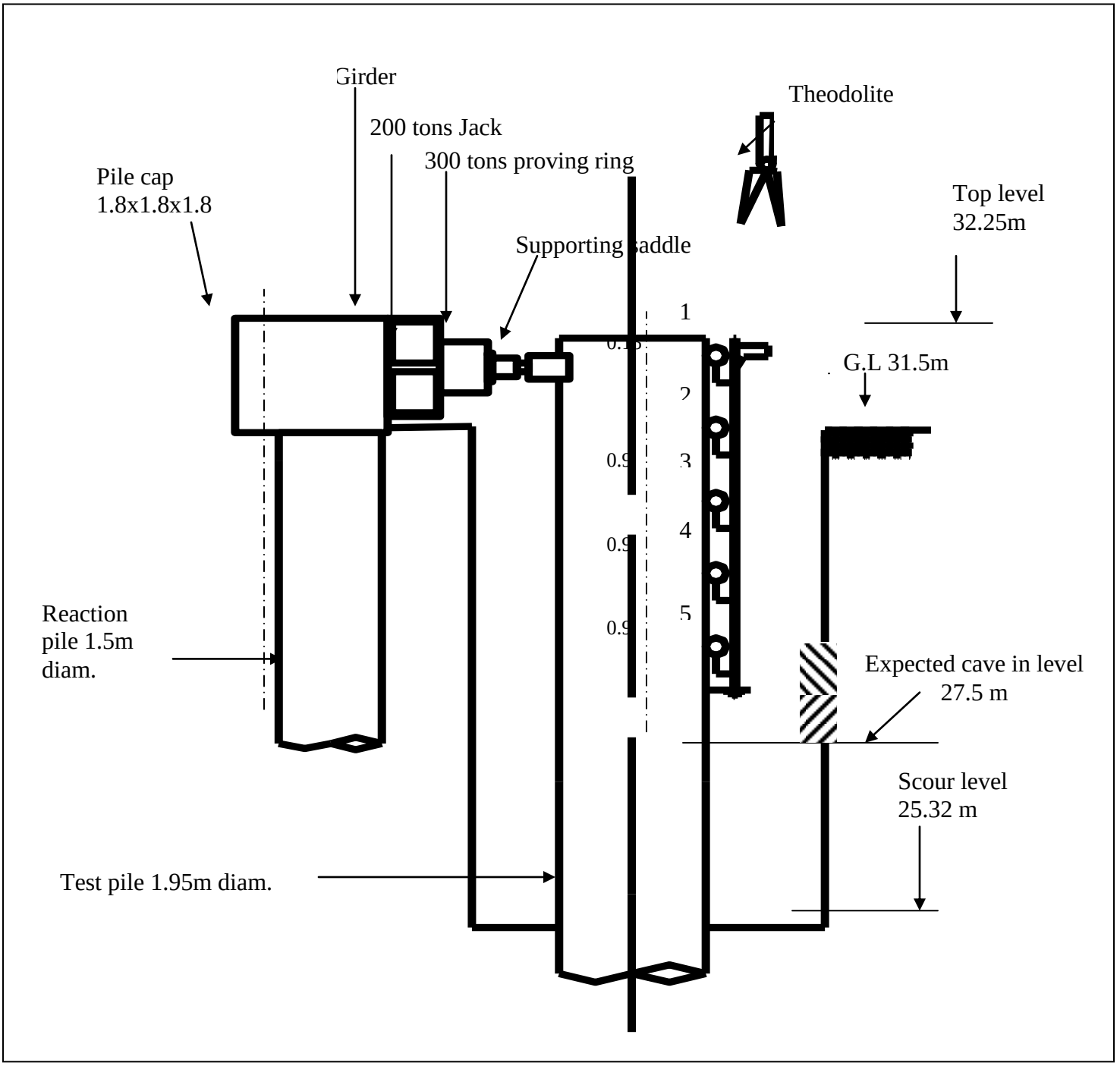

Figure 4. Lateral testing insulation (section).

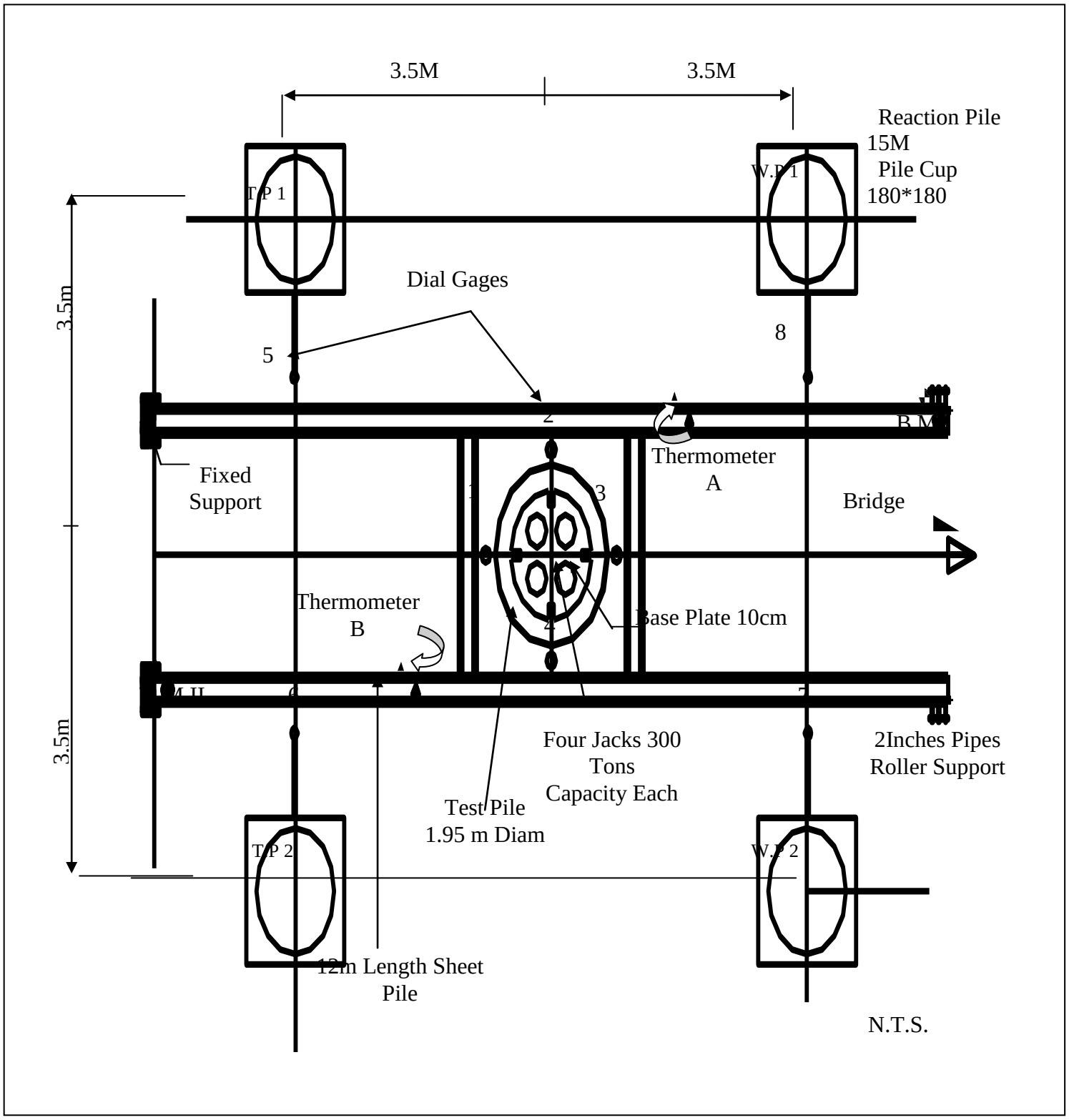

Figure 5. Vertical testing installation (plan).

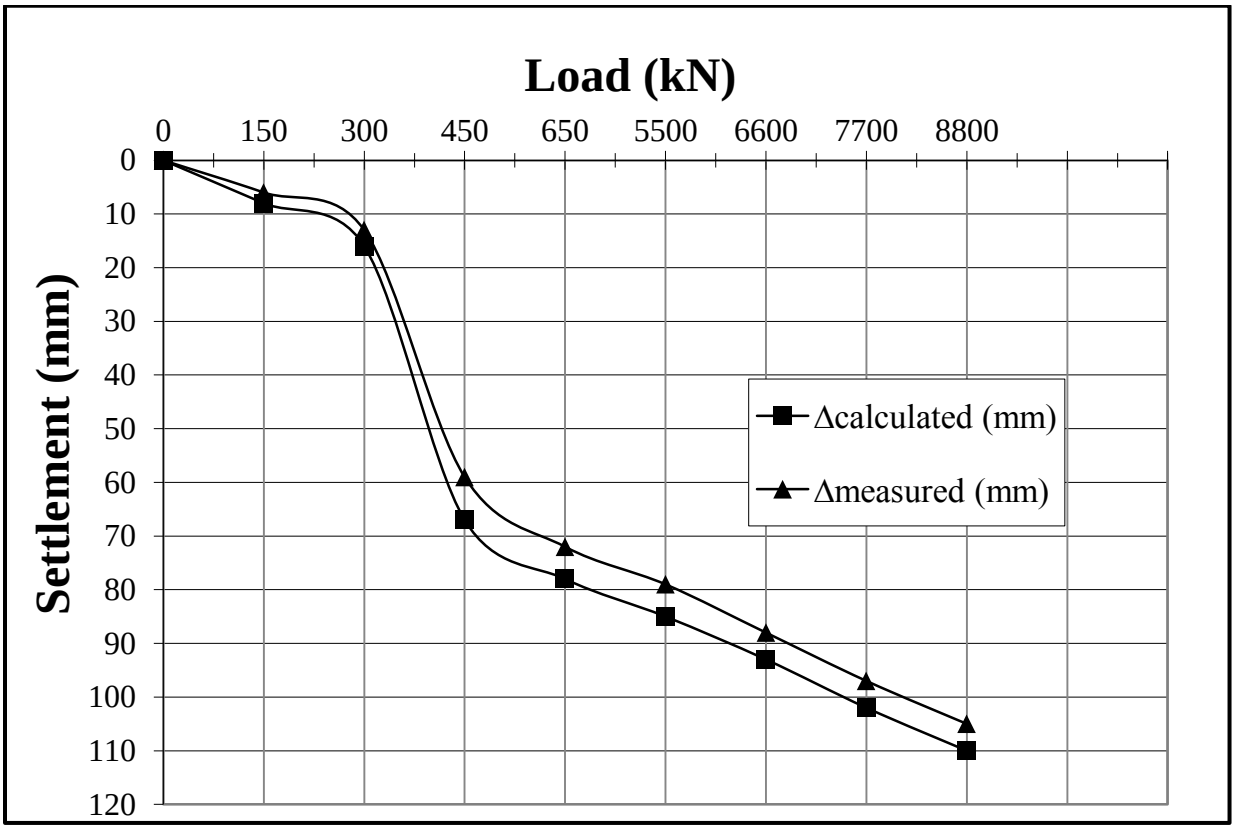

Figure 6. Load – Settlement curve for the pile head .

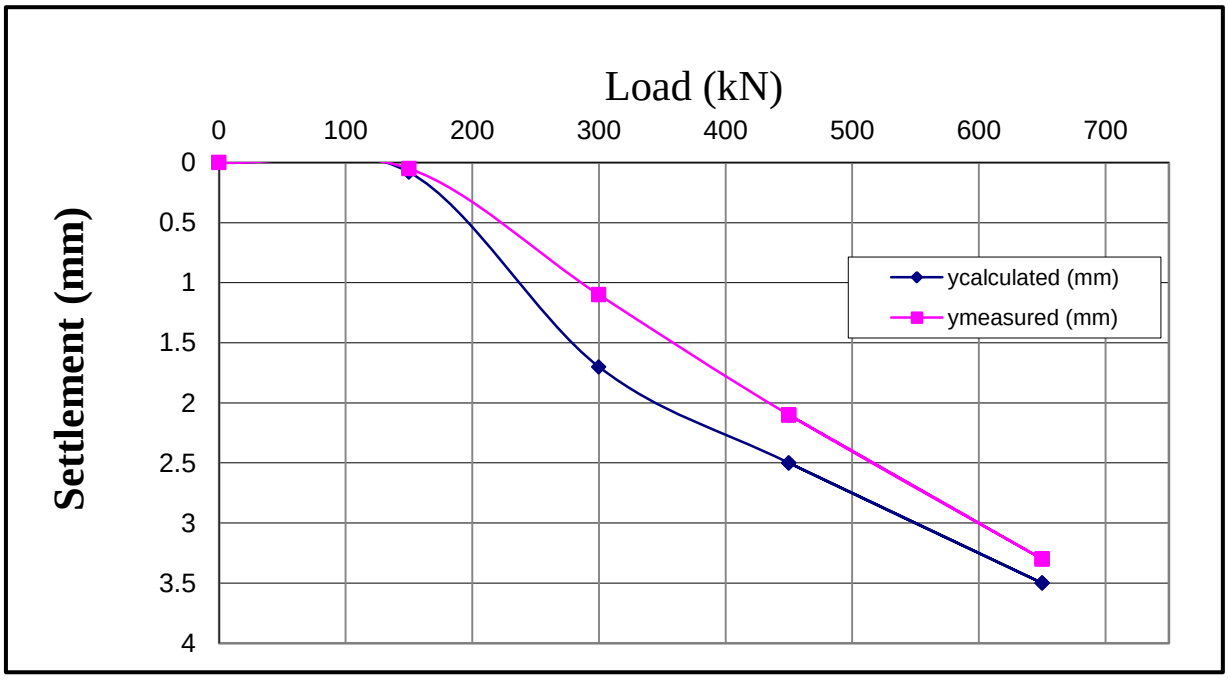

Figure 7. The calculated and measured lateral displacement for the pile head.